U. S. GEOLOGICAL SURVEY

SAUDI ARABIAN PROJECT REPORT 275

A TOTAL INTENSITY MAGNETIC ANOMALY MAP OF THE RED SEA AND ITS INTERPRETATION

by

Stuart A. Hall

U. S. Geological Survey
Jidda, Saudi Arabia

1979

The work on which this report is based was performed in accordance with a cooperative agreement between the U. S. Geological Survey and the Ministry of Petroleum and Mineral Resources, Kingdom of Saudi Arabia.

SA(IR)-275

UNITED STATES DEPARTMENT OF THE INTERIOR

GEOLOGICAL SURVEY

SAUDI ARABIAN MISSION

PROJECT REPORT 275

A TOTAL INTENSITY MAGNETIC ANOMALY MAP OF THE RED SEA AND ITS INTERPRETATION

by

Stuart A. Hall

PREPARED FOR
DIRECTORATE GENERAL OF MINERAL RESOURCES
MINISTRY OF PETROLEUM AND MINERAL RESOURCES
JIDDAH, SAUDI ARABIA
1979

PREFACE

In order to make widely available a useful contribution to Arabian geology, Stuart Hall's report on magnetic anomalies in the Red Sea area is reprinted herein directly from his doctoral thesis submitted in April 1976 to the University of Newcastle upon Tyne. Only page numbers have been changed and a list of illustrations added. Thus, the format of the report differs radically from that of other publications of the USGS Saudi Arabian Mission.

CONTENTS

	Page
ABSTRACT	1
ACKNOWLEDGEMENTS	3
CHAPTER 1. INTRODUCTION	
1.1 Introductory remarks	5
1.2 Plate tectonic framework	7
1.3 Evidence for crustal separation	10
1.4 Geological history of the Red Sea	16
1.5 Aims of the work	21
CHAPTER 2. THE TOTAL INTENSITY MAGNETIC ANOMALY MAP	
2.1 Introductory remarks	23
2.2 Sources of magnetic data	23
2.3 Data reduction	26
2.4 Corrections to data	30
2.5 Preparation of the magnetic anomaly map	35
2.6 Main features of the magnetic map	39
CHAPTER 3. SOME THEORETICAL CONSIDERATIONS OF SEA FLOOR SPREADING IN THE RED SEA	
3.1 Introductory remarks	41
3.2 Total intensity magnetic anomaly due to a two dimensional body	41
3.3 Seafloor Model	47
3.4 Variation in character of anomalies with latitude	48
3.5 Variation in character of anomalies with different depths to seafloor	49
3.6 Variation in character of anomalies with strike	54
3.7 Variation in character of anomalies with spreading rate	57
3.8 Predicted character of anomalies over the northern, central and southern Red Sea	57
CHAPTER 4. THE RED SEA NORTH OF 24°N	
4.1 Relevant geophysical data	63
4.2 Distribution of magnetic data	66
4.3 Description of magnetic anomalies	70
4.4 Ocean/continent boundary	78
4.5 Seafloor spreading history	80
4.6 Location of transform faults	86
4.7 Relation of magnetic anomalies to the deep holes	99
CHAPTER 5. THE RED SEA BETWEEN 18°N and 24°N	
5.1 Relevant geophysical data	107
5.2 Distribution of magnetic data	110
5.3 Description of magnetic anomalies	114
5.4 Ocean/continent boundary	128
5.5 Seafloor spreading history	130

Page

5.6 Location of transform faults..... 136
5.7 Relation of magnetic anomalies to deep holes..... 151
CHAPTER 6. THE RED SEA SOUTH OF 18°N
6.1 Relevant geophysical data..... 159
6.2 Distribution of magnetic data..... 162
6.3 Description of magnetic anomalies..... 167
6.4 Ocean/continent boundary..... 178
6.5 Seafloor spreading history..... 179
6.6 Location of transform faults from offsets of the magnetic anomalies..... 187
CHAPTER 7. RED SEA FLOOR SPREADING, TRANSFORMS AND PLATE GEOMETRY
7.1 Extent of oceanic crust..... 193
7.2 Seafloor spreading..... 200
7.3 Transforms..... 210
7.4 Poles of rotation for Nubia and Arabia..... 215
7.5 Plate movements and geometry..... 220
CHAPTER 8. IMPLICATIONS FOR THE FORMATION OF THE RED SEA DEEPS
8.1 Magnetic anomalies over deeps..... 235
8.2 Possible models for the formation of deeps..... 236
CHAPTER 9. CONCLUSIONS AND SUGGESTIONS FOR FURTHER WORK
9.1 Concluding remarks..... 245
9.2 Major conclusions..... 245
9.3 Suggestions for further work..... 247
REFERENCES..... 249

ILLUSTRATIONS

Page

Plate 1. Total intensity magnetic anomaly map of the Red Sea and adjacent coastal areas (Pocket)
Figure 1.1 Map showing present plate configuration of the Red Sea and Gulf of Aden..... 8
1.2 Map showing Bouguer gravity anomalies of the Red Sea area..... 12
1.3 Map showing epicenters in the Red Sea, Gulf of Aden, and Afar depression 1953-1968..... 13
1.4 Map showing heat flow measurements in the Red Sea area..... 15
1.5 Schematic geologic map of the Red Sea area..... 17
2.1 Map showing areas for which magnetic data are available..... 25
2.2 Diagram showing the subdivision of an irregularly shaped survey area into a number of rectangular outlines for digitisation of data..... 28

Page

Figure 3.1 Diagram showing geometry used for the calculation of the magnetic intensity due to a two-dimensional body..... 42
3.2 Synthetic magnetic profiles over seafloor spreading at various latitudes. 50
3.3 Graph showing amplitude of central anomaly versus latitude for the synthetic magnetic profiles shown in figure 3.2... 51
3.4 Synthetic magnetic profiles over seafloor at various depths..... 52
3.5 Graph showing amplitude of central anomaly versus depth of seafloor for the synthetic magnetic anomalies shown in figure 3.4..... 53
3.6 Synthetic magnetic profiles over seafloor with various strikes..... 55
3.7 Graph showing amplitude of central anomaly versus strike of seafloor for the synthetic magnetic profile shown in figure 3.6..... 56
3.8 Synthetic magnetic profiles over seafloor spreading at various rates..... 58
3.9 Graph showing amplitude of central anomaly versus spreading rate for synthetic magnetic profile shown in figure 3.8..... 59
3.10 Synthetic magnetic profiles over northern, central, and southern Red Sea predicted from geophysical and geological data... 61
4.1 Map showing geophysical data (excluding magnetic) available for the Red Sea between 24°N and 28°N..... 64
4.2 Map showing tracks of research vessels between 24°N and 28°N for which magnetic data are available..... 67
4.3 Map showing location of magnetic profiles selected from airborne surveys along the Arabian coast between 24°N and 28°N..... 69
4.4 Magnetic profiles and associated bathymetry from research vessels across the northern Red Sea near 26.5°N and the southern central Red Sea near 19°N.. 71
4.5 Magnetic profiles over the northern Red Sea from research vessels *Conrad* and *Dalrymple*..... 72
4.6 Aeromagnetic profiles over the Arabian coast between 24°N and 28°N..... 73
4.7 Magnetic profiles near 24.5°N from research vessels *Vema*, *Chain*, and *Aragonese*..... 75

Page

Figure 4.8 Map showing location of dominant peaks and troughs between 24°N and 28°N..... 77
4.9 Magnetic profile showing two seafloor spreading models, recent phase..... 82
4.10 Magnetic profiles showing two seafloor spreading models, early phase..... 85
4.11 Map showing location of transform faults inferred from offsets of the linear magnetic pattern in figure 4.8..... 89
4.12 Magnetic profiles across the traverse magnetic feature near 25°N, 36°E shown in figure 4.8..... 93
4.13 Magnetic profiles showing two seafloor spreading models of a leaky transform fault at 25°N, 36°E..... 96
4.14 Magnetic profiles near Oceanographer Deep from research vessels *Vema* and *Aragonese*..... 101
4.15 Magnetic profiles near Kebrit and Gypsum Deeps from research vessels *Dalrymple*, *Chain*, and *Aragonese*..... 102
4.16 Diagram of three-dimensional models of the Kebrit and Gypsum Deeps..... 104
5.1 Map showing geophysical data (excluding magnetic) available for the Red Sea between 18°N and 24°N..... 109
5.2 Map showing tracks of research vessels between 18°N and 24°N for which magnetic data are available 111
5.3 Map showing location of flight lines of aeromagnetic surveys between 16°N and 24°N..... 113
5.4 Magnetic profiles over central Red Sea... 115
5.5 Aeromagnetic profiles from Yanbu survey.. 117
5.6 Coast to coast aeromagnetic profiles between 21°N and 21.5°N..... 118
5.7 Aeromagnetic profiles from Al Lith survey 119
5.8 Project Magnet aeromagnetic profiles between 17°N to 19°N..... 120
5.9 Map showing location of dominant peaks and troughs between 18°N and 24°N..... 122
5.10 Northeast-southwest magnetic profiles over deep-water areas between 18°N and 19.5°N..... 123
5.11 Approximately west-east magnetic profiles over deep-water areas between 19.8°N and 20.3°N..... 124
5.12 Approximately northeast-southwest magnetic profiles over deep-water areas between 22°N and 22.4°N..... 125

Page

Figure 5.13 Aeromagnetic profiles across Arabian coast from 19°N to 27°N..... 127
5.14 Magnetic profiles showing seafloor spreading model, recent phase..... 132
5.15 Magnetic profiles showing two seafloor spreading models, early phase..... 134
5.16 Map showing location of dominant peaks and troughs in the area of transverse magnetic anomalies between 20.25°N and 21°N..... 140
5.17 Magnetic profiles over deep water between 20.25°N and 21°N..... 141
5.18 Map showing location of dominant peaks and troughs in the area of transverse magnetic anomalies between 21°N and 22°N..... 143
5.19 Magnetic profiles over deep water between 21°N and 22°N..... 144
5.20 Magnetic profiles showing seafloor spreading models for leaky transform faults between 20.3°N and 22°N..... 148
5.21 Map showing location of deep holes between 18°N and 24°N..... 154
5.22 Magnetic profiles over Suakin, Nereus, and Hardada Deeps..... 155
5.23 Magnetic profiles over Vema, Thetis, Port Sudan, Volcano, and Hatiba Deeps. 157
6.1 Map showing geophysical data (excluding magnetic) available for the Red Sea between 12°N and 18°N..... 160
6.2 Map showing tracks of research vessels between 12°N and 18°N for which magnetic data are available..... 163
6.3 Map showing location of aeromagnetic data between 12°N and 18°N..... 165
6.4 Magnetic profiles over southern Red Sea.. 168
6.5 Aeromagnetic profiles from the Jizan survey..... 169
6.6 Aeromagnetic profiles across Red Sea between 16°N and 17°N..... 170
6.7 Map showing location of dominant peaks and troughs between 12°N and 18°N..... 172
6.8 Approximately east-west magnetic profiles over deep water between 16°N and 18°N.. 173
6.9 Magnetic profiles over deep water between 12.6°N and 14°N..... 176
6.10 Magnetic profiles over shallow shelf near African coast from the research vessel *Discovery*..... 177

Page

Figure 6.11 Magnetic profiles showing seafloor spreading model, recent phase, between 17°N and 18°N..... 181
6.12 Magnetic profiles showing seafloor spreading model, recent phase, at at 15.3°N..... 182
6.13 Magnetic profiles showing two seafloor spreading models, early phase..... 184
6.14 Plot of separations of dominant magnetic features of Jizan survey versus distances from profile 1..... 186
6.15 Map showing location of transform faults inferred from offsets and (or) sudden changes in direction of the magnetic pattern shown in figure 6.7..... 191
7.1 Map showing crustal structure of the northern Red Sea deduced from the magnetic data..... 194
7.2 Map showing crustal structure of the central Red Sea deduced from the magnetic data..... 195
7.3 Map showing crustal structure of the southern Red Sea deduced from the magnetic data..... 196
7.4 Plot showing variation of intensity of magnetisation over two reversals of the geomagnetic field..... 203
7.5 Plots of intensity of magnetisation versus age of the seafloor for various spreading rates and intrusion zone widths..... 205
7.6 Magnetic anomalies showing seafloor spreading models for anomalies parallel and transverse to the axis of the northern and central Red Sea..... 206
7.7 Graph showing variation in TRM intensity with grain size for magnetite..... 209
7.8 Magnetic anomalies showing seafloor spreading model, recent phase..... 211
7.9 Map showing location of proposed transform faults..... 214
7.10 Diagram showing separation of continental crust and generation of oceanic crust..... 216
7.11 Regional map showing locations of rotation poles for the Red Sea determined from the magnetic data..... 218

Page

Figure 7.12 Sketch maps showing schematic two-stage reconstruction of Arabia and Nubia by rotation of Arabia about poles O and R in figure 7.11..... 221
7.13 Sketch maps showing schematically evolution of Red Sea..... 223
7.14 Sketch maps showing proposed reconstruction of Arabia-Sinai-Nubia deduced from the two-stage rotation..... 225
7.15 Sketch maps showing proposed evolution of Danakil plate deduced from the two-stage rotation of Arabia with respect to Nubia..... 230
7.16 Map showing present plate geometry at southern end of Red Sea..... 232
7.17 Map showing formation of the southern Red Sea by the counterclockwise rotation of Danakil with respect to Arabia 234
8.1 Diagram showing formation of deep holes by seafloor spreading with localised injection of seafloor into evaporites.... 237
8.2 Diagrams showing development of localised basins due to salt flowage and seafloor spreading..... 240
8.3 Plot of depth versus latitude of deep holes in the Red Sea..... 242

TABLES

Page

Table 2.1 Details of data used in the preparation of the total intensity magnetic anomaly map..... 24
2.2 Mean hourly values obtained from diurnal variation records..... 32
2.3 Values of secular variation obtained from cross-overs of ships' tracks..... 34
4.1 Locations and azimuths of proposed transform faults..... 91
5.1 Location of deeps in the central Red Sea including some of their physical and chemical properties..... 153
7.1 Amounts of recent and early seafloor spreading at various latitudes in Red Sea 197
7.2 Locations and relevant details of the proposed transform faults..... 213
7.3 Directions of motion of Arabia with respect to Nubia at various latitudes calculated from the poles of rotation shown in figure 7.11..... 219

ABSTRACT

All available total intensity magnetic field data have been used to prepare a total intensity magnetic anomaly map of the Red Sea at a scale of 1:2,000,000. These include airborne surveys at various elevations and numerous sea surveys. The data have been digitised at approximately one kilometre intervals and the International Geomagnetic Reference Field (IGRF epoch 1965.0) removed. The resulting values have been upward continued to a common height of 1.83 km (6000 ft), transferred to a base map and contoured at 100 nT intervals. The map is published in colour by the United States Geological Survey - Saudi Arabian Project.

The map reveals three distinct zones: (1) large amplitude (approximately 800 nT), short wavelength (15 km peak to trough) anomalies over the axial trough which form lineations roughly parallel to the coastlines, (2) smaller amplitude (approximately 300 nT), longer wavelength (30 km) anomalies over the main trough and shelves which also form lineations parallel to the coastlines, and (3) very variable amplitude (100 to 400 nT), short wavelength (5 to 30 km) anomalies over the shield areas on both sides of the Red Sea. The large, linear anomalies terminate in the north at about $23^{\circ}N$ and in the south at about $15^{\circ}N$. The anomalies over the main trough and shelves converge south of approximately $15.5^{\circ}N$. Several NE trending magnetic features offset the linear, axial anomalies. Such features are confined to zones (1) and (2) and are thought to indicate leaky transform faults.

The interpretation of the magnetic data is presented in three parts: the northern Red Sea (north of 24^{o}N), the central Red Sea (18^{o}N to 24^{o}N) and the southern Red Sea (south of 18^{o}N). For each part, there is a discussion of the extent of oceanic crust, the seafloor spreading history, the possible location of transform faults and the relationship of the magnetic anomalies to the deep holes. In Chapter 7, the results are brought together and their significance for Red Sea floor spreading, transforms and plate geometry discussed. The problems of the brine deeps are briefly discussed in Chapter 8.

ACKNOWLEDGEMENTS

I would like to thank Professor S.K. Runcorn for the opportunity of working in his department and Dr T.H. Kiilsgaard for providing logistical support during my employment with the U.S. Geological Survey - Saudi Arabian Project.

The idea for the map project came from discussions between Dr R.W. Girdler and Mr G.E. Andreasen, both of whom have provided much needed advice and encouragement at all stages of the work.

The work has benefitted from many useful discussions, especially those with P. Styles, R.C. Searle, G.F. Brown and R. Pearce on the plate tectonics of the region and those with D.G.Hadley, D. Schmidt and W. Greenwood on the geology of Arabia.

I should also like to thank R.H. Godson, L. North and B. North for their help in communicating with the giant IBM 360's and 370's; Mrs D Hewett who drew many of the final diagrams and A.J. Petty, to whose cartography the magnetic map owes so much.

The digitisation of the magnetic data was performed by several members of the Saudi Arabian Project, notably Abdeen Uthman and Mrs Diane Ghalib. Drs. R.W. Girdler, M.L. Richards and J.G. Mitchell read over early drafts of the thesis and made many constructive suggestions. To these and many more too numerous to mention I express my sincerest thanks.

This thesis was typed by Marion Turner who I thank not only for her painstaking care but also for her encouragement and support.

Finally, I wish to thank my wife and family for their patience and understanding throughout the course of the work.

The following kindly contributed data to the Magnetic Map Project:

T.D. Allan, NATO SACLANT;

R.C. Blakely, Tenneco Saudi Arabia Inc;

E. Blanton, Sun Oil Company;

N.D. Coggeshall, Gulf Research and Development;

R.W. Girdler, University of Newcastle upon Tyne;

R.L. Larson and W.C. Pitman III, Lamont-Doherty Geological Observatory;

P.L. Lawrence, Mobil Oil Corporation;

J.F. Mason, Continental Oil Company;

H.A. Roeser, Bundesanstalt fur Bodenforschung;

D.A. Ross, Woods Hole Oceanographic Institute;

R.B. Whitmarsh, Institute of Oceanographic Sciences.

Financial support for the map project was provided by the U.S. Geological Survey - Saudi Arabian Project.

CHAPTER ONE

INTRODUCTION

1.1 Introductory remarks

Except for the pioneering studies of the shape of the ocean bottom made by H.M.S. Challenger and U.S.S. Tuscarora towards the end of the nineteenth century, the oceans were little explored until after the second world war. Although Wegener's ideas on continental drift, presented in the early part of this century, pinpointed the oceans as areas of critical importance, the continents remained the subject of major interest. However, improved navigation and advances in geophysical instrumentation made during the war resulted in attention being increasingly focussed on the oceans. A rapid increase in marine surveys took place and bathymetric and geophysical data were collected from many areas.

In the mid-1950's, largely as a result of palaeomagnetic studies of N. America and Europe (e.g. Irving, 1956a; Runcorn, 1956), the ideas of continental drift were revived. Opposition to Wegener's hypothesis was mainly due to difficulties arising from the supposition that the continents moved through the oceanic crust. As the evidence for major movements of the continents grew during the late 1950's and early 1960's, the search for a mechanism for their transport became all important. As early as 1944, Holmes (1944) had suggested the continents were conveyed on seas of basalt rather than through them and that the gaps they left were filled with new seafloor; a process he called 'ocean floor development'. However,little further progress seems to have been made until Hess (1962) revived Holmes' model, updating it by incorporating results obtained during the intervening years. Hess' seafloor spreading model provides

a mechanism consistent with the geological and geophysical data and forms the basis of modern ideas on the generation of oceans.

In 1963, Vine and Matthews (1963) explained the large magnetic anomalies found over the mid-ocean ridges by combining Hess' seafloor spreading model with reversals of the geomagnetic field. Vine and Matthews pointed out that if seafloor was magnetised in the direction of the ambient magnetic field as it cooled then changes in the polarity of the geomagnetic field must be recorded by the seafloor as it spreads. This proved to be a major advance and it was quickly realised that magnetic field measurements over the ridges could be used to study their evolution.

Over the period 1963 to 1968 evidence accumulated which showed how the continents had moved over the surface of the earth and oceans had opened and closed during geological time. In a series of articles between 1965 and 1968 a dynamic view of the oceans developed which resulted in an entirely new approach to their study. This culminated in the now widely accepted New Global Tectonics (McKenzie and Parker, 1967; Morgan, 1968; Isacks et al, 1968) in which the surface of the earth is composed of several plates, each moving with respect to its neighbours. These 'plates' are considered to be rigid such that all activity is confined to their boundaries; consequently their interactions can be specified in terms of relative motions on a sphere. Magnetic field measurements are particularly important in the study of these relative motions as they indicate the age, extent and rate of development of the seafloor. Such measurements are still regarded as the single, most powerful tool in determining the history of ocean basins.

One area of outstanding interest in the New Global Tectonics is the initial break-up of continents and the early evolution of oceans. Very limited opportunities exist for studying these as there are few places where spreading axes intersect the continents or where continents appear to be breaking up. One such area is the Red Sea which, together with the Gulf of Aden and East African Rift, seem to represent three stages in the break-up of a continent : from a rift to an ocean. Previous work in the area has shown that major crustal separation has taken place in the Gulf of Aden (e.g. Laughton, 1966), minor extension in East Africa (e.g. Darracott et al, 1972), and a limited amount of crustal separation in the Red Sea (e.g. Vine, 1966). The Red Sea is of particular interest since not only is seafloor spreading taking place near land but also at either end of the Red Sea this activity is presumably transferred onto the continents. Furthermore, because of the proximity of the continents, it may be possible to relate tectonic events on the adjacent land to movements of the plates. The Red Sea, therefore, provides an ideal area to study the early evolution of oceans and the plate tectonic processes involved.

1.2 Plate tectonic framework

The Red Sea forms a divergent plate margin produced by the separation of Arabia from Nubia. The present plate configuration of the region is shown in fig. 1.1. Several reconstructions of the plates prior to separation have been made (e.g. Laughton, 1966; McKenzie et al, 1970; Freund, 1970; Girdler and Darracott, 1972). At both ends of the Red Sea there are small pieces of sialic crust, viz. Sinai and Danakil (fig. 1.1), which must be accommodated in any

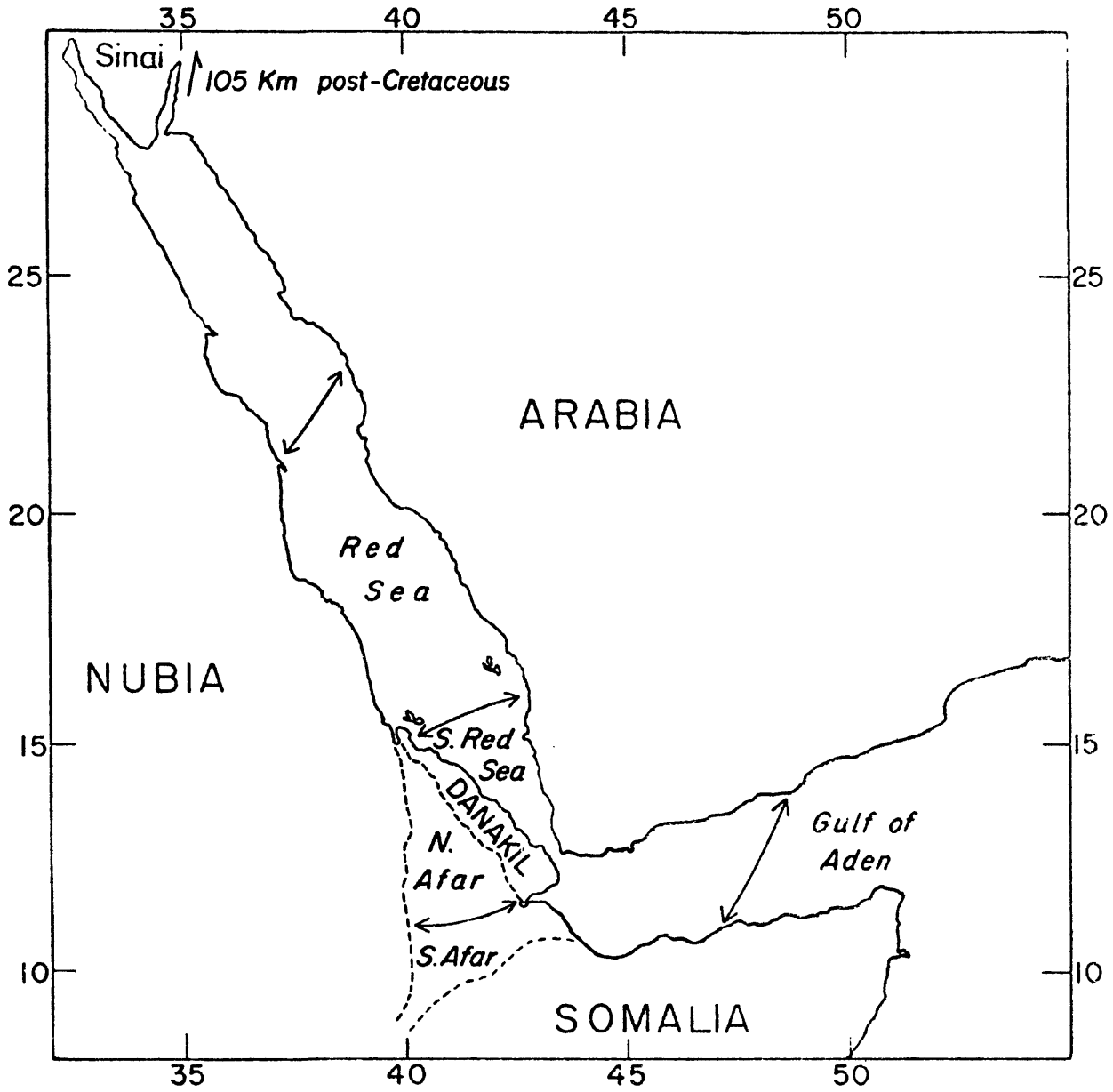

Figure 1.1 The present plate configuration of the Red Sea and the Gulf of Aden, from Girdler and Styles, 1976 (in press).

reconstruction of the area. The problems encountered at the southern end of the Red Sea in fitting back Arabia to Nubia and Somalia have been discussed by Laughton (1966). Closing the Gulf of Aden and the Red Sea produces an overlap of Arabia and Danakil which is not permitted by the rules of Plate Tectonics. To avoid this overlap, Laughton (1966) proposes a 35^{o} clock-wise rotation of Danakil which fits it back into Nubia closing the Afar depression. There are now extensive data which support Laughton's model. These include geological studies in Afar (e.g. Tazieff and Varet, 1969; Barberi et al, 1970; Marinelli et al, 1973) that indicate the depression is predominantly composed of oceanic material and palaeomagnetic data from the Danakil Horst which suggest a 25^{o} to 30^{o} counterclock-wise rotation of Danakil since the Miocene (Burek, 1970).

Although separated from Nubia by the Gulf of Suez, Sinai is often considered to be part of the Nubian plate. However, closing the Red Sea also results in an overlap of Arabia onto Sinai suggesting Sinai probably forms a separate plate. Reconstructions of the plates in the northern Red Sea have been proposed by McKenzie et al (1970) and Freund (1970) and discussed by Girdler and Darracott (1972) and Le Pichon et al (1973). The coast-to-coast reconstruction of Arabia and Nubia of McKenzie et al (1970) requires Sinai to have separated from Nubia by approximately 60 to 90 km. Such an amount is incompatible with the geological evidence (Said, 1962; Robson, 1971) which suggests the total extension across the Gulf is about 25 to 30 km (Freund, 1970). Although there is currently insufficient published evidence concerning the underlying structure of the Gulf it appears likely there is little oceanic crust present. It should be noted,

however, that most, recent reconstructions of Arabia and Nubia require some movement of Sinai with respect to Nubia.

Movement of Arabia with respect to Sinai is well documented in the form of offsets of surface and subsurface geological features along the Dead Sea rift (Quennell, 1958; Freund, 1965; Freund et al, 1970). The motion has been predominantly left-lateral, strike-slip and appears to have taken place in two stages: approximately 60 km post-Cretaceous but pre-Miocene and about 45 km since the Miocene (Freund et al, 1970).

Critical to any reconstruction of the plate geometry of the region is the relative displacement of Arabia to Nubia. The age and amount of crustal separation in the Red Sea provides the key to the plate tectonic evolution of the area and forms the central theme of this thesis. Evidence for crustal separation in the Red Sea prior to this work is reviewed below.

1.3 Evidence for crustal separation in the Red Sea

The earliest evidence for crustal separation in the Red Sea comes from a compilation of the gravity data of Triulzi (1898, 1901), Hecker (1910), Vening Meinesz (1934) and Harrison (Girdler and Harrison, 1957) made by Girdler (1958). This indicated a large, positive, Bouguer anomaly centered over the deeper water which Girdler (1958) interpreted as due to a large basic mass intruded into downfaulted basement rocks beneath the axial trough. As more gravity data were collected (Allan et al, 1964; Knott et al, 1966; Phillips et al, 1969) it became possible to define the extent of the positive anomaly more accurately. A Bouguer anomaly map was prepared by Allan (1970) and is reproduced in

fig. 1.2. The positive anomaly dominates the map extending from about 16^{o}N to the mouth of the Gulf of Suez. Its amplitude is typically 1000 g.u. (100 mgals) with localised maxima of 1200 to 1400 g.u. although it is somewhat smaller at the northern and southern ends. Smaller, positive anomalies (approximately 500 to 600 g.u.) are observed over the main trough although this area is not well covered.

Seismic refraction and magnetic surveys in the Red Sea (Drake and Girdler, 1964) show high seismic velocity material beneath the axial trough with lower velocity material beneath the main trough. Large magnetic anomalies were also observed over the axial trough and these together with the refraction data led the authors to propose a model in which a series of basic dykes were injected into downfaulted continental crust. Large magnetic anomalies were also reported by Allan et al (1964) and Knott et al (1966). These anomalies were explained by Vine (1966) in terms of seafloor spreading in which the axial trough is a site of recent spreading. As more refraction data (Tramontini and Davies, 1969) and magnetic data (Phillips et al, 1969) were collected the proposed crustal separation was confirmed. What remained to be shown was the extent of the oceanic crust, the direction of separation and whether it was continuing.

In their study of the seismicity of the Red Sea, Fairhead and Girdler (1970) show the activity is predominantly confined to the deep water (fig. 1.3). The events have shallow foci and form a pattern similar to that observed over mid-ocean ridges. This activity is generally associated with active seafloor spreading and indicates that parts of the Red Sea are currently spreading.

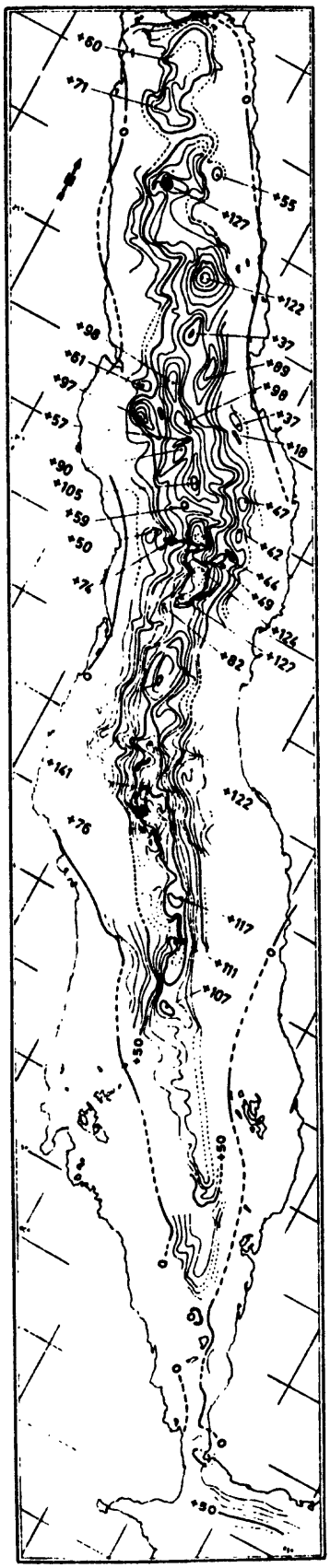

Figure 1.2 Bouguer gravity anomaly map of the Red Sea from Allan (1970). The water column is assumed to be replaced by rock of density 2.67 g cm . Contour interval 10 mgal (100 g.u.).

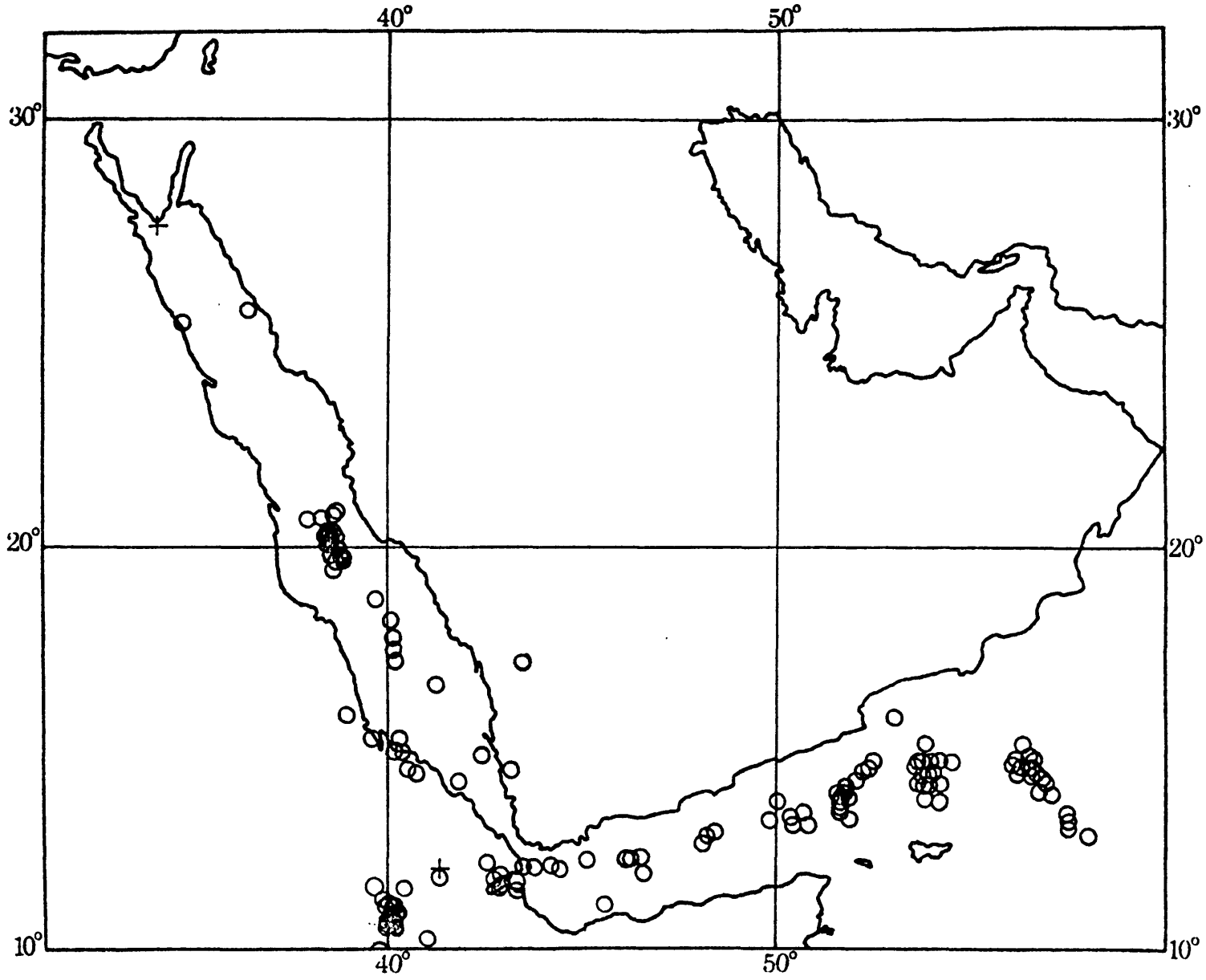

Figure 1.3 Epicentres for the Red Sea, Gulf of Aden (as far as the Owen fracture zone) and Afar depression for the period January 1953 through December 1968 from Fairhead and Girdler (1970).

A new heat flow map of the Red Sea has recently been compiled by Girdler (1975, unpublished) and is reproduced in fig. 1.4. The map shows the entire area has anomalously high heat flow; only 8 of the 83 measurements currently available are less than the world mean, viz 59 mW m^{-2}. Extremely high values are found in the deep water areas especially in the neighbourhood of the deep holes or 'deeps' where the world's highest value has been recorded, viz > 3306 mW m^{-2} (Erickson and Simmons, 1969). The heat flow data have been discussed by Girdler (1970a) who has shown that their distribution is similar to that predicted over seafloor spreading at a rate of 1 to 2 cm y^{-1}. Values along the coastal margins (Girdler, 1970a; Evans and Tammemagi, 1974) are typically two to three times higher than the world mean. Such values are difficult to reconcile with ancient continental shield and suggest that possibly more than the axial trough is underlain by oceanic crust.

Seismic reflection data (Knott et al, 1966; Phillips and Ross, 1970; Ross and Schlee, 1973) indicate the axial trough is floored by intensely deformed, acoustically opaque material which is interpreted as seafloor. Thick sedimentary sections are found throughout the main trough suggesting that the axial trough has been formed since the deposition of these sediments, i.e. since the late Miocene or early Pliocene (Knott et al, 1966).

Estimates of the present direction of separation of Nubia and Arabia have been obtained from first motion studies of earthquakes (Sykes, 1968; Fairhead and Girdler, 1970; McKenzie et al, 1970). There is considerable variation in the fault plane solutions obtained although all indicate an approximately north easterly movement of Arabia with respect to Nubia.

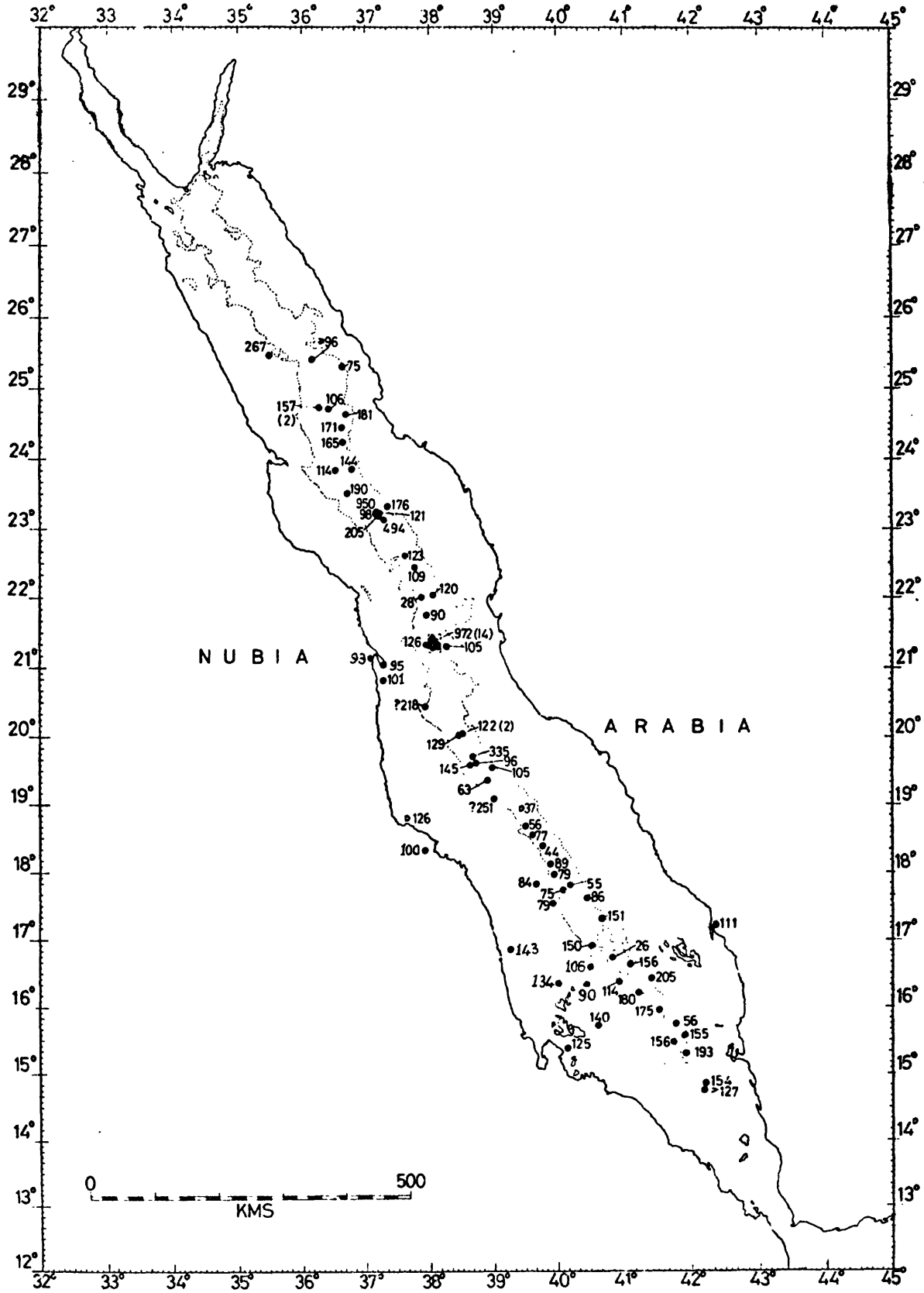

Figure 1.4 Heat flow measurements (in mW m^{-2}) available for the Red Sea, compiled by Girdler (1975, unpublished). Values in brackets are the number of measurements available in Kebrit, Atlantis II and Port Sudan Deeps.

Finally, a recent study of magnetic data over offshore Ethiopia (Girdler and Styles, 1974) suggests that a considerable part of the southern Red Sea is underlain by oceanic crust.

1.4 Geological history of the Red Sea

Geological summaries of the Red Sea have been given by Swarz and Arden (1960), Said (1969), Dubertret (1970), Ahmed (1972) and Coleman (1974). Detailed studies of individual areas have been reported by several authors, e.g. for Ethiopia by Mohr (1962), Tazieff et al (1969), Kazmin (1971) and Marinelli et al (1973), for Sudan by Carella and Scarpa (1962), Sestini (1965) and Whiteman (1971), for Egypt by Said (1962), for the Gulf of Suez and Sinai by Ball (1916), Barron (1917), Heybroek (1965), Schurmann (1966) and Robson (1971), for the Dead Sea rift and the Gulf of Aqaba by Dubertret (1932), Picard (1943, 1966), Quennell (1958, 1959), Freund (1965) and Freund et al (1970), for the eastern margin of Saudi Arabia by Richter-Bernburg and Schott (1954) and Brown et al (1962), Brown et al (1963a), Brown et al (1963b) and Brown (1970), for the Yemen by Geukens (1966). The following is a brief summary of the more important aspects of the geology. Figure 1.5 is a geological map of area taken from Said (1969).

The oldest sedimentary formations so far found are in the Gulf of Suez and consist of marine Carboniferous sandstones and dolomites (Ball, 1916; Beets, 1948). At that time an area encompassing the Gulf of Suez and Sinai, was submerged and the Tethyan Sea is thought to have extended as far south as Hurgada (27.3^{o}N, 33.8^{o}E) (Schurmann, 1966). South of this lay the Afro-Arabian Shield forming a continuous land barrier.

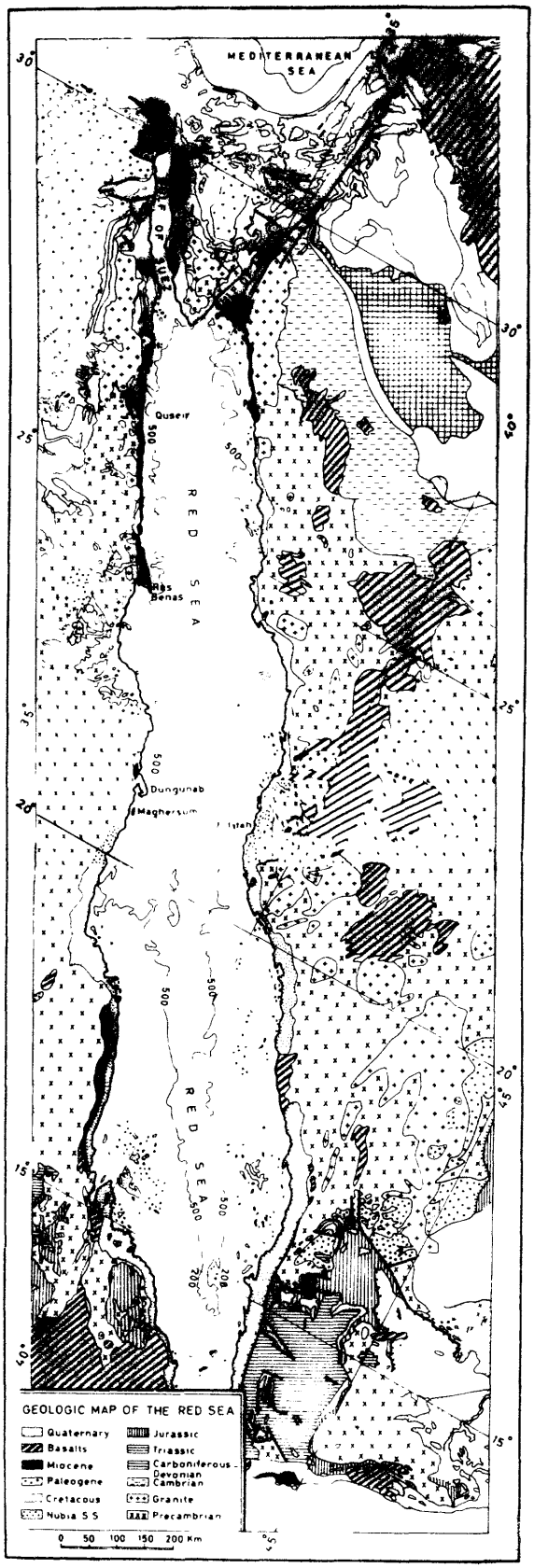

Figure 1.5 Schematic geologic map of the Red Sea from Said (1969).

This situation seems to have continued throughout the Jurassic with the Tethyan coastline stretching approximately E-W across the area at 29°N and shallow-water marine deposits being laid down across northern Egypt and Sinai. At the southern end of the Afro-Arabian Shield, the Jurassic Seas spread northwards across the Horn of Africa reaching Massawa (15.6°N, 39.5°E) and Jizan (16.9°N, 42.6°E). Upper Jurassic Amran series extend across Eritrea and the Yemen. Throughout this period the areas between 17°N and 29°N remained emergent and underwent erosion (Swartz and Arden, 1960).

During the Lower Cretaceous, there was a general uplift and emergence in the north and a submergence in the south. Major movements were probably epeirogenic as there is little evidence for major faulting at this time. The emergence in the north pushed back the Tethyan Sea to near the present Mediterranean coast. In the south, the embayment in Somalia extended further inland to the vicinity of Addis Ababa (9.1°N, 38.7°E). By the Middle Cretaceous, the vertical movements had reversed : the land subsided in the north permitting the sea to penetrate southwards and emerged in the south where regressive marine facies are found in Ethiopia and southern Yemen as far north as 13°N. At the end of the Cretaceous the Tethyan Sea extended at least as far south as 21°N where uppermost Cretaceous to Palaeocene rocks have been drilled on Maghersum Island (20.8°N, 37.3°E) (Carella and Scarpa, 1962). Rocks bearing Maestrichtian fossils have been reported along the Arabian coast near Usfan (21.9°N, 39.4°E) (Karpoff, 1957) although the dating of the fossils may be questionable (Brown, 1970). Volcanism seems to have begun at the southern end of the Afro-Arabian Shield towards the end of the Cretaceous as the Trap Series of volcanic rocks in the Yemen is thought to date from this time (Geukens, 1966). At the northern

end of the Red Sea, Cretaceous to Eocene formations have been preserved by faulting and now form limestone plateaux between Safaga (26.8°N, 34°E) and Quseir (26.1°N, 34.3°E) (Said, 1962). These strata bear a strong resemblance to those which lie west of the Red Sea hills suggesting they may have been deposited during a marine transgression which crossed Egypt from the north (Said, 1969).

During the Lower Eocene the sea continued to cover Sinai and northern Egypt extending possibly as far south as Maghersum Island where Eocene rocks may occur (Carella and Scarpa, 1962; Sestini, 1965; Whiteman, 1968). In the south, the uplift caused the sea to withdraw until by the end of the Eocene the Horn of Africa had completely emerged. Orogenic and epeirogenic movements began at the end of the Lower Eocene resulting in compression in the north and tension in the south (Swartz and Arden, 1960). These produced folding in northern Israel, Lebanon and Syria, uplift in Egypt and Sinai and strong NW-SE faulting and extensive volcanism in Ethiopia and Yemen . The uplift of Egypt and Sinai made the sea withdraw to the coastal areas in the Middle Eocene. With continued uplift in the Upper Eocene the sea withdrew northwards.

The Oligocene was a time of general uplift and consequently few sediments of this age have been preserved. The compressional forces continued in the north although some tensional forces must have been present as the Gulf of Suez in its present form probably formed at this time permitting the Tethyan Sea to penetrate at least as far south as Jeddah (21.5°N, 39.2°E) where Oligocene fossils have been reported in the Shumaysi formation (Shanti, 1966). Deep wells along the coast of Sudan have penetrated shale containing Oligocene fossils and interlayered basalts which give Oligocene radiometric ages (Whiteman, 1968).

Further south, the Red Series found in the Danakil Depression are thought to have been deposited during the late Oligocene. It appears very likely, therefore, that by the end of the Oligocene an extensive depression existed across the Afro-Arabian Shield, i.e. proto Red Sea. Towards the end of the Oligocene, but before Lower Miocene time, basalt flows occurred in northern Egypt, the Gulf of Suez and Sinai (Tromp, 1951).

In response to the general uplift in the Oligocene, the sea withdrew such that by the Lower Miocene the Red Sea occupied a narrow trough extending from the Mediterranean through the Gulf of Suez south to near Az Zuqar Island at about 15^{o}N. Extensive Miocene sediments are found throughout the Red Sea comprising mainly marls, shales, anhydrite and lenticular sandstones which contain Mediterranean fauna confirming that the waters came from the north. About late Middle Miocene, it is thought that an isthmus was formed along the present Mediterranean coast (Swartz and Arden, 1960) which converted the Red Sea and Gulf of Suez into a lagoon or series of lagoons (Ahmed, 1972). Arid conditions must have prevailed at this time since very thick sequences of anhydrite, salt and shale are found in boreholes drilled along the coastal margins (3.5 km or more evaporites are frequently encountered).

The isthmus was raised at the beginning of the Pliocene, permanently excluding the Mediterranean waters from the area. In the Middle Pliocene or possibly earlier, the southern end of the Red Sea subsided permitting the waters of the Indian Ocean to enter the Red Sea through the Straits of Bab-el-Mandeb. Indo-Pacific fauna of this age are reported as far north as Ismailia (30.6^{o}N, 32.3^{o}E) (Dubertret, 1970). The influx of water from the Indian Ocean resulted in an abrupt change in the sedimentation from anhydrites, salts, etc.

to marine oozes and marginal clastics (Coleman, 1974).

In Upper Pliocene to Pleistocene times evaporites were deposited in the Afar depression suggesting the area was intermittently connected with the Red Sea through the Gulf of Zula (Hutchinson and Engels, 1970). The modern Gulf of Aqaba was probably also formed at this time. Thick sections of coral reefs, gravels and continental deposits were formed along the present coastlines during the Pleistocene and Quaternary.

1.5 Aims of the work

Although throughout the past 20 years the Red Sea has received much attention and a great deal learned about it there are still several major problems. These include the extent of oceanic crust, the time or times of emplacement of this crust and the plate movements involved.

The work described in Chapters 2 to 7 is aimed at solving these problems by delineating the ocean/continent boundary, locating possible transform faults and determining the seafloor spreading history. From these it is possible to determine the present plate geometry and reconstruct the configuration of the plates prior to crustal separation.

A study of the magnetic data over the deep holes in the Red Sea is included and several possible mechanisms for their formation proposed. Unfortunately insufficient other information is available to restrict the possible models and those proposed are tentative.

CHAPTER 2

THE RED SEA TOTAL INTENSITY MAGNETIC ANOMALY MAP

2.1 Introductory remarks

The Red Sea magnetic map project forms part of a joint mineral investigations program of the Directorate General of Mineral Resources (DGMR) of Saudi Arabia and the United States Geological Survey (USGS). The objective of the project was to prepare a magnetic anomaly map using all available existing data. It was recognised that such a map would have several deficiencies, e.g. there would be areas where there were little or no data. Nevertheless, it was felt there were sufficient data to prepare a map which would show the more outstanding features. Preparation of the map began in July 1972 and was completed in February 1974.

2.2 Sources of magnetic data

Details of the magnetic data used in the preparation of the map (Plate 1) are given in Table 2.1 and the locations shown in fig. 2.1. Both sea and air data were available.

2.2.1 Sea data

Data collected by research vessels between 1958 and 1972 were used. During this interval eight vessels made a total of ten cruises mainly in the central and southern Red Sea. The data cover predominantly deep water areas (see fig 2.1) as difficult bathymetry restricts access to the shallow shelves in many areas. Proton precession magnetometers were used on all cruises except VEMA 14 which used a fluxgate magnetometer.

TABLE 2.1

Details of data used in the preparation of the total intensity magnetic anomaly map

Date	Code	Approximate survey area	Height (km)	Magnetometer type	Navigation type	Investigator
1958	A5	4350 km of track in main trough, VEMA 14	0.0	fluxgate	radar, celestial fixes	Lamont Doherty Geol Obs.
1959	A3	3000 km of track in main trough, DALRYMPLE	0.0	proton precession	radar, celestial fixes	Cambridge Univ., U.K.
1961	A4	Approx. 25 profiles in main trough, ARAGONESE	0.0	proton precession	radar and Loran	NATO SACLANT
1962	C3	Offshore Arabia at Jizan line spacing = 1.25 Km	0.30	fluxgate	Doppler	D.G.M.R. Saudi Arabia
1963	B3	Offshore Ethiopia at 17°N line spacing approx. 15 Km	0.61	fluxgate	Doppler	Mobil Oil Co.
1964	A7	10 long profiles in main trough, CHAIN 43	0.0	proton precession	radar, celestial fixes	Woods Hole Oceanographic Inst.
1964/66	C4	Arabian Shield, line spacing = 0.8Km	0.30*	fluxgate	Doppler, air photography	D.G.M.R. Saudi Arabia
1965	A6	Several long profiles in main trough, CONRAD 9	0.0	proton precession	radar, celestial fixes	Lamont Doherty Geol. Obs.
1966	A2	Concentrated over 'deeps', CHAIN 61	0.0	proton precession	radar buoys in 'deeps'	Woods Hole Oceanographic Inst.
1966	B2	Offshore Ethiopia at 16°N line spacing = 5 km	0.61	fluxgate	Shoran	Gulf Oil Co.
1966	C5	Offshore Arabia at Duba line spacing = 2Km	2.00	-	-	Ministry of Petroleum, Saudi Arabia
1967	C6	Offshore Arabia at Ranak line spacing = 2 Km	2.00	-	-	Ministry of Petroleum Saudi Arabia
1967	A1	Two long NW-SE profiles, DISCOVERY 16	0.0	proton precession	radar, celestial fixes	I.O.S., U.K.
1968	B1	Ethiopia, Afar and Isaas line spacing = 10 Km	1.83	fluxgate	Doppler, air photography	Newcastle Univ., U.K.
1968	B4/D4	Offshore Sudan at 19°N line spacing = 5 Km	0.30	fluxgate	Doppler	Continental Oil Co.
1968	D2	Coast to coast at 19°N line spacing approx 25 Km	0.30	caesium vapour	Doppler	Project MAGNET
1969	D3	Coast to coast at 21°N line spacing = 7 Km	0.30	caesium vapour	Doppler	D.G.M.R. Saudi Arabia
1970	C7	Offshore Arabia at Al Lisan line spacing = 2 Km	0.46	-	-	Auxerap
1970	C8	Offshore Arabia at Al Wajh line spacing = 1.5 Km	0.46	-	-	Auxerap
1971	A8	Southern Red Sea and 'deeps', CHAIN 100	0.0	proton precession	satellite fixes	Woods Hole Oceanographic Inst.
1971	A10	2 profiles at 14°N across Red Sea, VALDIVIA 1	0.0	-	Decca hi-fix	Bundesanstalt für Bodenforschung
1971	C1/D1	Offshore Arabia at Al Lith	0.61	caesium vapour	Doppler	Sun Oil Co.
1971	C2	Offshore Arabia at Yanbu line spacing = 3 Km	0.61	caesium vapour	Doppler	Sun Oil Co.
1972	A11	Southern andcentral Red Sea, GLOMAR CHALLENGER 23	0.0	proton precession	satellite fixes	D.S.D.P. Leg 23

*above mean terrain

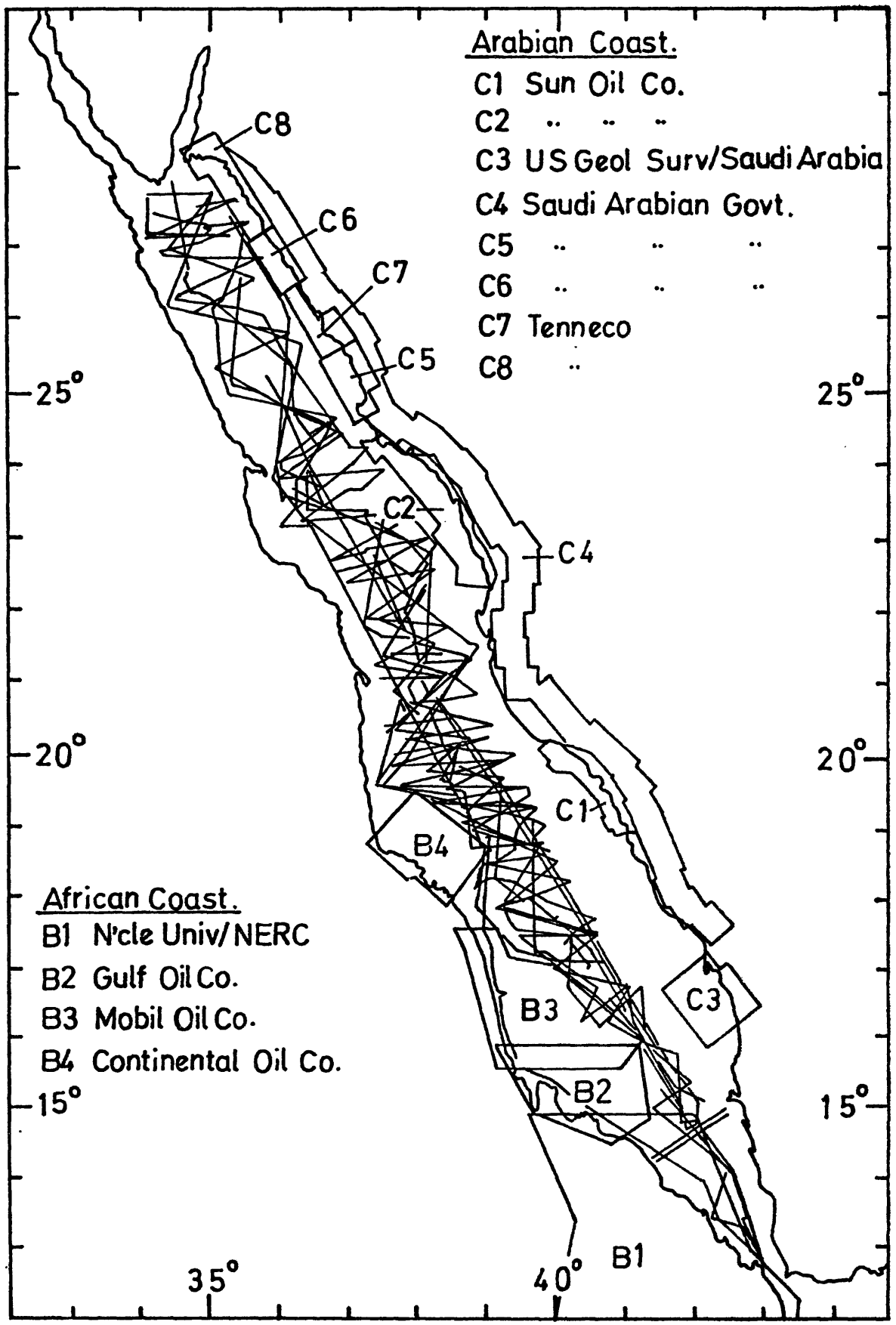

Figure 2.1 Index map showing areas for which magnetic data are available.

Although the methods of navigation varied (Table 2.1) most vessels used a combination of radar and celestial fixes. The more recent cruises, however, used satellite navigators and Decca Hi-fix which gave better positional control.

2.2.2 Air data

Data from several airborne surveys over the Red Sea and neighbouring parts of Arabia and Africa were used. A majority of these were flown for oil companies with concession areas along the coasts (fig 2.1) at elevations of typically 305 m (1000 ft) to 609 m (2000 ft).

The African coast has continuous coverage from 12^{o}N to about 17.5^{o}N with a further survey between approximately 18^{o}N and 19.5^{o}N. The Arabian coast has coverage from 16.3^{o}N to 17.25^{o}N, between 19^{o}N and 20.4^{o}N and from 22.4^{o}N to 28^{o}N. Surveys cover the Arabian Shield but only an approximately 50 km wide strip was used, viz.C4 in fig 2.1. Two coast-to-coast surveys have been made, one between 17^{o}N and 19^{o}N, the other between 21^{o}N and 21.5^{o}N, both of which recorded absolute values of the Earth's field. All other surveys recorded relative values. Doppler navigation was used in all surveys except that for Gulf Oil Co. (B2 in fig 2.1) in which Shoran was used.

2.3 Data reduction

The data were available in either of two forms : profiles or contour maps.

2.3.1 Profile data

Nearly all profiles were received in digital form. The digitising intervals were often irregular especially for the earlier sea data where somewhat

larger intervals (2 to 8 km) were common. Some profiles, however, needed digitising. These included DISCOVERY 16, ARAGONESE and air surveys B3 and D3 (Table 2.1 and fig 2.1). Original magnetometer records were used for DISCOVERY 16 and D3 and previously worked profiles for ARAGONESE and B3. The digitising interval used was either 0.4 km or 1.0 km. Most previously digitised values were supplied with latitudes and longitudes. For those without, the ship's position was calculated from track charts assuming uniform velocity between navigation points.

2.3.2 Contour map data

Magnetic anomaly contour maps at a scale of 1:100,000 were assembled for each survey area. The contour interval varied from 0.5 nT for air surveys C7 and C8 (fig 2.1) to 20 nT for surveys over the Arabian Shield (C4). To digitise the data several rectangular outlines were drawn on the maps. These were covered with a 1-cm square grid and the values of the anomaly field at each intersection recorded. This produced a 1 km digitising interval. Since many survey areas have irregular shapes, overlapping outlines were used (fig 2.2). The size of each data set was limited by the maximum array size handled by the computer in the upward continuation procedure (section 2.5.2). This was initially 64 x 64, i.e. 4096 values, and subsequently 100 x 100, i.e. 10,000 values. In cases where this size was exceeded, the array was subdivided into several overlapping arrays. Some overlap was required because of the edge effects produced by the upward continuation procedure.

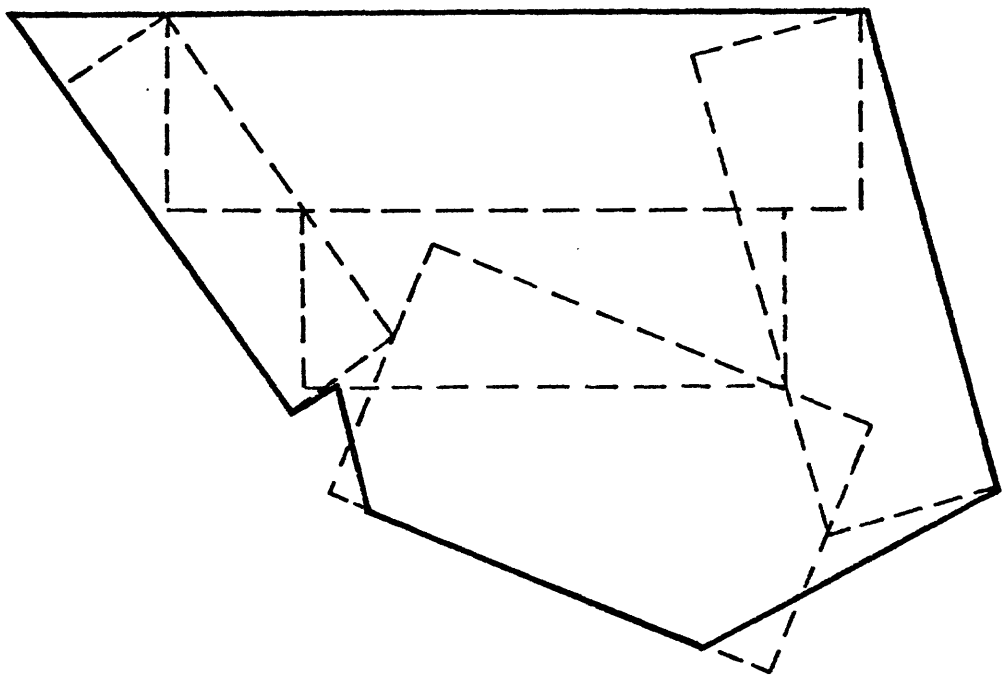

Figure 2.2 The subdivision of an irregularly shaped survey area into a number of rectangular outlines for digitisation of magnetic data.

——— boundary of survey area.

– – – – boundary of rectangular outlines.

2.3.3 Detection of errors

The magnetic map project involved processing an enormous number of values, consequently, the detection and correction of errors were especially important. Each digitised contour map was spot checked to ensure that the contours had been read correctly, the digital values corrected and transferred to punched cards. Line printer plots of the data were obtained using subroutine "PRPL3D" of GEOPAC (Godson, 1974) and compared with the original maps. Obvious errors were eliminated and the procedure repeated with the "corrected" data. Each new plot was compared with the original map until no further errors could be detected.

For profile data, the digitised values were plotted at a suitable scale and compared with the original records. Again, obvious errors were corrected and new plots obtained. The procedure was repeated in a similar manner to that for the contour maps.

The error detection threshold, i.e. the magnitude of the errors below which they are not detected, is directly related to the amplitude and wavelength of the anomalies. For those with long wavelengths and small amplitudes (e.g. in C5 and C6) which are contoured at 1 nT intervals, the detection threshold is approximately 5 nT. For those with large fluctuations (e.g. in C4), the threshold is much greater and errors as large as $\pm$ 50 nT possibly exist. Errors in excess of $\pm$ 100 nT were almost certainly detected and eliminated.

Finally, tracks of the sea data were plotted on a Mercator projection and checked for errors in their location.

2.4 Corrections to data

The following corrections were applied to the total intensity magnetic data : removal of a regional field, corrections for diurnal and secular variations.

2.4.1 Regional field

The contour maps and some profiles were supplied with a regional field already removed. These were restored where known. In some cases, the regional field removed was not known and consequently original records, where available, were used to estimate the field. With all data restored to their original form, it was possible to remove the International Geomagnetic Reference Field (IGRF 1965.0) and so make all the surveys compatible. Values for 1958.0 were used as the first survey was made in that year and a correction for secular variation was to be made. For surveys which did not record absolute values, only the gradient of the IGRF was removed.

2.4.2 Diurnal variation

The sea data were recorded over periods of several days and consequently corrections for diurnal variations of the geomagnetic field were made. The variations are large ($\sim$ 100 nT) in the southern Red Sea due to the proximity of the equatorial electrojet but decrease rapidly further north to between 20 nT and 40 nT.

Daily variations for various ranges of latitude were obtained from the records of magnetometers located at Al Wajh, Yanbu', Taif, Medinah, Jeddah and Asmara during aeromagnetic surveys. Mean hourly values calculated

from these are given in Table 2.2. Also given in Table 2.2 are the mean hourly values from the geomagnetic observatories at Helwan, Egypt and Addis Ababa, Ethiopia. Sea data were corrected using the mean hourly values for the appropriate latitude range in Table 2.2.

2.4.3 Secular variation

Since the magnetic surveys were made over a period of fifteen years from 1958 to 1972 it is necessary to correct the data for secular changes of the Earth's field. Only the sea data need correcting as secular changes are re moved from the air data by matching the overlapping values of adjacent surveys.

The IGRF includes a term for secular variation and corrections can be made using this value. However, an independent estimate was made from the absolute magnetic data using the various cross-overs of the ships' tracks. Care was taken to select only those cross-overs which satisfy the following criteria:

(1) The smaller cross-over angle between the ships' tracks is greater than 20^{o}.

(2) The closest values along the two ships' tracks are less than 1 km apart.

(3) The anomaly at the cross-over has a gradient of less than 100 nT per kilometre along each track.

Ninety-five of the 413 cross-overs available were found to satisfy these conditions, i.e. less than 25%. The remaining were rejected mainly on the

TABLE 2.2

Mean hourly values obtained from diurnal variation records

Latitude range (°N)	Stations used	Mean hourly values of variation in geomagnetic field																							No. of records used[1]
		0	1	2	3	4	5	6	7	8	9	10	11	12	13	14	15	16	17	18	19	20	21	22	23	
28-30	Helwan	9	10	9	10	14	21	23	33	31	24	14	3	-3	-4	-3	-3	-2	-1	1	2	3	4	4	6	*
26-28	Al Wajh	8	12	16	17	20	22	23	27	27	23	23	25	20	13	5	2	3	4	0	0	0	2	3	5	37
23-26	Yanbu /Medinah	7	7	8	13	17	23	29	32	33	30	27	24	19	16	14	11	7	4	4	0	2	1	2	5	81
19-23	Jeddah/Taif	8	11	10	11	12	14	17	22	26	30	32	31	27	21	14	10	6	4	3	2	1	2	4	4	87
14-19	Asmara	7	10	8	5	12	20	26	33	43	35	29	25	11	0	0	7	5	3	1	-3	-2	-1	3	-4	3
12-14	Addis Ababa	4	3	2	2	9	31	65	87	96	88	70	50	31	18	10	3	-1	-2	-3	-2	-1	1	2	4	*

*Several years of records available

[1]includes part records

basis of (1) and (3). Criterion (3) affects a majority of cross-overs as many of the ships' tracks are over deep water where there are large anomalies with steep gradients. Criterion (1) is more important in the southern Red Sea where many of the ships' tracks are close to one another and trend parallel along the narrow, navigable channels.

The ninety-five, selected cross-overs were used to obtain estimates of the secular variation and these combined to produce a mean value for the Red Sea over the period 1959 to 1972. Two estimates were obtained from each cross-over: one using the magnetic data before the diurnal variation had been subtracted, the other after. In each case, the estimates were assumed to follow a normal distribution and the standard deviation of the mean calculated. Estimates which lay more than three standard deviations from the mean were rejected and a new mean and standard deviation obtained from the remaining estimates. The procedure was repeated until all estimates lay within three standard deviations of the mean. Ten estimates were rejected from those obtained before diurnal correction and nine from those obtained after. Thus in Table 2.3 eighty-five of the ninety-five cross-overs were used to obtain the final mean before diurnal correction and eighty-six for the mean after correction.

A weighted mean calculation was also made in order to bias the result towards the few estimates obtained from areas of very small magnetic gradient, i.e. about 5 to 10 nT per kilometre. The weighting factor chosen was the inverse square of the standard error of the estimates (Topping, 1955).

TABLE 2.3

Values of secular variation obtained from cross-overs of ships' tracks

Stage of computation	No. of cross-overs used	Simple mean secular variation ($nT\ y^{-1}$)	Standard deviation of simple mean ($nT\ y^{-1}$)	Weighted mean secular variation ($nT\ y^{-1}$)	Standard deviation of weighted mean ($nT\ y^{-1}$)
before diurnal correction	95	21	$\pm$60	15	$\pm$60
before diurnal correction	85*	16	$\pm$27	15	$\pm$27
after diurnal correction	95	22	$\pm$60	18	$\pm$61
after diurnal correction	86*	18	$\pm$27	18	$\pm$27

Secular variation after diurnal correction = $+18nT\ y^{-1}$

Standard error of secular variation = $\pm 3nT\ y^{-1}$

*Spurious values removed

The standard error was obtained by dividing the standard deviation of the magnetic values one kilometre along each track in either direction by the time difference between the observations.

The values obtained for the simple and weighted mean (Table 2.3) differ noticeably when all 95 estimates are used but become almost identical when the spurious estimates are removed. The weighted mean remains constant indicating it is not seriously affected by the inclusion of some spurious values. Correcting the data for diurnal variation increases both means slightly by about +2 to +3 nT y^{-1} but does not reduce the rather large standard deviation, viz. $\pm$ 27 nT y^{-1}.

Using eighty-six estimates, corrected for diurnal variation, the mean secular variation obtained for the period 1959 to 1972 was + 18 nT y^{-1} with a standard error of $\pm$ 3 nT y^{-1}. The value given by the IGRF for the same period varies from + 22 nT y^{-1} at 15^{o}N to + 33 nT y^{-1} at 26^{o}N. The variation with latitude of the estimates obtained from the cross-overs was not studied.

The sea data were corrected using + 18 nT y^{-1}.

2.5 Preparation of the magnetic anomaly map

After the corrections had been made, two processes remained before constructing the magnetic map; viz. gridding the sea data and upward continuation of all data to a common height of 1.83 km (6000 ft).

2.5.1 Gridding of sea data

The sea values were recorded along various tracks (fig 2.1), consequently it was not possible to upward continue these unless the anomalies were assumed to be two dimensional, i.e. extending indefinitely in one direction. Such an assumption is, in general, unfounded although linear anomalies are known to be present over the axial trough (Drake and Girdler, 1964; Allan, 1970). It was necessary therefore to grid these data before upward continuation. This was done using the "GRID3D" subroutine from GEOPAC (Godson, 1974). Because of the size limitations set by the computer several arrays were necessary. The boundaries of these were obtained by studying the distribution of values in each one degree square. Where a large number of evenly distributed values were present the entire one degree square was used to form a grid. In such cases, a 2 km grid provided a suitable array size. Where there were either few values or the values were poorly distributed a smaller grid encompassing the area of denser coverage was used. Several one degree squares had too few values (< 100) to justify gridding and these data were not used in the magnetic map.

2.5.2 Upward continuation

The data were upward continued using the method described by Bhattacharyya (1965). The array data were first transformed into the frequency domain by a two dimensional Fourier analysis. The Fourier coefficients were then multiplied by a factor which was a function of frequency and the amount of upward continued required, and finally converted back to anomalies by an inverse Fourier transform.

The method has several advantages : first, it enabled the values to be upward continued by continuous rather than discrete amounts. This was important as the various data were upward continued by different amounts. If a discrete procedure had been used the digitising interval would have differed from survey to survey depending on the amount of upward continuation required. Secondly, a Fast Fourier Transform (Cooley and Tukey, 1965) could be used reducing the computation time dramatically.

The data were upward continued to 1.83 km (6000 ft) and the resulting values plotted as contour maps. This height was chosen to conform to the to the maximum topography within the map area. One survey (B1 in fig 2.1) was flown at this height and, therefore, required no processing. Only two surveys were flown higher, viz. C5 and C6 (fig 2.1) at 2.0 km. The land in these areas is low, typically 0 to 600 metres, and consequently, these data were downward continued by 170 metres. The difference in computation effort between upward continuing B1 to 2.0 km and downward continuing C5 and C6 to 1.83 km seems to justify this. An additional advantage is that more detail is retained in the other data by using the 1.83 km datum level.

All airborne surveys were flown at a constant height except those over the Arabian Shield (C4 in fig 2.1) which were contour flown at a constant terrain clearance. Before upward continuing these, a height correction was applied. Insufficient detailed topographic information was available to correct the data using sophisticated techniques such as that of Ducruix et al (1974). Consequently, an approximate method was used to obtain the 'constant' height of each C4 data set. The rectangular outlines, used in digitising the data,

were located on a 1:4,000,000 topographic map of the Arabian peninsula (U.S. Geological Survey, 1972). The topographic contours crossing these outlines separate the areas into small segments. The elevation of each segment was assumed to be the mean of the adjacent contours. The area of each segment was multiplied by its elevation and these products summed for each outline. A mean elevation was obtained by dividing this sum by the area of the outline. The mean aircraft elevation was obtained by simply adding the ground clearance to this value.

2.5.3 Construction of the map

To construct the magnetic anomaly map the individual upward continued contour maps were pieced together. In most cases, there were several kilometres of overlap and it was possible to follow corresponding contour lines from one to another. On some, edge effects, produced by the upward continuation, caused discrepancies between adjacent surveys. In such cases, the contours were adjusted manually and are, therefore, subjective.

Absolute values from the upward continued sea data were used to determine the zero datum of the overlapping air surveys. Since the locations of the sea and air data rarely coincide, it was necessary to interpolate between the appropriate sea values. A mean value for the difference in the magnetic values for the air and sea data was determined for each airborne survey and the air values adjusted by this amount.

The final map (Plate 1) was drawn with a contour interval of 100 nT and coloured using two shades of red and of blue. Anomalies between zero and + 100 nT were left white, those between + 100 nT and + 200 nT coloured light

red and those above + 200 nT dark red. Anomalies between zero to - 100 nT were coloured light blue and those below - 100 nT dark blue. The zero level was chosen to coincide with the boundary between the light blue and the white in order to make the map compatible with that of the Afar triangle (Hall, 1970). Since the IGRF produces a zero level approximately 200 nT above the zero level estimated from Red Sea magnetic data (Searle and Ross, 1975), the map is biased towards the blue.

Where the overlap of the air and sea data was small, the zero datum for the air data was poorly determined. As a result, several false level changes were generated on the anomaly map (Plate 1), e.g. in offshore areas of Africa near 18^{o}N the zero is apparently too 'high' producing a predominance of blue.

2.6 Main features of the magnetic map

Although the magnetic data are treated in some detail in Chapters 4, 5 and 6 it is convenient to mention briefly the dominant features of the magnetic map (Plate 1). The map reveals three distinct zones, each having anomalies of a different character, i.e. amplitude and wavelength. The zones are:

(1) The axial trough and adjacent parts of the main trough over which there are large amplitude (approximately 800 nT), short wavelength (15 km peak to trough) anomalies. These form a linear pattern approximately parallel to the coasts. The anomalies terminate in the north near 23^{o}N and in the south at about 15^{o}N.

(2) The main trough, shelves and parts of the coastal plain over which there are smaller amplitude (100 to 300 nT), longer wavelength (30 km) anomalies which are also approximately parallel to the coasts. These

are observed along the African coast between about 14°N and 19°N and along the Arabian coast at 17°N, 19°N and 23°N. The anomalies are present throughout the Red Sea but because of the 100 nT contour interval are not clearly displayed on the magnetic map.

(3) The Pre-Cambrian shield areas and parts of the coastal plain over which there are very variable amplitude (100 to 400 nT), short wavelength (typically 5 to 15 km) anomalies. These are remarkably different in character from those of (1) and (2) and do not form lineations but vary considerably in shape and size from place to place. The anomalies are observed throughout the area and may be traced from 12°N to near 19°N along the African side and from 17.5°N to about 27.5°N along the Arabian side.

Several NE trending features cross the map producing breaks in the linear patterns over the axial trough. For example, between 20°N and 21.5°N, southwest of Jeddah and at approximately 25.5°N, southwest of Al Wajh. These transverse features are confined to zones (1) and (2) and are, therefore, probably related to transform faults between Nubia and Arabia.

For convenience, discussion of the data is split into three parts : north of 24°N (Chapter 4), 18°N to 24°N (Chapter 5) and south of 18°N (Chapter 6). As much of the interpretation involves seafloor spreading a brief discussion of some theoretical aspects of seafloor spreading magnetic anomalies is given first.

CHAPTER THREE

SOME THEORETICAL CONSIDERATIONS OF SEAFLOOR SPREADING IN THE RED SEA

3.1 Introductory remarks

In the interpretation of the magnetic data presented in Chapters 4, 5 and 6, seafloor spreading models are used extensively to simulate the observed anomalies. The amplitude and wavelength of the synthetic anomalies depend not only on the depth, width and thickness of the magnetised layer but also the amplitudes and directions of the induced and remanent magnetisation vectors. Some appreciation of how these parameters control the character of the anomalies is, therefore, important. In this chapter, variations of these parameters and their affect upon the seafloor anomalies in the Red Sea are studied.

3.2 Total intensity magnetic anomaly due to a two dimensional body

In seafloor spreading, the magnetised bodies extend parallel to the spreading axis over large distances. Consequently each body may be considered to be two dimensional. In fig. 3.1, the block has a finite width (x - axis) and thickness (z - axis) but an infinite length (y - axis).

The magnetic potential, U, at the point O, due to a two dimensional body is:

$$U = \int_{x_1}^{x_2} \int_{z_1}^{z_2} \frac{2(M_x x + M_z z)\, dx\, dz}{(x^2 + z^2)} \qquad 3.1$$

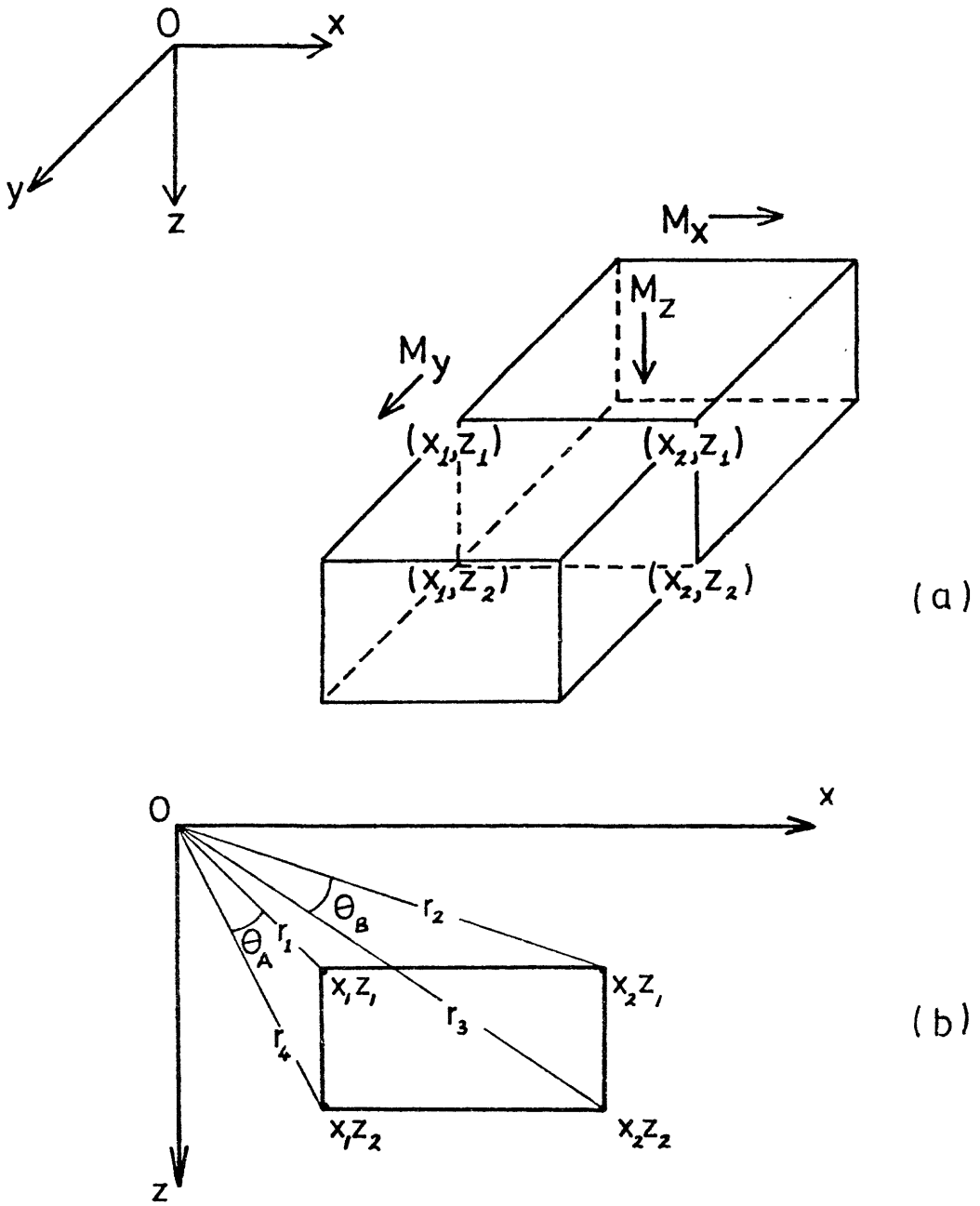

Figure 3.1 Geometry used for the calculation of the magnetic intensity due to a 2-dimensional body, infinite in the y direction.

where M_x and M_z are the x and z components of magnetisation (fig. 3.1) and x and z are the distances along the appropriate axes from O to the element dx dz of the body. The horizontal (H_x) and vertical (H_z) components of the magnetic field due to the body are:

$$H_x = \frac{dU}{dx} = [\,[\,2 M_x \tan^{-1}(\frac{x}{z}) + M_z \log(x^2 + z^2)\,]_{z_1}^{z_2}\,]_{x_1}^{x_2} \qquad 3.2$$

$$H_z = \frac{dU}{dz} = [\,[\,2M_z \tan^{-1}(\frac{x}{z}) + M_x \log(x^2 + z^2)\,]_{x_1}^{x_2}\,]_{z_1}^{z_2} \qquad 3.3$$

where the limits of integration specify the corners of the rectangle in fig. 3.1. Equations 3.2 and 3.3, when expanded, simplify to:

$$H_x = 2M_x(\theta_A - \theta_B) + 2M_z \log(\frac{r_1 r_3}{r_2 r_4}) \qquad 3.4$$

$$H_z = 2M_z(\theta_A - \theta_B) + 2M_x \log(\frac{r_1 r_3}{r_2 r_4}) \qquad 3.5$$

where θ_A, θ_B, r_1, r_2, r_3 and r_4 are shown in fig. 3.1(b).

The total intensity anomaly, ΔT, due to the body is assumed to be small compared with the Earth's field and consequently may be calculated by resolving H_x and H_z along the present total field vector, F :

$$\Delta T = H_z \sin I + H_x \cos I \cos(C - D) \qquad 3.6$$

where D and I are the declination and inclination of F and C is the angle between the positive x axis and geographic north, i.e. C defines the direction normal to the strike of the body.

The components of magnetisation may be written:

$$M_x = R_x + XF_x \qquad 3.7$$

$$M_z = R_z + XF_z \qquad 3.8$$

where R_x and R_z are the x and z components of the remanent magnetisation, X is the magnetic susceptibility (assuming no magnetic anistropy) and F_x and F_z are the x and z components of the present Earth's field. In the case of seafloor spreading the magnetised bodies consist of oceanic basalt whose remanent magnetisation is much greater than the induced magnetisation. The ratio of remanent to induced usually exceeds 10 but is often much larger (Pitman et al, 1968; Fox and Opdyke, 1973). Thus we can approximate equations 3.7 and 3.8 such that if $R \gg XF$ then:

$$M_x \simeq R_x = R \cos I_r \cos (C - D_r) \qquad 3.9$$

$$M_z \simeq R_z = R \sin I_r \qquad 3.10$$

where D_r and I_r are the declination and inclination of the remanent magnetisation vector, R. In the case of oceanic basalts their magnetisation is often specified in the form of an apparent or effective susceptibility, X_{eff}. This is defined by the equation:

$$X_{eff} = \frac{|R + XF|}{|F|} \qquad 3.11$$

i.e. the total magnetisation (remanent + induced) divided by the magnitude of the present Earth's field. If $R \gg XF$ then equation 3.11 can be approximated to:

$$X_{eff} = \frac{|R|}{|F|} \qquad 3.12$$

The magnitude of the remanent vector can be substituted for in equations 3.9 and 3.10 and the resulting magnetisations, M_x and M_z, inserted in equations 3.4 and 3.5 giving:

$$H_x = 2X_{eff}|F|[\cos i_r \cos(C-D_r)(\theta_A - \theta_B) + \sin I_r \log(\frac{r_1 r_3}{r_2 r_4})] \qquad 3.13$$

$$H_z = 2X_{eff}|F|[\sin I_r (\theta_A - \theta_B) + \cos I_r \cos(C-D_r) \log(\frac{r_1 r_3}{r_2 r_4})] \qquad 3.14$$

Substituting for H_x and H_z in equation 3.6 gives:

$$\Delta T = 2X_{eff}|F|[(\sin I_r(\theta_A - \theta_B) + \cos I_r \cos(C-D_r)\log(\frac{r_1 r_3}{r_2 r_4}))\sin I$$

$$+ (\cos I_r \cos(C-D_r)(\theta_A - \theta_B) + \sin I_r \log(\frac{r_1 r_3}{r_2 r_4}))\cos I \cos(C-D)] \qquad 3.15$$

Thus $\Delta T = f(X_{eff}, F, I, D, I_r, D_r, \theta_A, \theta_B, r_1, r_2, r_3, r_4)$ 3.16

In the case of seafloor the direction of the remanent magnetisation vector is obtained using the geocentric axial dipole approximation of the Earth's field. For normally magnetised seafloor $D_r = 0^o$ and for reversely magnetised seafloor $D_r = 180^o$. The value of I_r is obtained from the equation

$$\tan I_r = \pm 2 \tan \phi \qquad 3.17$$

where ϕ is the latitude (positive in the northern hemisphere); the plus sign is used for normally magnetised seafloor and the minus sign for reversely magnetised seafloor.

Calculation of I_r by equation 3.16 assumes that the latitude, ϕ, at which the remanence was acquired is known. Movement of the seafloor as the plates migrate means that in many cases this location is not known. In the Red Sea the seafloor is assumed to have been formed at the present latitudes. There is some evidence to suggest Africa has moved northwards since 70 My BP (Girdler, 1969) although the time of such movement is not known precisely. It is possible, therefore, that some seafloor may have been formed at lower latitudes. This would tend to reduce the amplitude of the anomalies but, unless the seafloor was formed south of the equator, their shapes would remain approximately the same.

Equation 3.16 shows that the parameters affecting the amplitude and wavelength of the anomaly are:

(1) the effective susceptibility, X_{eff}.

(2) the strength, inclination and declination of the Earth's field, F, I and D respectively.

(3) the inclination and declination of the remanent magnetisation vector, I_r and D_r respectively.

(4) the distance from O to the upper surface of the body specified by r_1 and r_2.

(5) the strike of the body, $(C + 90^o)$.

(6) the width and thickness of the body specified by θ_A, θ_B, r_1, r_2, r_3 and r_4.

In the case of seafloor spreading there are several two dimensional bodies, each of which contributes to the total intensity anomaly. If the area over which the anomalies are computed is small enough that I and D can be assumed to be

constant, the contributions from each body can be simply summed. Thus the total intensity magnetic anomaly T due to n two dimensional bodies is:

$$T = \sum_{i=1}^{n} \Delta T_i \qquad 3.18$$

where ΔT_i is calculated from equation 3.15.

3.3 Seafloor model

The model used is that presented by Vine and Matthews (1963) and modified by Vine and Wilson (1965) such that the magnetised layer is considered to be the upper 2 km of oceanic layer 2. There is still no general agreement on the thickness of the layer responsible for the anomalies although recent measurements of the magnetisation of pillow lavas from the ocean floor (Watkins et al, 1970; Marshall and Cox, 1971) indicate a few hundred metres of this material is sufficient to produce the observed anomalies.

The effective susceptibility, X_{eff}, of the seafloor is assumed to be constant at 0.01 emu cm^{-3} (0.02 emu cm^{-3} for the central body) unless otherwise stated. This value is typical of that found for oceanic basalts (Lowrie at al, 1973(b); Fox and Opdyke, 1973).

The reversal time scale used is that of Heirtzler et al (1968).

The synthetic magnetic anomalies are computed using a modified form of a computer program by Talwani and Heirtzler (1964) which calculates the anomaly due to a two dimensional body. The anomalies produced by each seafloor body are resolved along the direction of the Earth's field and summed.

This introduces a small error as the total field measured by the magnetometers used in the surveys is the vector sum of the main field, i.e. that specified by the IGRF, and the anomaly. However as even the largest anomalies observed in the Red Sea (1500 to 2000 nT) are small compared with the main field such errors are very small.

Equation 3.15 shows that X_{eff} and F act simply as scaling factors controlling the amplitudes of the anomalies; consequently the effect of variations of these parameters were not studied. Variations of the remaining parameters were studied under four headings: latitude, depth, strike and spreading rate. Variations of I, D, I_r and D_r in the Red Sea are predominantly due to latitude although, as noted above, some northward movement of the seafloor may have taken place. Consequently the effects of variations in parameters (2) and (3) (see section 3.2) can be considered together. Variations in parameter (4), i.e. r_1 and r_2 (fig. 3.1), are considered under depth of the seafloor and variations of parameter 5, C, under strike. Finally the widths of the seafloor bodies are controlled by the spreading rate; consequently the effects produced by varying parameter (6), i.e. r_1, r_2, r_3 and r_4, are considered under spreading rate.

3.4 Variation in character of anomalies with latitude

The Red Sea is located at low latitudes with a strike of about N145^{o}. The present declination and inclination of the Earth's field vary from about 0.6^{o} and 16^{o} at 16 ^{o}N to 1.5^{o} and 40^{o} at 28 ^{o}N. The dip of the remanent magnetisation vector varies from about 30^{o} (16^{o}N) to 47^{o} (28^{o}N). Synthetic magnetic profiles

over seafloor at various latitudes are shown in fig. 3.2. In each profile, the anomalies are those produced by 1 cm y^{-1} spreading over the past 5 My with seafloor striking N 145°. The shape of the anomalies varies little with latitude but their amplitude increases northwards reflecting the increasing influence of the vertical component of magnetisation, M_z. The amplitude of the central anomaly is plotted as a function of latitude in fig. 3.3. An increase of approximately 50% is observed between 15°N (1200 nT) and 28°N (1800 nT).

3.5 Variation in character of anomalies with different depths to seafloor

The amplitude of the anomaly due to each seafloor body decreases with increasing depth (d) by a factor mainly dependant on $1/d^2$. Synthetic magnetic profiles over seafloor at various depths are shown in fig. 3.4. The shapes of the profiles change such that for larger values of d the short wavelength anomalies due to the narrower bodies gradually disappear and the more prominent anomalies broaden. For large depths, d = 9 km, nearly all the anomalies are smoothed out and only the central anomaly can be seen clearly.

The amplitude of the central anomaly is plotted as a function of depth, d, of the seafloor in fig. 3.5. The amplitude decreases rapidly at first, falling from about 1450 nT at d = 2 km to approximately 750 nT at d = 4 km but slows down at greater depths to 500 nT at d = 6 km and 300 nT at d = 9 km. Also shown in fig. 3.5. is the curve of $1/d^2$ (dashed line) which has been set equal to the central anomaly amplitude for d = 2 km. It can be seen that this curve falls off more rapidly than the central anomaly amplitude.

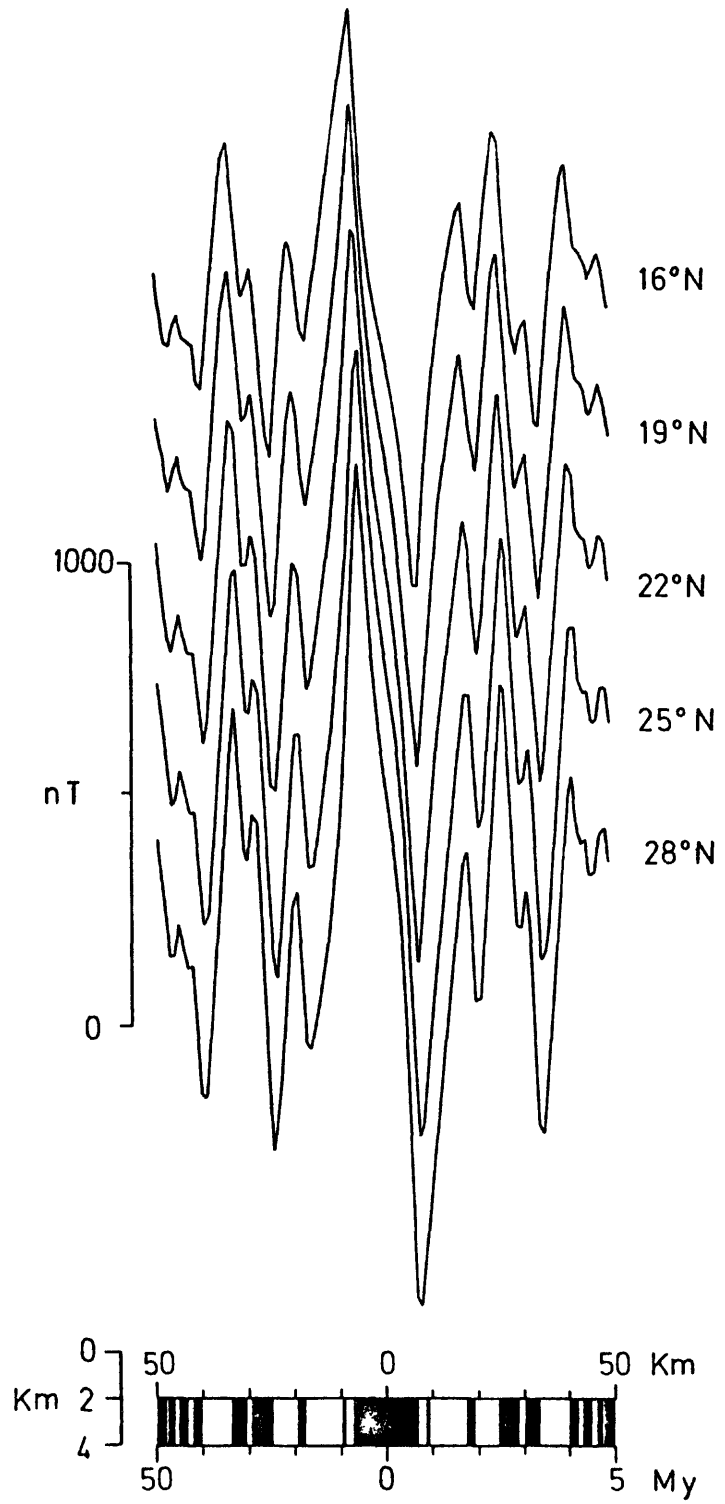

Figure 3.2 Synthetic magnetic profiles over seafloor spreading at 1 cm y^{-1} over the past 5My for various latitudes. Profiles are normal to the Red Sea axis.

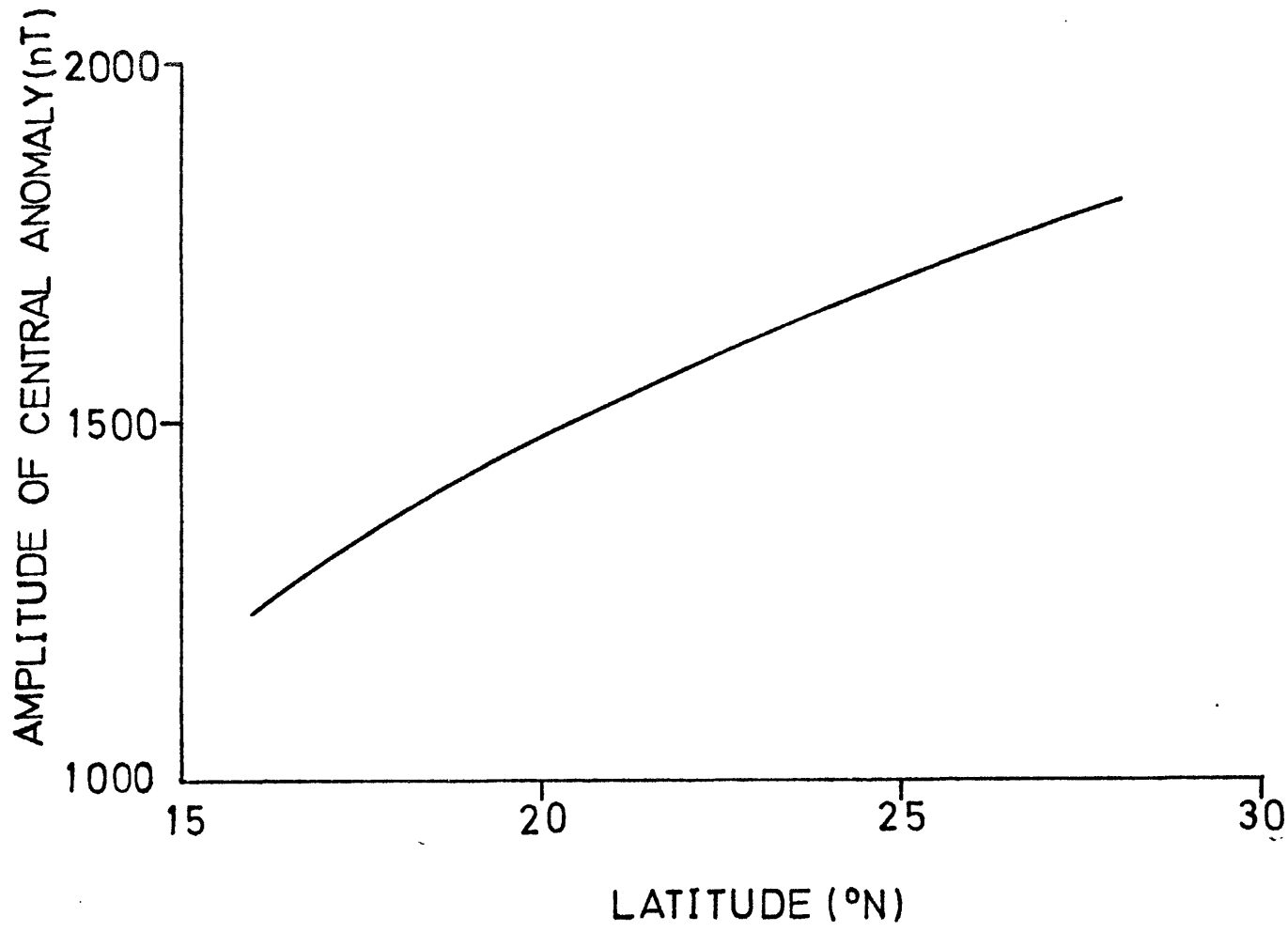

Figure 3.3 Amplitude of central anomaly versus latitude for the synthetic magnetic profiles shown in fig. 3.2.

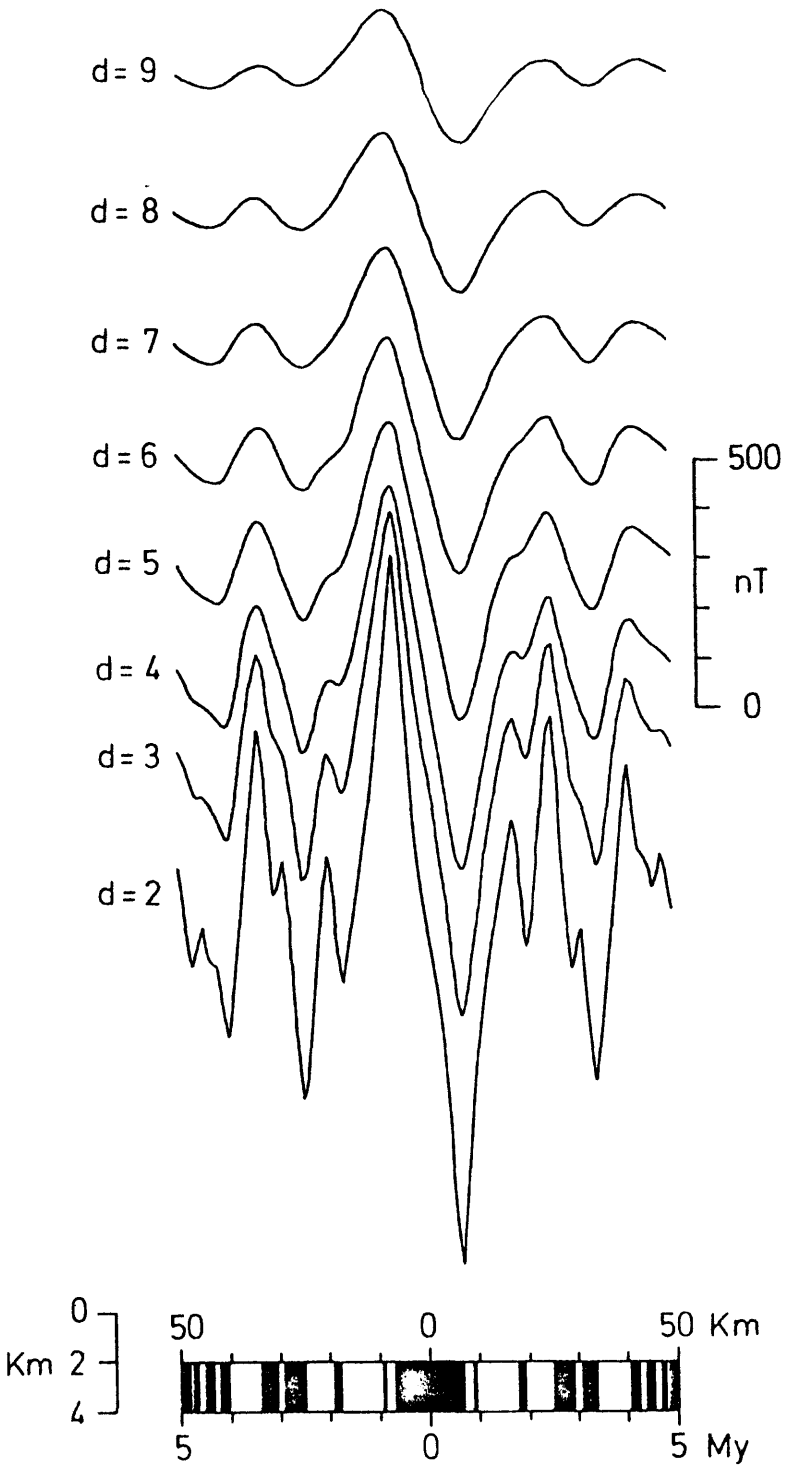

Figure 3.4 Synthetic magnetic profiles over seafloor at various depths (d). Profiles are computed for 1 cm y^{-1} spreading over the past 5 My and are normal to the Red Sea axis at 19°N.

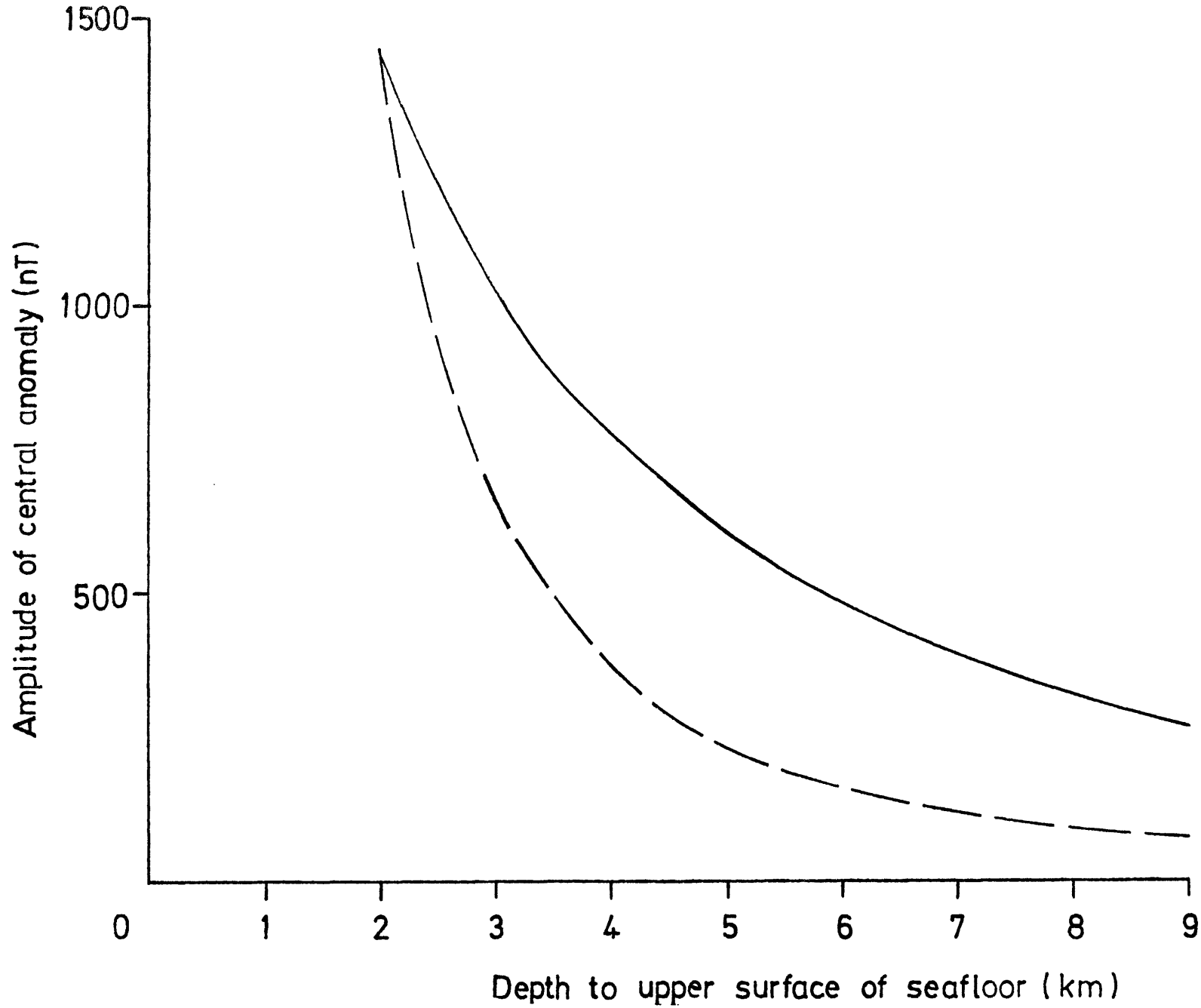

Figure 3.5 Amplitude of central anomaly versus depth of seafloor for the synthetic magnetic profiles shown in fig.3.4 .

3.6 Variation in character of anomalies with strike

The shape and size of the anomalies also depend on the strike of the seafloor ($C + 90^{o}$). The horizontal component of the anomaly field, H_x, combines with the horizontal component of the main field, F_H, enhancing or reducing it depending on the strike. The maximum effect occurs when the strike of the seafloor is normal to F_H, i.e. when H_x and F_H are either parallel or antiparallel depending on the polarity of the body.

For the Red Sea; the declination of the Earth's field is between 0^{o} and 1.5^{o}E and therefore approximately E-W striking seafloor produces the largest anomalies. Synthetic magnetic profiles over seafloor with various strikes are shown in fig. 3.6. The shapes of the anomalies vary considerably. For N-S striking seafloor ($\theta = 180^{o}$, fig. 3.6) H_x is normal to the F_H such that in equation 3.6 (C-D) is 90^{o}; consequently H_x does not effect the shape of the anomalies and the profile is symmetric about the central anomaly. The anomaly shapes reverse for strikes east of north (fig. 3.6), i.e. there is a peak to the east of the central body and a trough to the west. This effect has been used by Allan (1970) to infer the presence of seafloor striking east of north in the central Red Sea.

The amplitude of the central anomaly is plotted as a function of the strike of the seafloor in fig. 3.7. E-W striking ($\theta = 090^{o}$) seafloor produces the maximum amplitude, viz. 2660 nT and a N-S strike ($\theta = 180^{o}$) the minimum, viz. 370 nT. In the Red Sea, the seafloor strikes approximately 145^{o} and amplitudes of about 1400 nT are expected near 19^{o}N. Variations of about 10^{o} in this strike increase or decrease the amplitude by about 300 nT.

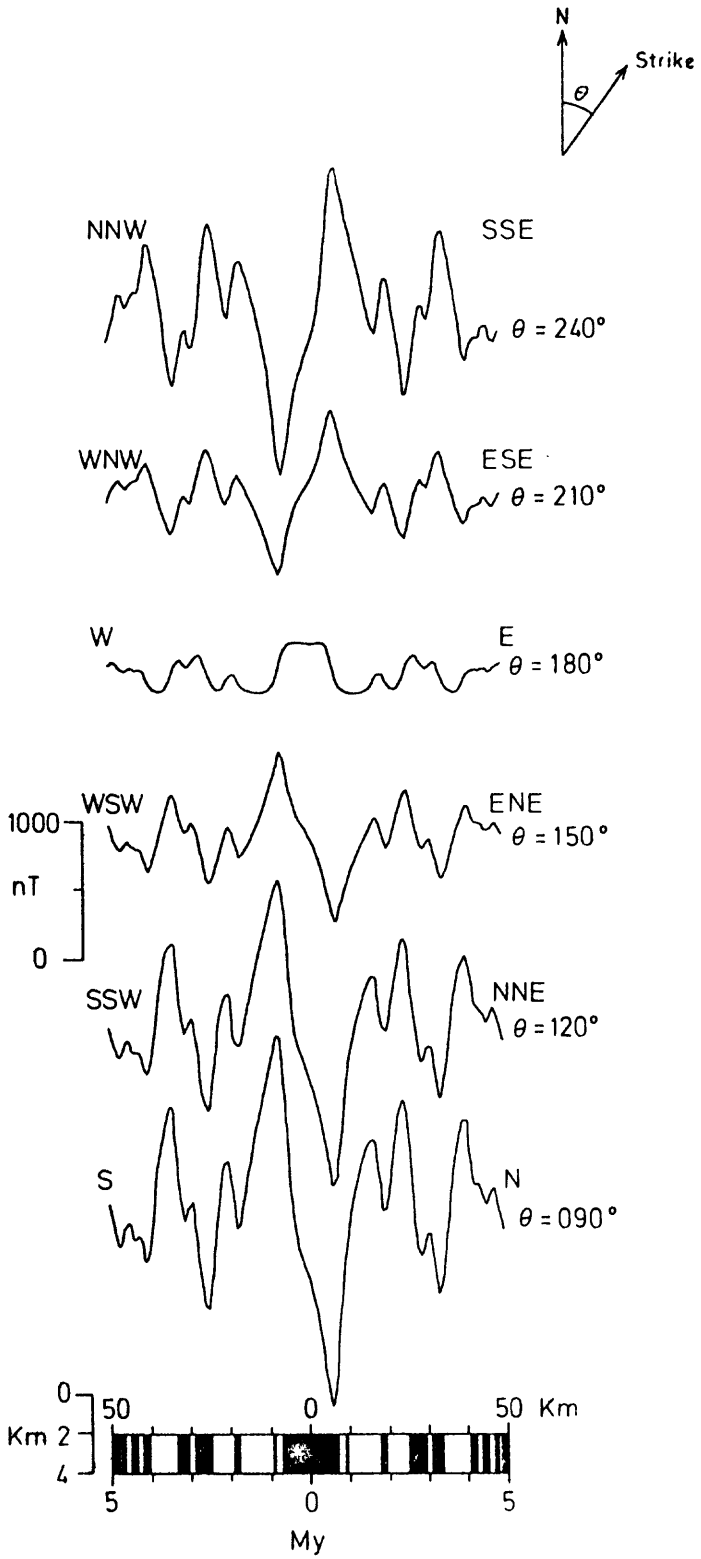

Figure 3.6 Synthetic magnetic profiles over seafloor with various strikes (θ). Profiles are computed for 1 cm y^{-1} spreading over the past 5 My at 19°N.

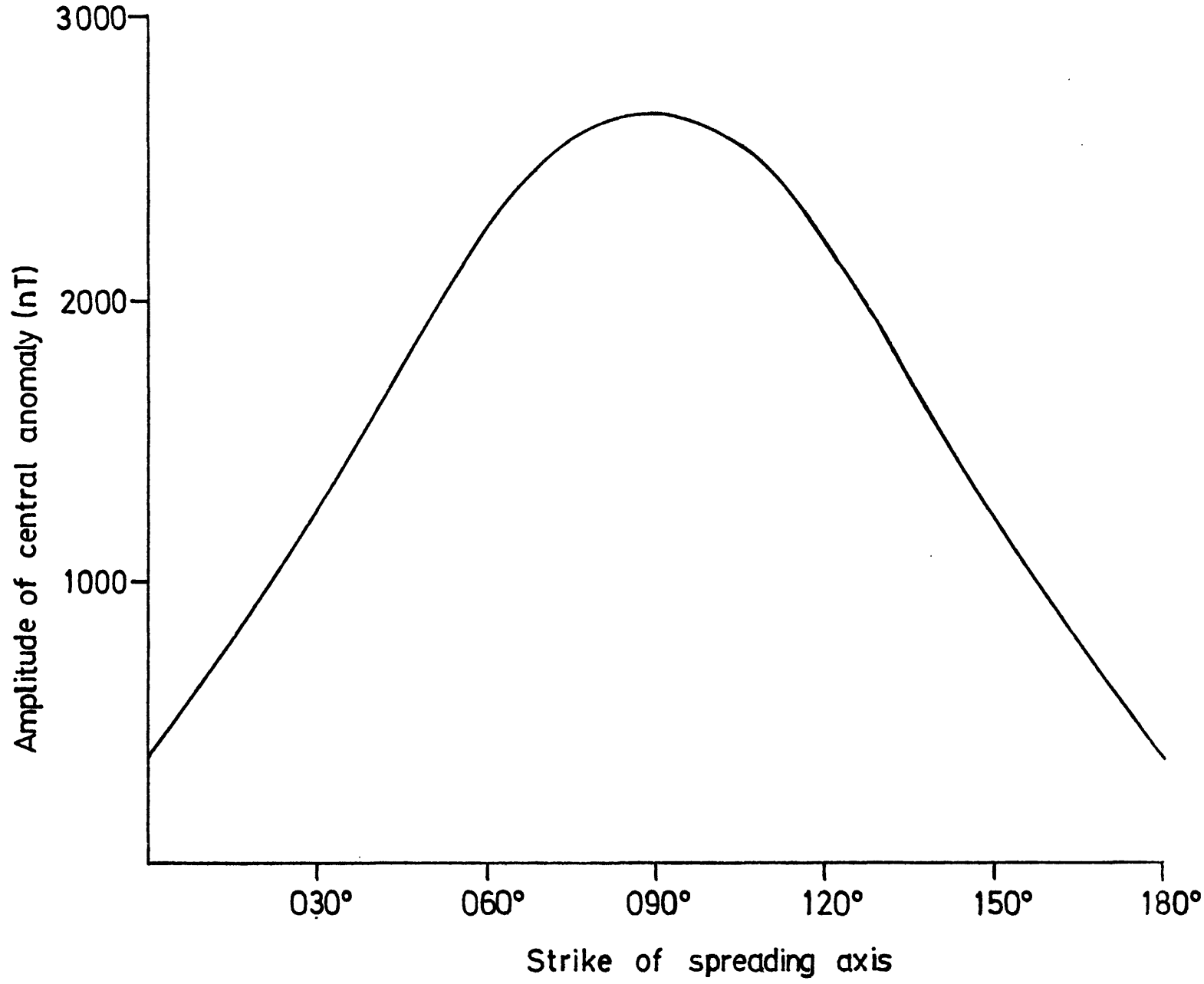

Figure 3.7 Amplitude of central anomaly versus strike of seafloor for the synthetic magnetic profiles shown in fig. 3.6.

3.7 Variation in character of anomalies with spreading rate

The spreading rate controls the width of the two-dimensional bodies. Synthetic magnetic profiles over seafloor formed at various spreading rates are shown in fig. 3.8. At 2.0 cm y^{-1} the anomalies are well defined and can be related to individual bodies. At smaller spreading rates, many of the anomalies combine to produce broad features similar to those produced by seafloor at greater depths (e.g. d = 7 in fig. 3.4). For spreading rates less than 0.6 cm y^{-1} the short wavelength anomalies are filtered out entirely leaving only the major features. For example, at 0.2 cm y^{-1} only the central anomaly can be seen clearly.

The amplitude of the central anomaly is plotted as a function of spreading rate in fig. 3.9. Between 2.0 cm y^{-1} and approximately 0.8 cm y^{-1} the amplitude does not change significantly : there is a decrease of approximately 100 nT which is about 6 to 7% of the amplitude at 2.0 cm y^{-1}. For spreading rates less than 0.8 cm y^{-1} the amplitude decreases more rapidly from about 1400 nT at 0.8 cm y^{-1} to near 600 nT at 0.2 cm y^{-1}.

3.8 Predicted character of anomalies over the northern, central and southern Red Sea

Estimates of the depth, strike and spreading rate of the seafloor beneath the deep water areas of the Red Sea may be obtained from geological and geophysical data. The depth of the magnetised layer, i.e. oceanic layer 2, may be found from seismic refraction data (Drake and Girdler, 1964; Tramontini and Davies, 1969). The strike can be determined from the linear anomalies in

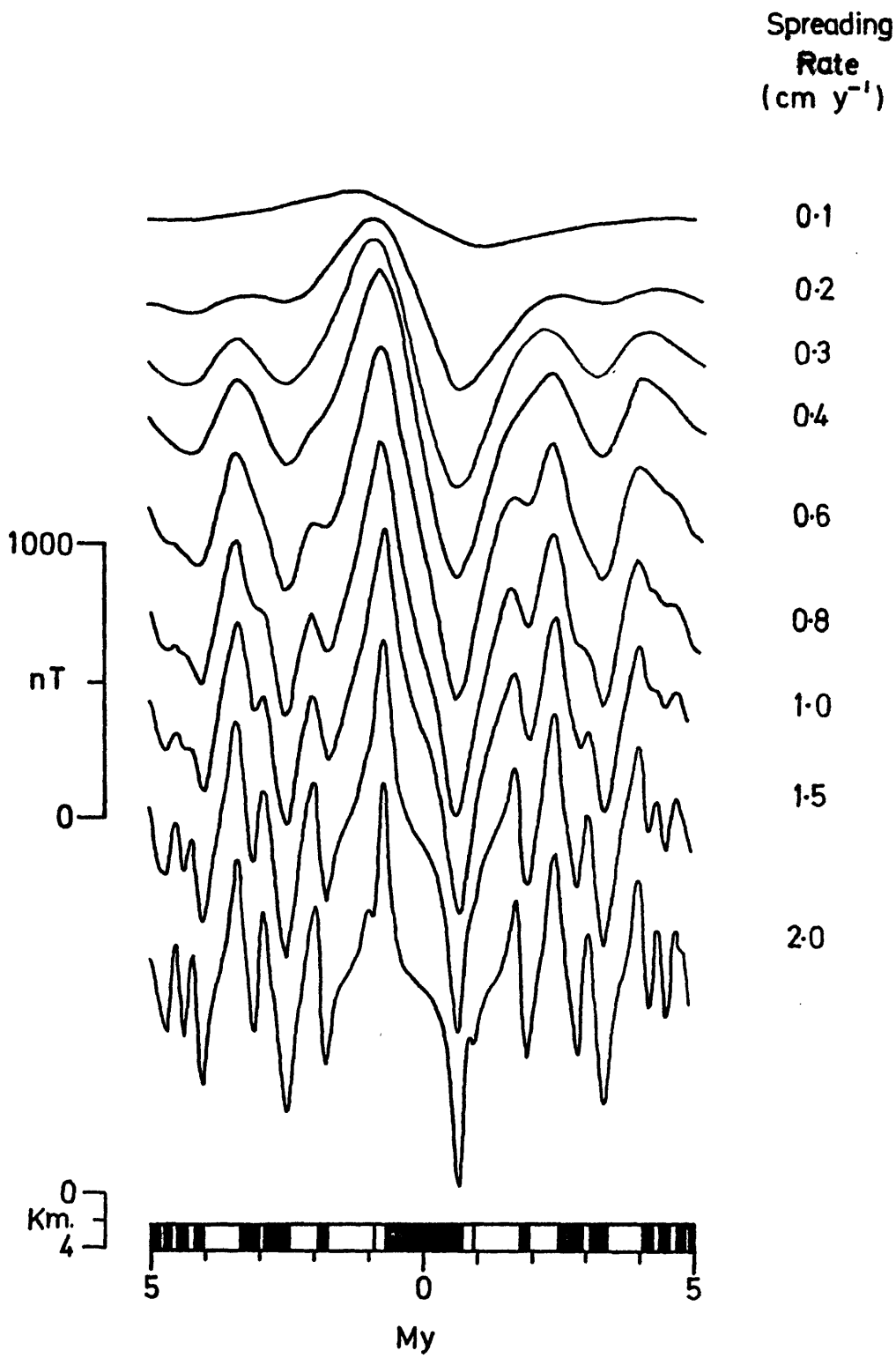

Figure 3.8 Synthetic magnetic profiles over seafloor spreading at various rates. Profiles are normal to the Red Sea axis at 19°N and are computed for the period 0 to 5 My.

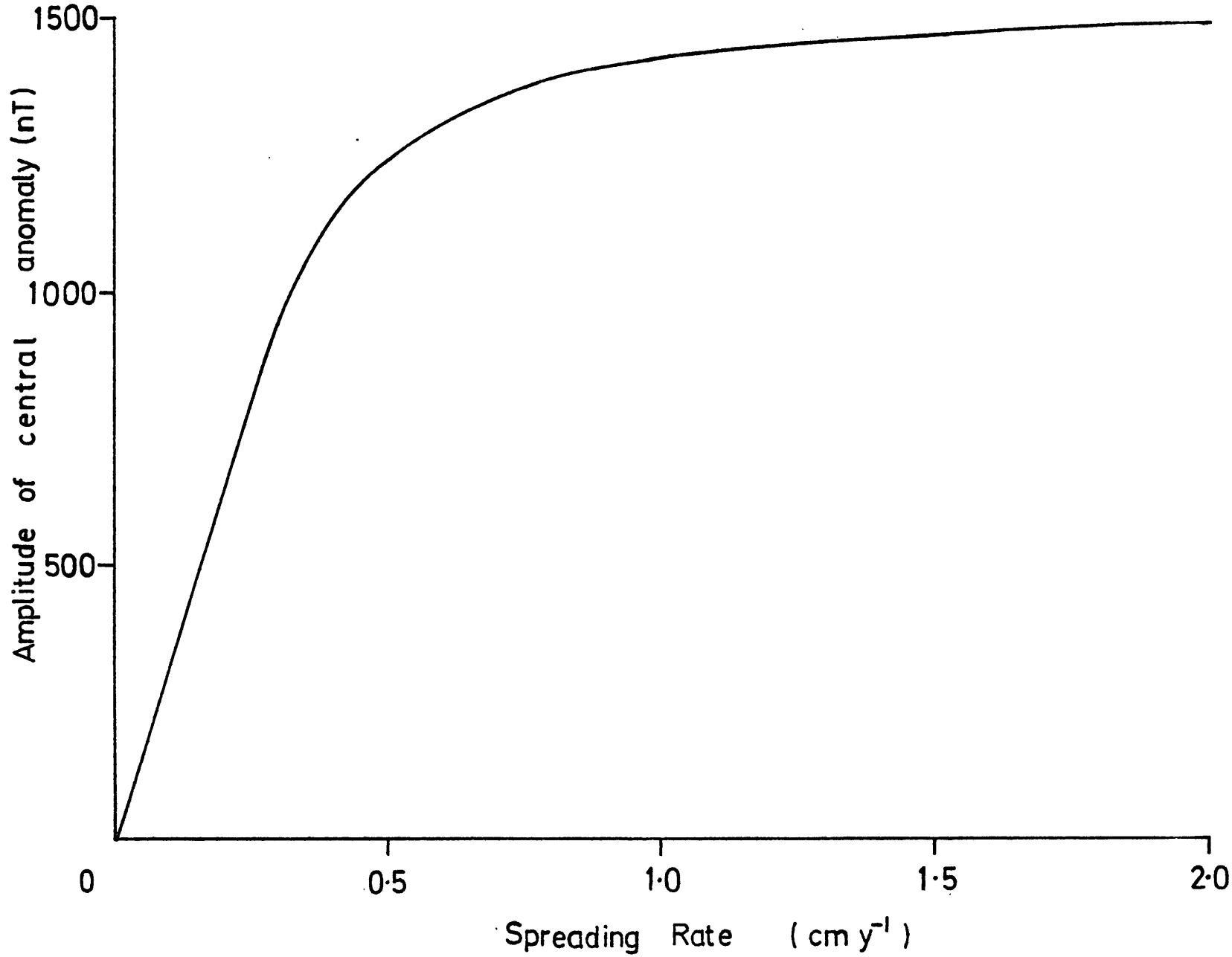

Figure 3.9 Amplitude of central anomaly versus spreading rate for synthetic magnetic profiles shown in fig. 3.8.

Plate 1. Spreading rates based upon correlations of the anomalies with synthetic profiles for the central and southern Red Sea have been given by Vine (1966), Allan (1970), Phillips (1970) and Girdler and Styles (1974). In the three areas considered in Chapters 4, 5 and 6 these data give the following values:

(1) Northern Red Sea. Layer 2 velocities at depths of 2 to 4 km. A strike of N 145^{o}, i.e. approximately parallel to the coastlines. Spreading rates of 0.4 to 0.5 cm y^{-1} in the extreme northern Red Sea inferred from the 45 km left lateral offset of geological features along the Dead Sea rift (Freund et al, 1970) since the Miocene. A synthetic magnetic profile over seafloor at 4 km spreading at 0.5 cm y^{-1} with a strike of N 145^{o} is shown in fig. 3.10 (profile 1). The anomalies are about 150 nT with many of the smaller features filtered out. The central anomaly amplitude is approximately 700 nT.

(2) Central Red Sea. Layer 2 velocities at depths of typically 2 km. A strike of either N-S or NE-SW between 20^{o}N and 22^{o}N and N 145^{o} elsewhere. A spreading rate of 1 cm y^{-1} for seafloor trending along N 145^{o}. A synthetic magnetic profile over seafloor at 2 km spreading at 1 cm y^{-1} with a strike of N 145^{o} is shown in fig. 3.10 (profile 2). The anomalies are typically 500 nT with a central anomaly amplitude of 1400 nT. Several more features are present than in profile 1.

(3) Southern Red Sea. Layer 2 velocities at depths of about 2 km. A strike of N 145^{o} and spreading rates of approximately 0.9 and 1.0 cm y^{-1}. A synthetic profile based on these parameters is shown

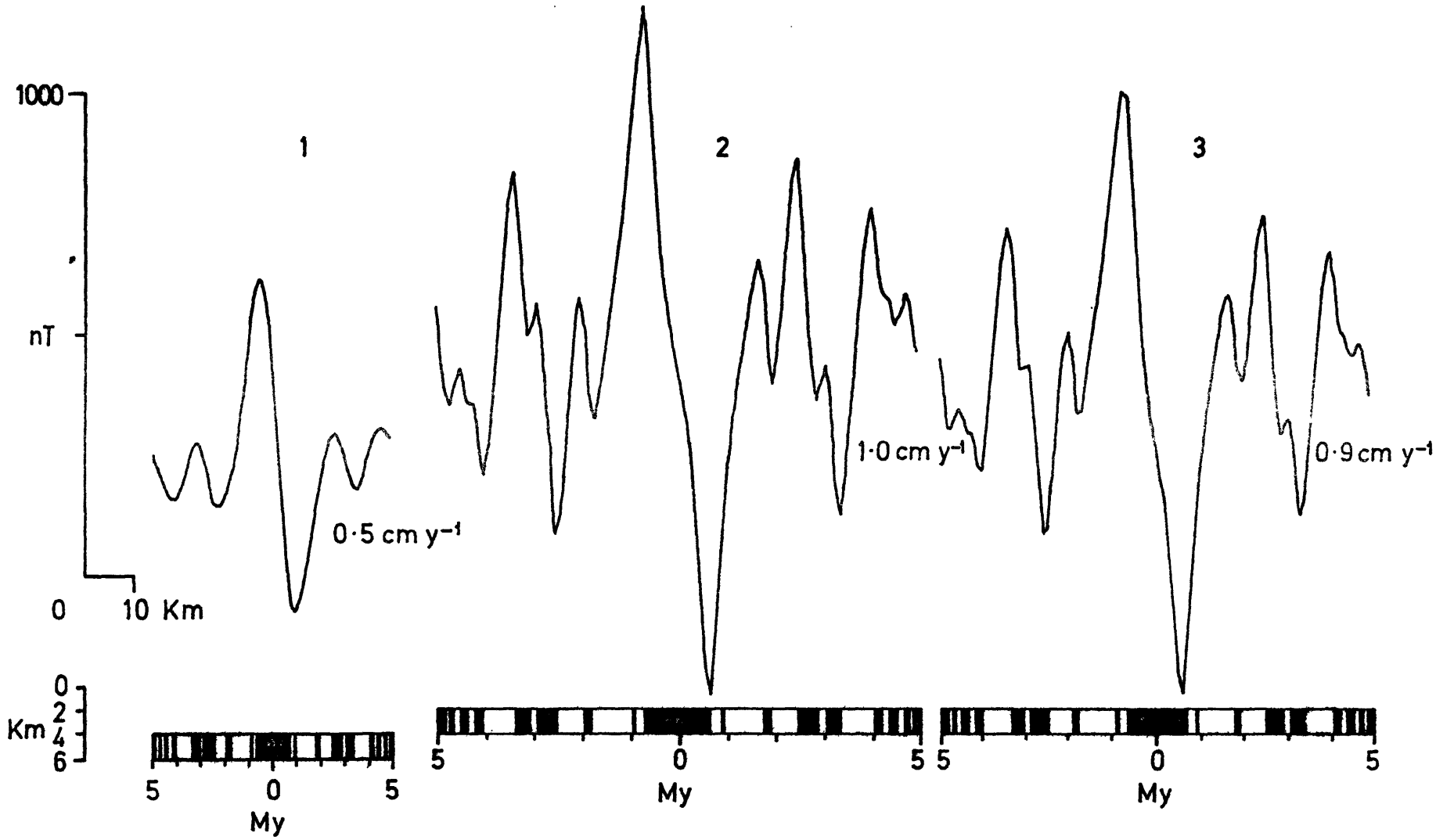

Figure 3.10 Synthetic magnetic profiles over 1) northern, 2) central, and 3) southern Red Sea predicted from geophysical and geological data . Profiles are for seafloor spreading over the past 5My with a strike of N 145° .

in fig. 3.10 (profile 3). The anomalies are very similar to those shown in profile 2. The central anomaly amplitude is 1200 nT.

Figure 3.10 indicates that smaller anomalies are expected in the northern Red Sea due to deeper seafloor and slower spreading and that where such seafloor exists, information on the short polarity intervals of the geomagnetic field is lost.

CHAPTER FOUR

THE RED SEA NORTH OF 24°N

4.1 Relevant geophysical data

The northern Red Sea has been much neglected in recent years especially since the closure of the Suez Canal in 1967. All the geophysical measurements were made prior to this closure and consequently there are no high quality data available. It is hoped that the recent re-opening of the Canal will revive interest in the area and lead to the collection of more detailed data. Nine heat flow measurements, all in deep water, have been made (Birch and Halunen, 1966; Langseth and Taylor, 1967; Scheuch, 1973) which are significantly higher than the world mean (59 mW m^{-2}).

Gravity stations (Girdler, 1958), not shown in fig. 4.1, and gravity profiles (Allan, 1970) indicate positive, Bouguer anomalies greater than 1000 g.u. are present over the central area as far north as 26°N. Further north the anomalies are still positive but smaller in amplitude (viz. 600-700 g.u.). The Gulfs of Aqaba and Suez are areas of negative Bouguer anomalies: -500 g.u. in Suez and -1000 g.u. for Aqaba (Girdler, 1969).

Seismic reflection and refraction studies have been made in the area (Drake and Girdler, 1964; Knott et al, 1966; Girdler, 1969; Phillips and Ross, 1970). The reflection data indicate the presence of a strong reflector, designated the S-reflector by Knott et al (1966), beneath the main trough. This has been correlated with a change in deposition from evaporites to marine oozes that occurred at the end of the Miocene. The reflector was

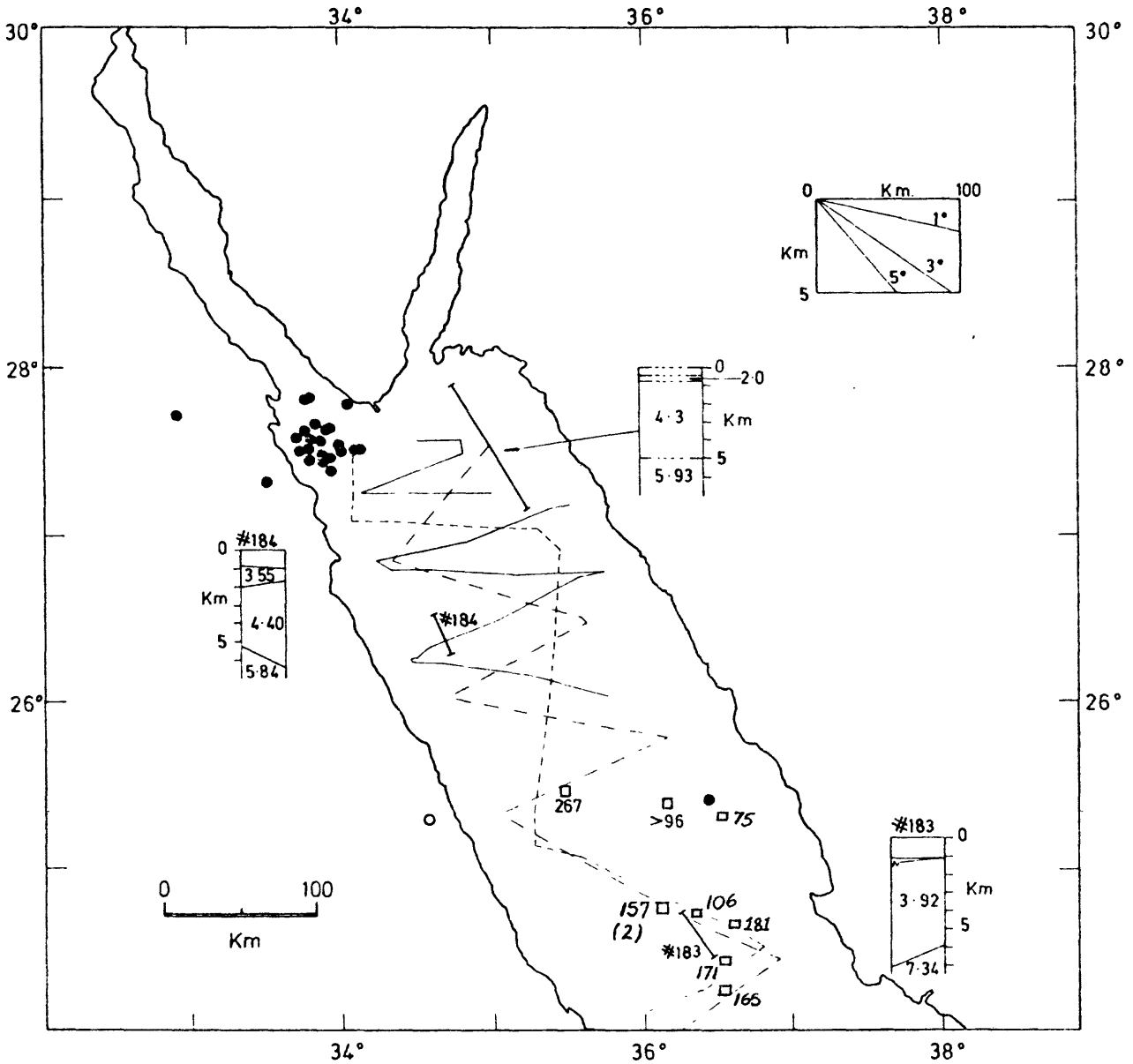

Figure 4.1 Geophysical data (excluding magnetic) available for the Red Sea between 24°N and 28°N. □ heat flow measurements (values in mW m^{-2}); O and ● earthquake epicentres before 1963 and since 1963 respectively. ⊢——⊣ seismic refraction profiles; ——— seismic reflection profiles; —— ··· —— gravity profiles; — — — — seismic reflection and gravity profiles. Seismic velocities in crustal models are in km s^{-1}.

was found along all tracks except those crossing a small area near 25^{o}N, 36^{o}E (see fig. 21, Phillips and Ross, 1970).

Three seismic refraction profiles, two by VEMA and ATLANTIS and one by DISCOVERY are shown in fig. 4.1. The northernmost two show a thin layer (less than 1.0 km) of 2.0 to 3.55 km s^{-1} material underlain by a thick layer (about 4 km) with velocities of between 4.3 and 4.4 km s^{-1}. These overlie a layer with a seismic velocity of 5.8 to 5.9 km s^{-1}, which has been interpreted as continental material (Drake and Girdler, 1964). The third seismic refraction profile indicates two layers: a 3.9 km s^{-1} layer underlain by a 7.3 km s^{-1} layer which is probably basic intrusive material.

Also shown in fig. 4.1 is the distribution of earthquake epicentres: solid circles represent epicentres of events occurring since the introduction of the World Wide Standard Seismograph Net (WWSSN) in 1963, open circle is for an event prior to 1963. A large number of epicentres are grouped near Shadwan Is. in the mouth of the Gulf of Suez; these include foreshocks and aftershocks of a large earthquake (m_b = 6.0) which occurred on March 31st 1969. The area has been seismically active since with earthquakes in August 1969, April 1970 and December 1970. Detailed studies of some of these earthquakes are given by Ben-Menahem and Aboodi (1971) and Pearce (in prep.). There are only two other epicentres both of which lie well outside the deep water and appear to be associated with faulting at the margins (Fairhead and Girdler, 1970).

4.2 Distribution of magnetic data

4.2.1 Sea data

Ships' tracks for which magnetic data are available between 24^{o}N and 28^{o}N are shown in fig. 4.2. All measurements were made between 1958 and 1967. Each vessel used celestial fixes and radar for navigation giving positional accuracies of about 1 to 2 km. Larger errors may be present as recent satellite photography from Landsat-1 has shown the position of the coastlines, as previously mapped, is not entirely accurate. Discrepancies as large as 5 km have been noted and some surveys probably contain similar positional errors.

The overall coverage is poor with the best distribution of tracks between 26.5^{o}N and 27.5^{o}N. Here, there are several E-W and NE-SW tracks spaced between 10 and 20 km apart. Between 26^{o}N and 26.5^{o}N the tracks are more widely spaced (about 30 km) and oriented in various directions. South of 25^{o}N there are several closely spaced (5 to 10 km), NE-SW tracks, e.g. EE', FF' and GG' (fig. 4.2). In general, the tracks are mainly over the deeper water with few tracks crossing the narrow, shallow shelves.

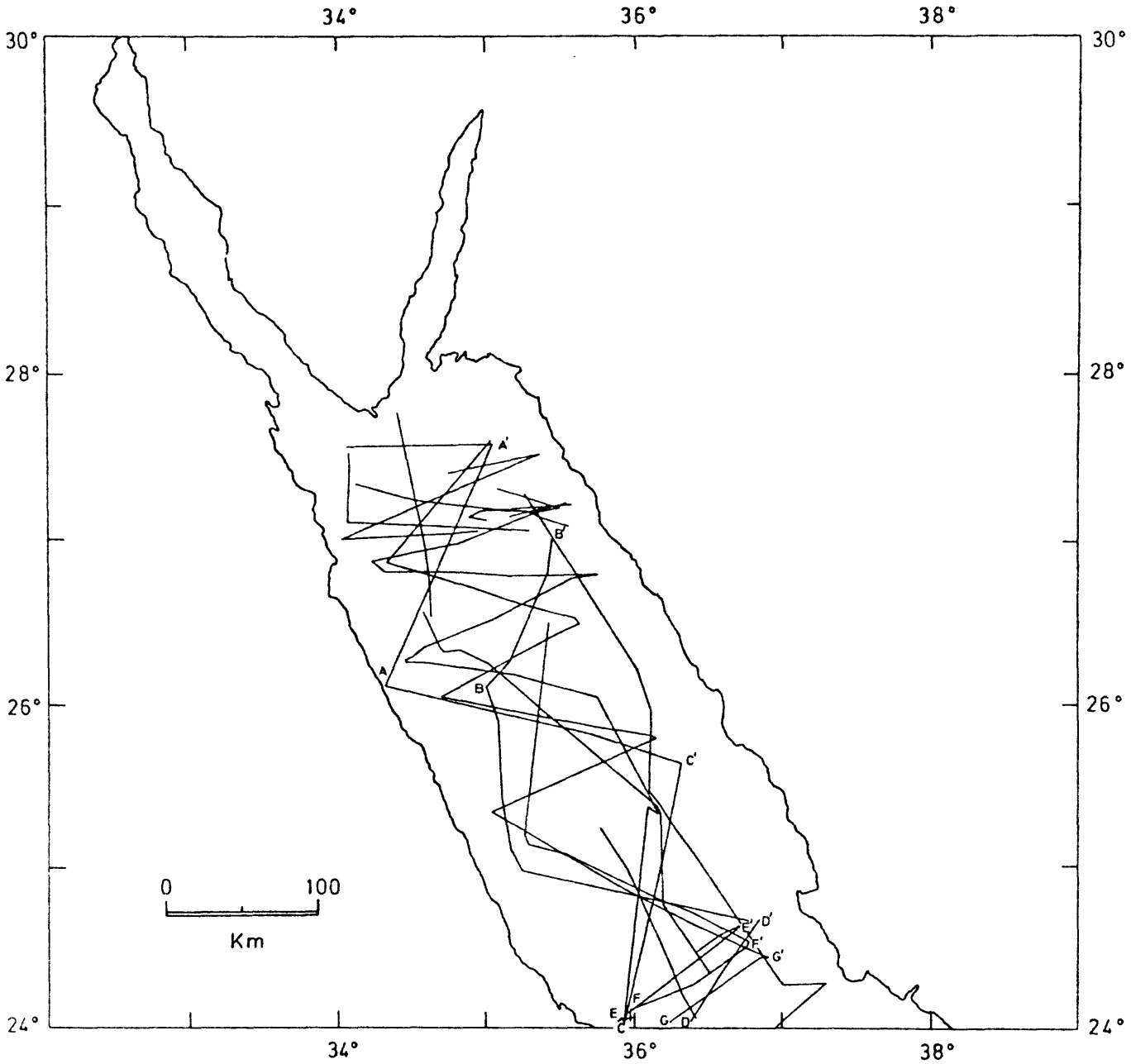

Figure 4.2 Tracks of research vessels between 24°N and 28°N for which magnetic data are available. Lettered tracks (AA', BB' etc.) indicate the location of magnetic profiles shown in figs. 4.5 and 4.7.

4.2.2 Air data

Five aeromagnetic surveys have been carried out along the Arabian coast between 22.3°N and 28°N (see fig 2.1 and Table 2.1). Each survey was flown at a constant height above mean sea level : two at 2000 metres, two at 457 metres (1500 feet) and one at 609 metres (2000 feet). All surveys used Doppler navigational systems giving accuracies of about ± 1 km over sea areas. For navigation over land, aerial photography was used in conjunction with the Doppler system producing better positional control (± 0.1 km).

The locations of 55 profiles selected from these surveys are shown in fig 4.3. As the original data are not available for four of the surveys (viz. C5, C6, C7 and C8, fig 2.1), 47 of the profiles (viz. profiles 1 to 47) were obtained by digitising contour maps using a 1 km interval. The remaining profiles, nos. 48 to 55, are original data from the Yanbu' survey (C2, fig 2.1). The profiles are spaced at about 10 km and vary in length according to the extent of the individual surveys. Those obtained from contour maps were extended inland using data from aeromagnetic surveys of the Arabian Shield. These surveys were flown at 300 metres above mean terrain, the height of which varies between 0 and 1800 metres.

The coverage of the coastal plain and offshore shelves is impressive with only two gaps: one at 25.8°N, the other at 24.5°N (fig 4.3). No similar airborne surveys along the African coast between 24°N and 28°N are currently available.

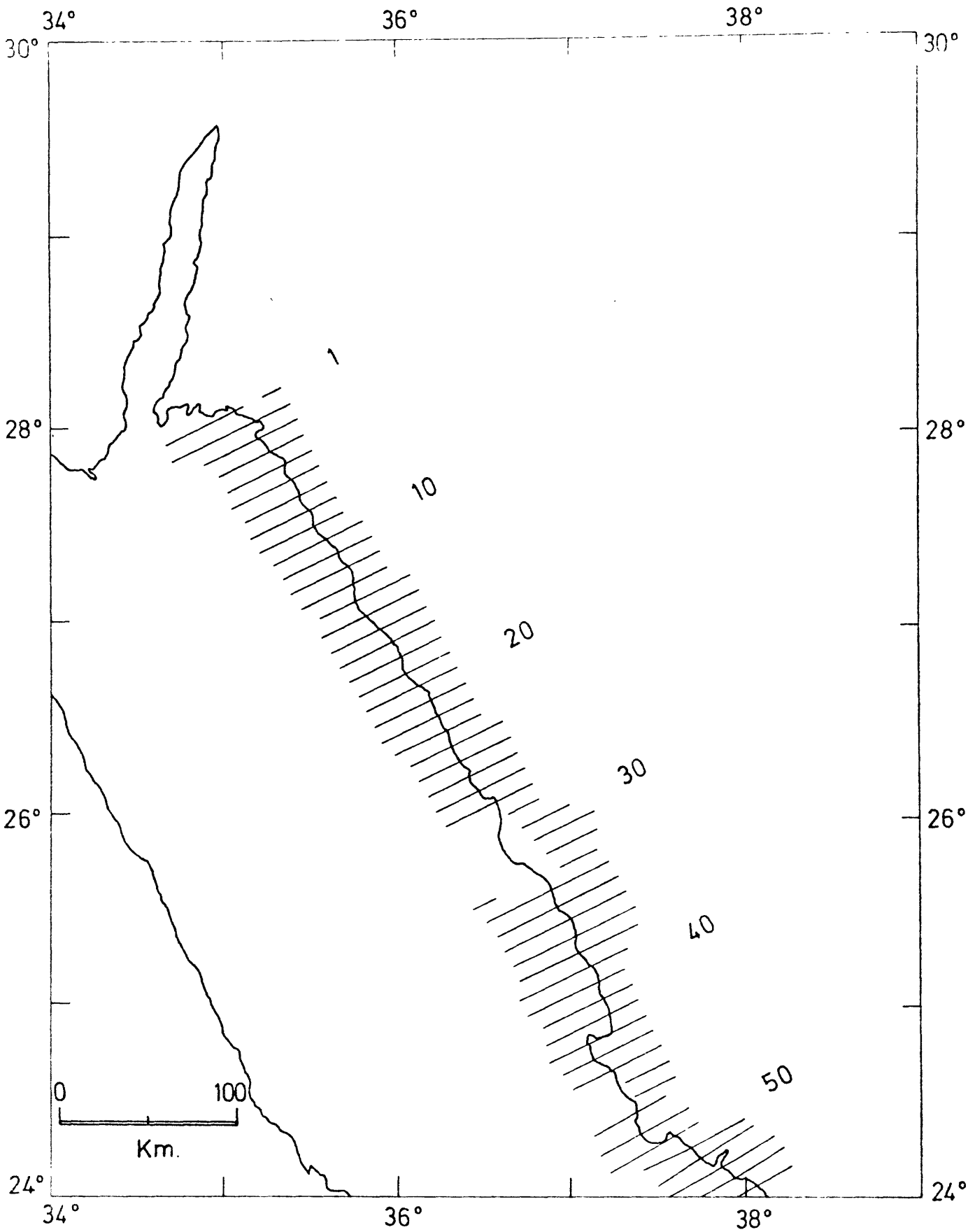

Figure 4.3 Location of magnetic profiles selected from airborne surveys along the Arabian coast between 24°N and 28°N.

4.3 Description of magnetic anomalies

4.3.1 Amplitude, wavelength and distribution of anomalies

In general, the magnetic anomalies observed over the northern Red Sea are smaller and smoother than those observed further south. A profile near 26.5°N (fig 4.4 (a)) displays anomalies with amplitudes of about 200 nT over the deeper water with 50 to 100 nT elsewhere. These are very smooth with wavelengths between 10 and 30 km(peak to trough). In comparison, the anomalies over the southern central Red Sea (fig 4.4(b)) are much larger (400 to 1100 nT) with shorter wavelengths ($\sim$ 5 km) giving the profile a distinctly "spikey" appearance. These differences are discussed more fully in Chapter 7.

A detailed examination of both the air and sea data reveals that the anomalies may be grouped into three types based upon their amplitude and wavelength. (1) Over the deep water areas the anomalies are typically 200 nT with wavelengths of 10 to 15 km (e.g. profiles AA' and BB' in fig 4.5). These anomalies are not, however, observed over all deep water areas (e.g. DD' fig 4.5). (2) The anomalies over the shallower water and parts of the coastal plain are smaller, typically 50 to 100 nT, with longer wavelengths of 20 to 30 km although 200 nT anomalies are present on airborne profiles in fig. 4.6. (3) Short wavelength (1 to 5 km), variable amplitude (10 to 500 nT) anomalies are observed on the coastal airborne data (fig 4.6) over the land. These contrast strongly with the smooth, uniform amplitude anomalies found over the shelves and parts of

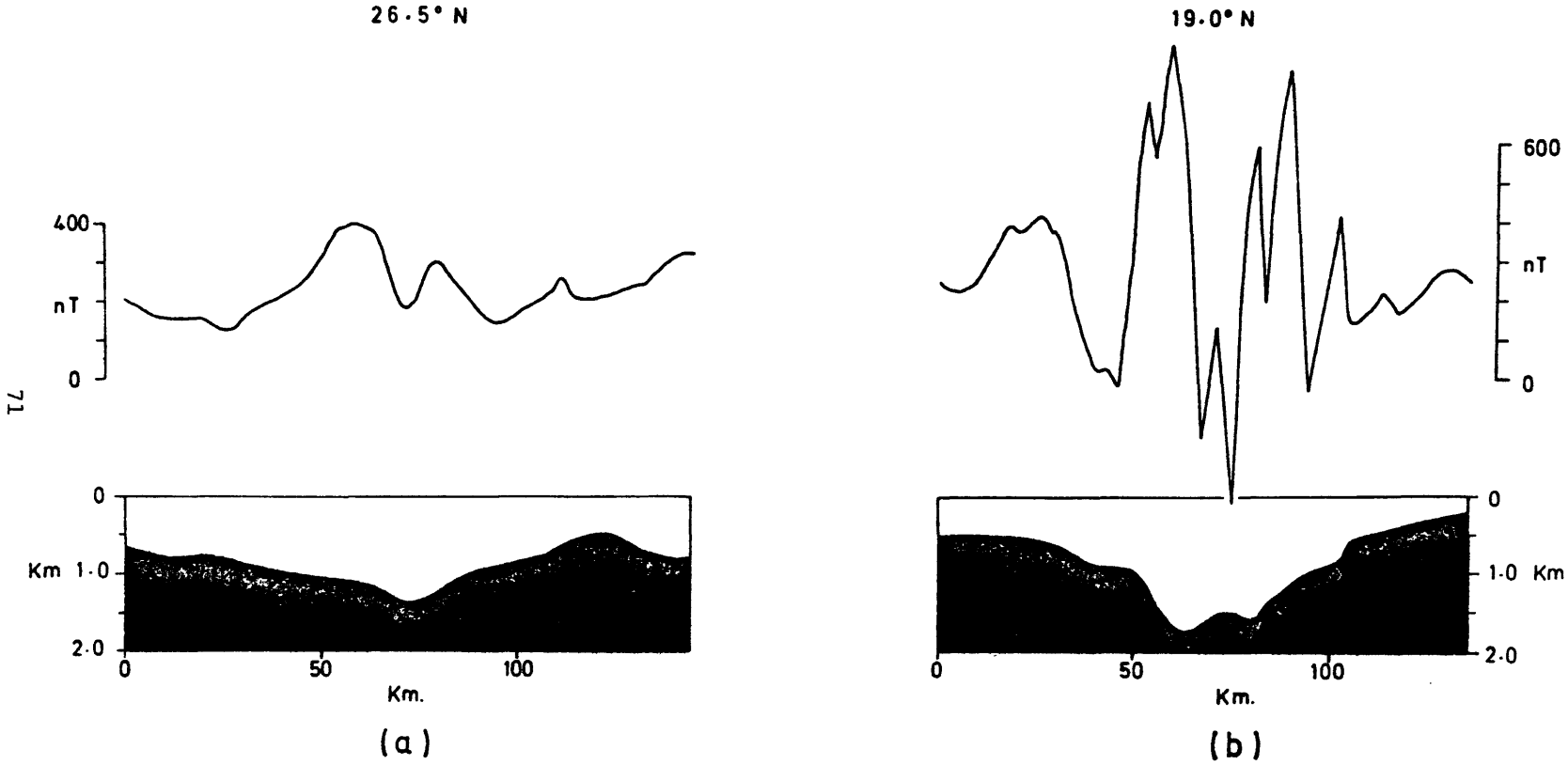

Figure 4.4 Magnetic profiles and associated bathymetry from research vessels across a) the northern Red Sea near 26.5°N and b) the southern central Red Sea near 19°N.

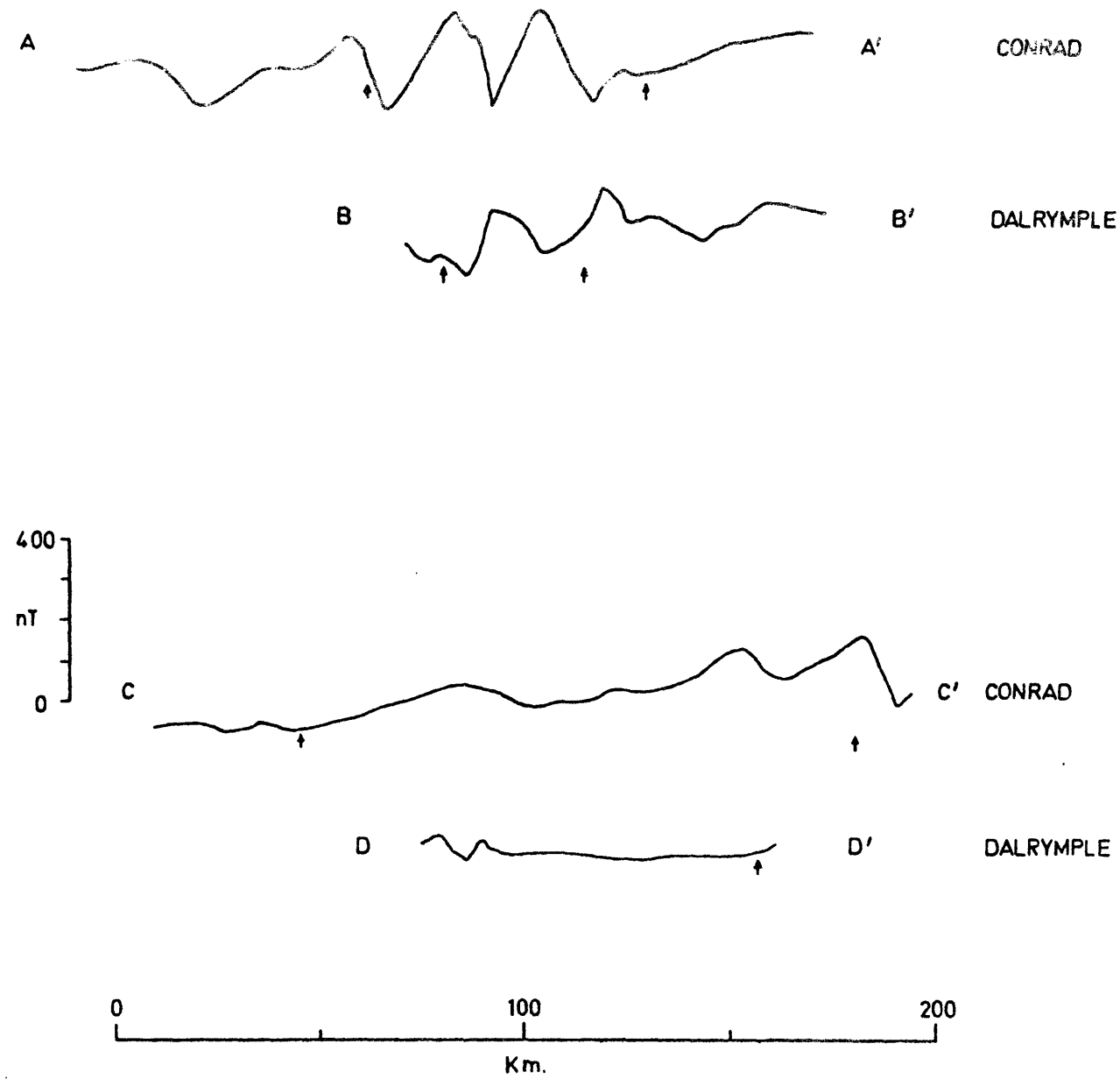

Figure 4.5 Magnetic profiles over the northern Red Sea from research vessels CONRAD and DALRYMPLE. Arrows indicate approximate position of 500 fathom contour. Locations of profiles are shown in fig. 4.2.

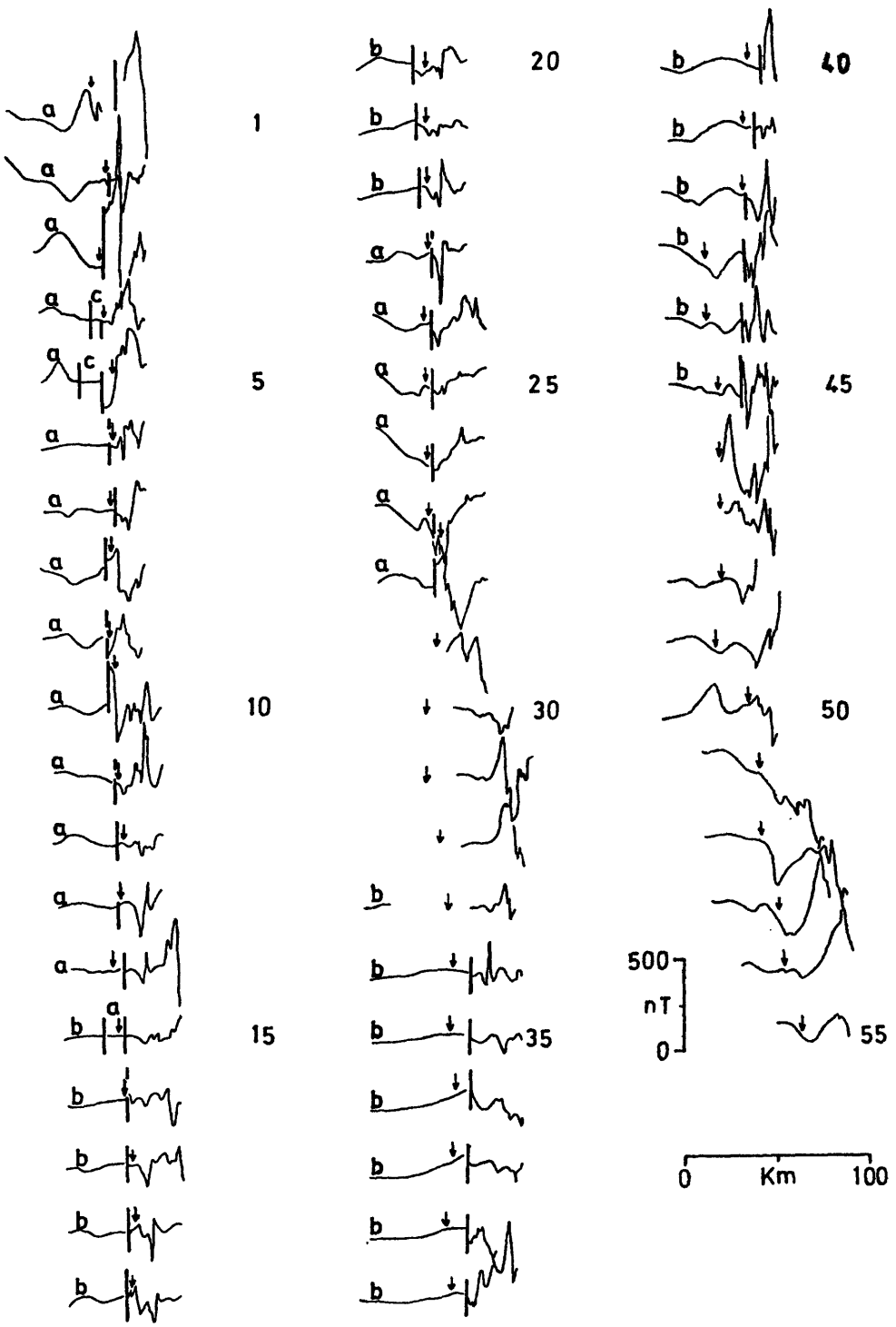

Figure 4.6 Aeromagnetic profiles over the Arabian coast between 24°N and 28°N. Locations of profiles shown in fig. 4.3. Arrows indicate approx. position of coast; vertical bars separate data collected at different elevations. Sections of the profiles west of the bar were flown at a) 0.46 km, b) 2.0 km, and c) 0.3 km; east of the bar were flown at 0.3 km above mean terrain. Profiles 48 to 55 were flown at 0.61 km.

the coastal plain (see fig 4.6). The high frequency anomalies seldom correlate over large distances but appear to be more or less randomly distributed. An exception to this is the sharp magnetic expression of several young dykes which have been mapped in Arabia. (e.g. on profiles 6 to 14 in fig 4.6).

The above classification is valid for all parts of the northern Red Sea except those sea areas over which no significant anomalies are observed. Such areas are generally located in shallow water where either the data coverage is poor or the flight height is large (viz. 2000 metres). However, one such area is over deep water near 24.5^{o}N where the data coverage is reasonably good. Three profiles over this area are shown in fig 4.7. Two of these, FF' and GG', have anomalies which are typically less than 20 nT, although a 50 nT trough is present at the extreme western end of FF'. A comparison of these three profiles with DD' of fig 4.5 indicates that the 'flat' area has a NW-SE width of at least 25 km. The exact NE-SW extent is unknown as the 'flatness' continues to the eastern limit of the sea data. Anomalies observed on profiles 42 to 45 of fig 4.6, however, indicate the area does not extend to the Arabian coast suggesting a maximum NE-SW extent of less than 100 km. No further 'flat' zones were discovered over the deep water and whilst the distribution of data is poor overall it is sufficiently good over the deep water to reveal any further zones unless their NW-SE extent is smaller than 20 km.

The differences in the nature of the anomalies observed are thought to reflect variations in the crustal structure beneath the various areas.

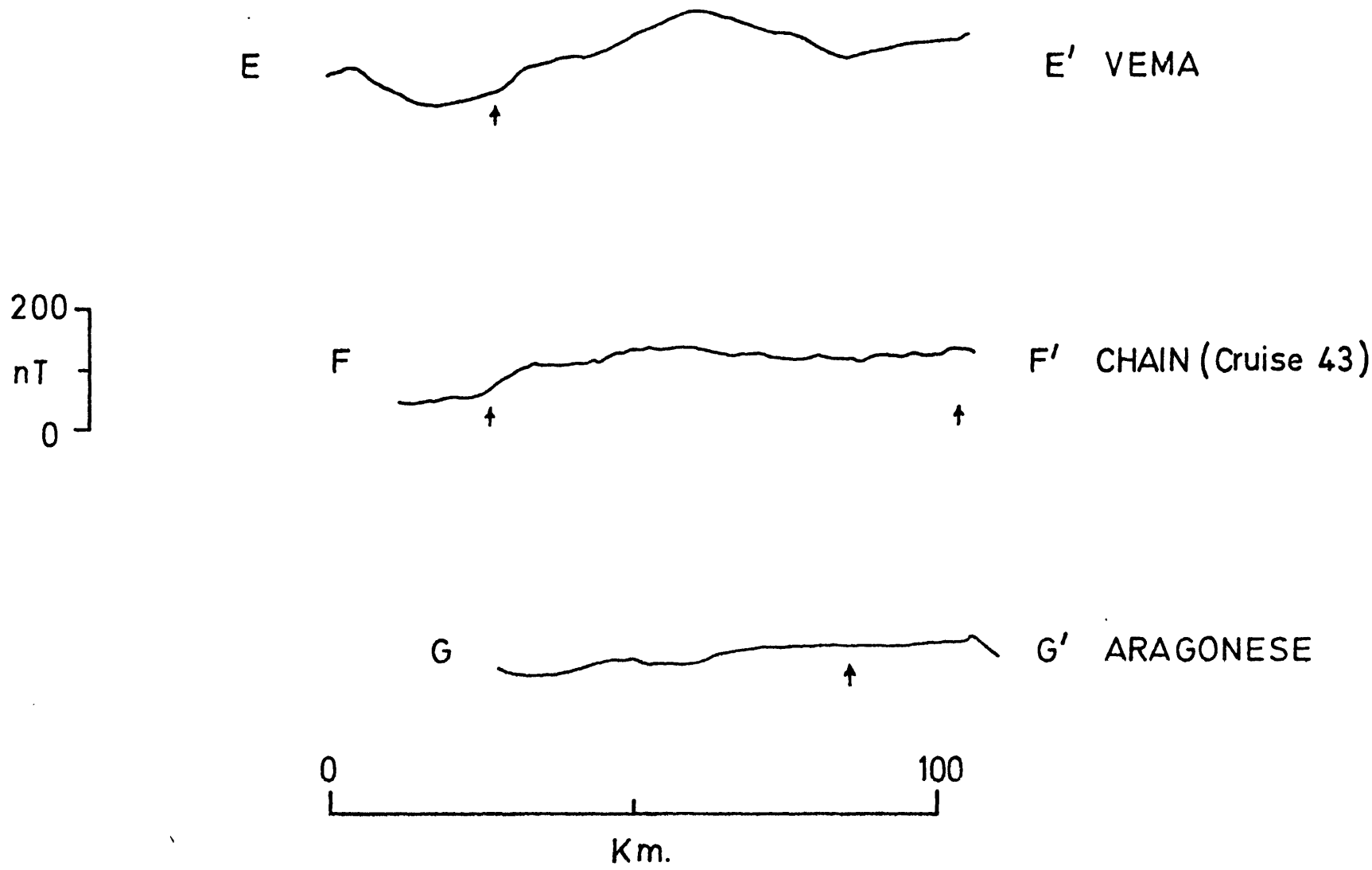

Figure 4.7 Magnetic profiles near 24.5°N from research vessels VEMA, CHAIN and ARAGONESE . Arrows indicate approximate position of 500 fathom contour. Locations of profiles shown in fig. 4.2 .

4.3.2 Correlations of the anomalies

The magnetic data were examined more closely to study the continuity of the anomalies in the various areas. Both air and sea magnetic profiles were inspected for dominant peaks (maxima) and troughs (minima) and their locations transferred to the map shown in fig 4.8. Anomalies were correlated from profile to profile and the corresponding features in fig 4.8 joined with straight lines. In the case of the sea data the smoothness of the anomaly field and the large gaps between adjacent profiles make correlations difficult. The air data, however, are more closely spaced and better correlations are obtained (cf. figs 4.6 and 4.8). Correlations of the high frequency anomalies over the shield and coastal plain are extremely poor, and rarely extend over more than two profiles. Consequently, peaks and troughs of these anomalies have been omitted from fig 4.8.

The distribution of peaks and troughs shown in fig 4.8 was studied in an attempt to distinguish trends. Lines of peaks and of troughs are observed which form lineations that extend approximately parallel to the coasts over distances of 60 km or more. These lineations are found over both the deep water areas and the shallow shelves extending over the land in several places (e.g. near 25.5^{o}N). The features have consistent trend directions in both the sea and air data, producing a fairly uniform and coherent magnetic pattern. It appears likely from this that the magnetic sources of the anomalies over the deep water and over the shelves are similar.

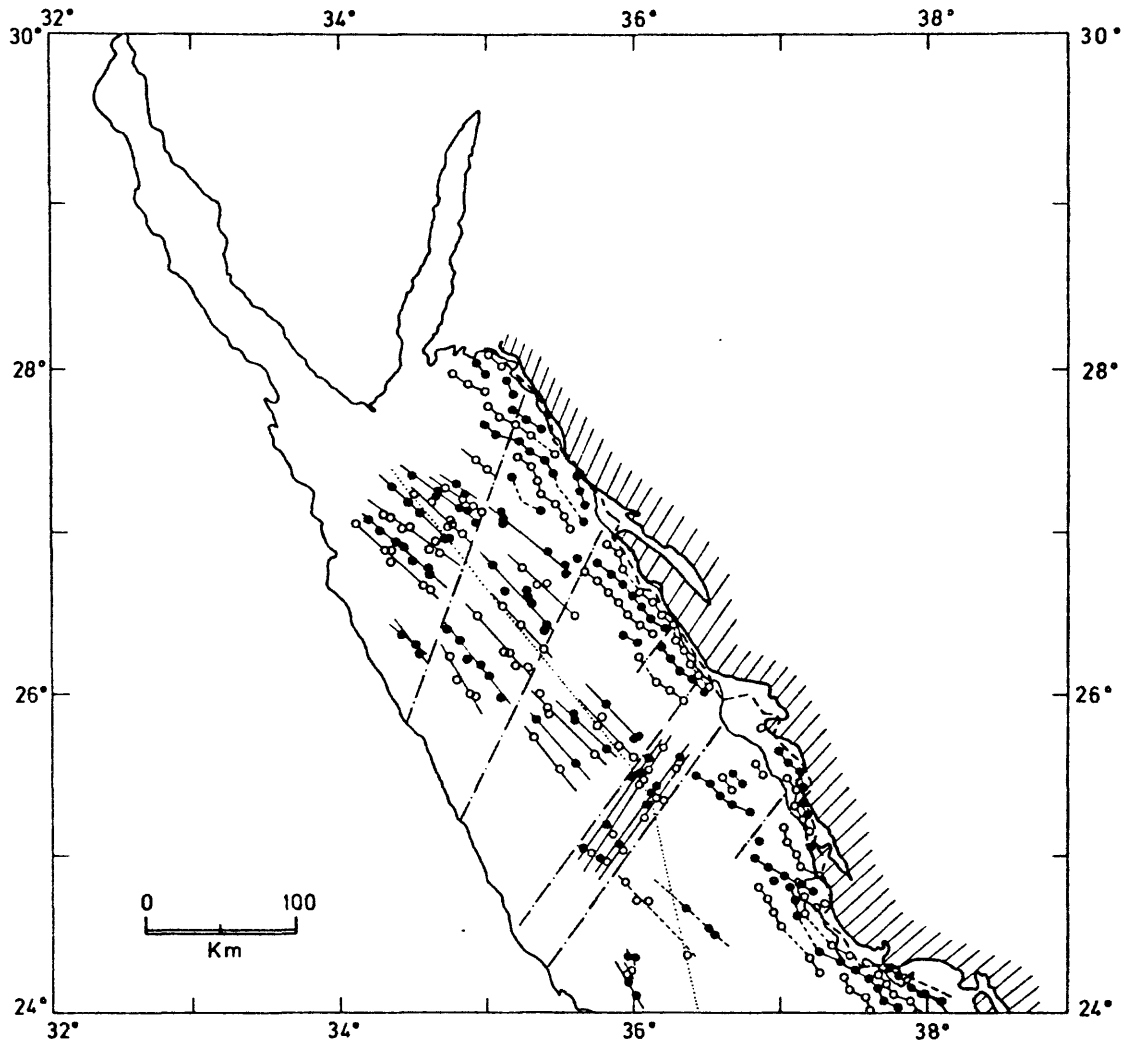

Figure 4.8 Location of dominant peaks, O (positive anomalies) and troughs, ● (negative anomalies). ..... deep water axis; —·— discontinuities in magnetic pattern. Heavy shaded line represents seaward limit of mapped Pre-Cambrian; heavy dashed line is seaward limit of high frequency anomalies. Firm correlations of features shown as solid lines; tentative correlations as light dashed lines.

Several discontinuities of the magnetic pattern were identified by consistent offsets of the lines of peaks and troughs and/or changes in the dominant trend direction. The discontinuities are more apparent over the deeper water than the shelves as more dominant features are present. The northern Red Sea is separated into five regions by the discontinuities (fig 4.8), four of which have trend directions approximately parallel to the Red Sea trend. The fifth region, near 25^{o}N, 36^{o}E, has a trend parallel to the discontinuity, i.e. normal to the Red Sea trend.

4.4 Ocean/continent boundary

The similarity of the anomalies found over the deep water areas and those over the shallow shelves has already been noted. Their shape, size and continuity make them very similar to the anomalies observed over the oceans. This together with the coherence of their magnetic pattern in fig 4.8 point convincingly to a seafloor spreading origin. Such an explanation is further supported by borehole information along the Arabian coast (Coleman, 1974) which indicates large thicknesses ($\sim$ 3.5 km) of sediments. Thus, strongly magnetised material is required to reproduce the anomalies. In contrast, the variability of the high frequency anomalies at the eastern ends of the profiles (fig 4.6) is typical of continental material and many of these anomalies are observed over mapped Pre-Cambrian areas. These differences in the character of the anomalies may be used to determine the extent of oceanic and continental material..

Estimates were made of the boundary between the high frequency anomalies and the smooth, long wavelength anomalies. The ocean/continent boundary obtained is shown in fig 4.8 (heavy dashed line). The estimates are rather subjective as the precise point at which the high frequency develops is difficult to determine. Also shown in fig 4.8 (shaded solid line) is the mapped edge of the Pre-Cambrian outcropping along the coastal plain. The near coincidence of this edge with the high frequency boundary in many places demonstrates the relationship between these anomalies and the crystalline basement rocks. Changes in the level of the Pre-Cambrian can result in the smoothing out of the high frequency anomalies. For example, in several of the magnetic profiles (fig 4.6) over the Tertiary and Quaternary sediments,the high frequency anomalies are almost entirely absent although Pre-Cambrian rocks probably exist beneath these sediments. It is apparent from this that the dashed line in fig 4. 8 only approximately delineates the ocean/continent boundary. An alternative estimate of this boundary may be obtained by studying the landward extent of the linear, seafloor anomalies. Again it is difficult to determine precisely the extent of these as many of the features do not appear on every profile. Also the most easterly peak of the magnetic pattern (fig 4.8) is often very close to the high frequency edge. A trough immediately west of this peak, however, is always located some way from this edge and this may be taken as the landward extent of the seafloor. That all the seafloor anomalies do not appear on every

profile may be explained partly by the offsets of the magnetic pattern noted above.

It can be seen from the above that the ocean/continent boundary cannot be determined exactly but must lie somewhere between the high frequency edge and the first correlatable seafloor linear anomaly. The zone between these two boundaries varies in width from 8 km near 26^{o}N to about 20 km near 27.5^{o}N. For simplicity it is assumed that the ocean/continent boundary is located along the middle of this zone. Thus assuming symmetrical seafloor spreading about the present deep water axis 170 ± 20 km oceanic material is present at 27^{o}N along N45^{o}.

4.5 Seafloor spreading history

The anomalies over the sea have been separated into two groups on the basis of their amplitude and wavelength (section 4.3.1). Both groups form coherent, linear patterns which suggest the presence of seafloor. Recently, Girdler and Styles (1974) have shown that the southern Red Sea has been formed by two phases of seafloor spreading separated by a long interval during which huge thicknesses of evaporites were deposited. Such a model explains very well the two different types of seafloor spreading anomalies observed in the northern Red Sea. An attempt has been made, therefore, to simulate these anomalies using seafloor spreading models.

4.5.1 Recent seafloor spreading

A detailed analysis of the peaks and troughs over the deeper water shows that the magnetic pattern is symmetrical about a line close to the deep water axis such that for a peak on one side of the axis there is a corresponding trough at an approximately equal distance on the other side. This suggests seafloor spreading about the present deep water axis. Consequently the peaks and troughs were compared with a seafloor spreading model based on the reversal time scale of Heirtzler et al (1968) and found to agree reasonably well with either of two possible models. The first (fig 4.9(a)) requires spreading at about 0.6 cm y^{-1} from about 5 My to the present whilst the second (fig 4.9(b)) requires the somewhat faster rate of 0.85 cm y^{-1} from 3.5 My to the present. The correlations obtained for either model are not good although they are slightly better for fig 4.9(b) as several of the sidepeaks and troughs of the synthetics in fig 4.9(a) are not found in the observed data. A clear change in the character of the observed anomalies (fig 4.9) occurs near the 5 My boundary (3.5 My in fig 4.9(b)) and this seems to indicate the outer limit of the recent spreading phase.

Analyses of magnetic data over the southern Red Sea reported by Girdler and Styles (1974) and Hall et al (1977), indicate that this area has been spreading continuously over the past 4.5 to 5 My at 0.8 to 0.9 cm y^{-1}. The correlations obtained with such a model are

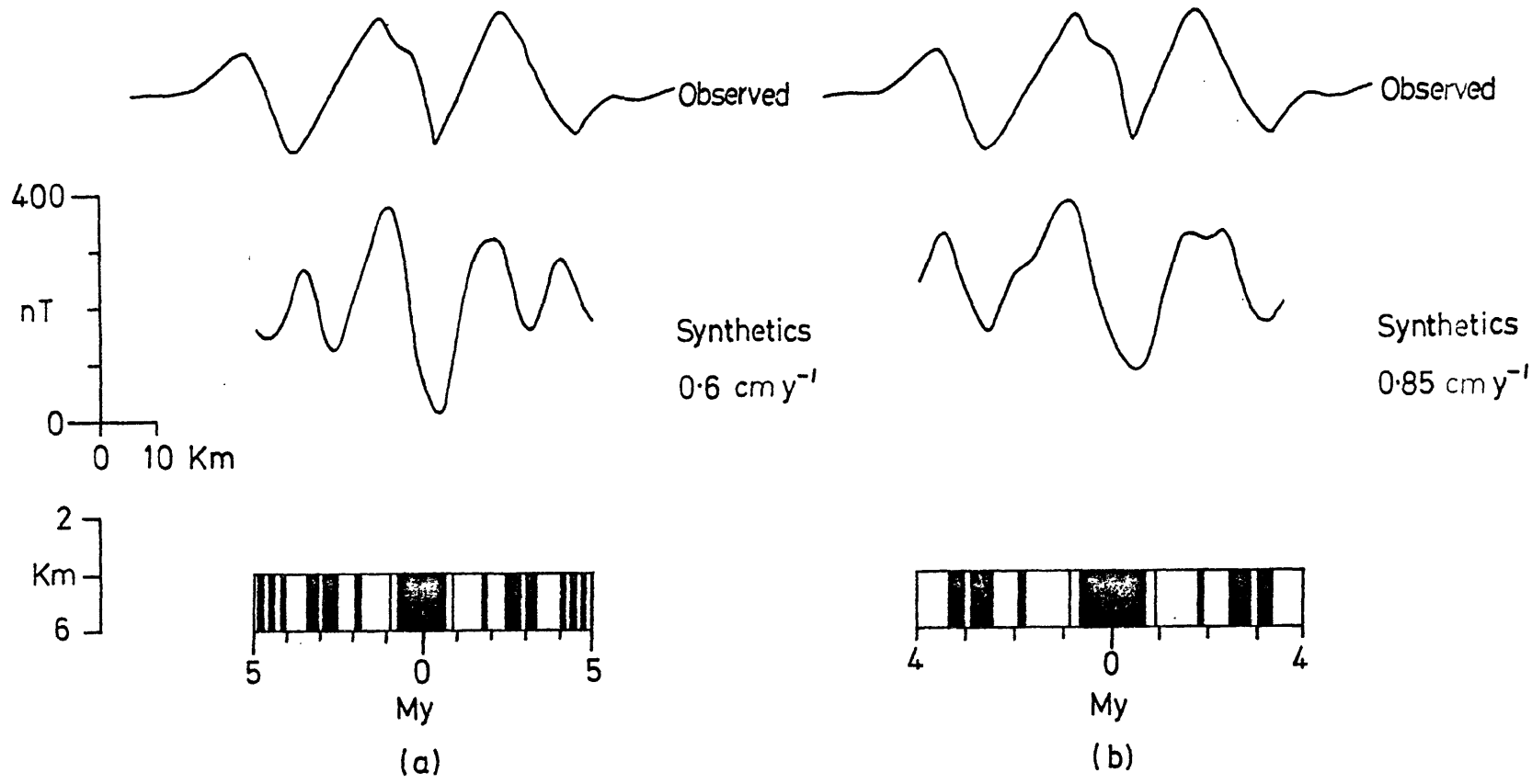

Figure 4.9 Two possible seafloor models of recent spreading phase. Observed profile is central portion of AA' (fig. 4.5). Location and strike of profile is shown in fig. 4.2.

impressive (see figs 5.14 and 6.9), consequently it appears very probable that of the two models presented in fig 4.9, that shown in (a) is the correct one.

In order to reproduce the amplitudes of the observed anomalies in fig 4.9 the effective susceptibility assumed for the seafloor (viz. 0.003 emu cm^{-3}) is less than the generally accepted value (viz. 0.01 emu cm^{-3}). Whilst the amplitude of the anomalies also depends on the depth of the seafloor the depth required to simulate the anomalies using an effective susceptibility of 0.01 emu cm^{-3} is large (about 9 km). This poses something of a problem as the depth of the bodies predicted from theoretical models (Sclater and Francheteau, 1970) is about 2 km for seafloor less than 5 My old although in this case the overlying evaporites will depress the seafloor. It seems more probable, therefore, that the seafloor is less strongly magnetised than elsewhere rather than very deep. Possible reasons for a weaker magnetisation in this area are discussed in Chapter 7.

The weaker magnetisation together with the small spreading rate (viz. 0.6 cm yr^{-1}) may be responsible for the smoothing out of the anomalies and the resulting absence of several of the side features predicted by the models. The smaller susceptibility contrast across adjacent seafloor bodies and the better opportunities for mixing (see section 4.6.2 and Chapter 7) provided by the slow rate would each contribute to an overall reduction of the magnetic expression of the spreading.

4.5.2 Early seafloor spreading

Fig 4.10(a)shows a model based upon Girdler and Styles (1974) in which spreading occurred continuously between 41 and 32.5 My at a rate of 0.7 cm y^{-1}. The observed data do not correlate very well with the synthetics although several similarities are present. A second model, shown in fig 4.10(b), is based upon the interval 29 to 23 My considered by Hall, et al (1976), and Girdler and Styles (in press) for magnetic data further south. For this period a spreading rate of 1.25 cm y^{-1} gives the best fit to the observed data. Correlations are again poor although several matching features exist.

The depth of the seafloor in the models is based upon three constraints. These are: the borehole information (Coleman, 1974), which sets a minimum depth of approximately 3.0 to 3.5 km; the effective susceptibility of the seafloor, which is typically 0.01 e.m.u. cm^{-3} for oceanic basalt; and the seismic refraction profiles in the area (Drake and Girdler, 1964; Girdler, 1969) which indicate up to 6 km of material with seismic velocities of 4.3 to 4.4 km sec^{-1}. A depth of 7 to 9 km was chosen. This compares favourably with the depth expected for seafloor of this age, i.e. 4 to 5 km (Sclater and Francheteau, 1970) if allowance is made for the effect of the large thicknesses of evaporites which depress the seafloor in the area.

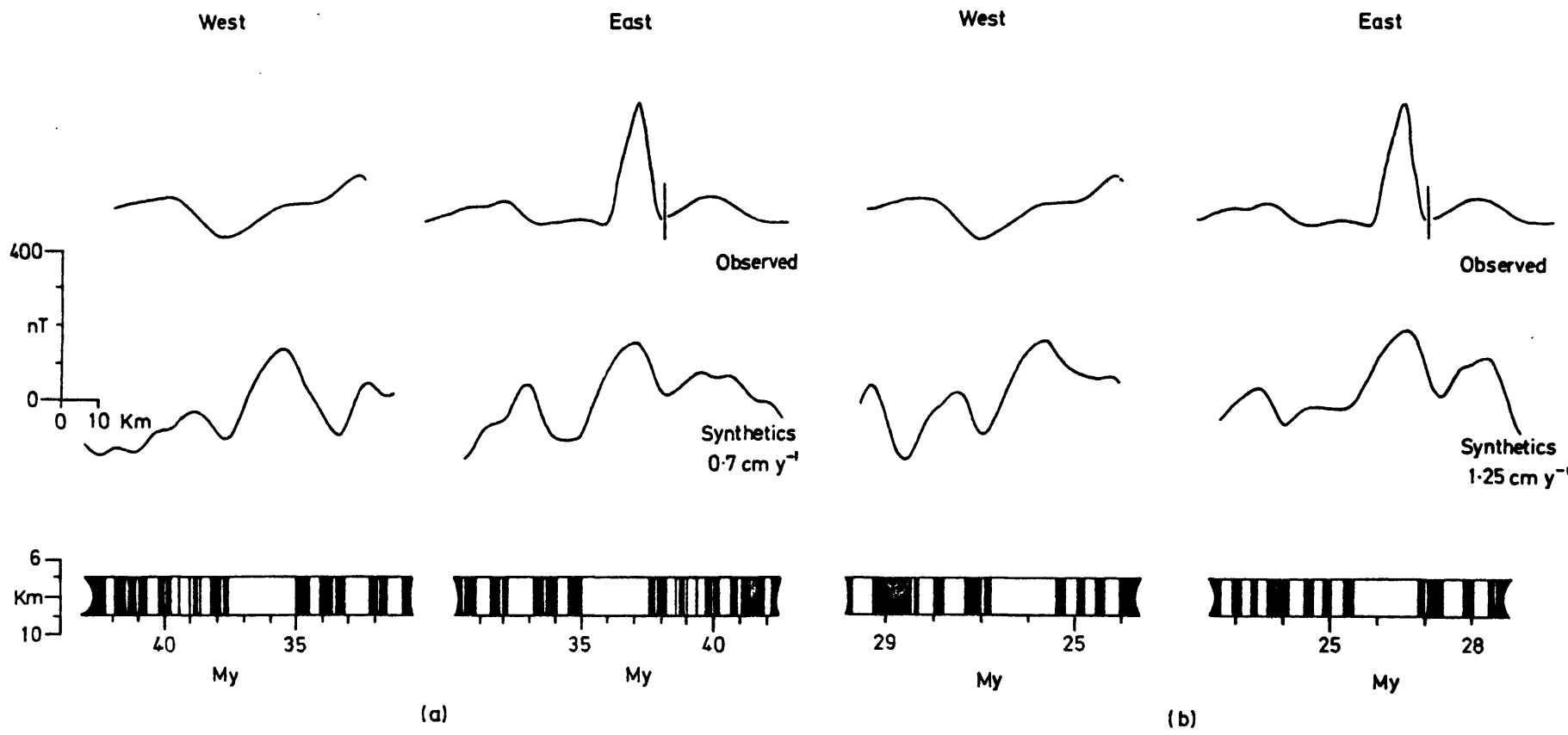

Figure 4.10 Two possible seafloor models for early spreading phase. Observed profiles are : West—western part of AA′ (fig.4.2), and East— sea data and western part of profile no. 12 (fig. 4.6)

4.6 Location of transform faults

4.6.1 Evidence from offsets of the magnetic anomalies

Several discontinuities are observed in the linear, magnetic patterns shown in fig 4.8. These extend across the northern Red Sea approaching the Arabian coast to within a few kilometres. At each,the magnetic pattern appears to be offset as a whole, i.e. the lines of peaks and of troughs are each offset by approximately the same amount and in the same direction. This suggests that the discontinuities mark the locations of transform faults. The discontinuities are described below from north to south.

1. Near 27^{o}N, 35^{o}E five features, three peaks and two troughs, of the sea data are displaced by approximately 10 to 12 km in a left lateral sense. The offset occurs near a NE-SW widening of the deep water trough (see Laughton, 1970). Evidence for an offset from the coastal airborne data is not so strong with only two features being displaced. Of a trough-peak-trough system next to the coast at 27.6^{o}N (fig 4.8) only the outer (most seaward) trough displays a definite offset. The peak also shows a small offset but this is much less definite. Such a small offset, though thought to mark a transform fault,may merely indicate a small bend in the magnetic pattern reflecting a similar bend in the initial continental fracture. There is, therefore, some doubt that the discontinuity marks a transform fault.

2. Another discontinuity occurs in the sea data near 26^{o}N, 35.4^{o}E where three features, two peaks and a trough, are displaced by about

7 km, this time in a right lateral sense. This offset is not related to any widening of the deep water. The discontinuity appears as a broad zone at the coast near 27^{o}N where the trough-peak-trough system is offset to the right by about 10 to 12 km. Thus the sense and amount of displacement of the anomalies at the discontinuity are approximately consistent on each set of data. A closer look at profiles 11 to 16 (fig 4.6) reveals that as this discontinuity is approached the amplitudes of the anomalies decrease. A similar effect has been reported near other transform faults (Matthews et al, 1965; Roberts and Whitmarsh, 1969).

3. Further south along the Arabian coast near 26.4^{o}N another discontinuity is observed. At this point only one continuous feature, a trough, is offset dextrally by about 10 km, although a peak to the east of this trough bends slightly producing an offset of about 4 to 5 km. Little support for the discontinuity can be found from the sea data which are poorly distributed in this area. Therefore the existence of the transform fault cannot be clearly demonstrated with the available data and its location should be considered tenuous.

4. A large zone bounded by two discontinuities appears near 25^{o}N, 36^{o}E in fig 4.8. In this zone the linear magnetic pattern trends transverse to the Red Sea trend and therefore simple offsets of the lines of peaks and troughs are not observed at either discontinuity. However the magnetic patterns north and south of the zone are displaced with respect to one another suggesting a transform fault may exist across this area. The pattern is displaced in a right lateral sense by about 50 km on both the air and sea

data although only 3 features, two troughs and a peak, display such an offset. The zone coincides with an area of deeper water within the main trough (see Laughton, 1970). The somewhat smooth appearance of the anomaly field south of the transverse zone makes correlations difficult and consequently the existence of a fault is not definite.

5. South of 25°N the sea data do not correlate well and few dominant peaks and troughs exist (fig 4.8). In the case of the coastal, airborne data correlations of the magnetic pattern between 24.5°N and 25.6°N are complicated by oblique trends which make the relationships between peaks and troughs unclear. A discontinuity near 25.3°N is, therefore, very tentative with only one feature, a trough, clearly offset. The offset is dextral by about 20 to 30 km but must be treated cautiously. More data are required in this area to clarify the magnetic pattern and identify any further offsets that may exist.

The offsets of the magnetic pattern described above are summarised in fig 4.11. In addition to the proposed transform faults based upon these offsets, a dashed line has been drawn in fig 4.11 between the end of the Magna block (Al Lisan) and the African coast which represents a southerly extension of the Dead Sea shear. This line coincides approximately with the northern limit of seafloor spreading obtained from the correlations in fig 4.8.

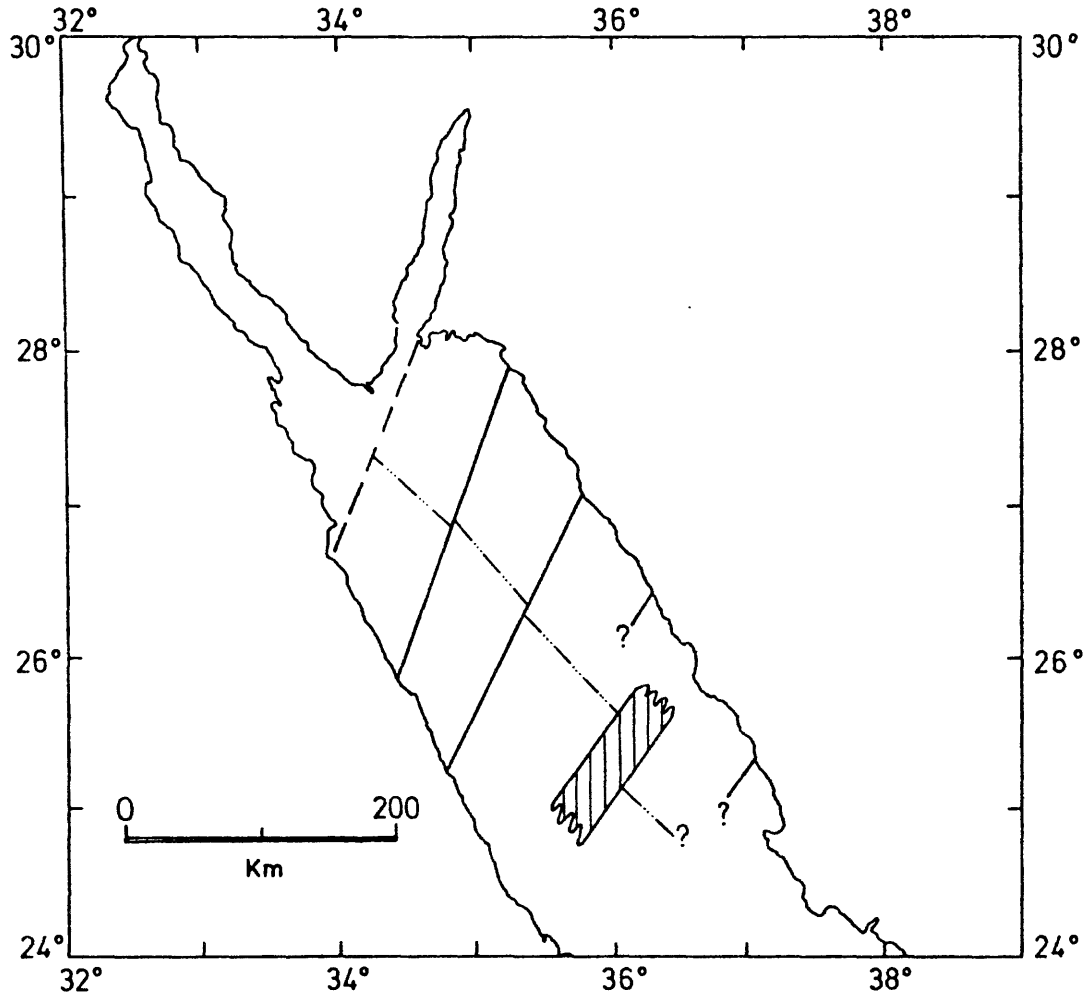

Figure 4.11 Location of transform faults inferred from offsets of the linear magnetic pattern (fig. 4.8). Shaded area at 25°N represents area of transverse magnetic anomalies. ——··· ——··· axis of symmetry of magnetic pattern; — — — — — southerly extension of the Dead Sea shear.

Unfortunately very little other geophysical or geological evidence is available to support the existence of the proposed transform faults. Only two earthquake epicentre determinations, other than those for Shadwan Is., are available but both lie well outside the deep water and appear to be associated with faulting near the coasts (Fairhead and Girdler, 1970). The positive Bouguer anomalies observed over much of the northern Red Sea (Allan, 1970) do not appear to be directly related to the proposed transform faults. Only that fault appearing near the zone of transverse magnetic anomalies coincides with a localised anomaly (1220 g.u.) and this is described more fully in section 4.6.2.

Azimuths of the proposed transform faults at 27^{o}N, 35^{o}E; 26^{o}N, 35.4^{o}E and 25^{o}N, 36^{o}E were measured using a best straight line fit along the discontinuities of the magnetic pattern. The values obtained are given in Table 4.1; also given are the azimuths predicted for such faults from the poles of rotation given by several authors. The measured azimuths are poorly defined owing to the sparse data coverage but agree reasonably well with those predicted, especially those of Freund (1970) and Girdler and Darracott (1972). Differences between the observed and predicted azimuths are small compared with the large errors found by fitting a maximum and minimum line to the discontinuities (i.e. 10^{o} or larger).

TABLE 4.1

Location and azimuths of proposed transform faults. Azimuths predicted for these faults from various poles of rotation are included for comparison

Location of transform fault		Azimuths for best fit to magnetic anomalies	Azimuths for McKenzie et al 1970	Azimuths for Freund 1970	Azimuths for Girdler & Darracott 1972
Lat.(^{o}N)	Long.(^{o}E)		(36.5^{o}N, 22.0^{o}E)	(32.0^{o}N, 22.0^{o}E)	(31.5^{o}N, 23^{o}E)
26.75	34.80	021^{o}	039^{o}	028^{o}	028^{o}
26.10	35.40	026^{o}	039^{o}	030^{o}	029^{o}
25.50	36.20	036^{o}	040^{o}	031^{o}	030^{o}

4.6.2 Zone of transverse magnetic anomalies

In fig. 4.8 there is a feature composed of a series of peaks and troughs at about 25^{o}N, 36^{o}E which trends in a direction N35^{o}, i.e. transverse to the Red Sea axis. This direction is approximately the same as the direction of motion between Arabia and Nubia suggested for this area by the poles of rotation given in Table 4.1. It seems possible, therefore, that the feature is caused by a transform fault. However, unlike those discussed above this fault has a well-defined magnetic expression: each trend line (fig. 4.8) is defined by 5 or 6 peaks or troughs. The zone is also much wider; approximately 40 km in a NW-SE direction.

Seven magnetic profiles which cross this feature are shown in fig. 4.12; each profile has been projected onto a line normal to the feature, i.e. N125^{o}, and the profiles stacked from NE (profile 1) to SW (profile 7). The amplitudes of the anomalies are impressive. Some are as large as 800 to 1000 nT which is four to five times greater than the amplitude of anomalies observed elsewhere in the northern Red Sea. A major peak-trough pair correlates well from profile to profile and several minor features appear on adjacent profiles.

Seismic reflection data from CHAIN cruise 43 indicate an acoustically opaque ridge which trends across the Red Sea (Knott et al, 1966) in the area of transverse magnetic anomalies. This ridge appears on Admiralty chart C6359 and trends NE-SW. The top of the ridge lies about 750 metres below sea level and has an irregular surface. The small arrows on profile 6 (fig. 4.12) indicate the approximate location and NW-SE extent of the ridge as defined by the seismic data. Its NE-SW extent is unknown but if the transverse

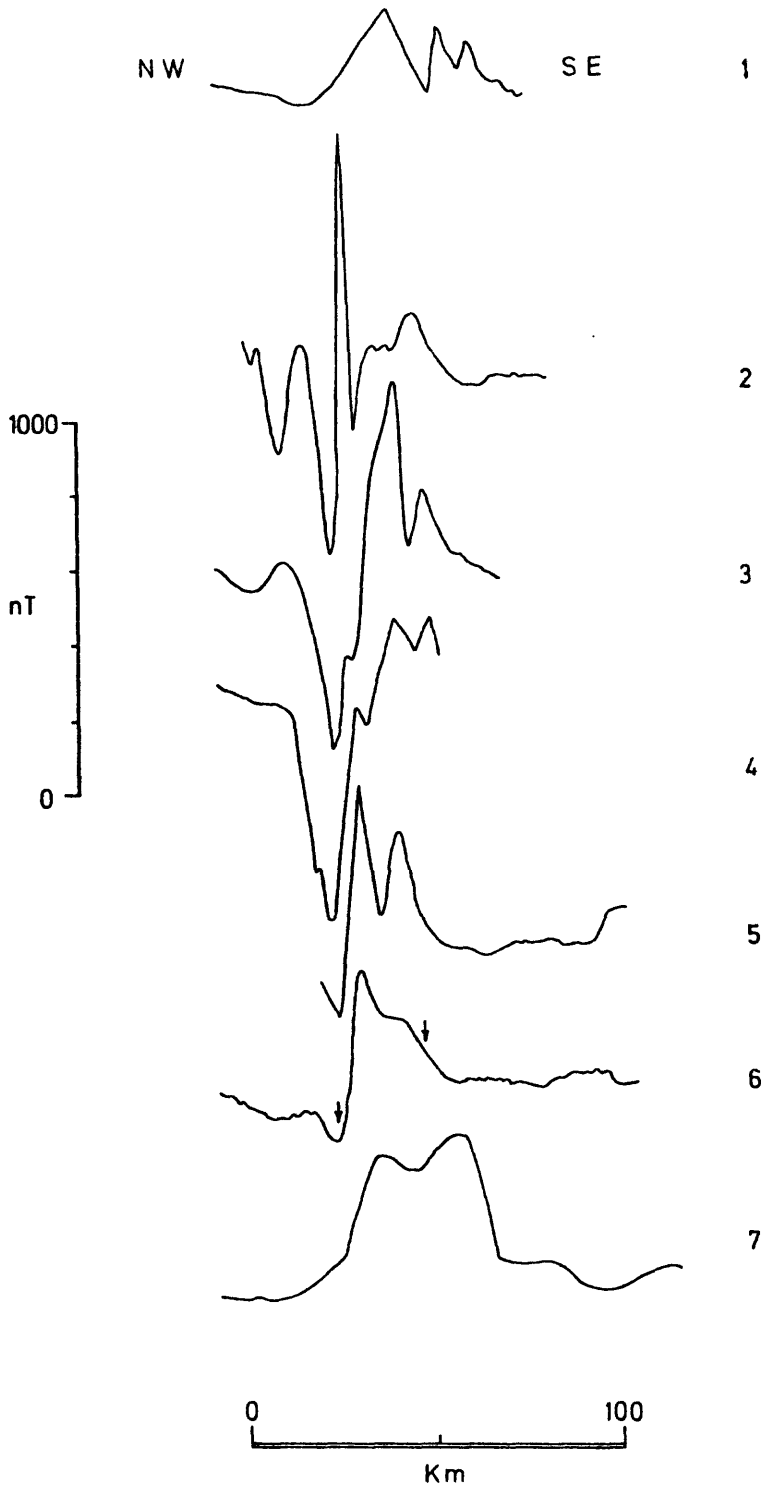

Figure 4.12 Magnetic profiles across the transverse magnetic feature near 25°N, 36°E shown in fig. 4.8. Profiles have been projected on to N125°, normal to the feature. Arrows on profile 6 indicate approximate position of ridge observed by CHAIN (cruise 43).

anomalies are caused by the ridge then it appears to extend to the limits of the sea data although profiles 1 and 7 (fig 4.12) have somewhat smaller amplitudes and longer wavelengths suggesting the ridge may be deeper at each end. The aeromagnetic data along the coast (fig 4.3) unfortunately do not cover the area north east of the ridge and so no estimate of its NE-SW extent is possible. The NW-SE width of the ridge visible on the seismic reflection data is about 25 km whilst the width of the zone of transverse magnetic anomalies is about 40 km. This suggests that the ridge probably extends some way beneath the sediments on either side. The profiles shown in fig 4.12 indicate the width of the ridge, as inferred from the anomalies, is not uniform varying from about 30 km on profile 6 to 40 to 50 km on profiles 2 and 3. The additional peaks and troughs on profiles 2, 3 and 4 suggest the feature has a more complicated structure at its north-east end.

In an attempt to simulate the anomalies shown in fig 4.12 several two-dimensional models of the ridge were computed using a block with a rectangular cross section composed of uniformly magnetised material. It is not possible to simulate all the observed anomalies using such models as the block gives only one peak and one trough (a trough to the north and a peak to the south for a normally magnetised body). In order to reproduce the anomalies using a body of uniform magnetisation it is necessary to choose an irregularly shaped block, varying the shape for each profile to obtain a fit with the observed data. Whilst the topography of the ridge is relatively rugged (Knott et al, 1966) such variations are too small to produce anomalies with

the correct wavelength but instead add high frequency noise to the broad anomaly over the block. It seems unlikely, therefore, that an irregularly shaped body provides a suitable source for the anomalies and that an irregularly magnetised body provides a better explanation.

As shown in sections 4.5.1 and 4.5.2, the area over which the transverse anomalies are observed is underlain by oceanic material. A realistic irregularly magnetised model is, therefore, more probably composed of normal and reversely magnetised blocks of the same material than variations in susceptibility due to materials of different compositions. This together with the offset of the magnetic pattern (section 4.6.1) suggests the ridge may have been formed at the site of a transform fault which has acted as a spreading centre and where, as a result, seafloor spreading anomalies have been generated. The similarity of the observed data (fig. 4.12) to seafloor spreading anomalies supports this explanation. Models of seafloor spreading over the past 5 My or so at between 0.2 to 0.4 cm y^{-1} were found to fit the data well, producing also the side peaks and troughs that are seen on some of the profiles. The widths and amplitudes of the major peaks and troughs match especially well in both models (fig. 4.13). Since the age of the model is compatible with the second, recent spreading phase (section 4.5.1) the anomalies have probably been produced by a transform fault 'leaking' in response to a change in the direction of motion of the Arabian and Nubian plates between the early and recent spreading.

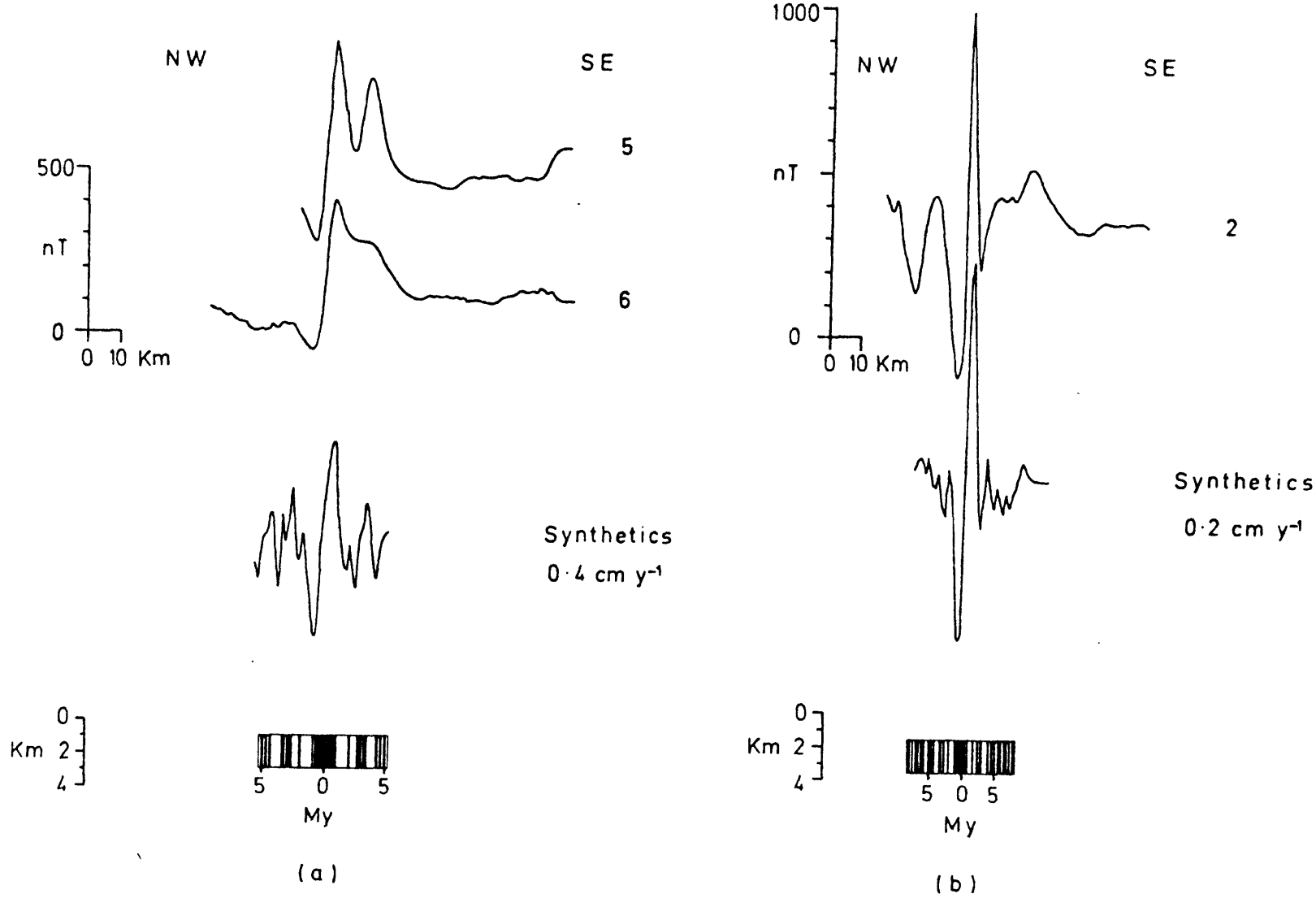

Figure 4.13 Seafloor spreading models of a leaky transform fault at 25°N, 36°E. Numbered profiles are observed data from fig. 4.12. Effective susceptibility of seafloor in (a) is 0.003 emu cm^{-3} (0.006 emu cm^{-3} for central body).

Difficulties were encountered in trying to reproduce the amplitudes of the observed anomalies (fig 4.12) using the generally accepted value of effective susceptibility for seafloor. Since the ridge lies only 750 metres below sea level as indicated by the seismic reflection data the anomalies expected are 2000 to 3000 nT compared with the 800 to 1100 nT anomalies that are observed. The effective susceptibility, therefore, has to be three times less than the generally accepted value. One possible explanation for this could be the influence of the small spreading rate on the mixing of the volcanic material. Since the intrusive and extrusive bodies are generally formed within a relatively narrow zone, e.g. at the Galapagos spreading centre current volcanic activity is confined to a zone 2 km wide over the centre (Klitgord and Mudie, 1974), slow spreading will mean that bodies of one magnetic polarity will not have spread outside of the intrusion zone when the field reverses. Thus fresh seafloor material will intrude into material of opposite polarity reducing the bulk effective susceptibility. Periods of constant field polarity last typically 0.3 to 0.4 My, therefore spreading rates of 0.2 to 0.4 cm y^{-1} will produce such a situation. This and other suggestions for the small amplitude anomalies are further discussed in Chapter 7.

Additional evidence for the presence of an intrusive body at 25^{o}N, 36^{o}E is available from gravity data. A positive, Bouguer gravity anomaly, maximum amplitude 1220 g.u. (122 mgal) (Allan, 1970), is observed over the zone indicating the ridge is composed of material denser than the surrounding sediments and this is compatible with oceanic basalt.

In a recent study of satellite photography and ground geology of Africa and the Arabian peninsula Abdel-Gawad (1969) describes two shear zones, one on each landmass, which are located at opposite ends of the zone of transverse anomalies. It has been suggested (Abdel Gawad, 1969) that these shear zones once formed a single continuous zone which implies that much of the Red Sea is oceanic. As sections 4.3, 4.4 and 4.5 have shown this is probably true, the shear belts may have been continuous prior to spreading. If so, the average direction of motion between the plates deduced from this must have been about $N35^{o}$.

4.6.3 Transform faults or transverse zones?

In section 4.6.1 the location of several transform faults were inferred from discontinuities in the magnetic pattern. These faults are narrow and appear to have no magnetic expression. In contrast, the transverse zone at $25^{o}N$ has a large area, about $40 \times 80\ km^2$, and a strong magnetic expression. If this latter feature has been produced by a 'leaky' transform fault the question arises why the other proposed transform faults have not also leaked. The most likely answer is that the offsets do not represent transform faults but merely bends in the original feature. Alternately there could be leaks at these faults which are not detected because of the poor data coverage. However such features appear to generate large anomalies (cf. fig 4.12) and these are not observed. The main difference between the proposed transform fault across the transverse zone and the others is the amount of offset, viz. 50 km compared with about 10 km. If the amount of leak is related to the offsets, smaller leaks would

be expected over the other faults. No evidence is available for such leaks. No leak would occur at the fault near 27°N, 35°E as the offset is sinistral. This is because the change in relative motion of the plates is such that only dextrally offset transform faults can 'leak'. Sinistral faults instead fracture across the old plate (cf.fig 4,Menard and Atwater, 1968) to produce a new transform fault. An alternative explanation is that the offsets represent transform faults and the transverse anomalies are not produced by a leaky transform fault. The results of Chapters 5 and 6, however, appear to preclude such an explanation.

4.7 Relation of magnetic anomalies to the deep holes

4.7.1 Location and properties of deep holes

North of 24°N, three deep holes or 'deeps' have been discovered: Oceanographer, Kebrit and Gypsum Deeps. All three are situated in deep water near the axis of the Red Sea. Oceanographer Deep is located at 26.29°N, 35.02°E and has a maximum recorded depth of 1446 metres with a free brine surface at 1364 metres. Kebrit and Gypsum Deeps are located south of Oceanographer Deep and close to one another near 24.7°N, 36.3°E. Kebrit Deep has a maximum recorded depth of 1550 metres and a brine surface at 1466 whilst Gypsum Deep with a maximum recorded depth of 1196 does not contain a brine pool. The physical and chemical properties of the water and sediments found in these deeps have been reported by several authors, e.g. Ostapoff, 1969; Backer and Schoell, 1972. Only Gypsum Deep contains important hydrothermal sediments being especially rich in iron. Temperature measurements are only available for Kebrit Deep;

these give a maximum temperature of 23.3°C which is a little higher than normal Red Sea water (~22°C) but much lower than the temperatures recorded in deeps in the central Red Sea (e.g. Atlantis II has a maximum temperature of 60°C).

4.7.2 Magnetic anomalies over the deep holes

None of the ships' tracks shown in fig. 4.2 cross directly over the deeps but several pass close by. The magnetic profiles for two tracks passing to the south of Oceanographer Deep are shown in fig. 4.14. Among the anomalies observed are several long wavelength (about 20 to 30 km) peaks and troughs, e.g. a broad trough at the eastern end of the ARAGONESE profile in fig. 4.14 of nearly 200 nT and wavelength about 25 km. However, near the deep the field is very smooth, with variations of less than 30 nT. The long wavelength anomalies are part of the magnetic pattern shown in fig. 4.8 which can be correlated over tens of kilometres. Consequently these anomalies are not directly related to the deep but as the deep lies within the pattern formed by the recent seafloor spreading,it must be younger than 5 My.

The magnetic profiles for tracks near Kebrit and Gypsum Deeps are shown in fig. 4.15. Two of the profiles, those of DALRYMPLE and CHAIN (cruise 43) pass north of the deeps. Anomalies on these are small, less than 50 nT, with a broad positive near Kebrit Deep and a shallow negative near Gypsum Deep. In the case of the CHAIN profile, short wavelength anomalies (1 to 2 km) are superimposed upon the smooth anomalies. The third profile, from ARAGONESE, shows a large, sharp positive anomaly (500 nT) very close to Kebrit Deep and a broad negative (100 nT), approximately 40 km long,

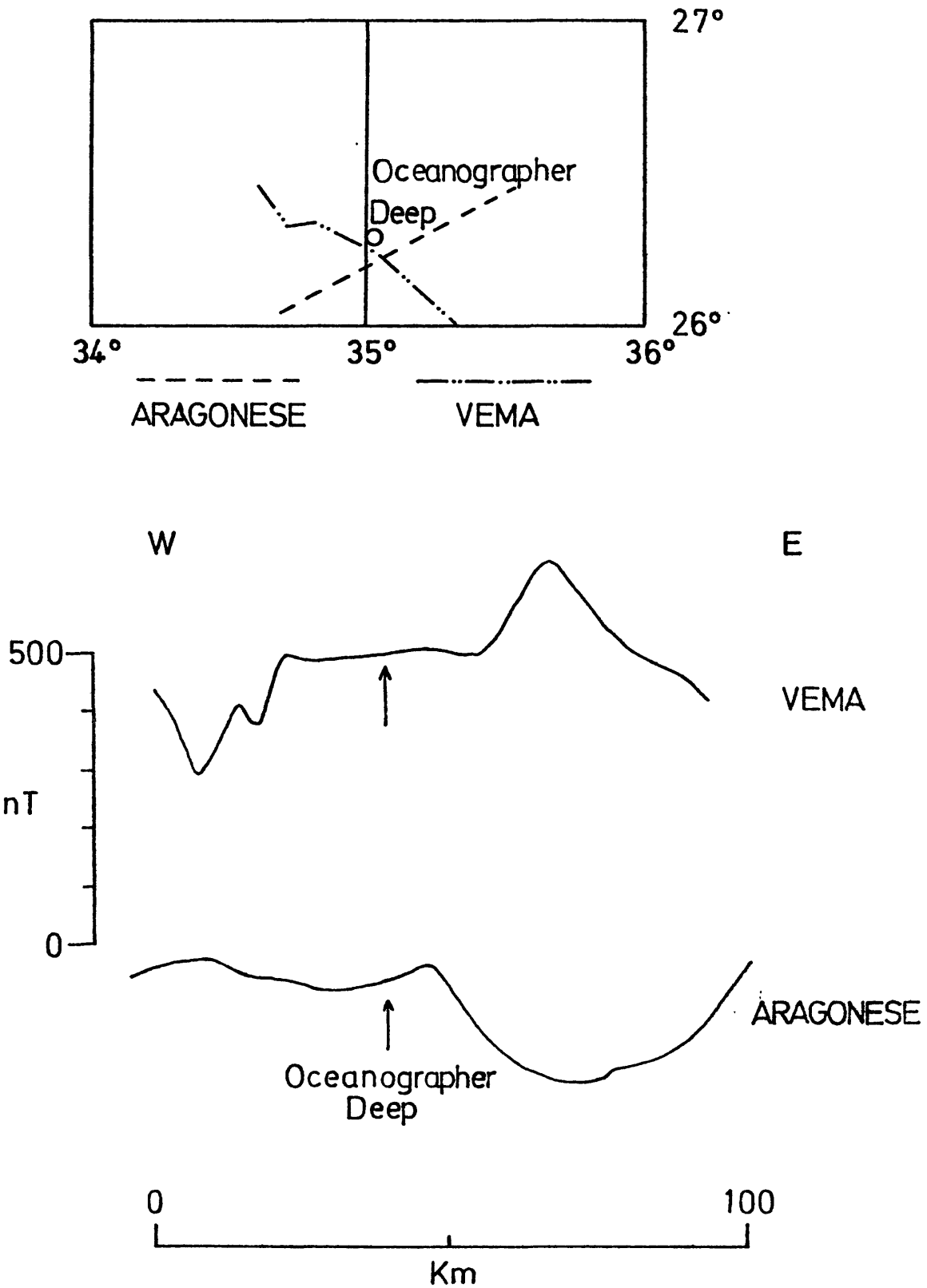

Figure 4.14 Magnetic profiles near Oceanographer Deep from research vessels VEMA and ARAGONESE. Arrows indicate approximate position of deep. Inset map shows location of profiles.

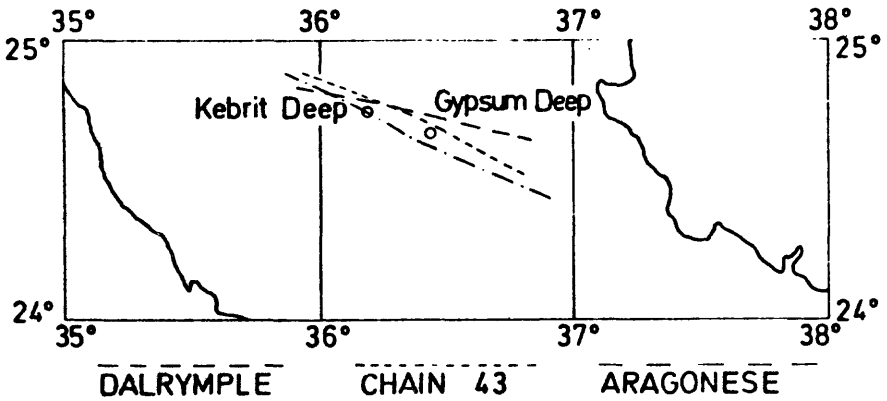

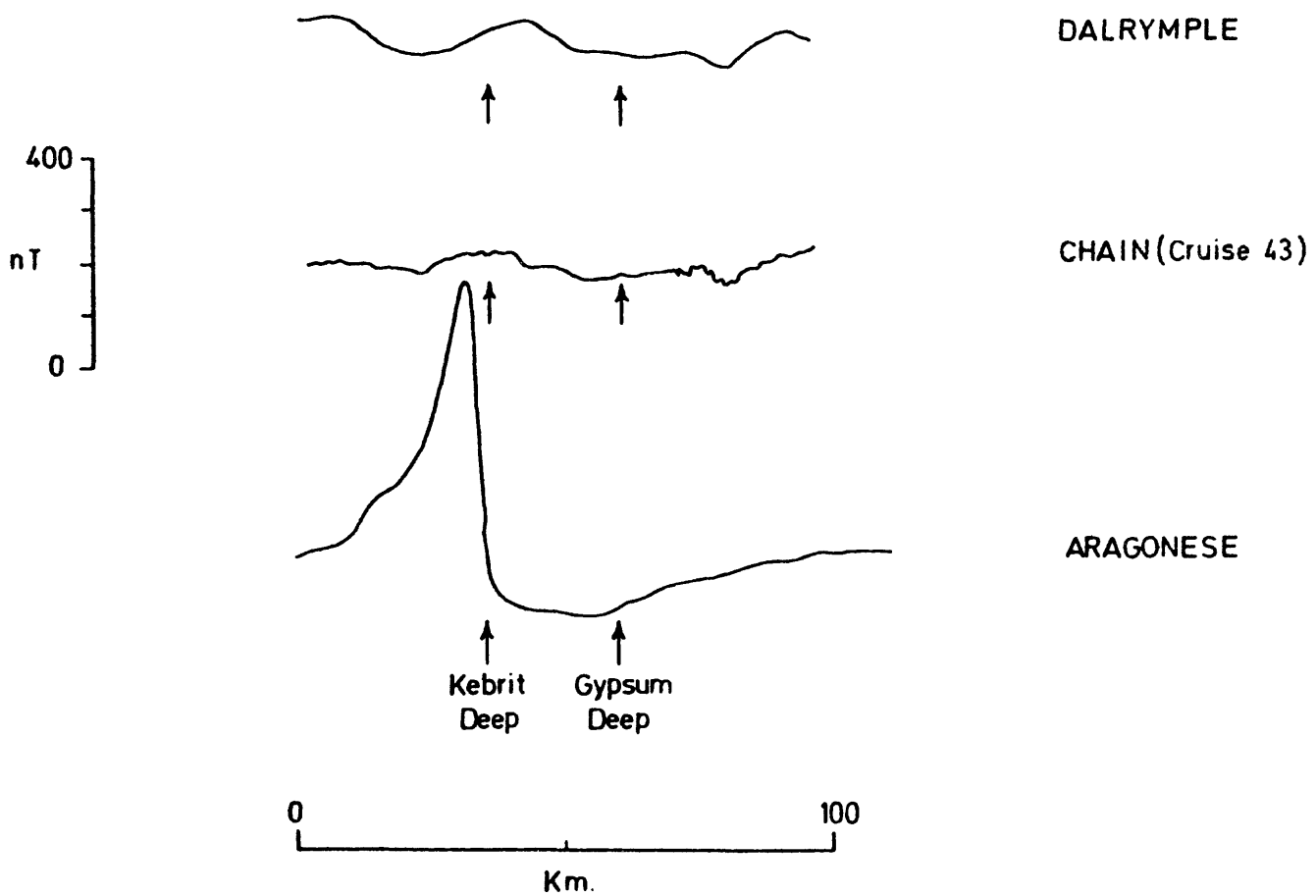

Figure 4.15 Magnetic profiles near Kebrit and Gypsum Deeps from research vessels DALRYMPLE, CHAIN (cruise 43) and ARAGONESE. Arrows indicate approximate position of deeps. Inset map shows location of profiles.

south of Gypsum Deep. To the south east of this negative, the profile is smooth and flat. The impressive peak appears to be directly related to Kebrit Deep. It is possible that strong, localised anomalies are associated with each of the deeps but that in the case of Oceanographer and Gypsum Deeps the available tracks pass too far away to detect them. Certainly the amplitude of the peak near Kebrit Deep (fig. 4.15) must decrease rapidly if the positive observed on the DALRYMPLE profile, 4 km away, is the same feature. Unfortunately insufficient data are currently available to determine if the magnetic expressions of the deeps are similar but the 3-dimensional nature of the deeps suggests that any anomalies associated with them will be very localised. Because of this, no model can be constructed from the magnetic data for Oceanographer Deep. A model of Kebrit and Gypsum Deeps may, however, be constructed using the single profile from ARAGONESE.

4.7.3 Simple model of Kebrit and Gypsum Deeps

A 3-dimensional model of Kebrit and Gypsum Deeps has been computed using volcanic bodies as the magnetic sources. The model, (fig. 4.16), has two bodies, one beneath each deep, which have either intruded into the overlying evaporites or have been covered by the evaporites during or after deposition, possibly by flowage of the evaporites. The model was calculated using a computer program based upon the method of Talwani (1965). In this the shapes of the bodies are specified and the directions of the polarization vectors computed using a least squares fit of the calculated field to the observed data.

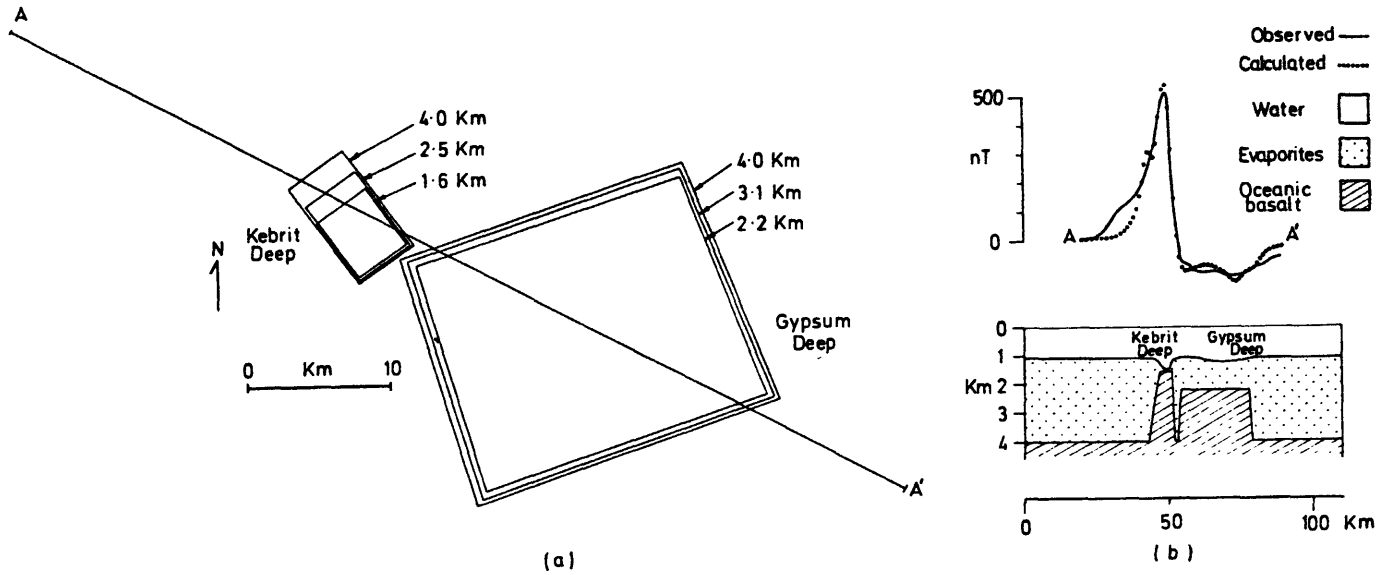

Figure 4.16 3-dimensional magnetic model of Kebrit and Gypsum Deeps. (a) Plan view of bodies used to simulate anomalies observed on ARAGONESE profile (fig.4.15). (b) Elevation view along profile AA' showing observed and calculated anomalies. Magnetic parameters for the bodies are: Kebrit— DIP= -27^{o}, DEC. = 234^{o}, Intensity of magnetisation = 0.009 emu cm^{-3}.
Gypsum—DIP= 6^{o}, DEC. = 44^{o}, Intensity of magnetisation = 0.004 emu cm^{-3}.

Unfortunately there are few constraints on the shapes of the bodies and the model must be considered as one of many possible solutions. Only two parameters can be assumed with any confidence; (i) the shallowest part of each body (i.e. top contour) is located directly beneath the appropriate deep and (ii) the effective susceptibility is approximately that of oceanic basalt. The depths to the upper surfaces of the bodies are limited on the one hand by the depths of the holes themselves and on the other by the effective susceptibility of the magnetic material. The base of each body is assumed to be 4.0 km, i.e. the depth of the recent seafloor given in section 4.5.1 and fig 4.9. This depth may be too shallow as the linear seafloor spreading pattern expected of seafloor at this depth is not observed. However a seismic refraction profile nearby (# 183, figs. 4.1) indicates a depth of 6 km for material whose seismic velocity is 7.34 km sec^{-1}. The refraction data show a 5 km thick layer of 3.92 kms^{-1} material, presumably evaporites but no oceanic layer 2 velocities (viz. 4.5 to 5.5 km s^{-1}). The 7.34 km sec^{-1} is assumed to represent the low velocity upper mantle layer found under oceanic ridges. Thus, if a 2 km layer of basalt overlies this as is commonly assumed, this would give a depth of the upper surface of the magnetic seafloor of about 4 km.

The polarization vectors obtained by minimising the variance of the residuals suggest different polarities for each body: that underlying Kebrit Deep is reversely magnetised whilst that beneath Gypsum Deep is normally magnetised. This difference is not difficult to explain as the volcanic bodies were probably formed at different times and therefore correspond

to different parts of the reversal scale. Also if the bodies were formed in a comparatively short time ($< 10^4$ y) the effects of secular variation may not be entirely averaged out and declinations and inclinations other than those predicted for an axial dipole may be present. Such a possibility could explain the calculated directions for the vectors (fig 4.16). As Kebrit Deep is located almost directly over the deep water axis, the body should be normally magnetised to be consistent with the seafloor spreading model but this was not found to be true. For Gypsum Deep, situated approximately 17 km from the axis, the polarity predicted from the seafloor spreading is less certain. The body beneath the deep is large and its relationship to the linear seafloor bodies is not known, consequently it may have been formed during any normal polarity interval between 2 and 3 My.

The amplitude of the observed anomalies require shallow, strongly magnetised sources and for this reason buried seamounts rather than depressions in the seafloor have been used. If the seafloor was shallow in this area large anomalies forming a linear seafloor spreading pattern would be present but these are not observed. It appears more likely that the spreading at depth gave rise to localised injections of oceanic basalt into the base of the evaporites producing slumping of the salt and/or the re-dissolving of the evaporites into solution in response to the increased temperature. The hot volcanic material could, therefore, have produced both the depression and the brine pool. In the case of Gypsum Deep, 17 km from the spreading axis; the heat may have subsided and the salt been precipitated and this could account for the absence of a brine pool in this deep.

CHAPTER FIVE

THE RED SEA BETWEEN 18°N AND 24°N

5.1 Relevant geophysical data

Several marine geophysical surveys have been carried out between 18°N and 24°N the most recent of which have been concentrated in the region of the deep brine pools (Scheuch, 1973; Searle and Ross, 1975).

Forty nine heat flow measurements have been made (Sclater, 1966; Erickson and Simmons, 1969; Girdler, 1970a; Haenel, 1972; Scheuch, 1973; Girdler et al, 1974; Evans and Tammemagi, 1974), of which all but five are higher, some being many times greater, than the world mean of $\cdot 59 mWm^{-2}$. Forty four measurements were made in deep water areas, twenty-three of these in the deeps, and five along the coastal and offshore areas of Africa (fig. 1.4). The latter measurements are surprisingly high and indicate the entire width of the Red Sea is associated with anomalously high heat flow. The heat flow values from the deeps, vary somewhat suggesting different thermal conditions of the crust beneath.

Gravity measurements (Plaumann, 1963; Allan, et al, 1964) indicate that the axial trough and parts of the main trough are associated with a large, positive Bouguer anomaly ($\sim$ 1000 g.u.) with localised larger values of 1400 to 1500 g.u. (fig 1.2). Somewhat smaller, positive anomalies (500 to 600 g.u.) are found over the main trough although this area has been relatively poorly covered. The area covered by data is large but the density of tracks is such that a detailed structural picture is not yet possible.

Integration of the recently collected data from CHAIN Cruise 100 (1971) into the existing maps will, no doubt, result in a more detailed picture.

Seismic reflection studies (Knott, et al, 1966; Phillips and Ross, 1970; Ross and Schlee, 1973) have detected the S-reflector beneath the main trough in each area covered. The reflector is absent from most parts of the axial trough but has been found in certain areas (see fig. 3 , Ross and Schlee, 1973). The seismic refraction data available include four profiles from VEMA and ATLANTIS (1958) and a detailed survey by the ASSAB at 22.5^{o}N, 37^{o}E comprising thirteen profiles, many of which were reversed. The profile locations are shown in fig. 5.1. Crustal models based upon these data have been described by Drake and Girdler, (1964) and Tramontini and Davies, (1969). All profiles except nos. 12 and 182 gave similar results. Three layers were found; a topmost layer with seismic velocities of 1.7 km sec^{-1} to 3.0 km sec^{-1} varying in thickness from about 0.1 km (profile no. 180)to 0.39 km (profile no. 4). A second layer with velocities of 3.0 to 5.0 km sec^{-1} between 3 and 5 km thick and a third layer with a velocity of 6.6 to 7.0 km sec^{-1} which is typical of that found for oceanic layer 3 Profiles 12 and 182 gave a third layer velocity of 6.1 km sec^{-1} which is more typical of continental basement.

Also shown in fig. 5.1 is the distribution of earthquake epicentres : solid circles represent epicentres of events occurring since the introduction of the WWSSN in 1963, open circles represent events prior to 1963. Many events are grouped near 19.8^{o}N, 38.8^{o}E where an earthquake swarm started on 13th March 1967. Detailed analyses including first motion studies

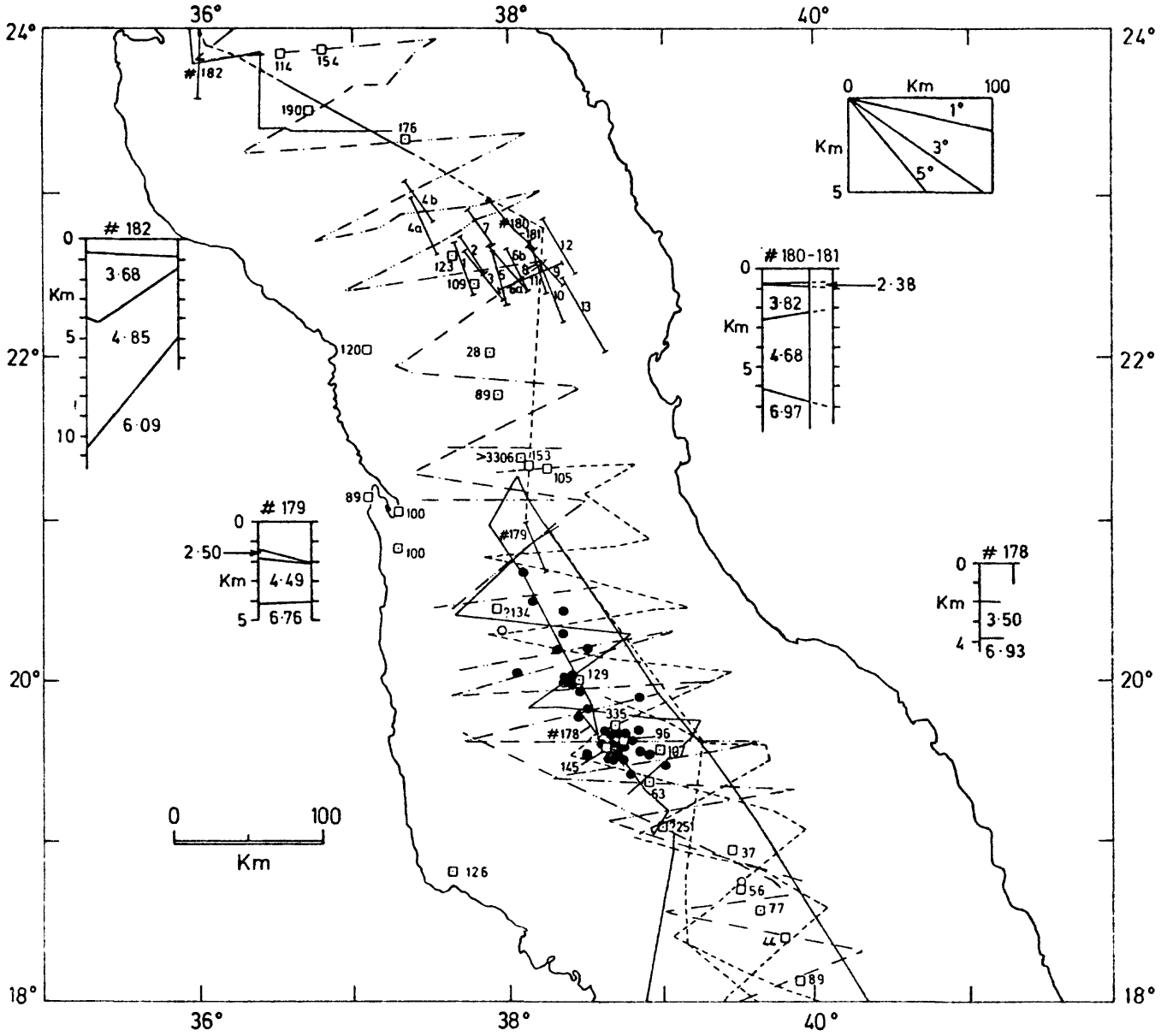

Figure 5.1 Geophysical data (excluding magnetic) available for the Red Sea between 18°N and 24°N. □ heat flow measurement(values in mW m^{-2});O and ● earthquake epicentres before 1963 and since 1963 respectively. ⊢——⊣ seismic refraction profiles; ——— seismic reflection profiles; —— · · · —— gravity profiles; — — — — seismic reflection and gravity profiles. Seismic velocities in crustal models are in km s^{-1}.

of one of these earthquakes have been made by Fairhead and Girdler (1970), and McKenzie et al (1970) which gave dextral shear along N53^{o} (Fairhead and Girdler 1970) or N68^{o} (McKenzie et al, 1970). Seismicity elsewhere in the area is restricted to south of 20.6^{o}N. This does not, however, preclude small magnitude earthquakes occurring north of 20.6^{o}N which have not been detected by the WWSSN. Fairhead and Girdler (1970) have shown that only events with magnitudes $\geqslant$ 5.0 are well determined.

5.2 Distribution of magnetic data

5.2.1. Sea data

Ships' tracks for which magnetic data are available in the central Red Sea between 18^{o}N and 24^{o}N are shown in fig 5.2. Two vessels, CHAIN during cruise 100, and GLOMAR CHALLENGER on Leg 23, used satellite navigation giving good positional accuracy of about 100 to 200 metres. The remaining vessels relied upon celestial fixes and radar giving an overall accuracy of about 1 to 2 km but occasionally larger. Coverage of the area is good especially between 18^{o}N and 22^{o}N: north of 22^{o}N the tracks are somewhat more widely spaced (approximately 25 km). In general the tracks are over the deeper water with the shallow shelves only partly covered. This is particularly evident south of 20^{o}N where the shelves widen and the E-W extent of the data is more restricted. Only one track, profile DD' in fig 5.2, extends across most of the Red Sea reaching to within 15 to 20 km of the coast on either side.

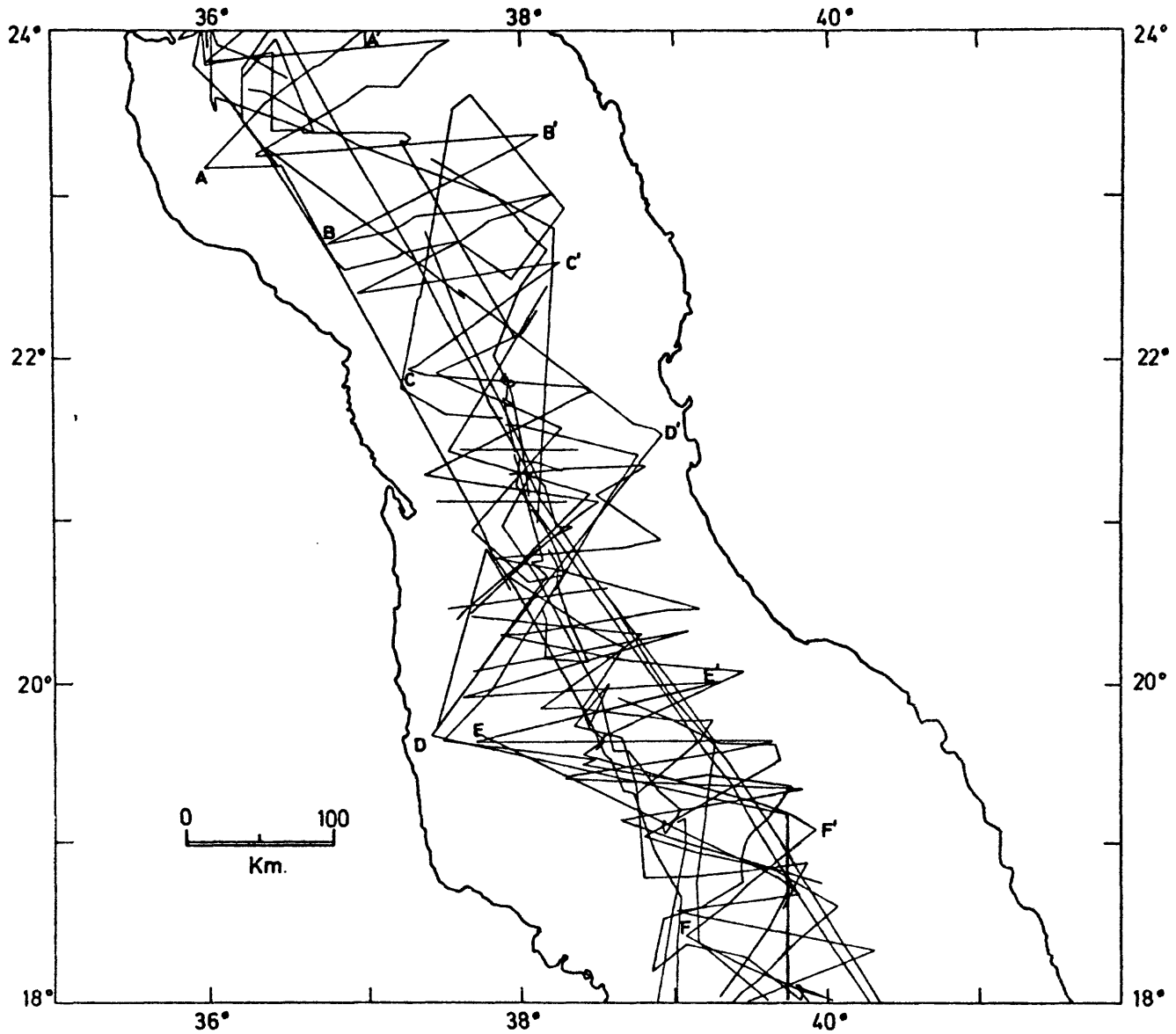

Figure 5.2 Tracks of research vessels between 18°N and 24°N for which magnetic data are available. Lettered tracks (AA', BB' etc.) indicate the location of magnetic profiles shown in fig. 5.4.

The tracks are oriented in many directions (fig. 5.2) although a majority are approximately transverse to the Red Sea axis. Two long tracks trending approximately NNW-SSE cross the entire area from north to south. E-W, ENE-WSW and ESE-WNW tracks predominate south of 21°N. Between 21°N and 24°N fewer ESE-WNW tracks are present but two, long (200 to 300 km) NW-SE tracks cross the area. Data from the detailed survey of the Chain, Discovery and Atlantis II Deeps by CHAIN during cruise 100 are not included but are reported by Searle and Ross (1975).

5.2.2 Air data

Two extensive aeromagnetic surveys have been flown along the Arabian coast between 18°N and 24°N; the Yanbu survey between 22.3°N and 24.6°N and the Al Lith survey between 19°N and 20.4°N (fig. 5.3). Each was flown at a constant height of 609 metres (2000 feet) A.M.S.L. with a flight direction of approximately N60° and a line spacing of 3 km. In addition, there are eight long profiles flown in an approximately E-W direction from the Arabian coast to the African coast near 21°N. These profiles (L1 to L8 in fig. 5.3), which have been discussed by Kabbani (1970), are about 7 km apart and were flown at 300 metres A.M.S.L. A further eight coast to coast profiles, four at an elevation of 305 metres (1000 feet), A1 to A4 (fig. 5.3), and four at 3,658 metres (12000 feet), B1 to B4, were flown by Project Magnet between 17°N and 19°N. These have a flight direction of N 60° and are irregularly spaced (approximately 10 to 30 km).

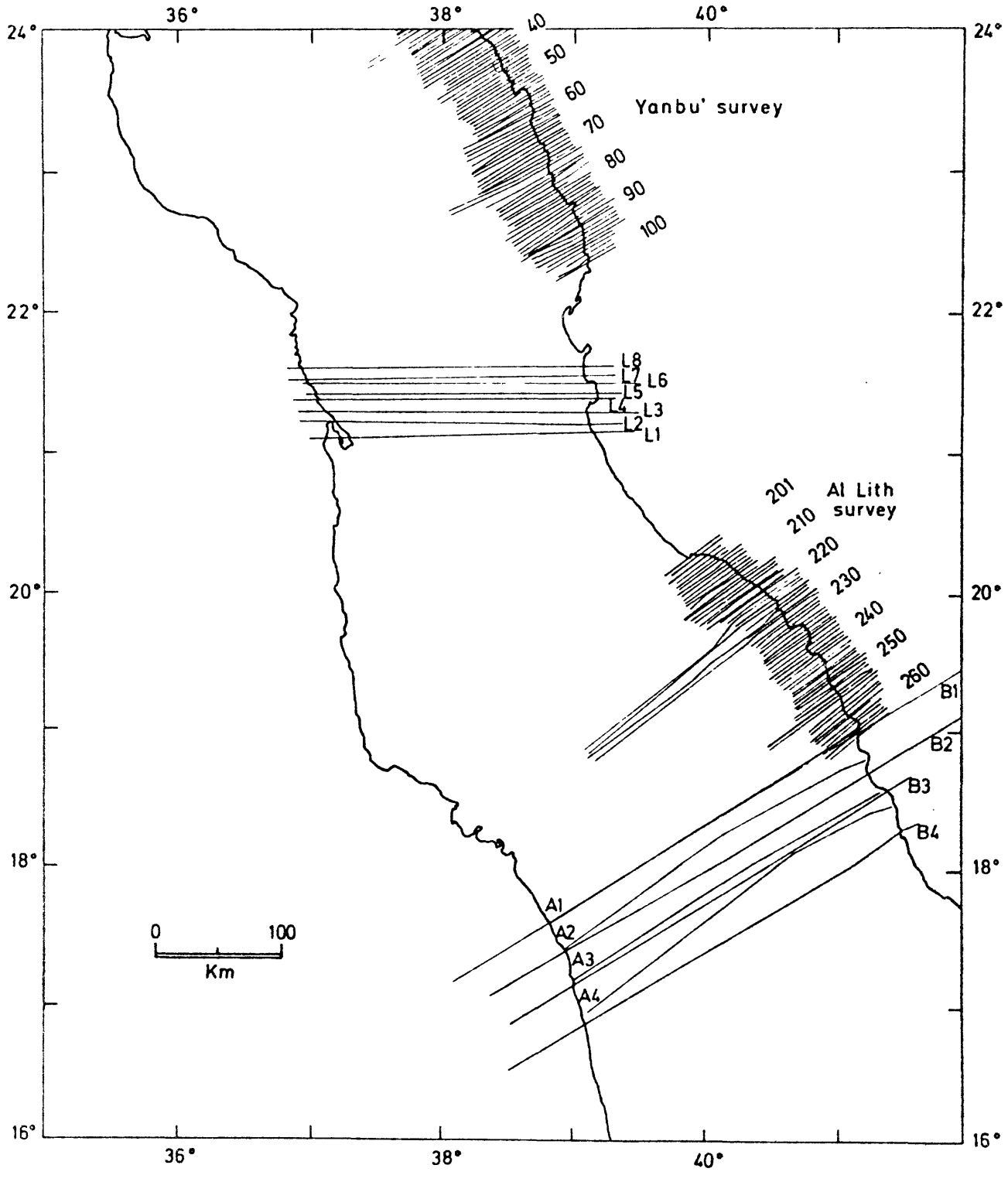

Figure 5.3 Location of flight lines of aeromagnetic surveys between 16°N and 24°N.

Each survey used a Doppler navigational system resulting in positional accuracies of better than ± 0.1 km over land. However as there are few islands in the area the Doppler navigator must rely upon memory over sea areas. Furthermore the effectiveness of the navigational system is directly dependant on the state of the sea; a smooth sea returns a reduced signal resulting in poor positioning. Hence positional errors of about 1 km are probably present over the sea. The coverage of the Arabian coast and immediate offshore areas provided by these surveys is good although over two areas, one between 20.4^{o}N and 21.1^{o}N, the other between 21.7^{o}N and 22.3^{o}N, there are no data. Data from an aeromagnetic survey along the African coast between approximately 18^{o}N and 20^{o}N (Conoco), are not discussed but are described in detail by Styles (in prep.)

5.3 Description of magnetic anomalies

5.3.1 Wavelength, amplitude and distribution of anomalies

In a similar manner to that described in section 4.3.1. separation of the anomalies according to their wavelength and amplitude produces three zones:

(1) Anomalies over the deep water are usually large (approximately 1000 nT) with short wavelengths, typically 5 to 10 km (peak to trough), although profiles AA' and BB' (fig. 5.4) show that between 23^{o}N and 24^{o}N the amplitudes are somewhat smaller ($\sim$ 300 nT) similar to those observed in the

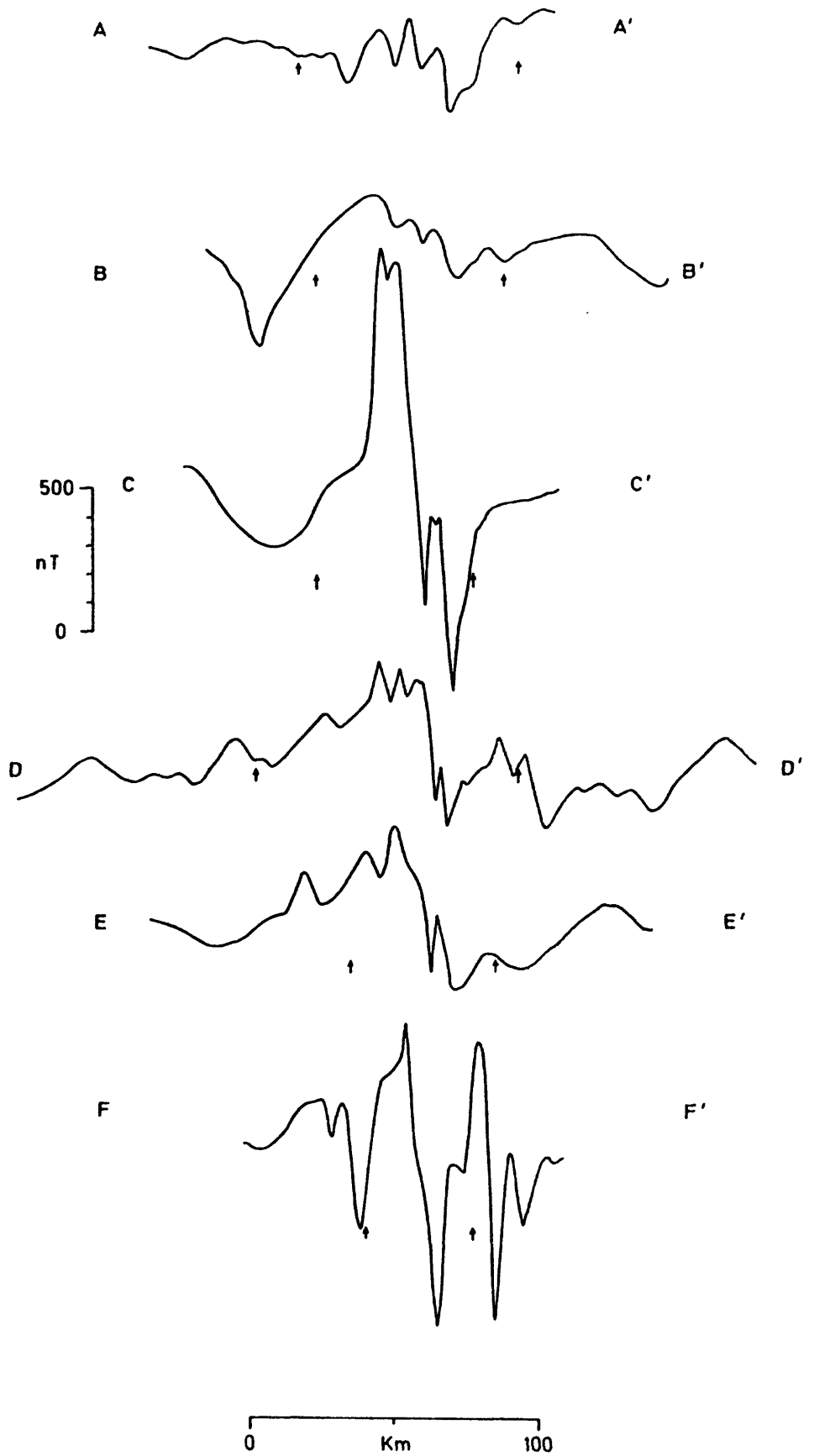

Figure 5.4 Magnetic profiles over central Red Sea. Location of profiles given in fig. 5.2. Arrows indicate position of 500 fathom contour.

northern Red Sea. The large anomalies are first recorded at about 22.6°N slightly south of the first appearance of the deep axial trough at approximately 24°N (Drake and Girdler, 1964). South of 22.6°N the large anomalies are observed over the deep water on many but not all profiles. The anomalies occur mainly over the deep water but are sometimes also observed over parts of the main trough (e.g. profile FF' in fig 5.4). A possible explanation of this has been given by Girdler and Whitmarsh (1974).

(2) Smooth, long wavelength (20 to 30 km) anomalies of about 100 to 300 nT are found over the main trough, shelves and parts of the coastal plain (figs. 5.4 to 5.8). These are remarkably uniform and tend to correlate well (see section 5.3.2), in contrast to the variability of the larger anomalies over the deep water. Profiles 222, 224, 226 and 228 from the A1 Lith survey (fig. 5.7) demonstrate clearly the change in character from the larger to the smaller anomalies.

(3) At the eastern end of the airborne profiles in figs. 5.5 to 5.7 the anomalies are typically 10 to 100 nT but have variable amplitudes and short wavelengths of 1 to 5 km. They are similar to the high frequency anomalies observed in the northern Red Sea at the eastern end of fig. 4.6. The anomalies do not appear in the sea data nor in the airborne profiles shown in fig 5.8. Four of these profiles (B1 to B4), however, are flown high over land, viz. 3,685 metres (12000 feet), thereby filtering out any short wavelength anomalies. Profiles A1 to A4 (fig 5.8) do not overfly the land but indicate the high frequency anomalies are not observed over offshore areas south of 19°N.

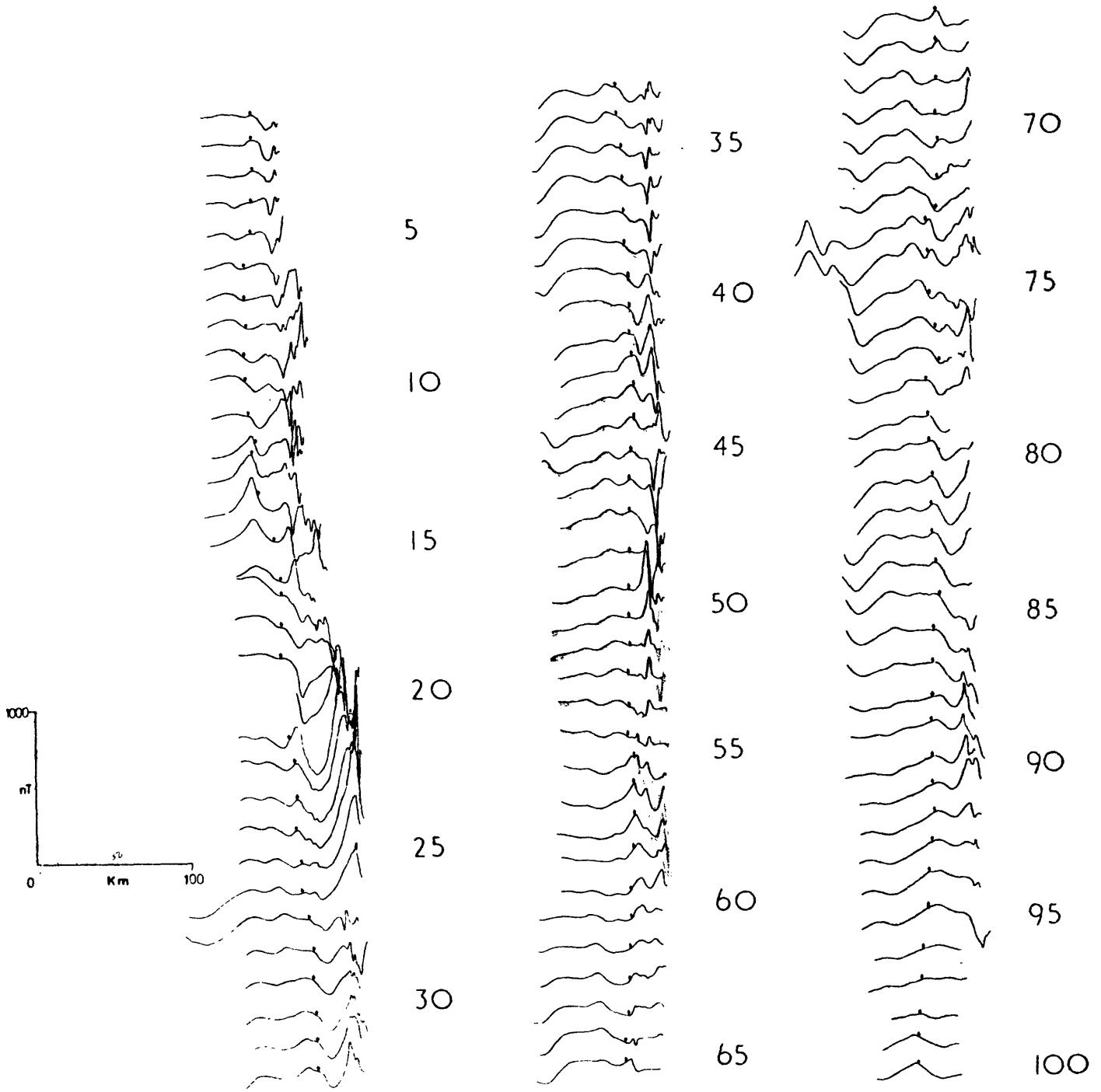

Figure 5.5 Aeromagnetic profiles from Yanbu' survey. Location of profiles shown in fig. 5.3. Small arrows indicate approximate position of Arabian coast. All profiles flown at 609 metres (2000 ft.).

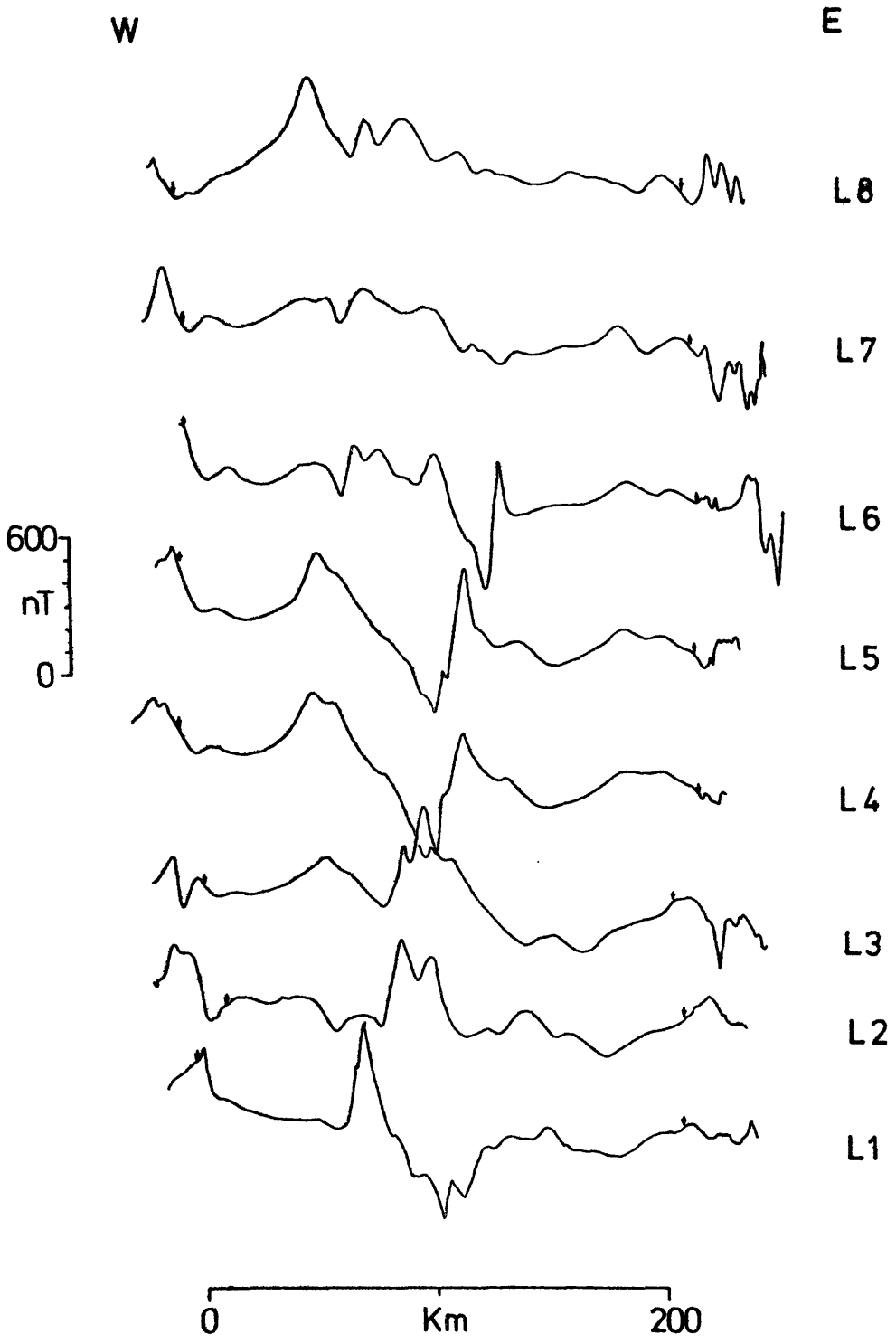

Figure 5.6 Coast to coast aeromagnetic profiles between 21°N and 21.5°N. Location of profiles shown in fig. 5.3. Arrows indicate positions of coasts. All profiles flown at 300 metres.

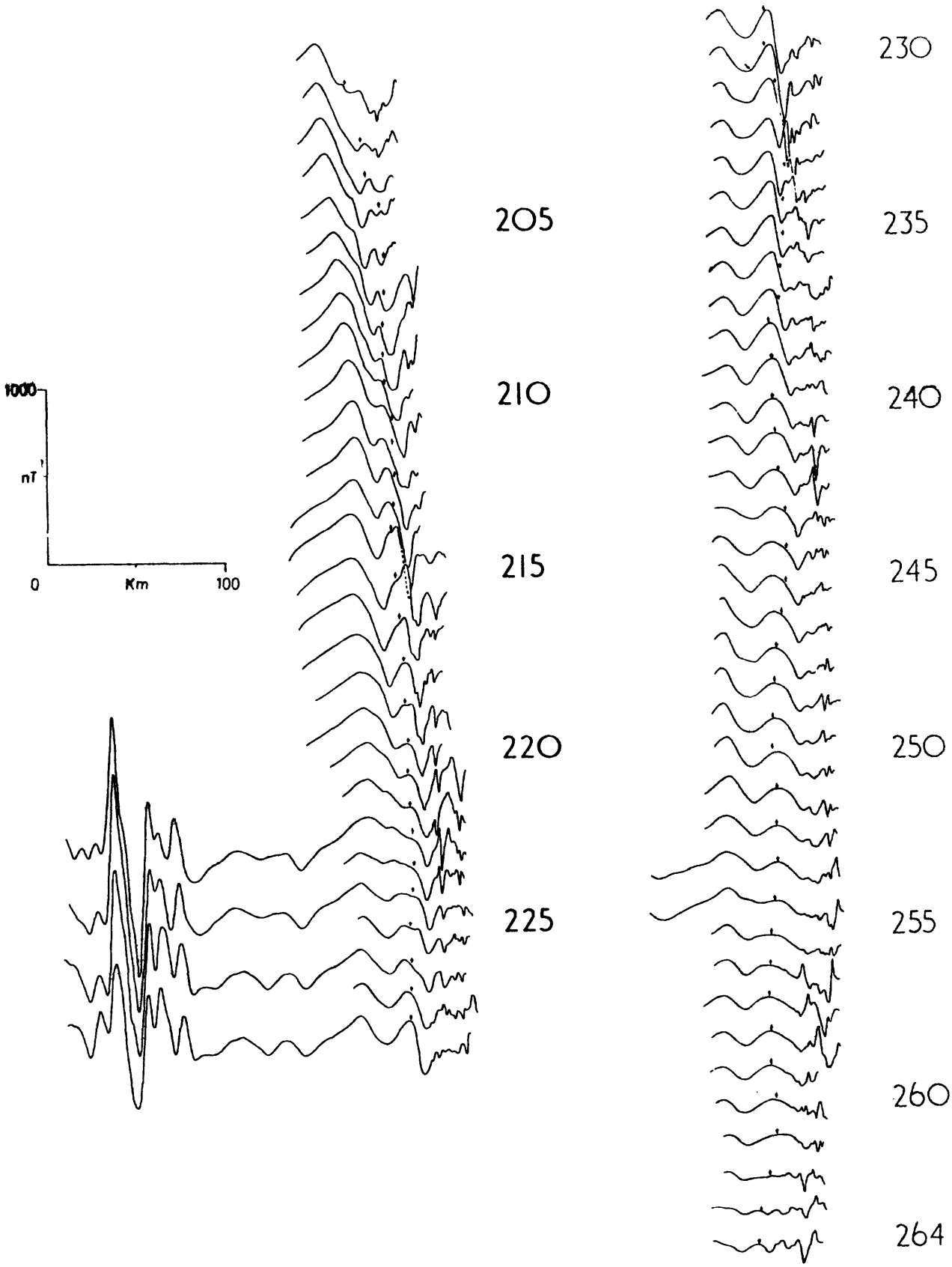

Figure 5.7 Aeromagnetic profiles from Al Lith survey. Location of profiles shown in figure 5.3. Small arrows indicate approximate position of Arabian coast. All profiles flown at 609 metres (2000 ft.).

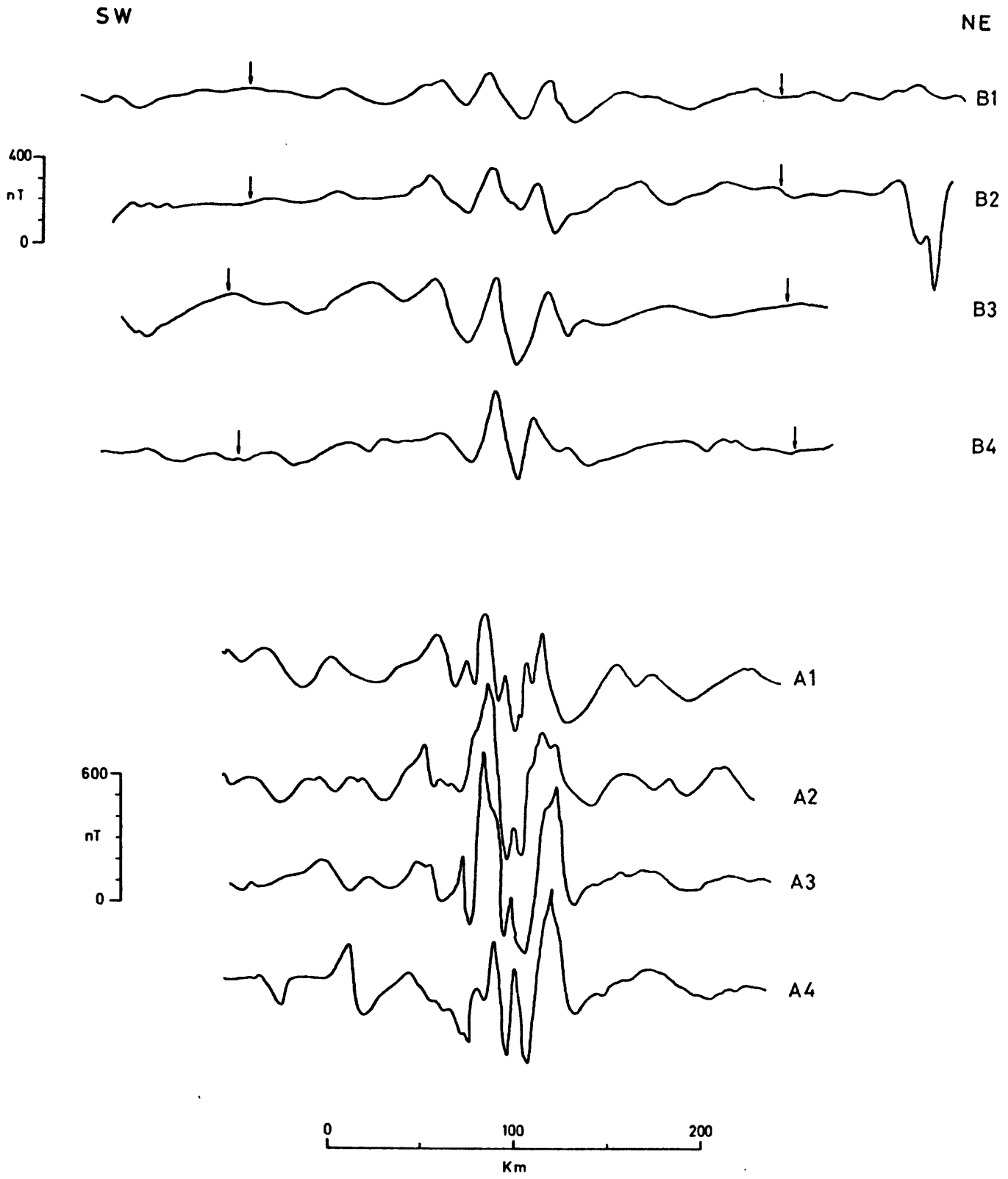

Figure 5.8 Project Magnet aeromagnetic profiles between 17°N and 19°N. Location of profiles shown in fig. 5.3. Arrows indicate position of coasts. Profiles A1 to A4 flown at 304 metres (1000 feet), B1 to B4 at 3658 metres (12000 feet).

5.3.2 Correlations of the anomalies

To study the continuity of the anomalies the locations of dominant peaks and troughs from both sea and air data were transferred to the map shown in fig. 5.9. Correlations of these peaks and troughs were made and the corresponding features in fig. 5.9 joined by solid lines. Tentative correlations are represented by light dashed lines. The flight line spacing of the Al Lith and Yanbu' surveys is such that each peak and trough cannot be shown without cluttering the diagram, consequently only features from approximately every fourth line are shown. In general, correlations of the large anomalies over the deep water areas are not good although in some areas they are excellent. The large variations in amplitude and shape make reliable correlations difficult especially north of 22^{o}N where there is a poorer distribution of tracks (fig. 5.2). Examples of the correlations obtained are shown in figs 5.10 to 5.12. In fig. 5.10, several profiles between 18^{o}N and 19.5^{o}N are shown which display major features that correlate remarkably well, including an approximately 1000 nT peak-trough pair that appears on each profile. Several minor features also correlate but do not appear on all profiles. These anomalies form a linear pattern which trends parallel to the deep water axis (dotted line in fig. 5.9) until 19.5^{o}N at which point several of the dominant features appear to correlate better in an approximately NE-SW direction. Several profiles north of this transverse zone are shown in fig. 5.11; correlations of features on these are not as good as those in fig. 5.10. The anomaly amplitudes are smaller and fewer features are observed although a dominant peak-trough pair appears on all but the most southerly profile. The correlations may be followed

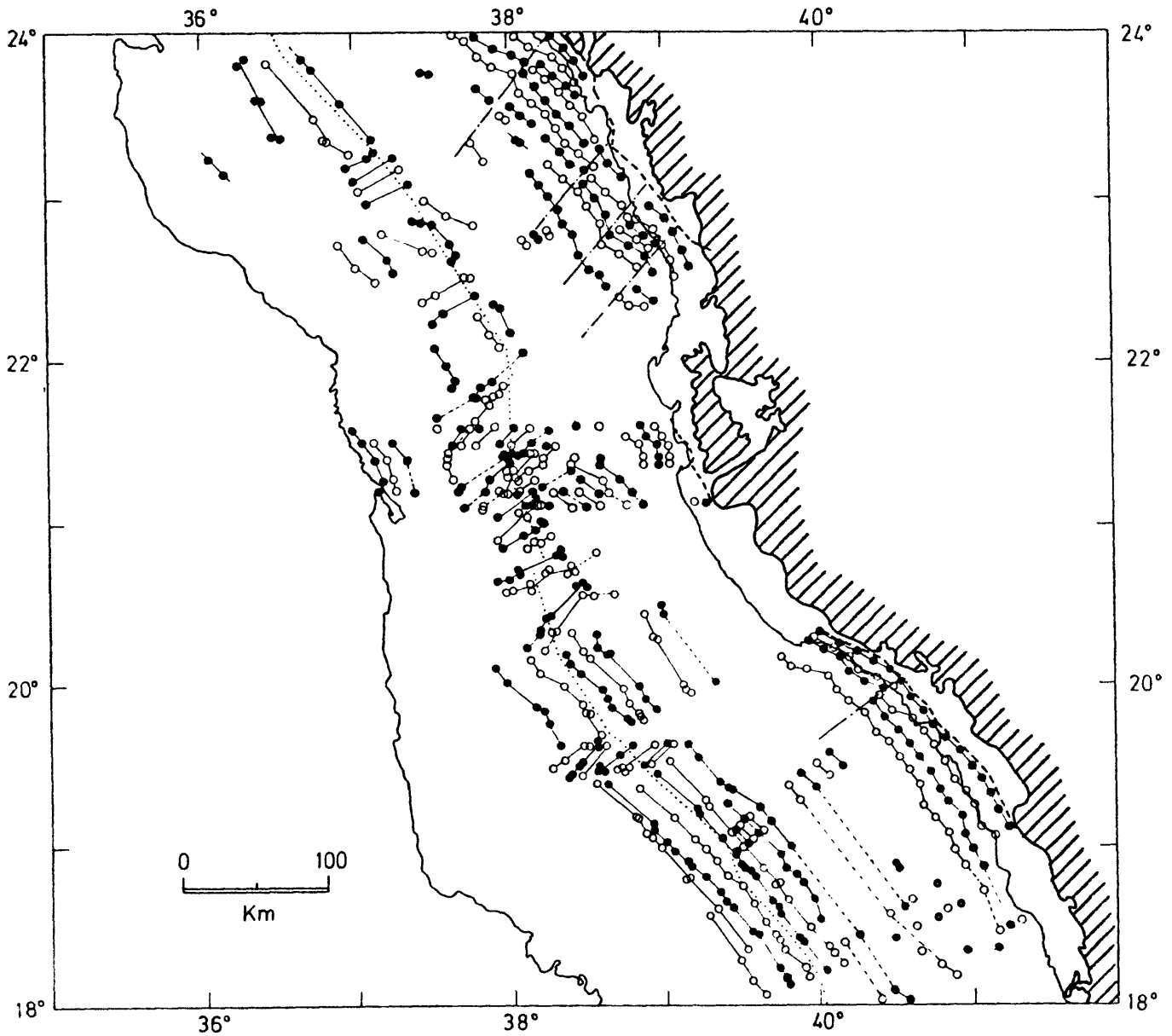

Figure 5.9 Location of dominant peaks, O (positive anomalies) and troughs, ● (negative anomalies). ····· deep water axis; ——·—— discontinuities in magnetic pattern. Heavy shaded line represents seaward limit of mapped Pre-Cambrian; heavy dashed line is seaward limit of high frequency anomalies. Firm correlations of features shown as solid lines; tentative correlations as light dashed lines.

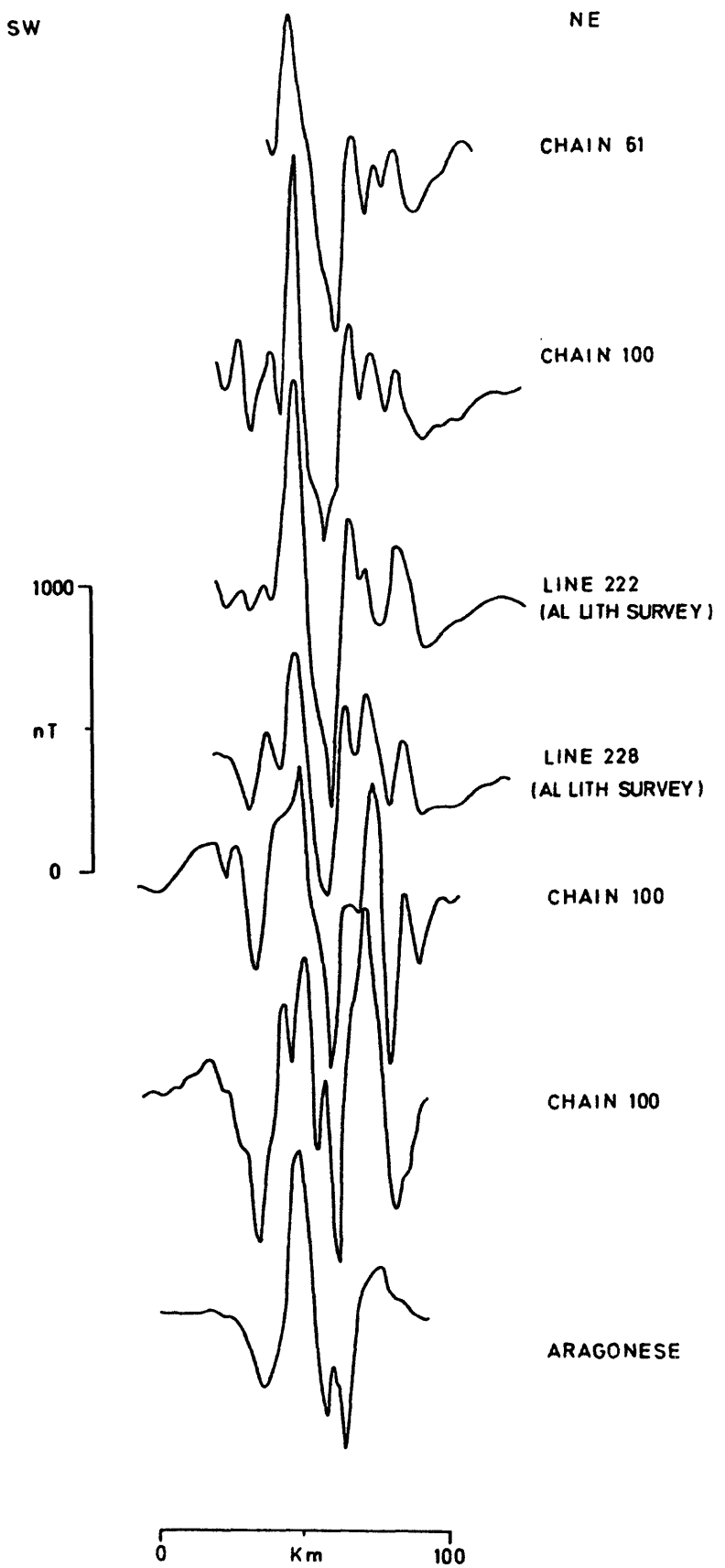

Figure 5.10 NE - SW magnetic profiles over deep water areas between 18°N and 19.5°N. Profiles aligned along large, central anomaly.

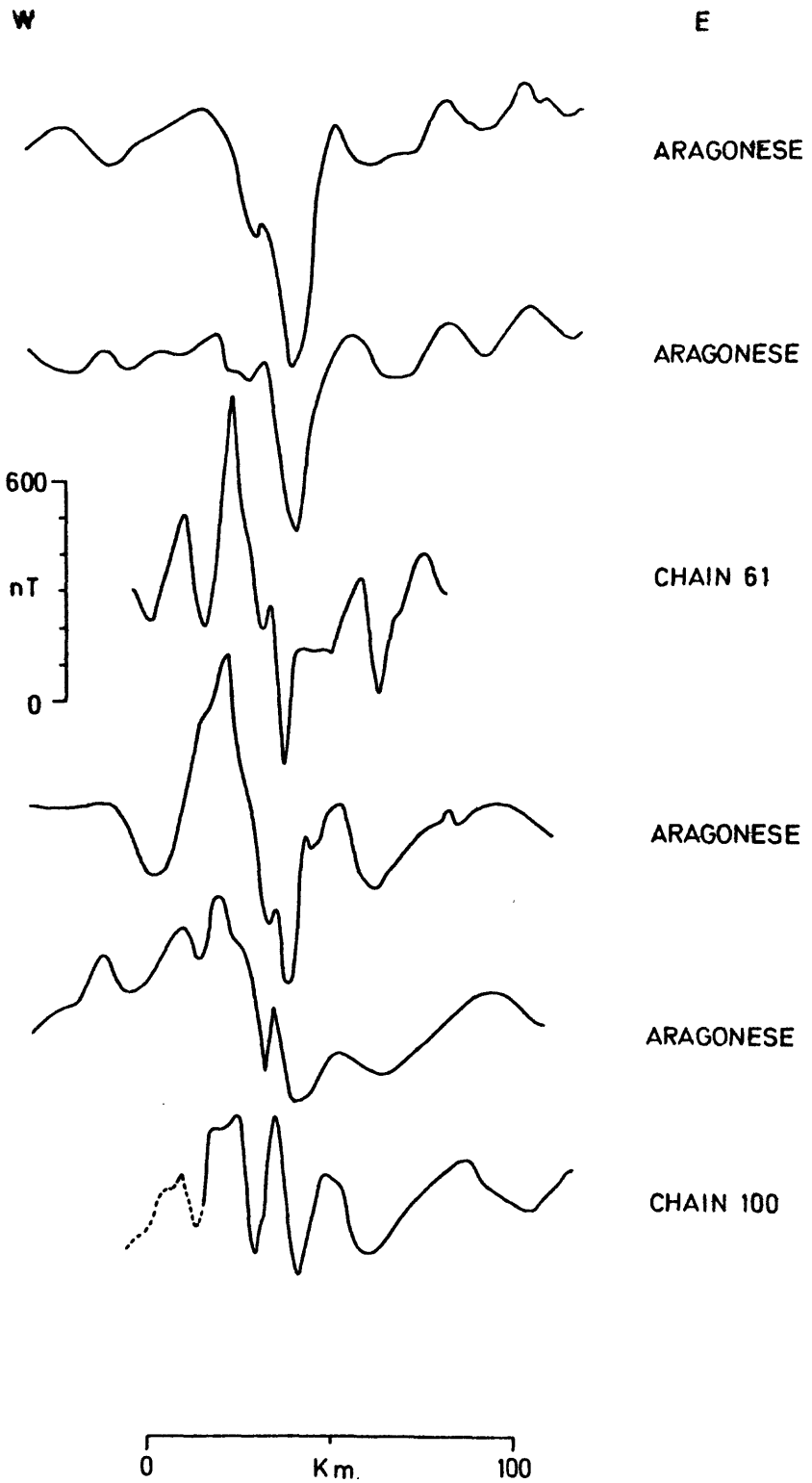

Figure 5.11 Approximately W - E magnetic profiles over deep water area between 19.8°N and 20.3°N. Profiles aligned along major, central anomaly.

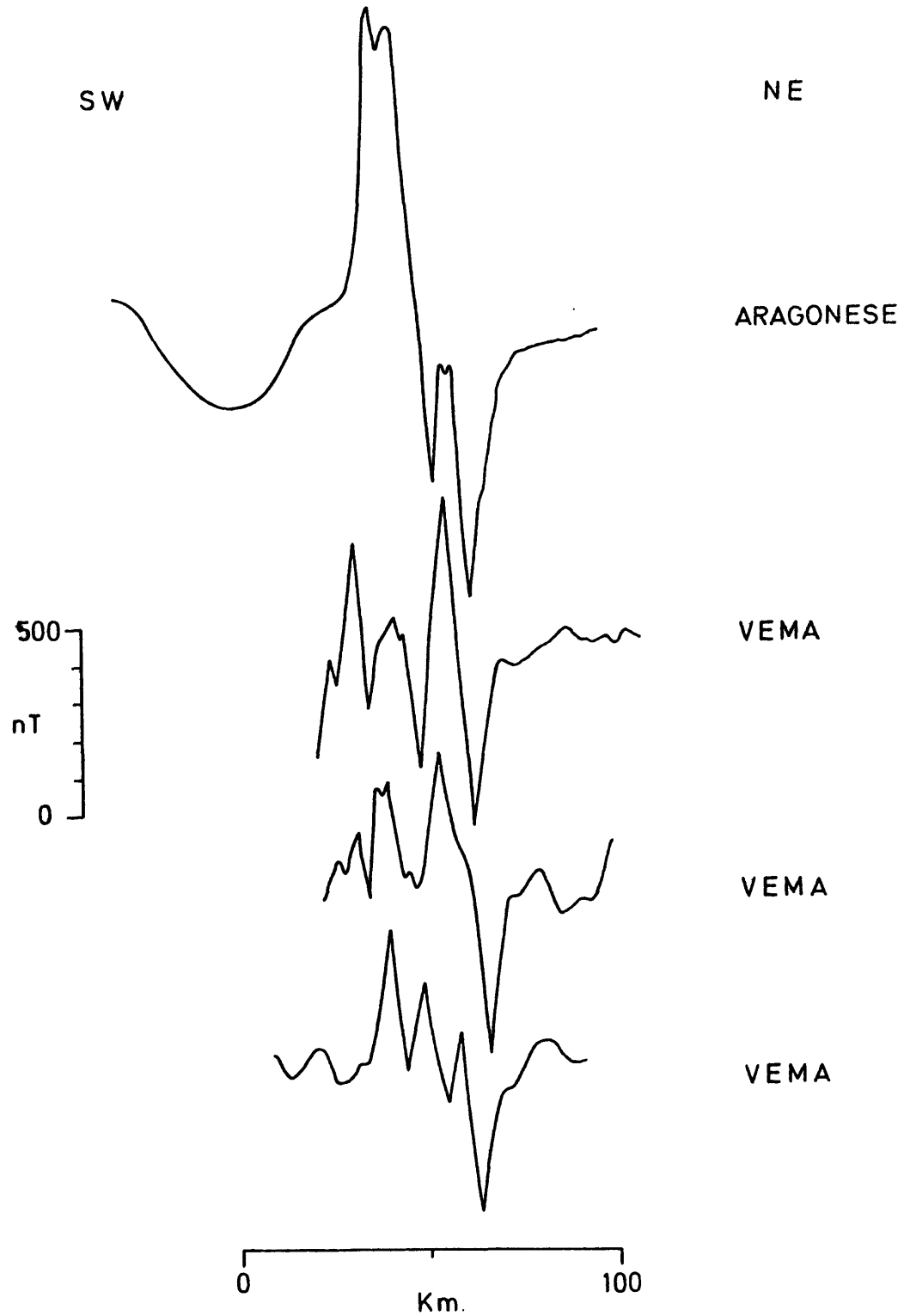

Figure 5.12 Approximately NE - SW magnetic profiles over deep water areas between 22°N and 22.4°N. Profiles aligned along major central anomaly.

northward until 20.3°N where they encounter another transverse feature (fig. 5.9).

Between 20.3°N and 22°N correlations of anomalies over the deep water are difficult to obtain parallel to the axis which trends approximately N-S in this area. A great many profiles exist (see figs. 5.2 and 5.3) but correlations over more than a few kilometres do not appear to be present. Better correlations are obtained, however, in the directions NE-SW and E-W where large anomalies appear to trend transverse to the axis (see section 5.6.2.) Such transverse features predominate between 20.3°N and 22°N.

North of 22°N the correlations are very tenuous as the data coverage is poor and the anomaly amplitudes smaller (400 to 800 nT). Four profiles over the deep water area between 22°N and 22.4°N are shown in fig. 5.12; the correlations are moderate with a sharp minima occurring on the eastern side of each profile. A large peak on the topmost (most northerly) profile is not reproduced in the others but appears to be replaced by several smaller peaks. Two further transverse zones are located at 22.4°N and 23.2°N although insufficient data are available to identify such features well.

Correlations of the anomalies over the main trough and shelves are excellent. Comparison of profiles in figs. 5.5 to 5.8 indicate the remarkable similarity of the anomalies which appear to trend approximately parallel to the coast for hundreds of kilometres. Selected profiles from these data have been stacked from north to south in fig. 5.13 with an extra

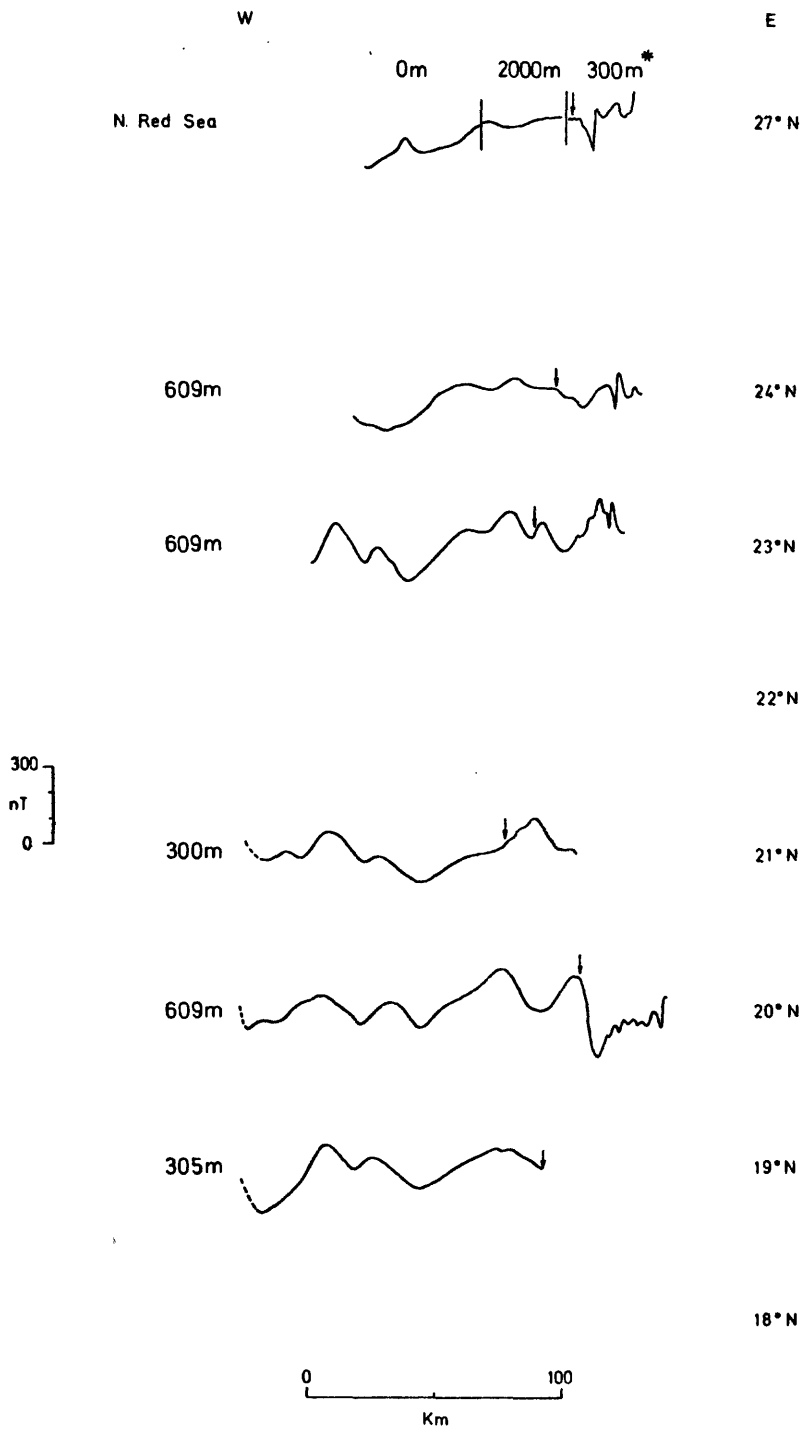

Figure 5.13 Aeromagnetic profiles across Arabian coast at various latitudes. Arrows indicate position of coast. Dashed line at end of profile indicates profile extends westward. *This part of profile flown at 300 metres above mean terrain.

profile from the northern Red Sea added for comparison. These show that the same anomalies are observed at each latitude and confirm the lineations extend throughout the area.

The high frequency anomalies observed at the eastern end of the airborne profiles seldom correlate from line to line over more than short distances (10 km maximum) and therefore are not included as peaks and troughs in fig. 5.9. The great variability in amplitude makes reliable correlations almost impossible and from figs. 5.5 to 5.8 it appears these anomalies are more or less randomly distributed over the land areas. There are exceptions to this : several sharp features which appear to be directly related to the young dykes mapped in the area are found on many of the profiles (e.g. profiles 240 to 255 fig. 5.7).

5.4 Ocean/continent boundary

Of the three types of anomalies only those over the axial trough and main trough and shelves correlate over distances greater than 10 km. Both types contrast strongly with the high frequency anomalies found over the land. The smooth, linear nature of the anomalies together with their symmetry about the deep water axis suggests a seafloor spreading origin. Conversely the high frequency anomalies are thought to be due to the presence of crystalline continental material. The boundary between the anomalies over the shallow shelves and those over the Shield were used, therefore, to delineate the ocean/continent boundary.

An estimate of the position on each profile (figs. 5.5 to 5.7) at which the high frequency anomalies first appear was made. A heavy dashed line representing the maximum westerly extent of the high frequency anomalies, based upon these estimates, is shown in fig. 5.9. The mapped edge of the Pre-Cambrian outcropping along the coastal plain is also shown in fig. 5.9 (shaded solid line). Unlike the northern Red Sea (section 4.4) the mapped Pre-Cambrian edge in most areas is located some distance to the east of the high frequency boundary although at 20.2°N and 23.7°N the two are nearly coincident. Thus if the high frequency anomalies are due to continental material then Pre-Cambrian rocks probably exist beneath the sediments of the coastal plain. Field work in progress along the Arabian coast may result in a revision of the extent of the Pre-Cambrian.

The ocean/continent boundary may also be defined by the smooth seafloor anomalies over the shelves and parts of the coastal plain. Between 19°N and 20.4°N fig. 5.9 shows that the innermost (most easterly) continuous feature, a trough, almost coincides with the high frequency boundary. Thus the ocean/continent boundary determined by either method is the same in this area. Between 21.1°N and 21.7°N there are insufficient dominant features to delineate the boundary. The innermost feature, a peak, is observed on five of the eight profiles (fig. 5.6) but may also appear on profile L1. If so then the trough immediately east of the peak (fig. 5.9) may indicate the boundary. This feature again more or less coincides with the high frequency edge. A somewhat different situation

occurs in the case of the Yanbu' survey where as fig. 5.9 shows, the seafloor anomalies are not continuous but appear to be broken into small segments which are offset. Only between 23.7°N and 24°N is a continuous feature, a trough, present which coincides nearly with the high frequency boundary. South of 23.7°N there is a gap of approximately 15 km between the seafloor anomalies and the dashed line (fig. 5.9) although near 22.9°N this gap is reduced to less than 5 km.

It appears, in general, the ocean/continent boundary lies between 0 and 25 km inshore. Thus there is about 330 km of seafloor material at 19°N measured along an azimuth of N 60° and about 280 km at 23°N along a similar direction. Both amounts are based upon the assumption of symmetry about the present deep water axis.

5.5 Seafloor spreading history

Almost the entire width of the Red Sea between 18°N and 24°N appears to be composed of oceanic crust generated by seafloor spreading. The anomalies were examined to study the evolution of this oceanic material. In section 5.3.1 these anomalies were separated into two types on the basis of their wavelength and amplitude although both types form linear patterns. The two anomaly types are thought to represent two phases of seafloor spreading separated by an hiatus of 20 to 30 My (Girdler and Styles, 1974; Hall et al, 1970; Girdler and Styles, in press).

5.5.1 Recent seafloor spreading

The large anomalies observed over the axial trough which form a symmetric, linear pattern parallel to the deep water axis (fig. 5.9) have been discussed elsewhere (Drake and Girdler, 1964; Allan et al, 1964; Knott et al, 1966; Vine, 1966; Phillips et al, 1969; Allan, 1970; Phillips, 1970). It is now generally accepted that these anomalies are produced by recent seafloor spreading. A seafloor spreading model based upon the reversal time scale of Heirtzler et al (1968) was therefore computed to simulate the observed anomalies, e.g. those in fig. 5.10. The model obtained (fig. 5.14) involves spreading over the past 5 My at approximately 0.8 cm y^{-1}. Such a model compares favourably with that described in section 4.6 and elsewhere (Girdler and Styles, 1974). The correlation of the observed and synthetics in fig. 5.14 is remarkably good. Beyond 5 My, point B in fig. 5.14, the observed data display an abrupt change of character such that the smaller amplitude, longer wavelength anomalies replace the larger anomalies (see profiles 222, 224, 226 and 228, fig. 5.7). Thus B represents the boundary between the two phases of spreading.

Individual seafloor models for each area where the large anomalies parallel the axis were not computed as the correlations are often poor. However the data in these areas in general support similar models with spreading rates between 0.7 and 0.9 cm y^{-1}.

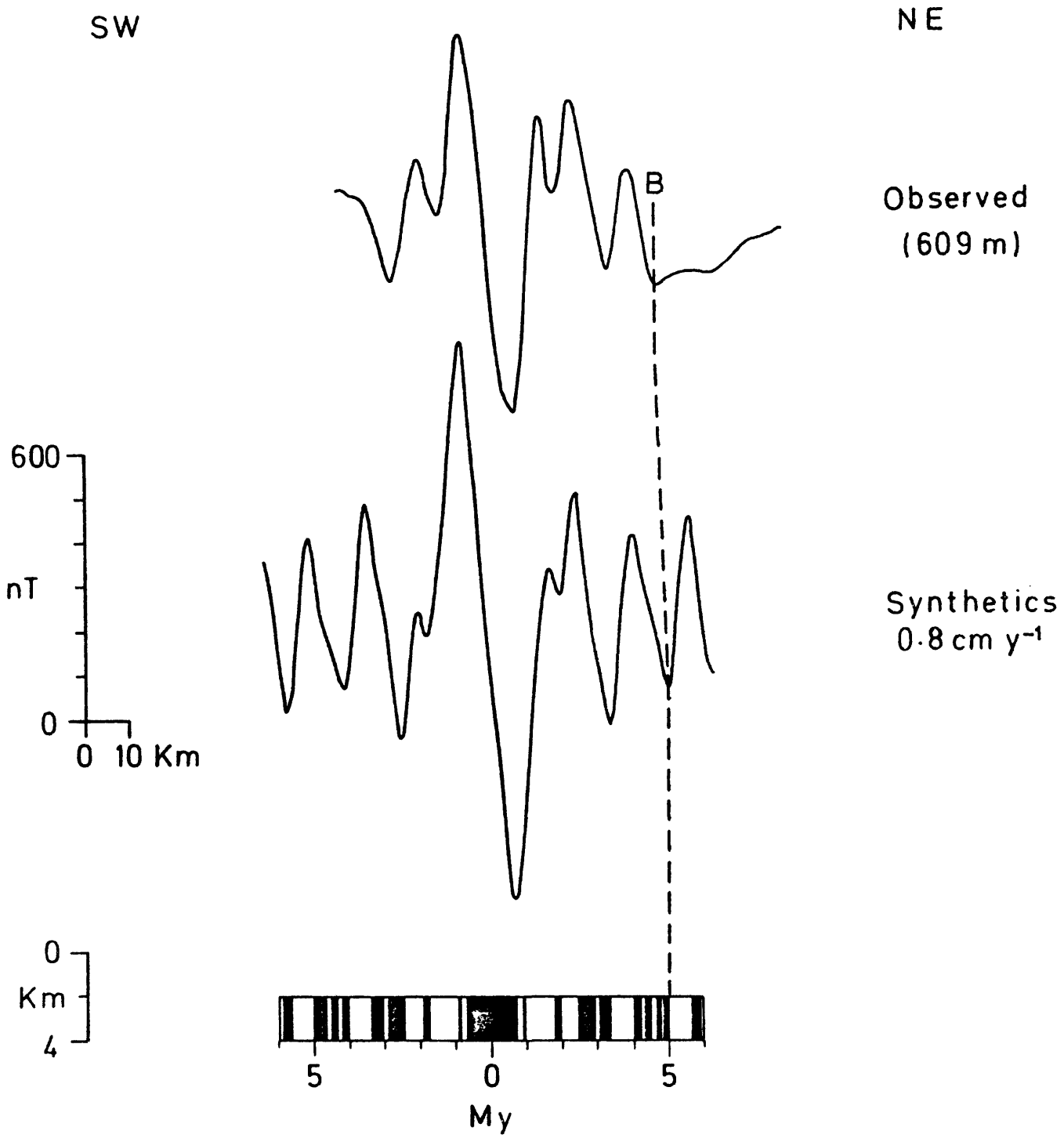

Figure 5.14 Seafloor model of recent spreading phase. Observed profile is from western part of profile no. 228 (Al Lith survey) near 19°N. B represents eastern limit of good correlation between synthetics and observed.

Seafloor spreading models for this area presented by other authors favour a larger spreading rate over a slightly shorter period. Vine (1966) presented a model in which the seafloor has spread over the past 2 to 3 My at approximately 1.0 cm y^{-1} at 20°N. A similar model is described by Phillips (1970) who also includes a discussion of a model spreading along N 10° at 1.6 cm y^{-1}. Allan (1970) using different magnetic data suggests a rate of 1.1 cm y^{-1} near 19°N with spreading having been continuous over the past 3 to 4 My. The model presented in fig. 5.14 is in better agreement with recent work in the southern Red Sea (Girdler and Styles, 1974) and the models described in Chapters 4 and 6. Irrespective of the model chosen, the recent seafloor spreading phase has created about 80 ± 10 km of new oceanic material at 19°N, measured along N 60°, and about 70 ± 10 km at 23°N along a similar direction.

5.5.2 Early seafloor spreading

Seafloor spreading models were computed to simulate the smooth, linear anomalies observed over the main trough and shelves. Two possible models similar to those described in section 4.5 were found to reproduce most of the observed features. The first, shown in fig. 4.15(a) is based upon Girdler and Styles (1974) and involves continuous spreading between 41 and 34 My at approximately 1.3 cm y^{-1}. Correlation of the observed and synthetics is good over much of the profile; the long reversal (35 My to 37.61 My) and the minimum at 40 My agree remarkably well. However the twin peaks between these two features are not found in the observed profile.

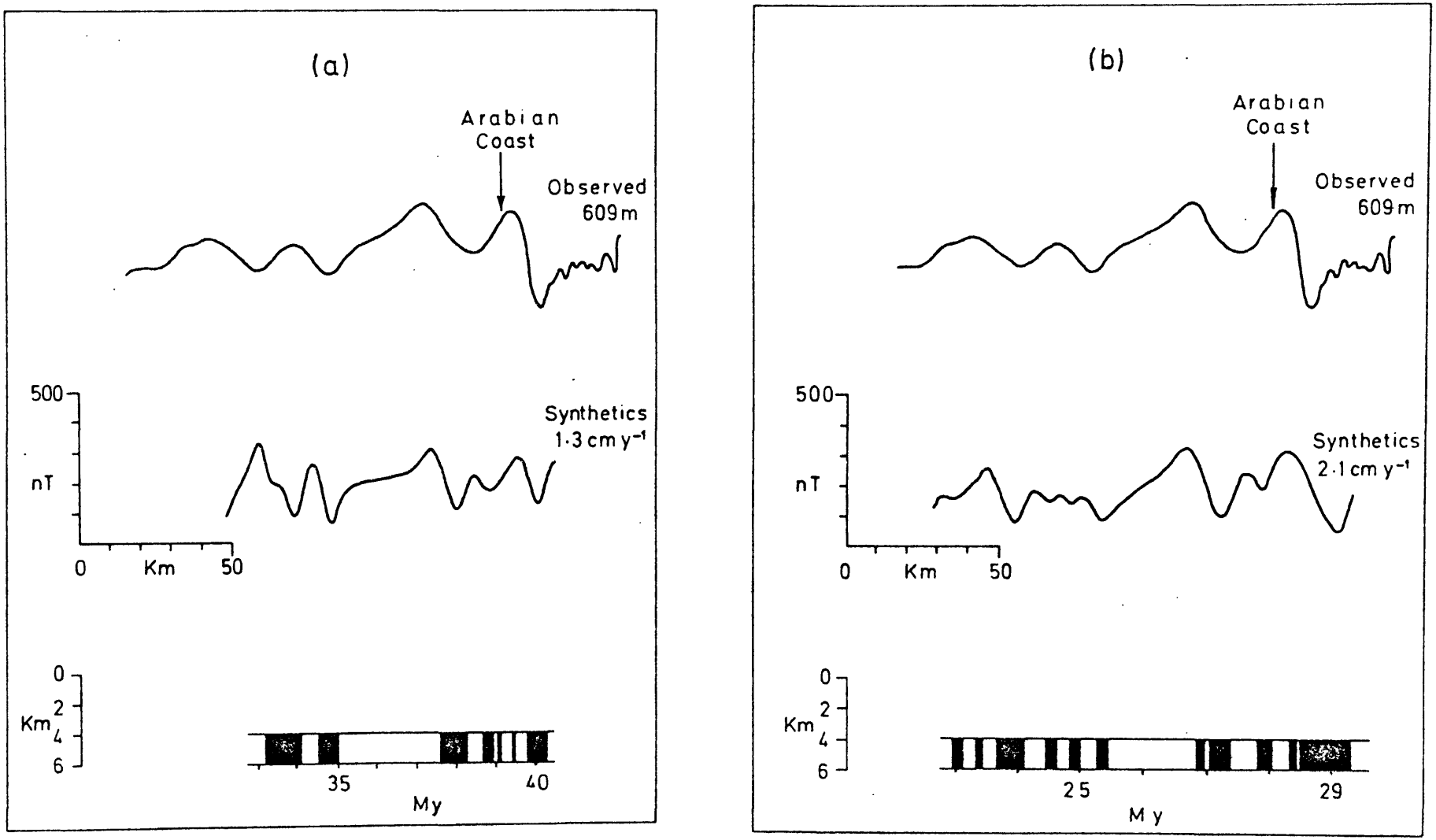

Figure 5.15 Two possible seafloor models of early spreading phase. Observed profile is from profile no. 228 (Al Lith survey) near 19.5°N.

Those features at the western end of the observed profile have longer wavelengths than those of the model possibly indicating a somewhat faster spreading rate. Alternately the poorer correlation on the west may be due to inaccuracies of the reversal time scale used in the model (Heirtzler et al, 1968). The observed data appear to support a period of seafloor from spreading 40 My to 32.5 My.

The second model (fig. 5.15(b)) is that discussed by Hall et al (1976) and Girdler and Styles (in press). In this, the long reversal chosen in the shorter interval between 25.43 My and 26.86 My which consequently requires a somewhat faster spreading rate, viz 2.1 cm y^{-1}. The correlation of the observed and synthetics is good over much of the profile although not all the features predicted are observed. Again a twin peaked feature, this time between 27 and 29 My, is not found in the observed. Between 23 and 25 My the observed profile appears as a smoothed out version of the synthetics. The locations of major features, however, are correct and seem to indicate an almost constant spreading rate. Only the major trough predicted at 29 My appears to be displaced suggesting the initial spreading was slightly slower. The data, therefore, support a spreading phase between about 29 My and 23 My.

Whichever model is correct the amount of seafloor generated on the Arabian side during the earlier phase is approximately 125 $\pm$ 10 km at 19^{o}N along N 60^{o} and about 105 $\pm$ 10 km at 22.5^{o}N along the same direction. Assuming symmetrical spreading the earlier phase accounts for about 250 km of the present width of the Red Sea at 19^{o}N and 210 km at 22.5^{o}N : both amounts measured along N 60^{o}.

These amounts together with the estimates for the recent spreading (section

5.5.1) give a total of 330 ± 30 km of seafloor at 19°N and 280 ± 30 km at 22.5°N. Both amounts are based upon the assumption of symmetrical spreading about the present deep water axis and are similar to those predicted from the location of the ocean/continent boundary in section 5.4.

5.6 Location of Transform faults

Unlike the northern Red Sea, the magnetic pattern over the deep water in the central Red Sea (fig. 5.9) does not display any simple discontinuities or offsets. Instead several transverse magnetic features are observed at which the pattern as a whole undergoes an abrupt change of direction; these features are discussed in some detail in section 5.6.2. In contrast, the magnetic anomalies over parts of the main trough and shelves display offsets and these are considered first.

5.6.1 Offsets of the magnetic anomalies over main trough and shelves

The magnetic pattern over the main trough and shelves displays several discontinuities which indicate possible sites of transform faults. Such discontinuities are apparent where either a continuous line of peaks (troughs) becomes a line of troughs (peaks) as for example near 23.2°N, 38.6°E or an abrupt change in direction of the lineations occurs such as at 23.85°N, 38.05°E. Combining these two types of discontinuity five possible transform faults were located:

(1) at 23.85°N, 38.05°E, six features, three peaks and three troughs, are discontinuous but only three show an offset. These suggest a dextral offset of about 8 km with an approximate azimuth for the fault of N30° to N40° although this direction cannot be determined precisely because of the limited extent of the data.

(2) at 23.0°N, 38.5°E four features are discontinuous but only two show a clear offset. The offset is again dextral, this time by about 9 km. Two other features to the west of these appear to be continuous suggesting the offsets may not indicate a transform fault. The azimuth is about N25° to N40° but again must be treated cautiously.

(3) A less definite discontinuity is located at 22.85°N, 38.75°E where five features, two peaks and three troughs, are discontinuous. Two of these display a dextral offset of about 10 km. However two other features appear continuous across the proposed fault which must therefore be considered tentative. A trend of about N30° to N40° can be assigned but there are too few features to enable a reliable estimate to be made.

(4) Near 22.5°N, 38.85°E there is a discontinuity (fig. 5.9) which is less certain as the lineations to the south are defined by only a few peaks and troughs. Five features, two peaks and three troughs, are discontinuous but only two display a clear offset. The offset is dextral by approximately 15 to 20 km along N40° to N50°. However as the two offset features are close to one another this direction is probably subject to a large error.

(5) The lineations along the coast between 19^{o}N and 20.4^{o}N show a discontinuity at about 20^{o}N, 40.4^{o}E which offsets two of the four features by approximately 10 to 12 km to the right. However as the remaining two features are continuous throughout it is not clear whether the offset marks a transform fault or not. If it does, an approximate direction of $N55^{o}$ can be assigned to the fault.

The locations and approximate azimuths of the proposed faults are shown in fig. 5.9 (dot dashed line). Azimuths were obtained by fitting the best straight line to the discontinuities; large errors are probably present and the directions chosen should be considered tentative.

5.6.2 Transverse magnetic features

The correlations of the dominant magnetic anomalies over the deeper water trend either parallel to or approximately normal to the deep water axis (fig. 5.9). Those lineations almost normal to the axis form transverse magnetic features at about 19.5^{o}N, 22.4^{o}N, 23.2^{o}N and between 20.3^{o}N and 22^{o}N (fig. 5.9). The features at 22.4^{o}N and 23.2^{o}N are not well defined as the data are sparse in these areas. Two or three anomalies are present but do not correlate very well and, as a result, the identification of transverse features in these areas is questionable. Those features between 20.3^{o}N and 22^{o}N and at 19.5^{o}N are based on many tracks and are, therefore, considered genuine transverse features. Those between 20.3^{o}N and 22^{o}N are discussed in some detail below.

A detailed map of the area between 20.25°N and 21°N is shown in fig. 5.16. The ships'tracks are mainly those which trend approximately parallel to the Red Sea axis and, therefore, normal to the magnetic trends (fig. 5.9) but several oblique tracks are also included where these help to delineate the transverse features. Magnetic profiles from these tracks are shown in fig. 5.17: the profiles have been projected normal to the dominant magnetic trend, i.e. N160°. The anomalies have large amplitudes, 500 to 1000 nT, and short wavelengths, typically 10 km, but vary considerably (fig. 5.17). For example,profiles 1, 10, 11 and 12 display smaller anomalies, 300 to 400 nT. A distinctive asymmetric peak observed on several profiles is characterised by a sharp gradient to the NW and a shallow gradient to the SE. This peak appears on profiles 2, 3, 5 and 6 (fig. 5.17) and is located near a dextral offset of the deep water axis (fig. 5.16). Correlation of the peak from profile to profile is good and tracks 15 to 20 km apart all record it. On the other hand the excellent correlation of profiles 10, 11 and 12 is probably not significant as these profiles are located very close to one another. A large trough, NW of the asymmetric peak, correlates well appearing on all profiles except 1, 10, 11 and 12 (fig. 5.17). There are large gaps, however, between the profiles and it is not clear whether the anomalies observed on profiles 10, 11 and 12 are the same as those found on the other profiles. Consequently it is difficult to determine the NE-SW extent of the transverse features but a minimum amount of 55 km may be assigned on the basis of the correlations of profiles 2 to 9.

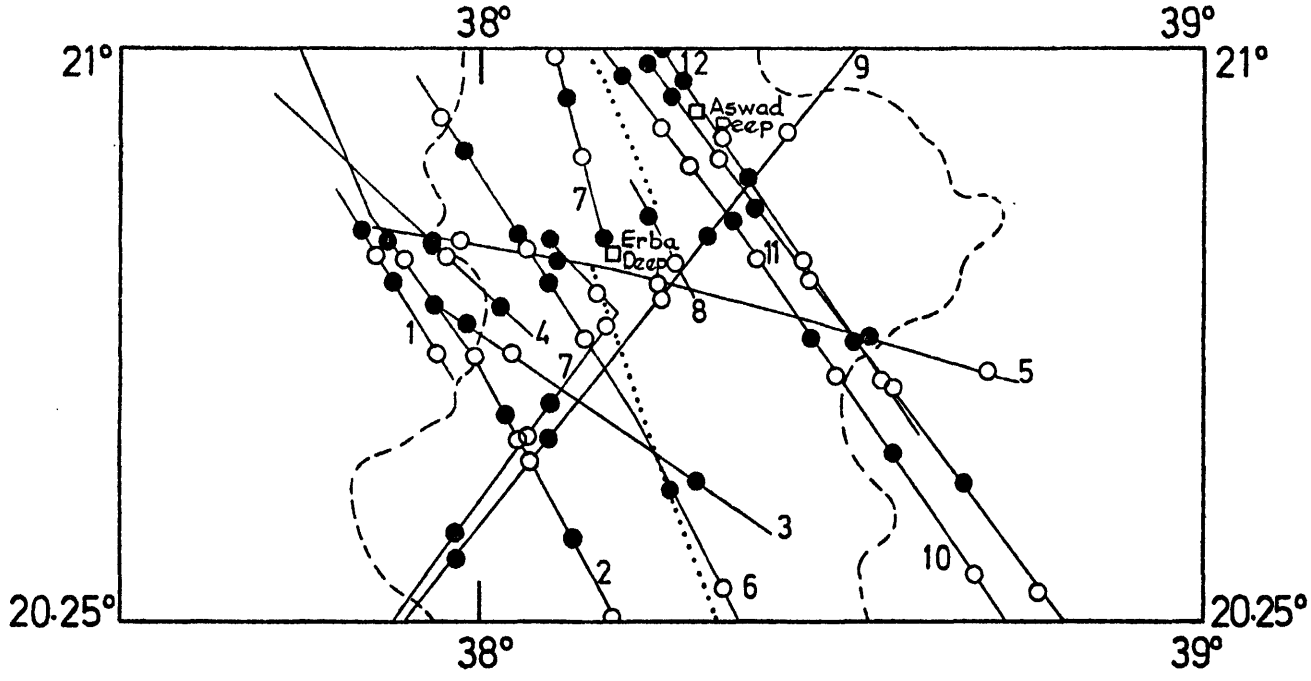

Figure 5.16 Location of dominant peaks, O,and troughs, ●, in the area of transverse magnetic anomalies between 20.25°N and 21°N. Solid lines are ships' tracks, dashed line is 500 fathom bathymetric contour, dotted line is deep water axis. Numbered tracks show locations of profiles in fig.5.17 .

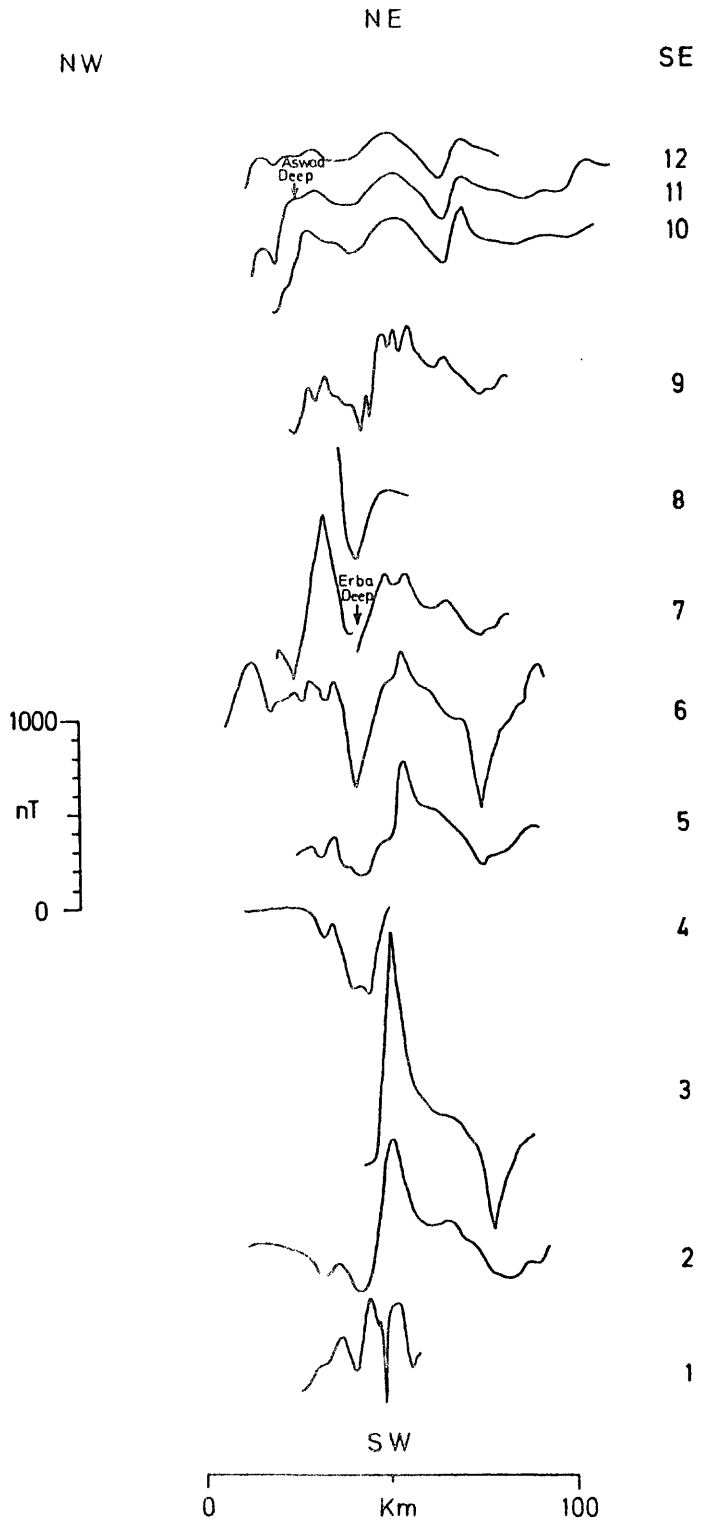

Figure 5.17 Magnetic profiles over deep water between 20.25°N and 21°N. Location of profiles shown in fig. 5.16. Profiles have been projected on to the direction N160°.

The magnetic pattern shown in fig 5.16 extends westward beyond the 500 fathom bathymetric contour near 20.6°N for at least 10 km and possibly more. Oblique tracks west of profile 1, not shown in fig. 5.16, do not record the anomalies but as these are not favourably oriented the anomalies may be present. Further data are required to delineate the SW extent of the anomalies. The transverse magnetic features coincide with a dextral offset of the deep water axis (dotted line in fig. 5.16) of about 10 km which occurs near Erba Deep. This deep is located between a line of peaks and a line of troughs in a NE trending depression produced by an abrupt widening of the axial trough near 20.6°N. The area is seismically active (fig. 5.1). A smaller deep, Aswad Deep, also occurs within the area covered by the transverse features lying about 25 km NE of Erba Deep and some 10 km from the deep water axis.

A detailed map of the area between 21°N and 22°N is shown in fig. 5.18. The ships' tracks are again those which trend approximately parallel to the axis together with several oblique tracks which link the anomalies across the larger gaps. The magnetic profiles from these tracks are shown in fig. 5.19 where again the data have been projected normal to the transverse features, N144°, and stacked NE to SW. Large amplitude anomalies, 500 to 1000 nT, are common with wavelengths typically 10 km. The absence of such anomalies on profiles 1 and 12 indicates a maximum NE-SW extent of less than 90 km. In general, the largest anomalies are observed over the centre of the area with somewhat smaller amplitudes, 300 to 500 nT, at either end e.g. profiles

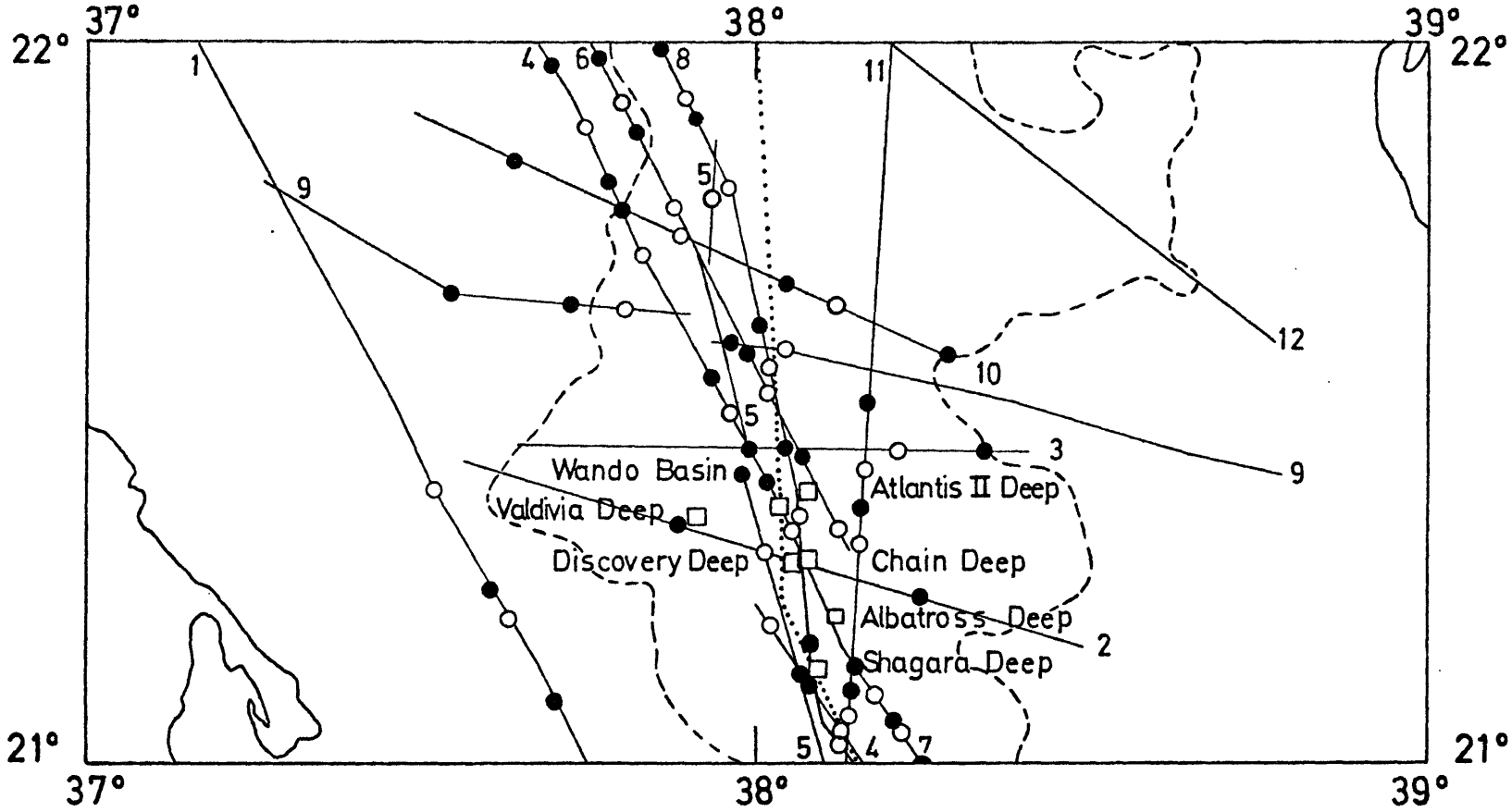

Figure 5.18 Location of dominant peaks, O, and troughs, ●, in the area of transverse magnetic anomalies between 21°N and 22°N. Solid lines are ships' tracks, dashed line is 500 fathom bathymetric contour, dotted line is deep water axis. Numbered tracks show location of profiles in fig 5.19 .

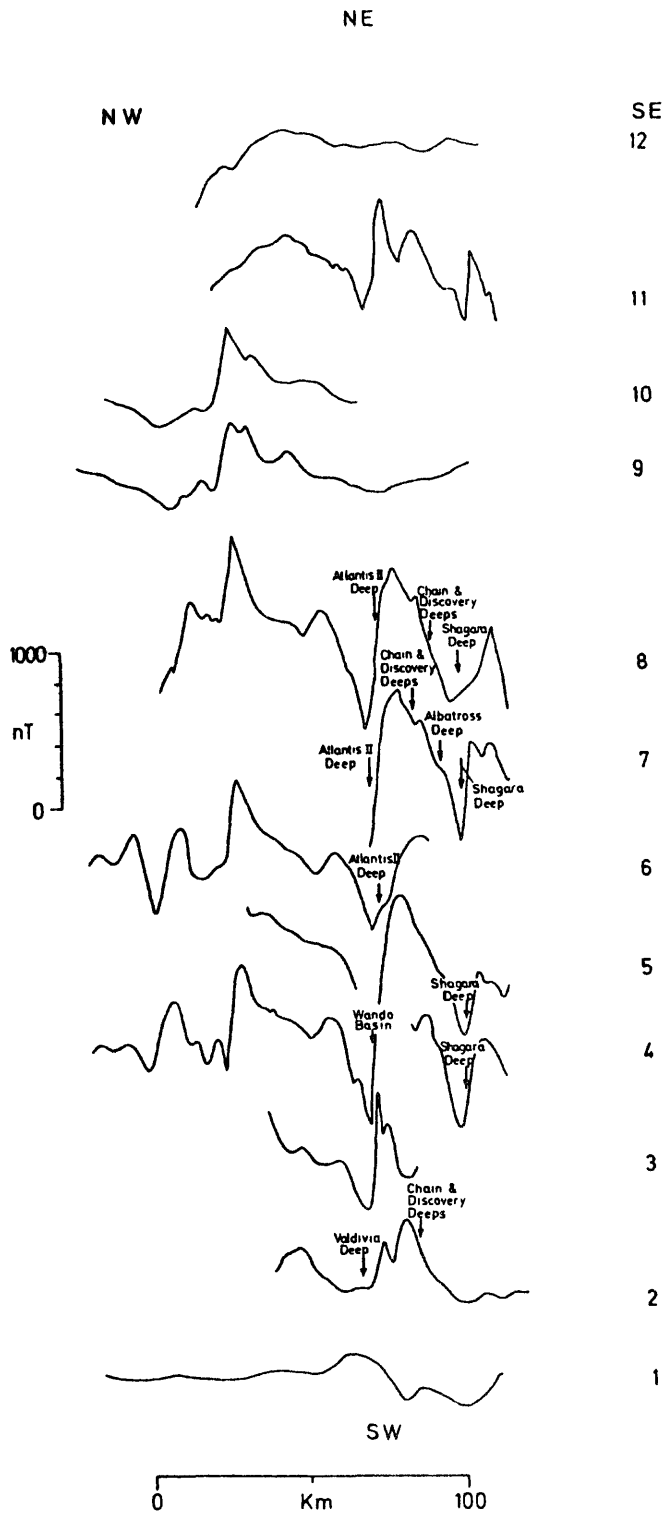

Figure 5.19 Magnetic profiles over deep water between 21°N and 22°N. Locations of profiles are shown in fig. 5.18. Profiles have been projected on to the direction N144°.

2 and 11 in fig. 5.19. Profiles 4, 6 and 8 which are separated by approximately 15 km correlate remarkably well each displaying an asymmetric peak similar to that found on profiles 2, 3,5 and 6 of fig. 5.17. Several other features are present which correlate well from profile to profile. For example,a large peak-trough pair, SE of the asymmetric peak, on profiles 3, 5, 6, 7, 8 and 11 produces a linear feature over a line of 3 deeps, Valdivia Deep, Wando Basin and Atlantis II Deep (fig. 5.18).

The patt ern of peaks and troughs in fig 5.18 is quite uniform and trends along approximately N55^{o} although individual trend lines vary somewhat in direction. Peaks and troughs are again observed outside the axial trough where they extend westward 20 km beyond the 500 fathom bathymetric contour. The axial trough in this region widens considerably from about 50 km at 22 ^{o}N to over 100 km at about 21.6^{o}N producing a N60^{o} trending depression. A furt her widening takes place near 21.4^{o}N when the trough becomes 70 km wide. No major offsets of the deep water axis are observed at either widening but several deeps, some located some distance from the axis e.g. Valdivia Deep, have been discovered between 21.1^{o}N and 21.4^{o}N.

Studies of the transverse features at 19.5^{o}N, 22.4^{o}N and 23.2^{o}N reveal similar anomalies to those found between 20.3^{o}N and 22^{o}N. For those at 22.4^{o}N and 23.2^{o}N the data coverage is such that the NE-SW extents cannot be determined. Their NW-SE extents, however, are found to be approximately the same, viz. 30 km. In the case of the 19.5^{o}N feature the data are more extensive and the size of the feature is approximately 80 km (NE-SW) by 30 km (NW-SE). Deeps have been discovered within each of these three areas:

at 19.5°N (Suakin Deep), at 22.4°N (Hardaba Deep) and at 23.2°N(Nereus Deep). Of these, only Suakin Deep lies within a known seismically active area (see fig. 5.1), whilst Hardaba Deep is located near the only apparent widening of the axial trough. No major offsets of the deep water axis are observed in any of the areas.

An explanation of the anomalies that form lineations parallel to the Red Sea trend has been given in section 4.5.1 and elsewhere (Vine, 1966; Phillips et al, 1969; Allan, 1970; Phillips, 1970; Girdler and Styles, 1974) which involves the presence of oceanic crust beneath the axial trough and part of the main trough. This has now been confirmed by recent geophysical evidence. Thus the large transverse magnetic anomalies must be due to oceanic crust. Since the features are more or less normal to the Red Sea axis they might be due to transform faults. This is supported in part by the fact that some features occur over known seismically active areas and some where offsets of the deep water axis are observed. However, transform faults do not, in general, have strong magnetic expressions associated with them (Matthews et al, 1965; Bergh, 1971; Schouten, 1974) nor are they very wide, typically 1 to 5 km. Consequently a simple transform fault does not seem to provide an adequate explanation.

The transverse anomalies are similar in amplitude and wavelength to those parallel to the axis over the deeper water. They are also similar to those observed over a NE-SW trending ridge in the northern Red Sea described in section 4.6.2. It appears possible, therefore, that the

features are produced by seafloor generated at transform faults which act as spreading centres i.e. "leaky" transform faults. Seafloor spreading models similar to those in fig. 4.13 were computed and compared with the observed profiles (figs. 5.17 and 5.19). The data were found to agree with models having spreading rates of 0.3 to 0.5 cm y^{-1} over the interval 0 to 5 My and these are shown in fig 5.20. The gross features of the observed data are reproduced but too few anomalies are present to provide a reliable test. The major peak-trough pair fits well in each case but the anomalies over the sides are smoother than those of the synthetics. The value of effective susceptibility used in the model (fig. 5.20) is 0.01 emu cm^{-3}. It is apparent from fig. 5.20 that whilst a 'leaky' transform fault provides a promising explanation of the transverse features further evidence is required to substantiate such a model.

The geometry of a leaky transform fault depends on certain factors which are difficult to assess. Menard and Atwater (1968) suggest that where leaks occur in response to changes in the motion of two plates the line of a transform fault will rotate until it reaches a direction compatible with the new direction of motion. The fault will then cease to leak and become a true transform fault. How quickly this occurs is difficult to determine. However the fit of the major peak-trough pair in fig. 5.20 indicates the transform is probably still spreading at between 0.3 and 0.5 cm y^{-1}. If the rate has been constant between 0 and 5 My then the NW-SE extent expected is between 30 and 50 km. This amount compares favourably with the widths of the features

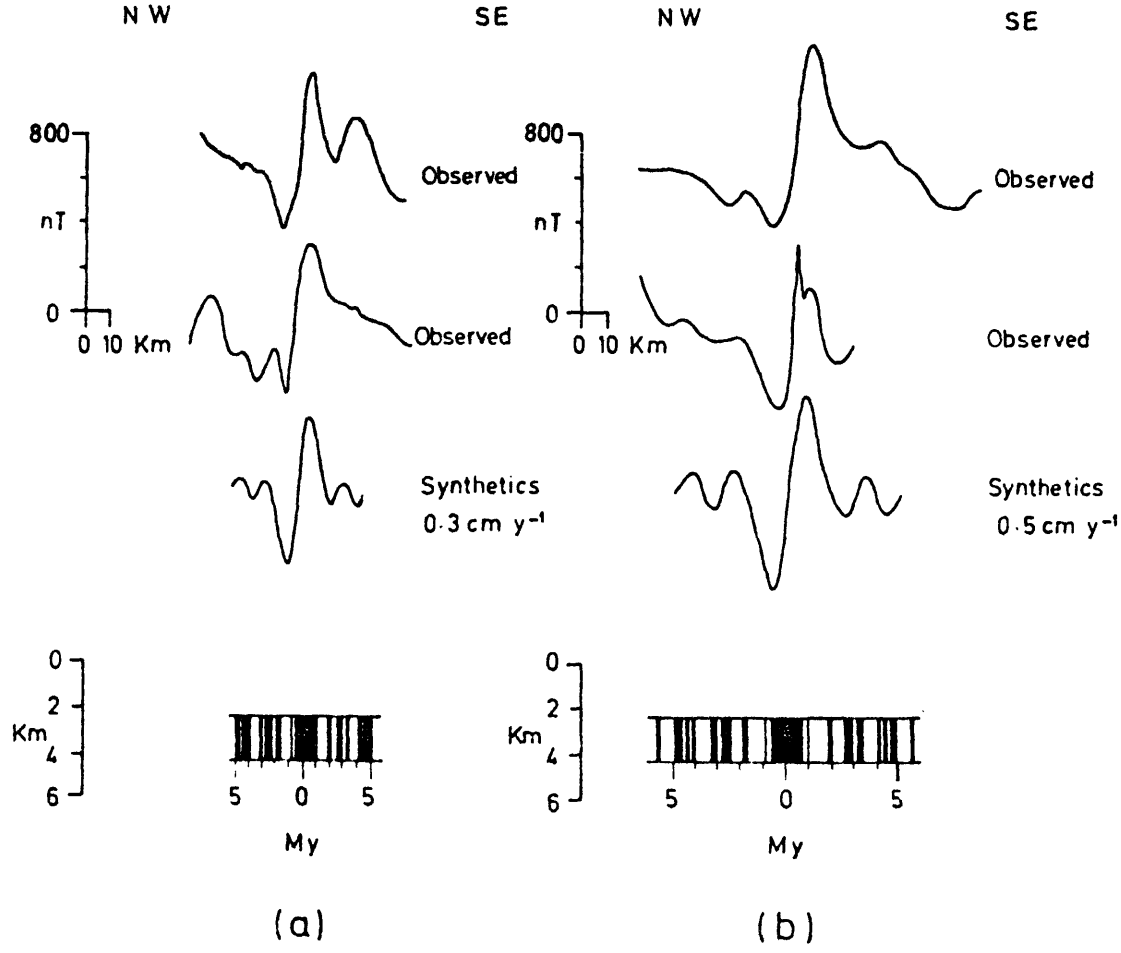

Figure 5.20 Seafloor spreading models for leaky transform faults found between 20.3°N and 22°N. Observed profiles in (a) are numbers 4 and 11 (fig.5.19); in (b) number 2 (fig.5.17) and number 3 (fig.5.19).

at 19.5°N, 22.4°N and 23.2°N. The NE-SW length of the feature depends on spreading normal to the deep water axis which was found to be approximately 0.8 cm y^{-1} at 19°N. Using this value and assuming constant spreading over the past 5 My the NE-SW length expected is about 80 km plus the offset at the transform fault prior to the recent spreading. This again compares favourably with the lengths estimated above, viz. 80 to 90 km. Leaky transform faults, therefore, provide a reasonable explanation of the transverse anomalies.

In the models (fig. 5.20) the major feature of the synthetics is the central peak-trough pair. Consequently to locate the leaking axes of the transform faults this feature must be identified. This was done by correlating feature by feature the synthetics with the observed data in figs. 5.17 and 5.19. Three axes were found: one along the large peak-trough feature on profiles 2, 3, 5, 6, 7, 8 and 9 of fig. 5.17 i.e. over Erba Deep and the dextral offset of the deep water axis (fig. 5.16). Another along the large anomalies over Valdivia Deep, Wando Basin and Atlantis II Deep on profiles 2, 3, 4, 5, 6, 7 and 8 (fig. 5.19) and a third along the trough and asymmetric peak on profiles 4, 6 and 8 (fig. 5.19) about 50 km NW of Atlantis II Deep. These three leaky transform faults account for approximately 90 to 150 km of the 180 km covered by the transverse features between 20.3°N and 22°N. Thus there are about 30 to 90 km over which anomalies parallel to the deep water may be present. Such anomalies, if present, are probably split into at least two or three short sections and this may explain why the anomalies have not been detected. However, a detailed study of the Atlantis II, Chain and Discovery Deeps (Searle and Ross, 1975) indicates an approximately 40 km long section

of anomalies parallel to the deep water axis near 21°N.

The seafloor geometry which results from the leaking axes is discussed further in Chapter 7.

5.6.3 Correlation of anomaly offsets and transverse features

Additional support for the proposed transform faults may be obtained by correlating the locations of the transverse features with the discontinuities in the magnetic pattern along the Arabian coast. The two offsets of the linear magnetic anomalies between 23°N and 24°N each correspond to a transverse feature: one at 22.4°N, the other at 23.2°N (see fig. 5.9). On the other hand, the offset at 22.85°N, 38.75°E is not related to the transverse features but corresponds instead to part of the magnetic pattern parallel to the deep water axis. The discontinuity at 22.5°N, 38.85°E, although based on the offsets of only two features corresponds with the northern part of those transverse features between 20.3°N and 22°N (fig. 5.9). Finally, the offset of the two linear features along the Arabian coast near 20°N, 40.4°E corresponds to an area where lineations parallel to the axis are well defined on the basis of excellent correlations (see fig. 5.10) and extensive data. In this latter case it is almost certain that there is no leaky transform fault in the area. Conversely the transverse features may be used to locate discontinuities in the magnetic pattern along the coast. The transverse features between 20.3°N and 22°N indicate three transform faults (see section 5.6.2) and those at 19.5°N one such fault. Four offsets, therefore, are inferred near the coast between 20.7°N and 22.6°N. Unfortunately there are relatively few magnetic

data in this area (fig. 5.3) and consequently the linear patterns are not well defined. Only the discontinuity at 22.5°N, 38.85°E, noted above, is located within this area and this appears to correspond to the most northerly leaky transform between 20.3°N and 22°N, i.e. the one near 21.85°N, 38°E.

From the above it would appear that those transform faults proposed at 23.85°N, 38.05°E, 23.0°N, 38.5°E and 22.5°N, 38.85°E are probably genuine whilst those at 22.85°N, 38.75°E and 20°N, 40.4°E must be considered doubtful. Insufficient data are available to confirm those faults at 19.5°N, 38.85°E, 20.75°N, 38.2°E and 21.35°N, 38°E which have been inferred from the transverse features (section 5.6.2).

5.7 Relation of magnetic anomalies to deep holes

5.7.1 Location and properties of deep holes

Eighteen deep holes or deeps have been discovered in the seabed between 18°N and 24°N. The physical and chemical properties of several samples of water and sediments from these deeps have been reported, see for example, Backer and Schoell, 1972; Backer, 1973; Baumann, et al 1973; Backer and Richter, 1973; Bignell, et al 1974. In particular, extensive analyses of samples from Chain, Discovery and Atlantis II Deeps have been carried out (see for example "Hot brines and recent heavy metal deposits in the Red Sea", Degens and Ross (eds.) 1969.
Of the deeps, all but six (viz. Vema, Thetis, Aswad,

Hatiba, Hardaba and the unnamed deep near Vema Deep) contain brine pools, some of which are associated with high temperatures. Some of the more important physical and chemical properties of samples obtained from the deeps, based upon the above sources, are summarised in Table 5.1. Unfortunately the properties of an unnamed deep near Vema Deep have not been reported although metalliferous sediments have been found (Backer et al, (1975). The location of the deeps are given in Table 5.1 and shown in fig. 5.21.

5.7.2 Magnetic anomalies over deep holes

Twelve of the eighteen deeps are located in areas where the magnetic data display transverse features although Shagara and Albatross Deeps lie in an area where these are not well developed (fig. 5.18). Profiles over nine of these deeps are shown in figs. 5.17 and 5.19. Profiles over the remaining three, viz. Nereus, Hardaba and Suakin Deeps, are shown in fig. 5.22. In general, the anomalies over each deep are large ($\sim$ 1000 nT) and have short wavelengths ($\sim$ 10 km) although near Valdivia Deep (profile 2, fig. 5.19) the magnetic field is comparatively smooth. These anomalies have been examined in section 5.6 and interpreted as due to leaky transform faults. If this is true then the deeps must be formed as a result of seafloor spreading. Several of the deeps are located near the centres of spreading given by the models (see section 5.6.2) and this may account for the high temperatures and heat flow associated with them. From figs 5.19 and 5.20 it can be seen that three deeps, Valdivia, Wando Basin and Atlantis II, lie on or very near a spreading centre. However a comparison of the properties

TABLE 5.1

Location of deeps in the central Red Sea including some of their physical and chemical properties

Name of Deep	Latitude (^{o}N)	Longitude (^{o}E)	Total Depth (metres)	Brine pool present?	Temperature of brine (^{o}C)	Thickness of brine layer (m)	Chlorimity (%Cl) of most concentrated brine	Heat Flow (mW m^{-2})
Vema	23.87	36.51	1611	No	-	-	22.7[3]	-
unnamed	23.67	36.43	1500	No	-	-	-	-
Nereus	23.19	37.23	2445[1]	Yes	30.2	39	129.5	374[1]
Thetis	22.72	37.60	1970	No	22.6	-	22.9[3]	-
Hardaba	22.47	37.77	2250	No(?)	-	-	-	-
Hatiba	22.0	37.9	>2300	-	-	-	-	-
Valdivia	21.34	37.95	1673	Yes	29.8[2]	123	144.7[2]	126
AtlantisII	21.38	38.08	2194	Yes	60.1[2]	178	156.5	921[1]
Wando Basin	21.36	38.04	2013	Yes	29.3[2]	28	73.5	-
Discovery	21.28	38.05	2224	Yes	44.8	209	155.5	29
Chain	21.29	38.08	2122[1]	Yes	53.2[2]	167(?)[2]	156.0	-
Albatross	21.20	38.12	2133	Yes	24.4	72	143.3	-
Shagara	21.13	38.09	2496	Yes	-	8	113[3]	-
Aswad	20.92	38.28	2400	No	-	-	-	-
Erba	20.73	38.18	2395	Yes	27.9	19	86.5	-
Suakin	19.62	38.75	2840[1]	Yes	24.6[2]	74[2]	85.9	-
Port Sudan	20.06	38.51	2836	Yes	36.2	322	125	122[1]
Volcano	20.02	38.45	2440	No	-	-	-	-

1 mean value

2 max value

3 from connate water

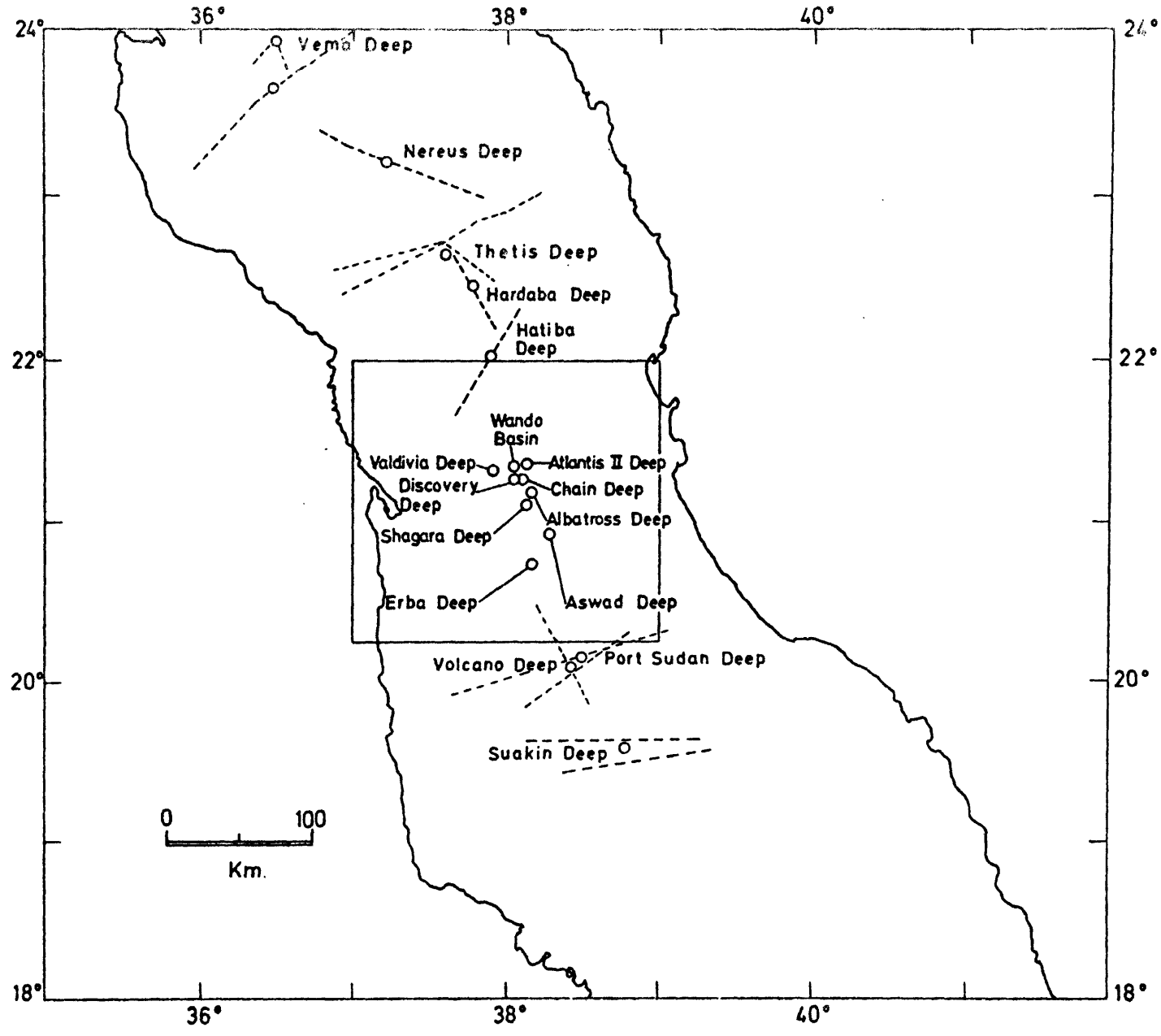

Figure 5.21 Location of deep holes between 18°N and 24°N. Dashed lines represents ships' tracks that pass near or over the deeps. Tracks over deeps in inset are shown in figs. 5.16 and 5.18.

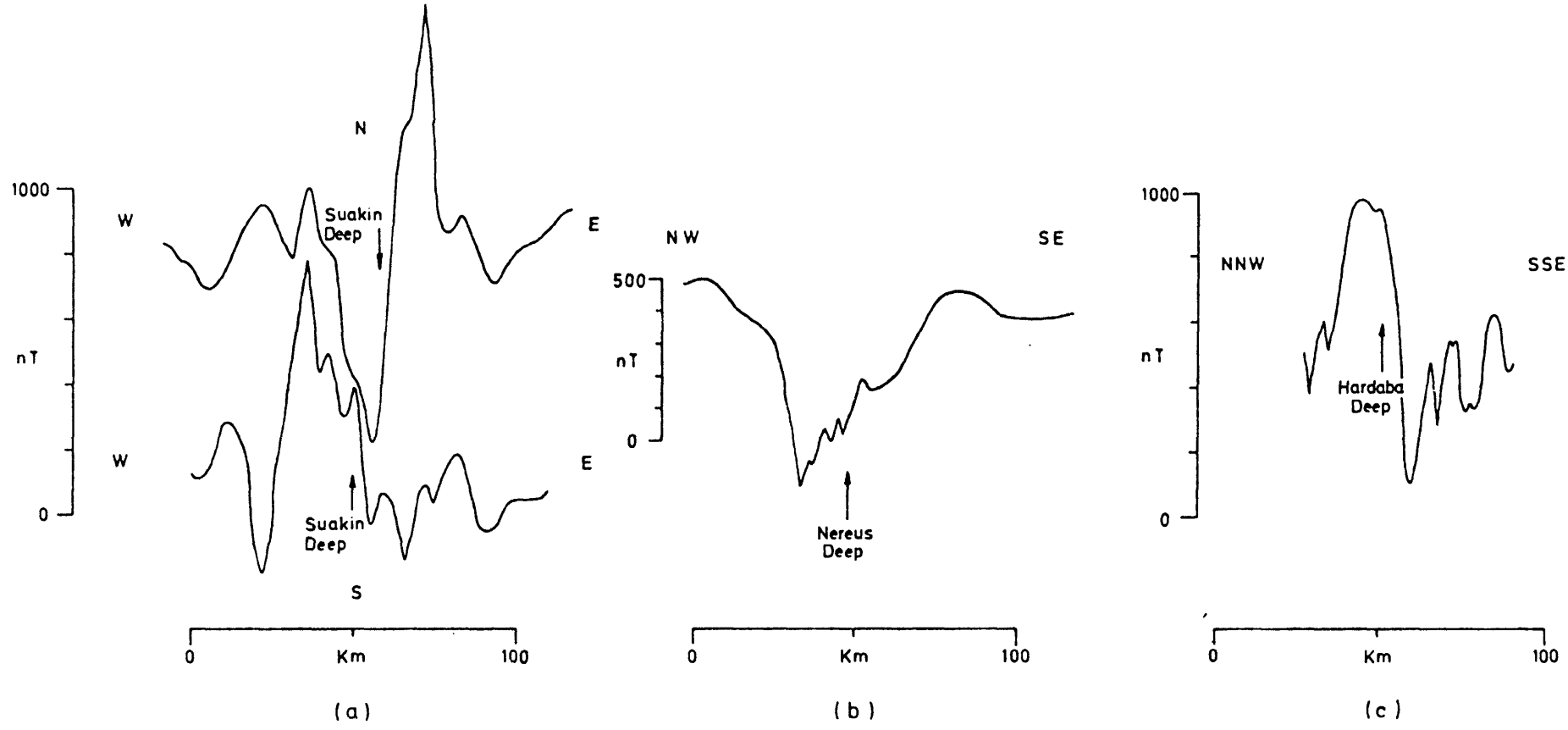

Figure 5.22 Magnetic profiles over (a) Suakin, (b) Nereus and (c) Hardaba Deeps. Locations of profiles shown in fig. 5.21.

of these deeps (Table 5.1) indicates several important differences. For example, Atlantis II Deep has very high temperatures and heat flow whilst Valdivia Deep has only slightly elevated temperatures and lower heat flow values (fig. 1.4). These differences suggest the 'activity' of the leak varies along its length with a maximum close to the deep water axis. It seems, therefore, the Red Sea axis has a noticeably larger influence on the temperature and heat flow than the "leaking" axis. This probably reflects the presence of a relatively narrow, elongated magma chamber beneath the deep water axis the depth to which increases with distance from the axis.

Six of the eighteen deeps are located within areas over which the anomalies are parallel to the axial trough although in the case of the most northerly four,these are poorly defined. The location of the deeps (Vema, Thetis, Hatiba, Port Sudan, Volcano and an unnamed deep) together with adjacent ships' tracks are shown in fig. 5.21. Three of the deeps, Vema, Hatiba and the unnamed deep, have tracks which pass over them within the limits of navigational accuracy whilst the others have several that pass close by. Magnetic profiles from these tracks are shown in fig. 5.23(a) to (e). Thetis, Volcano and Port Sudan Deeps are located in areas over which large (500 to 1000 nT), short wavelength (5 to 10 km) anomalies are present. Smaller (100 to 200 nT), slightly longer wavelength (10 to 15 km) anomalies are observed on those profiles directly over Vema and the unnamed deep (fig. 5.23 (a) and (b)). In the case of Hatiba Deep the anomalies are

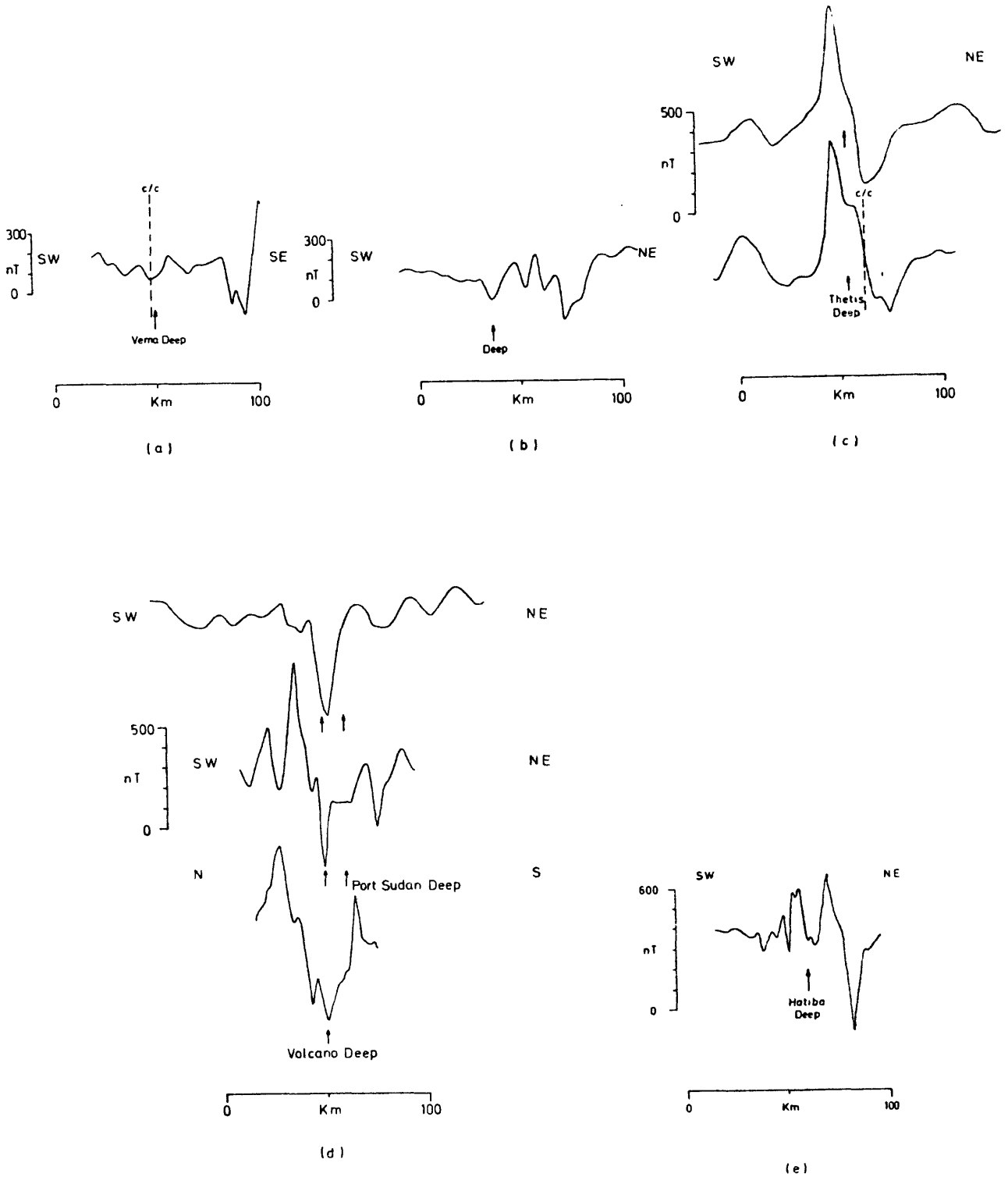

Figure 5.23 Magnetic profiles over Vema, Thetis, Port Sudan, Volcano and Hatiba Deeps and an unnamed deep near Vema Deep. Location of profiles shown in fig. 5.21.

typically 200 to 300 nT with 5 to 10 km wavelengths. These anomalies form part of the pattern shown in fig. 5.9 which is due to seafloor spreading (see section 5.5.1). Consequently individual models for the deeps were not computed. However, as the tracks occasionally pass some distance from them (fig. 5.21) the presence of localised anomalies over the deeps cannot be ruled out completely (cf. northern Red Sea, section 4.7).

CHAPTER SIX

THE RED SEA SOUTH OF 18°N

SECTION ONE

6.1 Relevant geophysical data

South of 18°N the Red Sea has a narrow, deep water trough which terminates at about 15.2°N and shallow shelves (< 100 fathoms) that widen southwards to 16°N. Consequently, marine surveys are mostly restricted to the narrow deep water areas. Figure 6.1 shows the locations of the geophysical information available excluding the magnetic data.

Twenty-five heat flow measurements have been made (Sclater, 1966; Langseth and Taylor, 1967; Girdler, 1970a; Haenel, 1972; Girdler et al, 1974), of which all but three are higher, some being several times greater than the world mean value . Nineteen measurements were made in deep water and six along the shallow shelves and coastal plain. All the latter measurements are high, two to three times the mean, indicating the entire width of the Red Sea is associated with anomalously high heat flow. The highest values are found in the deeper water where they are typically three times greater than the mean, with a maximum value of 205 mW m^{-2}. One deep water value (26 mWm^{-2}) is much lower than the mean, although a large topographic correction has been applied (Haenel, 1972). This measurement was obtained just south of a shallow area of the axial trough at 16.9°N, 40.8°E and is probably, therefore, considerably influenced by the bathymetry.

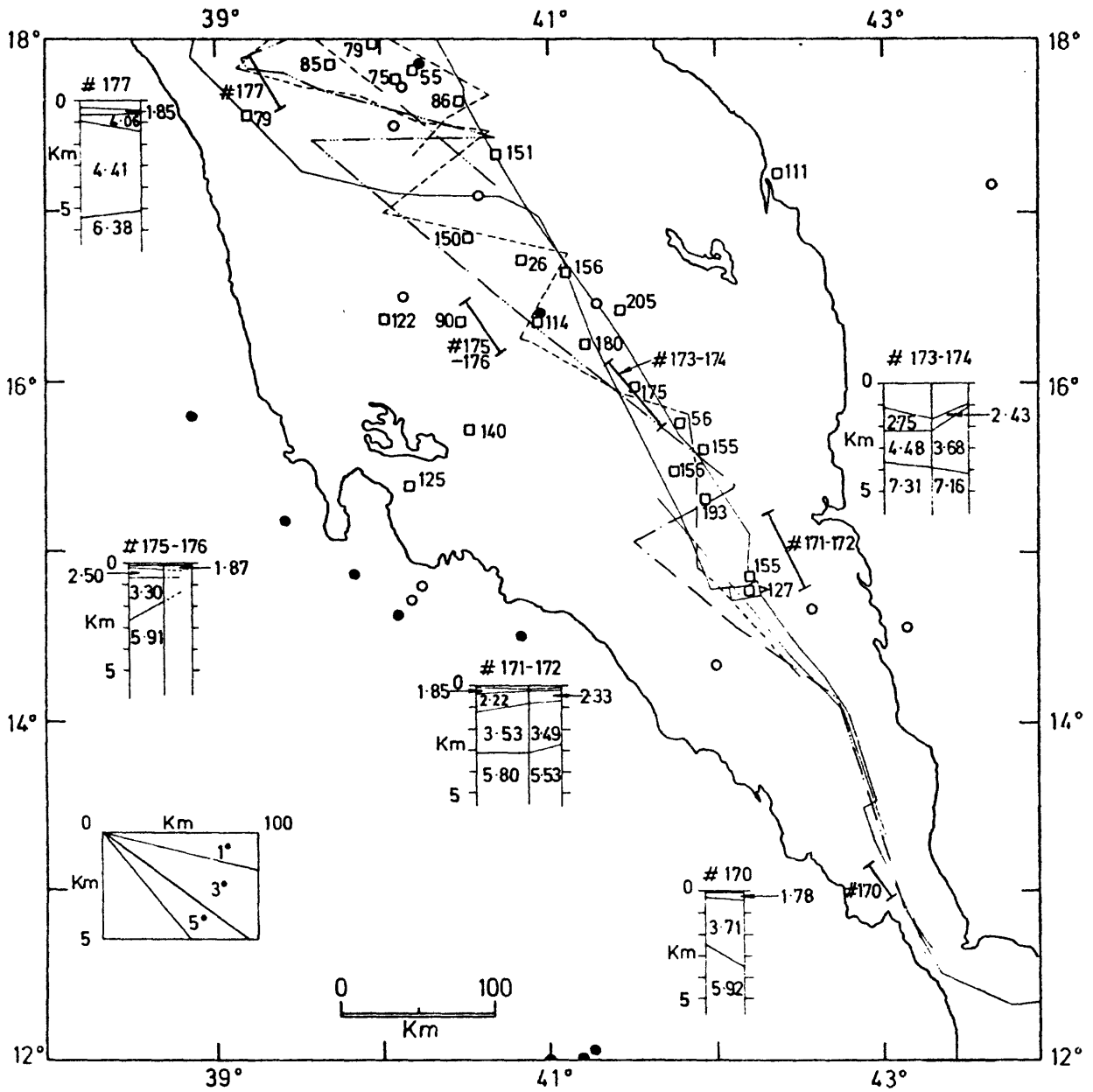

Figure 6.1 Geophysical data (excluding magnetic) available for the Red Sea between 12°N and 18°N. □ heat flow measurement (values in mW m^{-2}); O and ● earthquake epicentres before 1963 and since 1963 respectively. ⊢——⊣ seismic refraction profiles; ——— seismic reflection profiles; —— · · · —— gravity profiles; — — — — seismic reflection and gravity profiles. Seismic velocities in crustal models are in km s^{-1}.

Gravity measurements (Girdler and Harrison, 1957; Plaumann, 1963; Allan et al, 1964) are limited to a few tracks (Fig. 6.1) and several gravity stations (see Girdler, 1958) south of 17.0°N (not shown in Fig. 6.1). These measurements are over the deeper water and indicate a large positive Bouguer anomaly (1000 g.u.) which narrows southwards. The Bouguer map of Allan (1970) shows the anomaly narrowing and becoming smaller such that it is only 500 g.u. at 15.5°N.

Seismic reflection studies (Knott et al, 1966; Ross and Schlee, 1973) have detected the S-reflector beneath each area of the main trough covered. Existing measurements only extend south as far as 16°N and consequently its presence south of this remains to be shown. However, the measurements of interstitial salinity by GLOMAR CHALLENGER at sites 229 and 230 (Whitmarsh et al, 1974) suggest the reflector is present at 15.3°N but ends between 14.8°N and 15.3°N. The reflector is absent, in general, from the axial trough.

The seismic refraction data available comprises five reversed profiles from VEMA and ATLANTIS (1958). The profile locations and seismic velocities obtained by Drake and Girdler (1964) are shown in Fig. 6.1. Each profile except 173-174 gave similar results. Layer 1, the topmost layer, has a seismic velocity between 1.8 km sec^{-1} and 2.8 km sec^{-1} and varies in thickness from 0.13 km on profile 173-174 to 1.1 km on profile 171-172. Layer 2 has velocities of 3.3 to 4.5 km sec^{-1} and a thickness of approximately 2 to 3 km. Underlying these is a layer with velocity of 5.5 to 6.4 km sec^{-1} (mean value $\sim$ 5.9 km sec^{-1}). Profile

173-174 which lies over the deeper water gave similar velocities and thicknesses for the top two layers but the third layer has a velocity of 7.2 to 7.3 km sec^{-1}.

Also shown in Fig. 6.1 is the distribution of earthquake epicentres : solid circles represent events occurring since the introduction of the WWSSN, in 1963, open circles represent events prior to 1963. The events are widely scattered although the small number of earthquakes for which there are epicentre determinations may be responsible for this. In general, the two most active areas are the axial trough north of 16^{o}N and a broad area near the Gulf of Zula. Six events have occurred in the axial trough, two since 1963, for one of which there are first motion studies (Sykes, 1968; Fairhead and Girdler, 1970). This earthquake, which was located at 17.1^{o}N, 40.6^{o}E and had magnitude 5.6, gave fault plane solutions involving sinistral movement along either $N23^{o}$ (Sykes, 1968) or $N49^{o}$ (Fairhead and Girdler, 1970).

Events occurring near the Gulf of Zula and those along the continental margins (Fig. 6.1) are probably the result of normal faulting although some of this activity may be associated with the rotation of the Danakil plate.

6.2 Distribution of magnetic data

6.2.1 Sea data

Ships' tracks for which magnetic data are available south of 18^{o}N are shown in Fig. 6.2. One vessel, VALDIVIA, used a Decca Hi-fix navigational system giving positional accuracies better than 50 metres. Two tracks at approximately 14.5^{o}N (EE' and adjacent parallel track, fig. 6.2)

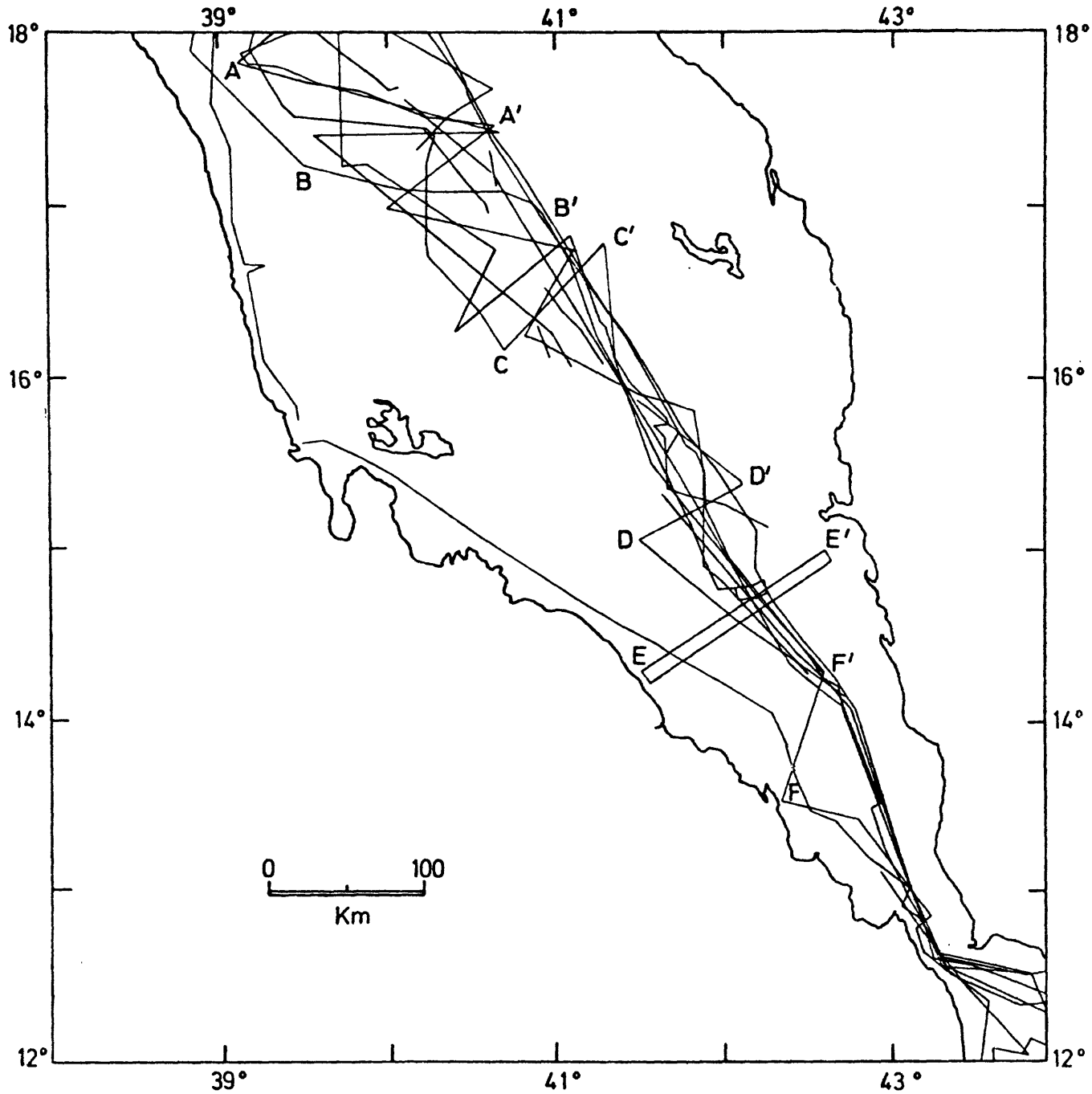

Figure 6.2 Tracks of research vessels between 12°N and 18°N for which magnetic data are available. Lettered tracks (AA , BB etc.) indicate the location of magnetic profiles shown in fig.6.4.

were used from this survey. Two other vessels, CHAIN (cruise 100) and GLOMAR CHALLENGER (Leg 23) used satellite navigators giving accuracies of about 100 to 200 metres. The remaining vessels used radar and celestial fixes giving accuracies of typically 1 to 2 km but considerably better in the south where there are many islands and the coastlines converge.

The coverage is poor, with a majority of tracks trending approximately NW-SE in the narrow, deep water areas. Between 17^{o}N and 18^{o}N several long ($\sim$150 km) tracks cross the axial trough and extend some way over both sides of the main trough; most of these trend either W-E or WNW-ESE. South of 17^{o}N, seven tracks cross the deeper in an approximately NE-SW direction. Five of these are shorter (about 80 to 90 km) than those north of 17^{o}N and two (EE' and adjacent track, fig. 6.2) are of similar length, viz. 140 km. Except for the single track along the African coast (fig. 6.2) from DISCOVERY (cruise 16) the wide, shallow shelves are not covered.

6.2.2 Air data

Two aeromagnetic surveys have been made along the Arabian coast south of 18^{o}N. The surveys, whose locations are shown in fig. 6.3, cover almost the same area near Jizan. The first (dotted outline, fig. 6.3) was flown in 1962 at a height of 300 metres AMSL by Hunting Survey Corporation of Canada for the DGMR, Saudi Arabia. The lines were flown along N55^{o} at a spacing of 1.25 km. Doppler navigation was used giving positional accuracies of about 0.1 km over land and 1 km over the sea away from the Farasan Islands.

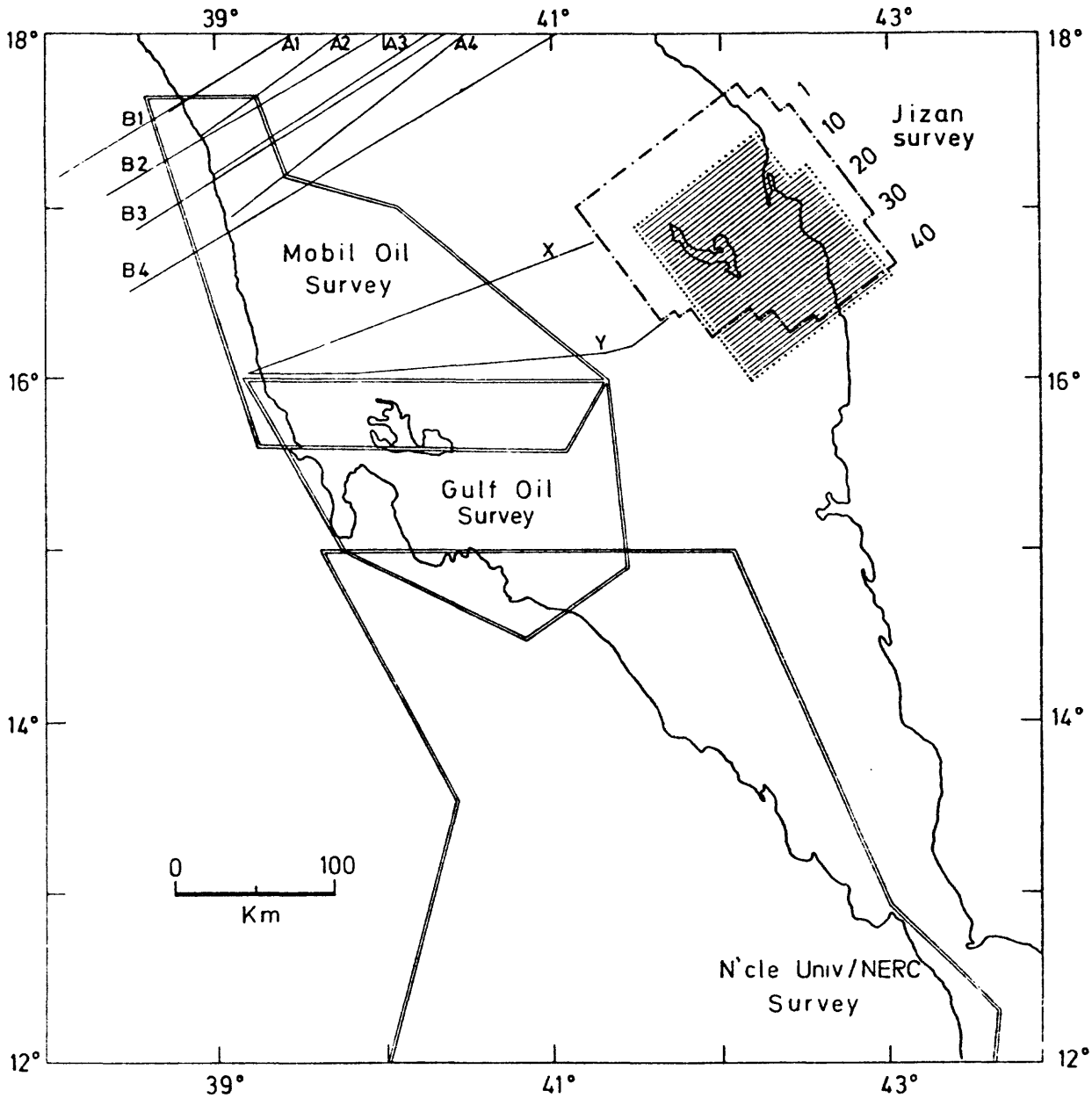

Figure 6.3 Location of aeromagnetic data between 12°N and 18°N. Flight lines inside dotted outline show location of Jizan profiles in fig. 6.5. Dot-dashed outline is Auxerap Jizan survey for which data are not currently available.

The second survey (dot-dashed outline, fig. 6.3) was flown in 1966 at a height of 2500 metres by Arabian Geophysical and Surveying Co. for the Auxerap Oil Co. The lines were flown along N50^{o} at a spacing of 1.5 km in some areas and 3 km elsewhere. Radar beacons, located on the Farasan Islands were used giving extremely good positional control of tens of metres. Unfortunately, data from this survey are not currently available.

Three aeromagnetic surveys have been made along the African coast between 12^{o}N and 18^{o}N. These include: (i) the northern part of a survey flown over the junction of the Red Sea, Gulf of Aden and Ethiopian Rift (Girdler, 1970b; Girdler and Hall, 1972), (ii) a Gulf Oil Co. survey between 15^{o}N and 16^{o}N (Girdler and Styles, 1974), and (iii) several, widely spaced, profiles flown for Mobil Oil Co. between 15.6^{o}N and 17.6^{o}N (Hall et al, 1970; Styles, in prep.) Outlines of the appropriate survey areas are shown in fig. 6.3.

Finally, there are two long profiles (X and Y, fig. 6.3) flown at a height of 2500 metres as part of the 1966 Auxerap survey and eight coast - to-coast Project Magnet profiles (see section 5.2.2 and fig. 5.3) which cross the African coast between 16.9^{o}N and 17.6^{o}N.

The coverage of the African coast and shelf areas is extremely good with only a minor gap between 17.6^{o}N and 18^{o}N, although the line spacing in the Mobil survey area is wide (15 km). Coverage of the Arabian side, on the other hand, is poor with no data over the Farasan Bank between 17.5^{o}N and 18^{o}N or over offshore areas south of 16^{o}N.

6.3 Description of magnetic anomalies

6.3.1 Wavelength, amplitude and distribution of anomalies

Anomalies observed on both sea and air data were separated into groups on the basis of their wavelength and amplitude. Anomalies of a particular group were again found in specific areas or zones. Three zones were found: (1)Over the axial trough there are large amplitude (1000 to 1500 nT), 5 to 10 km wavelength anomalies, cf. profiles AA', BB' and CC' (fig. 6.4), which vary considerably in shape and size becoming smaller (approximately 500 nT) towards the south (e.g. DD' and EE', fig. 6.4). In some areas the anomalies are also observed outside of the deeper water beyond the 500 fathom contour (e.g. CC', fig. 6.4). (2)Over the main trough and parts of the wide, shallow shelves there are smooth, long wavelength (15 to 30 km) anomalies of 100 to 150 nT. These are observed at the western ends of profiles AA' and BB' (fig. 6.4), on each profile of the Jizan coastal survey (fig. 6.5) and at the western ends of profiles X and Y (fig. 6.6). The anomalies have a remarkably uniform appearance, quite different to the large, axial anomalies. (3) Over the southern part of the area (FF', fig. 6.4) and at the extreme eastern ends of profiles 32 to 40 of the Jizan survey (fig. 6.5) there are small amplitude (5 to 50 nT), very short wavelength (approximately 1 to 2 km) anomalies. Those on the airborne profiles are larger but more variable (20 to 700 nT). On profile FF' they appear to be superimposed on broader features of 10 to 20 km and amplitudes 200 to 300 nT. It is not possible to detect the broader features, if present, on profiles 32 to 40 (fig. 6.5) as only a few kilometres of each display the high frequency anomalies.

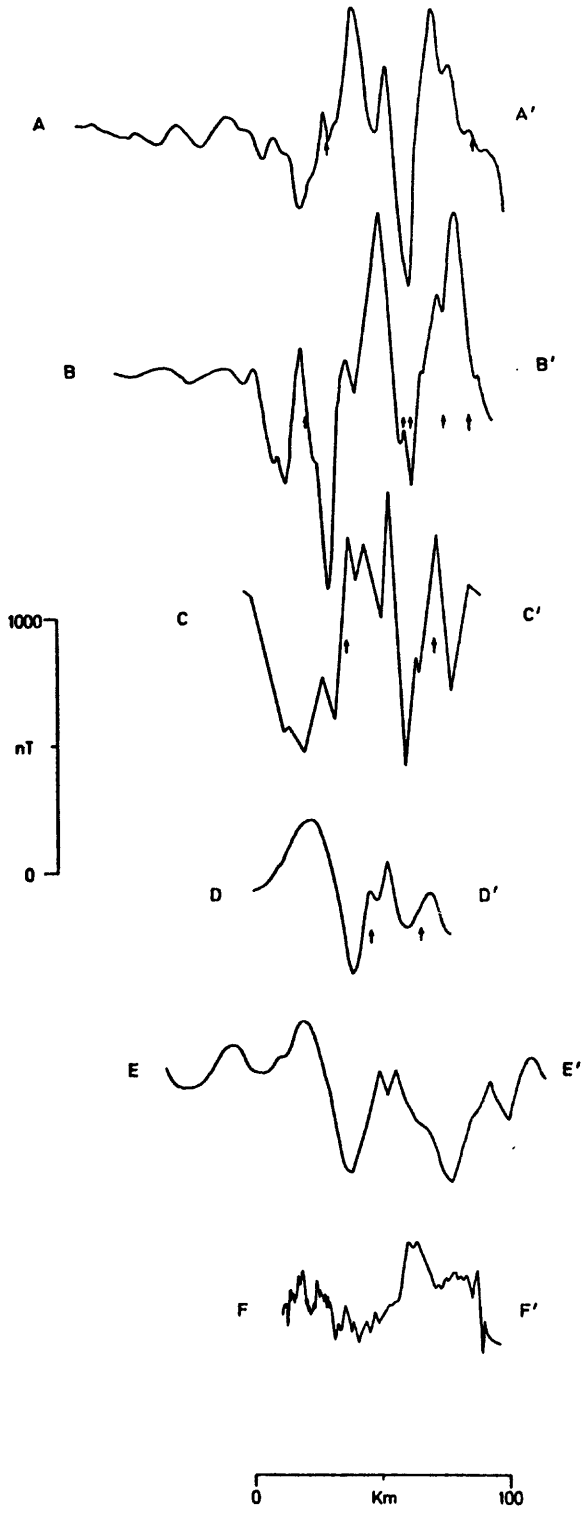

Figure 6.4 Magnetic profiles over southern Red Sea. Location of profiles are shown in fig.6.2. Arrows indicate approximate position of 500 fathom contour.

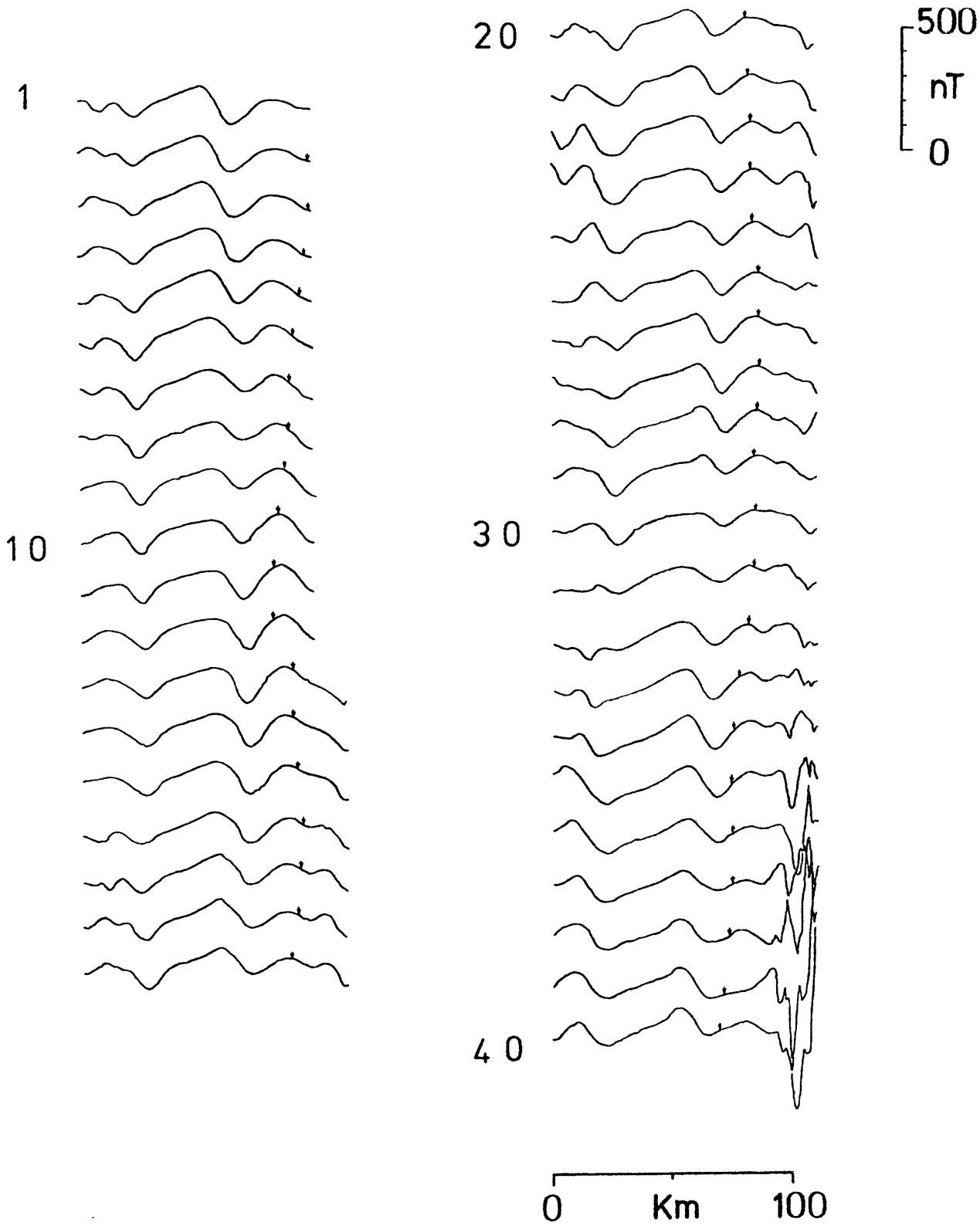

Figure 6.5 Aeromagnetic profiles from the Jizan survey. Location of profiles shown in fig. 6.3. Small arrows indicate approximate position of Arabian coast. All profiles flown at 300 metres.

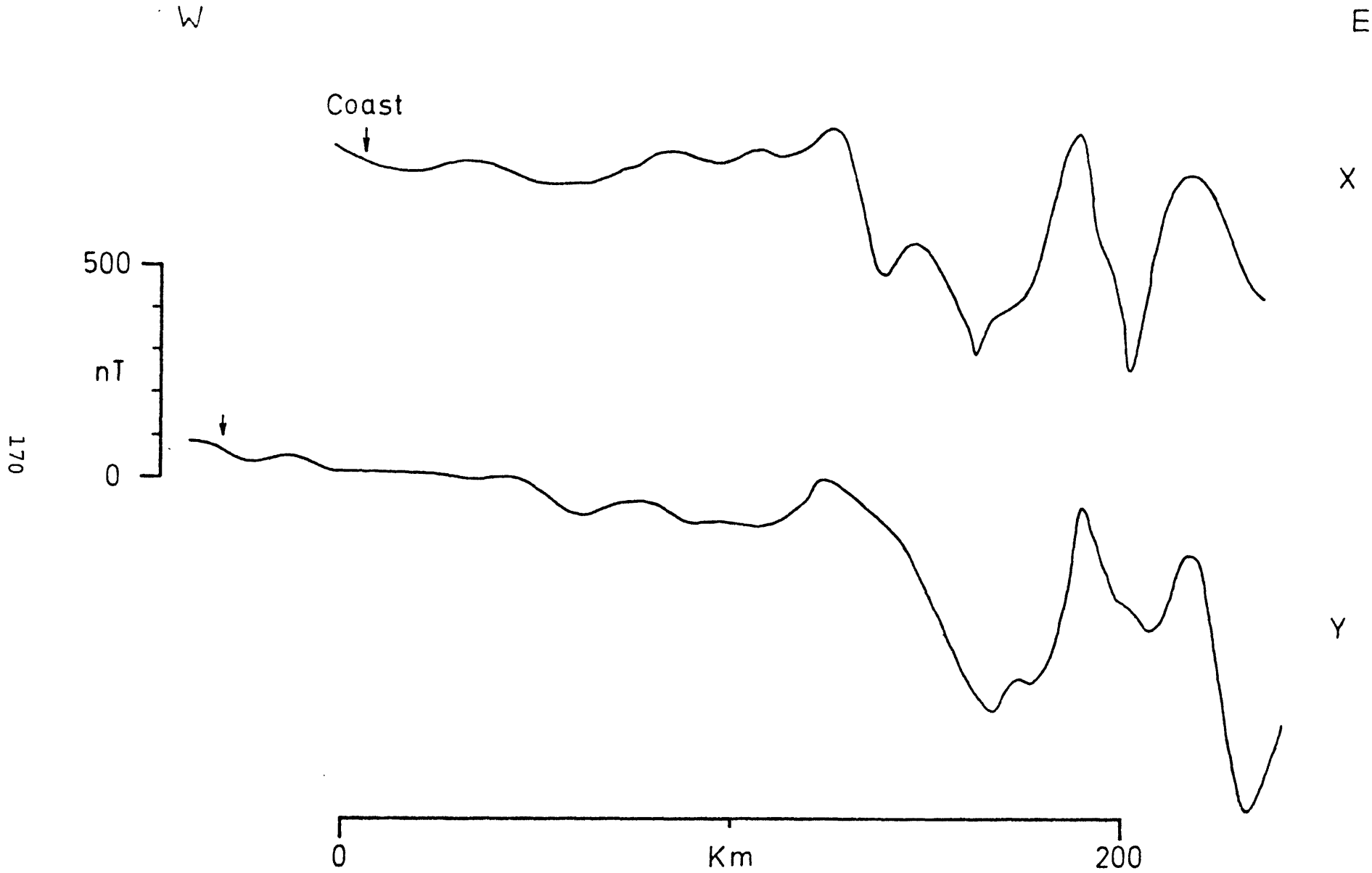

Figure 6.6 Aeromagnetic profiles across Red Sea between 16°N and 17°N. Location of profiles shown in fig. 6.3. Arrows indicate approximate position of African coast. Both profiles flown at 2500 metres.

There are high frequency anomalies in the northern and central Red Sea but these are found over coastal sediments and outcrops of Pre-Cambrian rocks (see Chapters 4 and 5). Their presence over sea areas in the southern Red Sea is, therefore, particularly significant and a more detailed description of the anomalies is given in section 6.3.3.

6.3.2 Correlations of the anomalies

The anomalies were separated into groups on the basis of their continuity. Anomalies of zones 1 and 2 (see section 6.3.1) are fairly continuous whilst those of zone 3 cannot be correlated very well. The locations of dominant peaks and troughs in zones 1 and 2 were transferred to the map shown in fig. 6.7. Peak and trough locations within the Gulf survey area (fig. 6.3) were kindly provided by P. Styles; those to the south were obtained from the magnetic anomaly map of Hall (1970). Correlations of the anomalies were made and the corresponding features in fig. 6.7 joined by straight lines. Tentative correlations are shown by light dashed lines. In the case of the Jizan survey the density of flight lines is such that to avoid cluttering the diagram only the peaks and trough from every other line are shown in fig. 6.7.

In general, the correlations are good, especially along the African and Arabian coasts (cf. profiles 1 to 40, fig. 6.5 and fig. 3, Girdler and Styles, 1974). Several profiles from the sea data, between 16^{o}N and 18^{o}N, are shown in fig. 6.8; major features which correlate well, include a large peak-trough-peak on each profile and a dominant trough approximately 30 to 40 km west of the central trough. Variations in the size and shape

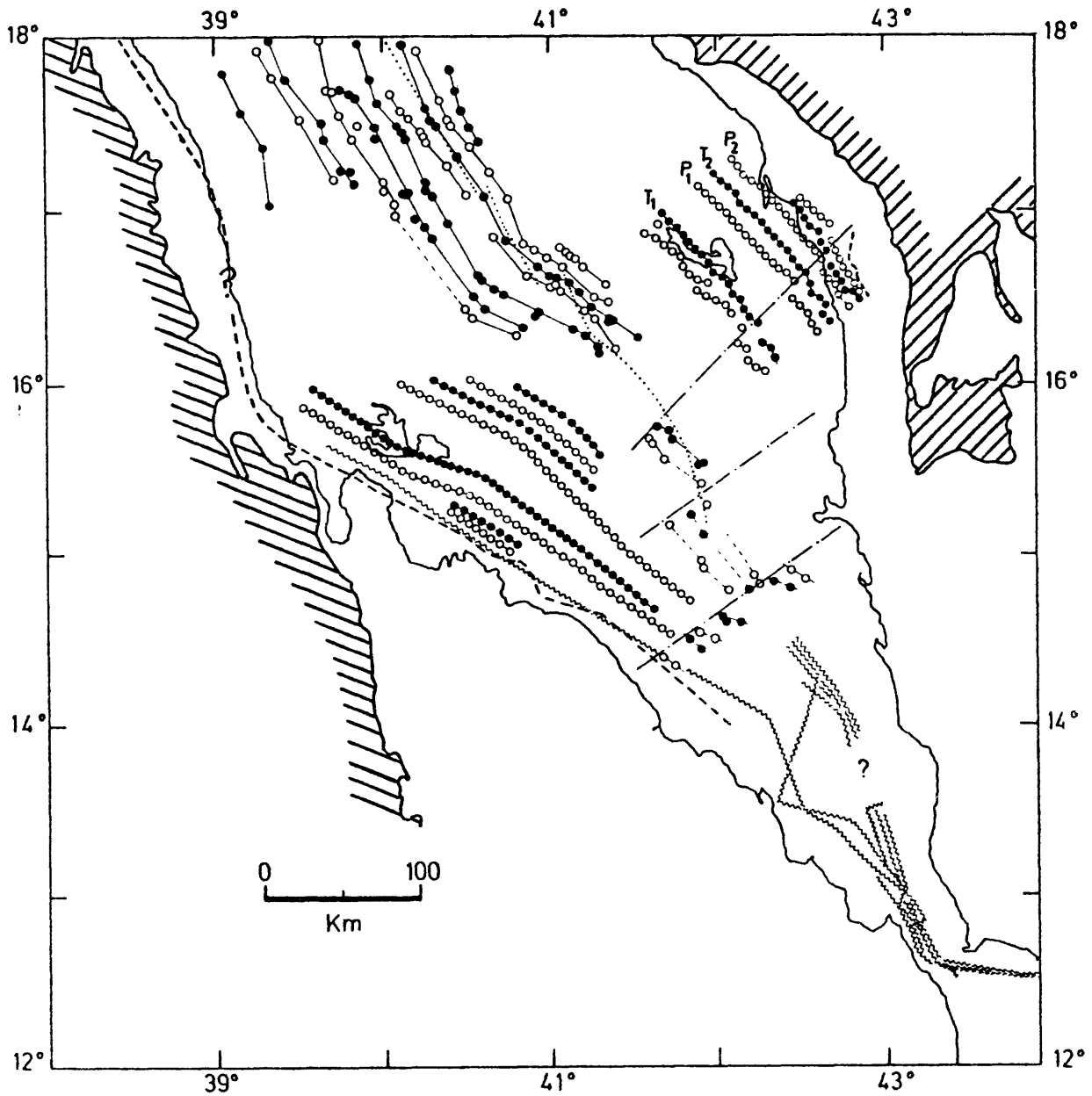

Figure 6.7 Location of dominant peaks, O (positive anomalies) and troughs, ● (negative anomalies. ····· deep water axis; —— · —— discontinuities in magnetic pattern. Heavy shaded line represents seaward limit of mapped Pre-Cambrian; heavy dashed line is seaward limit of high frequency anomalies. Firm correlationsof features shown as solid lines; tentative correlations as light dashed lines. Saw shaped symbol denotes ships' tracks along which high frequency anomalies are observed.

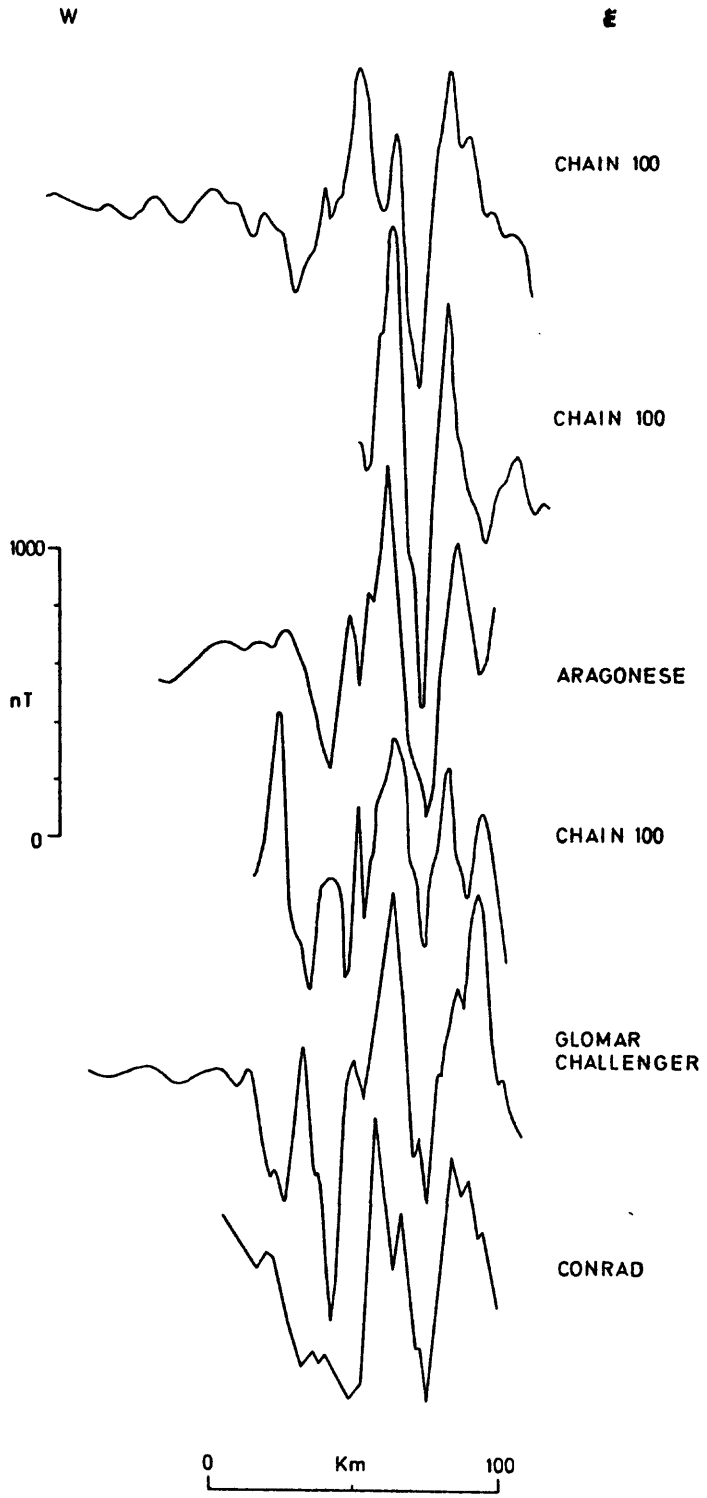

Figure 6.8 Approximately E - W magnetic profiles over deeper water between 16°N and 18°N. Profiles are aligned olong large, central anomaly.

of the anomalies over the deep water make reliable correlations difficult in many cases. In particular, where the tracks are oblique to the trend of the anomalies, it is difficult to identify corresponding features. No correlations were attempted in those areas south of 14.2°N where all the tracks trend approximately parallel and are located very close to one another.

The anomalies form lineations approximately parallel to the deep water axis (dotted line, fig. 6.7) with the largest peak-trough feature lying near, often directly over, this axis. The linear pattern can be traced along the African coast from about 14°N to 17.7°N, the Arabian coast between about 16°N and 17.5°N (i.e. throughout the Jizan survey) and over the deep water between 16.3°N and 18°N. South of 16.3°N the absence of suitably oriented ships' tracks does not permit all the anomalies to be traced. At 15.8°N, the large, central peak-trough feature is observed and may be followed southward to 15.3°N where it is offset dextrally by about 30 km. South of this, the anomalies are more difficult to identify as they become smoother (e.g. DD' and EE', fig. 6.4). Tentative correlations south of 15.3°N indicate the anomalies trend N 145° to 14.6°N where they appear to be offset dextrally again, this time by about 25 km. South of this there are no suitably oriented tracks and consequently correlations could not be made.

6.3.3 High frequency anomalies in the southern Red Sea

Magnetic profiles from each research vessel were examined for high frequency anomalies. None was found over the deeper water north of

14.5°N. However, along the track near the African coast (fig. 6.2) and over the deeper water south of 14.5°N the anomalies are common. An attempt was made to annotate those parts of the tracks where the high frequency anomalies are present although there are difficulties locating exactly where they first appear. The presence of the anomalies are indicated in fig. 6.7 by a saw-shaped symbol.

South of 14.1°N the anomalies are observed on all sea profiles. Four magnetic profiles from tracks over the deeper water south of 14°N are shown in fig. 6.9. The tracks trend parallel to the deep water channel (N145°) and are located close to one another. The correlation of the anomalies, therefore, is due to the proximity of the tracks and does not signify NE-SW trending features. A short section (AB, fig. 6.9) of each profile appears smoother than the rest and consequently the presence of high frequency anomalies in these areas is questionable. A question mark has been used in fig. 6.7 to indicate these sections of the tracks.

The magnetic profile from the DISCOVERY 16 track along the African coast is shown in fig. 6.10. The character of the profile changes from smooth, 15 to 20 km wavelength anomalies near A to very variable, high frequency anomalies between D and E. Beyond E the anomalies are larger (~700 nT), similar to those observed over the deeper water in the Red Sea. Volcanoes and extensive lavas have been reported in the area (Lamare, 1930; MacFadyen, 1932; Gass et al, 1965; Gass et al, 1973) and it seems likely that these constitute the magnetic sources. The differences in character of the anomalies between B and E (fig. 6.10) are more difficult to explain.

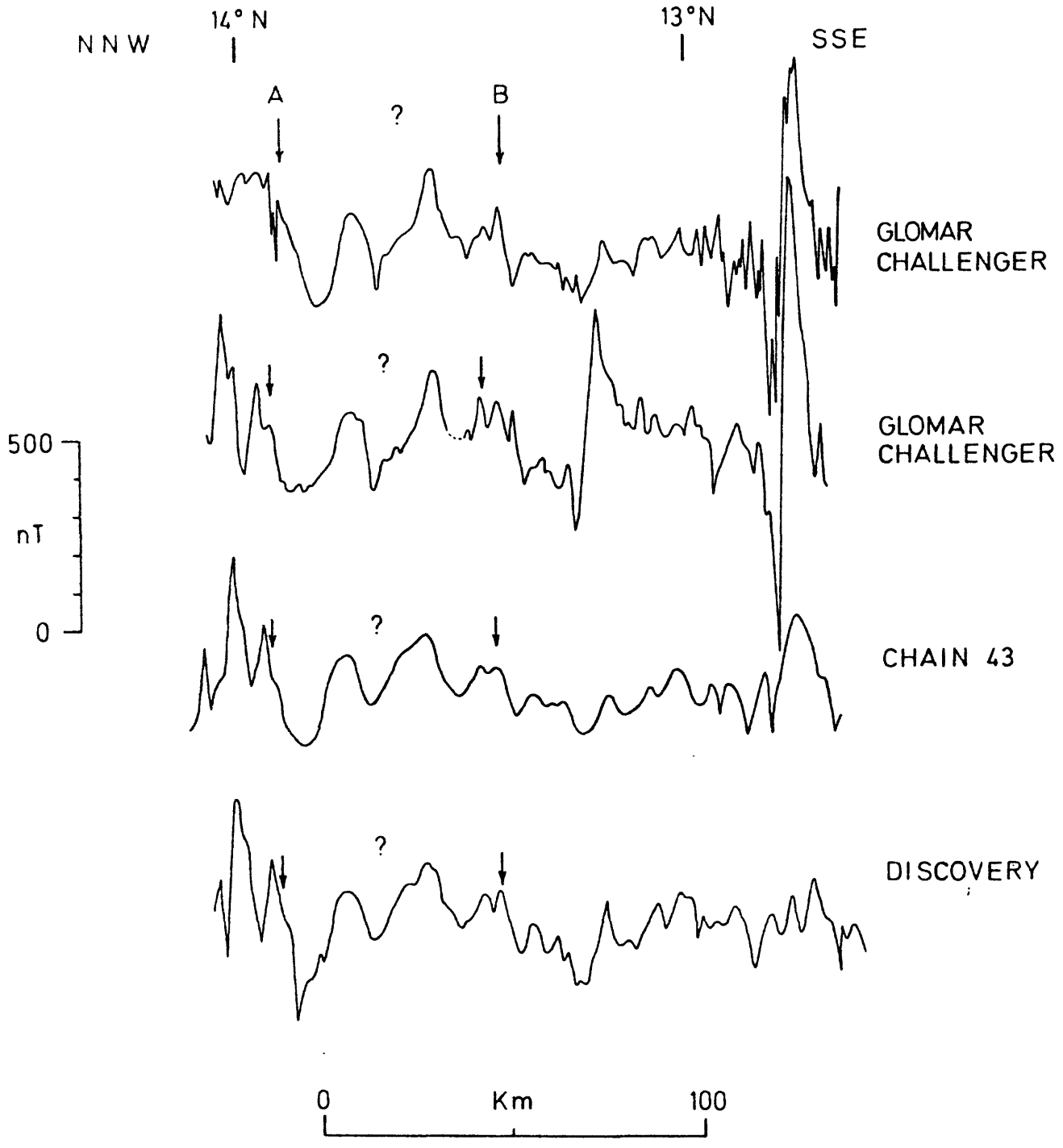

Figure 6.9 Magnetic profiles over deeper water between 12.6°N and 14°N. Profiles trend N160° along the narrow navigable channel east of Hanish Island. AB denotes somewhat smoother portion of each profile.

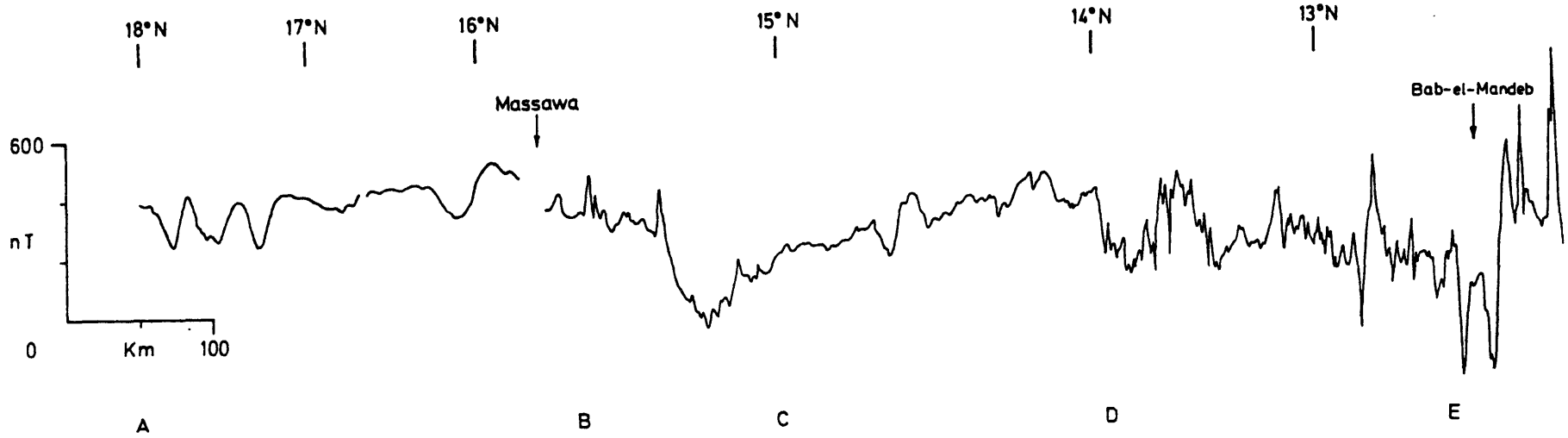

Figure 6.10 Magnetic profile over shallow shelf near African coast from the research vessel DISCOVERY. Location of profile is shown in fig. 6.2.

Anomalies between B and D are smaller, in general, and seem to be superimposed on broader features. These may be due to deeper lavas but could also be produced by Pre-Cambrian rocks underlying the African coastal margin. There is an abrupt change in character at D (fig. 6.10) to larger, high frequency anomalies similar to those seen on profile FF' (fig. 6.4). This change suggests the lavas may be limited to shelf areas south of 14°N although, as fig. 6.7 shows, beneath the deeper water they are probably present at least as far north as 14.5°N.

6.4 Ocean/continent boundary

Unlike the northern and central Red Sea the air data along the Arabian side in the southern Red Sea do not, in general, extend sufficiently inland to record the high frequency anomalies associated with the Pre-Cambrian crystalline basement. Estimates of the ocean/continent boundary could be obtained only from profiles 32 to 40 (fig. 6.5) as these recorded the high frequency anomalies. The western limit of the anomalies on these profiles is shown by a heavy dashed line in fig. 6.7. Along the African side each survey records some high frequency anomalies and it is possible to locate the high frequency edge more reliably. This edge was obtained from Girdler and Styles (1974) and Plate 1.

Also shown in fig. 6.7 (shaded solid line) is the mapped edge of the Pre-Cambrian outcropping along each side. On the Arabian side south of 17.5°N this edge is about 50 km inland, well to the east of the Jizan survey area. Therefore, the high frequency anomalies on profiles 32 to 40 may indicate either the shield rocks extend beneath the coastal sediments or,

since the amplitudes are rather large (~500 nT), the presence of basaltic dykes or flows. Along the African side, the high frequency edge and Pre-Cambrian edge are separated by a similar distance but since the anomalies are smaller (~ 100 nT) they are probably due to shield rocks beneath the shelves.

An alternative estimate of the ocean/continent boundary may be obtained from the eastern and western limits of the smooth, seafloor anomalies. Along the African coast, the western extent of these anomalies is well defined and appears to coincide more or less with the high frequency edge. There is a gap of approximat ely 10 km between the final correlatable seafloor anomaly and the high frequency edge at 15^{o}N. On the Arabian side, profiles 1 to 31 (fig. 6.5) have seafloor anomalies at their eastern ends; consequently, only profiles 32 to 40 may be used. Using these profiles the final correlatable feature seems to be a peak, 15 km inshore, on profile 32 (fig. 6.5). This peak is about 2 km west of the high frequency edge (heavy dashed line, fig. 6.7) indicating the ocean/continent boundary is well defined by the high frequency anomalies. Combining the results from each side there appears to be 320 ± 20 km of oceanic crust at 17^{o}N measured along N55^{o}. This is slightly less than the amount estimated at 19^{o}N, viz. 330 km, suggesting the Red Sea may begin to narrow near 17^{o}N.

6.5 Seafloor spreading history

The detailed analysis of the Gulf survey between 15^{o}N and 16^{o}N on the African side (Girdler and Styles, 1974) has clearly demonstrated the existence of an older phase of seafloor spreading. The Jizan survey (fig. 6.3) enables

the symmetry of this seafloor to be studied and the anomalies examined for evidence of narrowing due to the rotation of the Danakil plate. The plate geometry of the area is discussed further in Chapter 7. The recent spreading is examined first.

6.5.1 Recent seafloor spreading

The linear anomalies over the axial trough and adjacent parts of the main trough have been interpreted as being due to a recent phase of seafloor spreading (Vine, 1966). Further models, based on Vine's work have been given by Phillips et al (1969), Phillips (1970), Allan (1970) and Girdler and Styles (1974). A seafloor model of this recent phase of spreading was computed and is shown in fig. 6.11. In this model, the seafloor at 17^{o}N was spread continuously between 5 My and the present at a constant rate of approximately 0.8 cm y^{-1}. The observed profiles in fig. 6.11 have been projected onto the direction $N55^{o}$, i.e. normal to the magnetic trends shown in fig. 6.7. The correlation of the observed and synthetic profiles is remarkably good between 0 and 5 My; beyond this (B in fig. 6.11) the observed anomalies are smaller and have longer wavelengths than the synthetics. This is similar to the central Red Sea (fig. 5.14). and B probably represents the boundary between the two phases of spreading.

Another seafloor model was computed for profile DD' (fig. 6.4) at 15.3^{o}N. The model, shown in fig. 6.12, involves a slightly smaller spreading rate, viz. 0.7 cm y^{-1}. Insufficient dominant features are present to obtain more than a fair correlation and the profile is too short to record

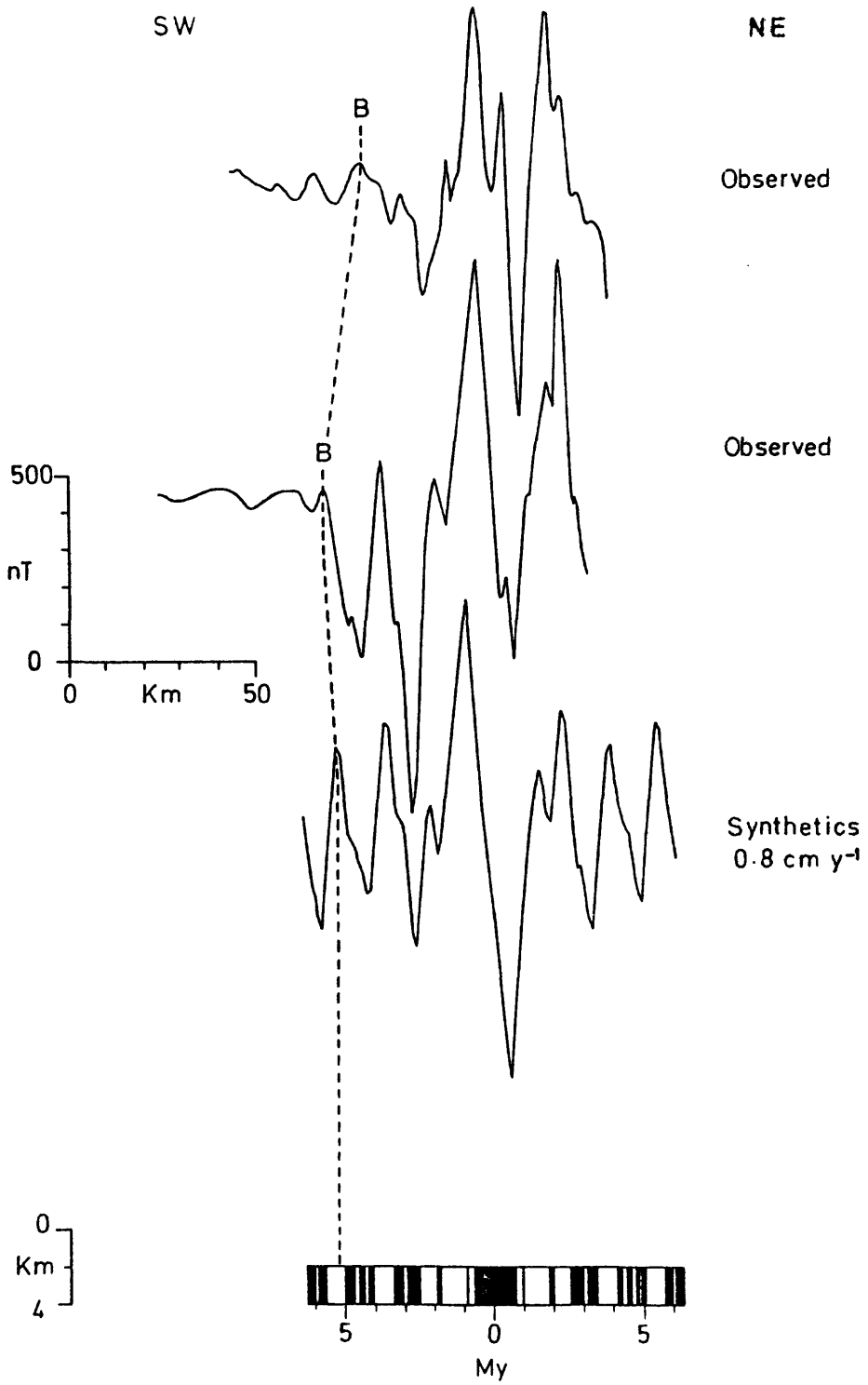

Figure 6.11 Seafloor model for recent spreading phase. Observed profiles are from sea data between 17°N and 18°N and have been projected on to N55°, normal to linear pattern. B represents south western limit of good correlation between synthetics and observed.

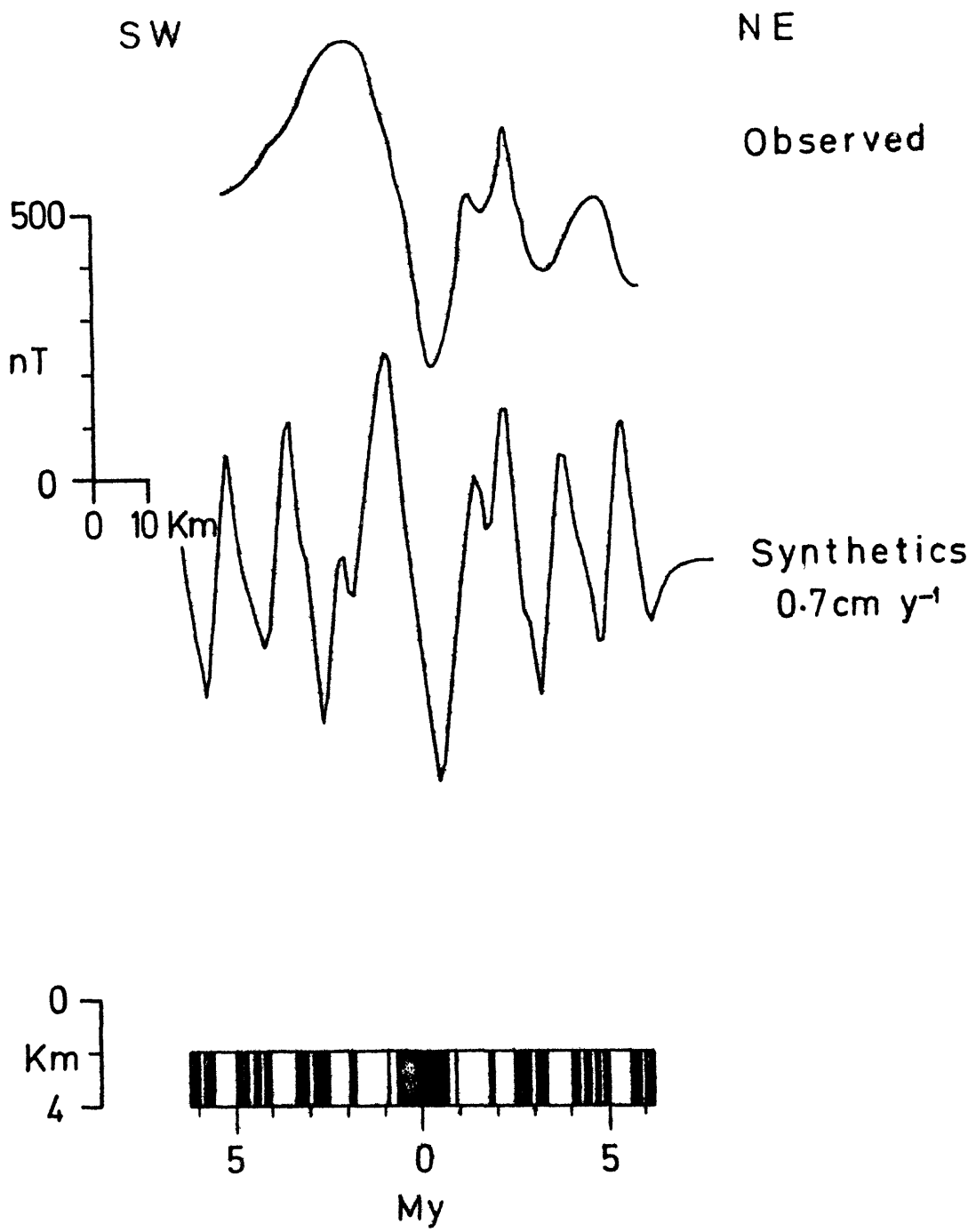

Figure 6.12 Seafloor model for recent spreading phase. Observed profile (DD , fig.6.4) is located at approximately 15.3°N. Effective susceptibility of central body is 0.01 emu cm^{-3}.

the hiatus in spreading. Only a major trough and the twin peaked feature east of this match the synthetics well. The slightly smaller spreading rate, although based on only one profile, may be significant in view of other evidence (palaeomagnetic, geological, magnetic) for a counterclockwise rotation of the Danakil plate, causing the narrowing of the Red Sea. A similar decrease in spreading rate for the older seafloor has been noted by Girdler and Styles (1974). It seems possible, therefore, that spreading at 15.3°N is controlled by the motion of Danakil and Arabia.

6.5.2 Early seafloor spreading

Seafloor models were computed for the earlier phase of spreading using the intervals chosen by Girdler and Styles (1974) and Hall, et al, (1977) and are shown in fig. 6.13. The models agree reasonably well with the observed profiles over the intervals 34 to 41 My (fig. 6.13(a)) and 24.5 to 29 My (fig. 6.13(b)) for spreading rates of 1.3 cm y^{-1} and 2.2 cm y^{-1} respectively. None of the airborne profiles from the Jizan survey (fig. 6.5) extends sufficiently far seaward to record the larger axial anomalies and therefore can be used to determine the boundary between spreading phases. X and Y (fig. 6.6) extend over the deeper water but unfortunately are too smooth to determine the boundary accurately. The Gulf profiles (Girdler and Styles, 1974) record anomalies from the recent phase and these have been used to determine the hiatus in spreading. This appears to have occurred at either 34 My or 24 My (P. Styles, pers.comm.) The earlier spreading appears to have created approximately 240 km of oceanic crust at 17°N along N 55°.

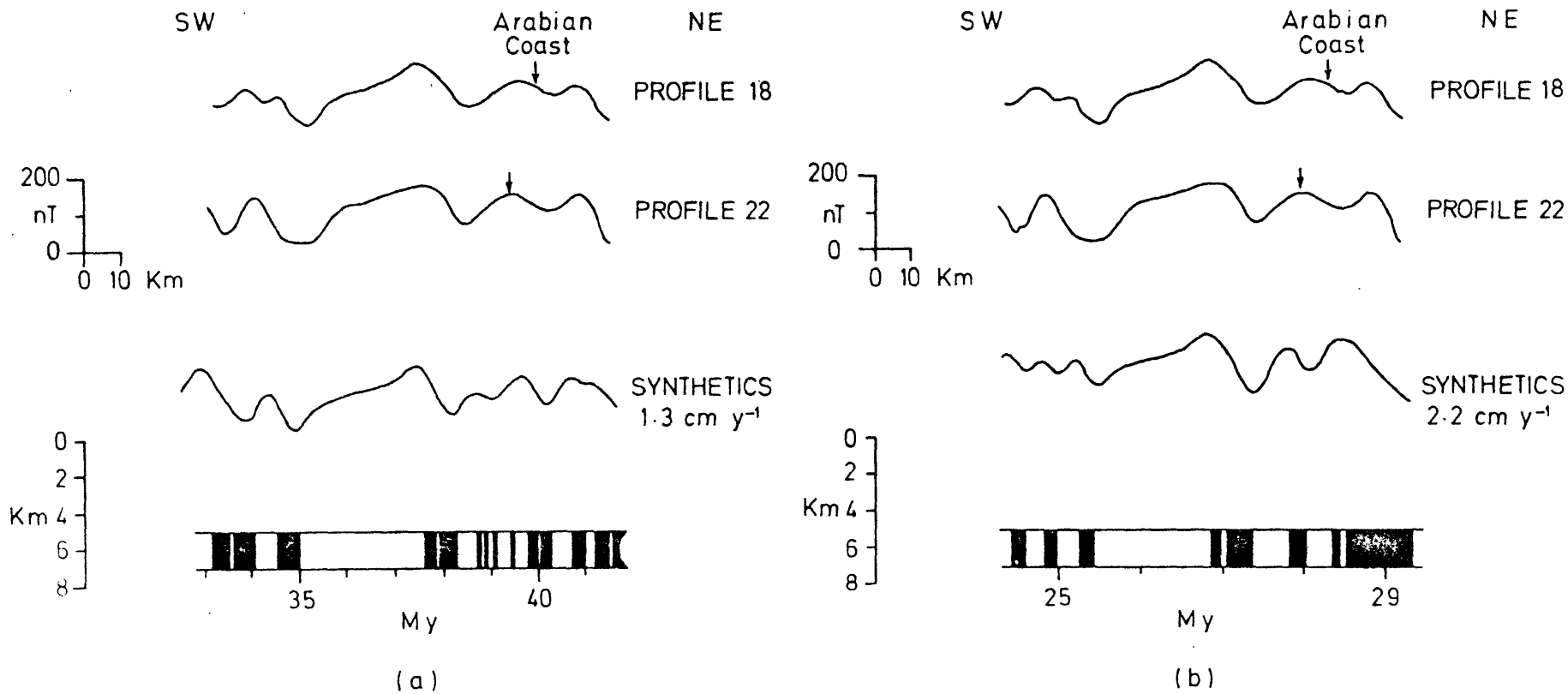

Figure 6.13 Two possible seafloor models of early spreading phase. Locations of profiles 18 and 22 are shown in fig. 6.3. Observed profile height = 300 metres AMSL.

The depth of the seafloor chosen in each of the models shown in fig. 6.13, viz. 5 km, is based on the effective susceptibility of oceanic basalt and the information available for a borehole at Mansiyah (17.2°N, 42.4°E) (Gillman, 1968) which indicates a minimum depth of 3.9 km to the magnetic sources.

6.5.3 Narrowing or widening of seafloor anomalies over the main trough?

A narrowing towards the south of the anomalies over the main trough and shelves has been reported by Girdler and Styles (1974). This narrowing is also seen in the aeromagnetic map of the junction of the Red Sea, Gulf of Aden and Ethiopian Rift (Hall, 1970). The magnetic profiles from the Jizan survey (fig. 6.5) were examined for evidence of narrowing along the Arabian coast in order to detect any influence on the spreading by the Danakil plate. The separations of the four major features (T1, P1, T2, P2 in fig. 6.7) were determined for every other profile (fig. 6.5) and the results plotted in fig. 6.14. None of the features indicates a narrowing of the anomalies, instead all support a small but significant widening. It is perhaps interesting to note that the transform fault proposed at 15.8°N, 41.7°E (see section 6.6) slightly disturbs the slow increase where it crosses the survey area. Least squares straight lines were computed for each of the separations and these are also shown in fig. 6.14. The least squares gradients (m in fig. 6.14) obtained are all positive. Each requires an error of three times the respective standard deviation (σ) for the gradient to be zero or negative. As the probability of this occurring is less than 1% there appears little doubt the anomalies do widen between 17.2 °N and 16.3 °N. It seems likely from this that the

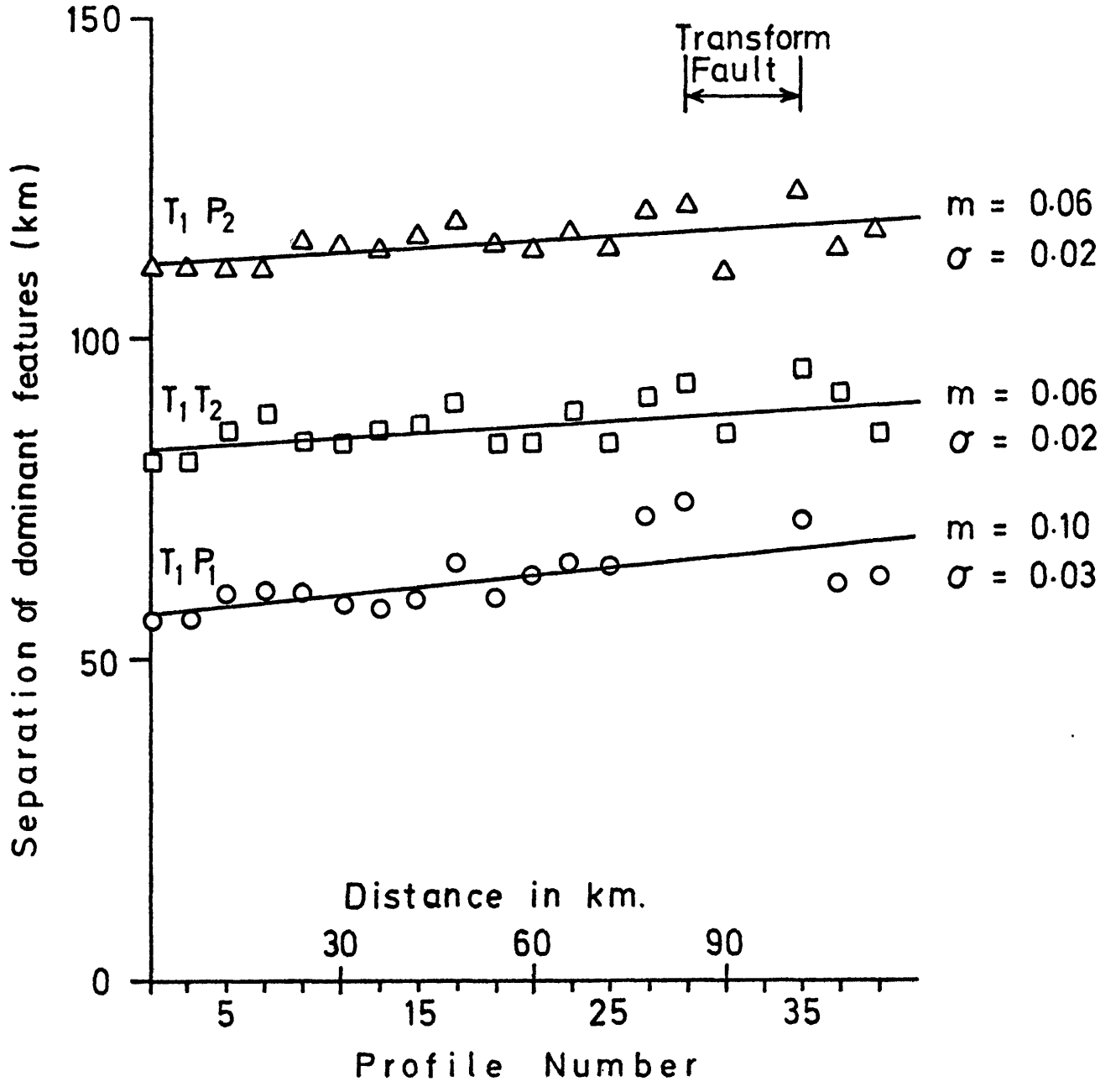

Figure 6.14 Plot of separations of dominant magnetic features of Jizan survey versus distances from profile 1. Locations of P_1, P_2, T_1 and T_2 are shown in fig. 6.7. m is the least squares gradient of the lines through the separations, σ is the standard deviation of the gradient.

Danakil plate has not influenced the spreading observed in the Jizan survey area.

6.6 Location of transform faults from offsets of the magnetic anomalies

The linear magnetic pattern (fig. 6.7) was examined for offsets which might indicate the presence of transform faults. Three such offsets were found and are shown in fig. 6.7 as dot dashed lines. The offsets are discussed below from north to south.

1. 15.8^{o}N, 41.7^{o}E. The correlations of the magnetic profiles from the Jizan survey (fig. 6.7) reveal a dextral offset of the linear anomalies of about 9 km. The offset occurs between profiles 28 and 35 trending N $45^{o} \pm 5^{o}$ and displaces all seven features shown in fig. 6.7. The offset seems related to the appearance of high frequency anomalies on profiles 32 to 40 (fig. 6.5). The western limit of these anomalies (heavy dashed line, fig. 6.7) displays a bend near the proposed fault which may indicate the continental edge is also offset dextrally in this area.

The seaward extension of the fault crosses between profiles CC' and DD' (fig. 6.2) meeting the African coast near 15^{o}N. Correlations of the sea data north and south of this line indicate a larger offset of the magnetic pattern, viz. approximately 30 km. The impressive linear pattern of the anomalies, north of profile 28, indicates there are no further offsets within the Jizan survey area. Therefore, the difference in the offsets deduced from the air and sea data is probably due to either a change in the anomaly trends over the deep water between 15.8^{o}N and 16.2^{o}N or further offsets south of

the survey area. There is supporting evidence for the fault from a similar offset of the magnetic lineations along the African coast (P. Styles, pers. comm.). In addition, detailed bathymetric charts (Backer et al, 1975) indicate a small, shallow area near 15.8^{o}N, 41.7^{o}E which coincides with the projected location of the fault over the deeper water. The small, shallow area separates the deep water into pools which are dextrally offset by about 10 km. No earthquakes have been located for the area.

2. 15.3^{o}N, 41.9^{o}E. There is a dextral offset of the magnetic pattern in this area but the scarcity of suitably oriented tracks and the comparative smoothness of the magnetic profiles make the location of a transform fault less reliable. The dominant peak-trough feature which is tentatively correlated north and south of the proposed fault (fig. 6.7) appears offset by approximately 30 km. The azimuth of the fault cannot be determined accurately as the data available do not adequately delineate the fault. An azimuth of $N55^{o}$ has been tentatively assigned.

There is little supporting evidence for the fault. No epicentres have been located for the area. A study of the bathymetry reveals a localised high (Jebel Tair) near the fault which separates the deep water into pools. These pools are displaced dextrally by about 5 km although it is difficult to make precise correlations of the bathymetric features. The large disparity between the offsets of the magnetic pattern (30 km) and the deep water pools (5 km) is difficult to explain, unless the magnetic features have been incorrectly identified. The poor distribution of ships' tracks increases this possibility and the proposed fault should be considered tentative.

3. 14.8^{o}N, 42.1^{o}E. The magnetic pattern in this area is based on few tracks (fig. 6.2) and is, therefore, poorly defined. The two, long VALDIVIA lines, south of the proposed fault correlate well, whilst the shorter tracks north of the fault give only tentative correlations. Comparison of profiles DD' and EE' (fig. 5.3) suggests the dominant features are offset dextrally by about 25 km. The three main features are observed on a short profile north of EE' (fig. 6.7) indicating the transform fault is narrow (approximately 2 km) and trends approximately $N55^{o}$. The magnetic contour map of Hall (1970) shows a break in the contours near the proposed line of the fault. At the break, a dominant, negative anomaly is displaced dextrally by about 25 km along an azimuth of $N55^{o} \pm 5^{o}$. These contours are based entirely upon airborne data and therefore provide additional evidence for the proposed transform fault.

Epicentres of two earthquakes have been determined (fig. 6.1) which lie close to the line of the fault. These events occurred in 1958 and 1960, prior to the introduction of the WWSSN, and consequently, their locations may be subject to large errors. Furthermore, the epicentres lie well outside the zone between the spreading axes where, in general, most seismic activity occurs. No topographic expression of the fault is observed on the bathymetric charts although the recent, detailed soundings of VALDIVIA (Backer et al, 1975) do not entirely cover the area.

A fourth, possible transform fault may be present at approximately 16.8^{o}N, 40.8^{o}E where some lineations although continuous undergo a somewhat large change in their directions, viz. 30^{o} (fig. 6.7). The magnetic

pattern in this area is based upon extensive data and the change in direction is therefore, well defined. A similar bend is observed in the anomaly pattern along the African coast near 15.6°N (Girdler and Styles, 1974) suggesting the feature may extend across the western half of the Red Sea.

Several seismic events have occurred nearby and a first motion study of one of these has been reported by Fairhead and Girdler (1970). This indicates strike-slip sinistral motion along azimuth N49°. The detailed bathyme try again displays a local high (340 metres) near the proposed fault with the deep water areas north and south displaced left laterally. The amount of displacement is difficult to determine accurately but appears to be about 10 to 15 km. As noted above no offset of the magnetic lineations is observed.

The location of the proposed transform faults are shown in fig. 6.15: also shown are the earthquake epicentres and the spreading axis deduced from the magnetic patterns in fig. 6.7.

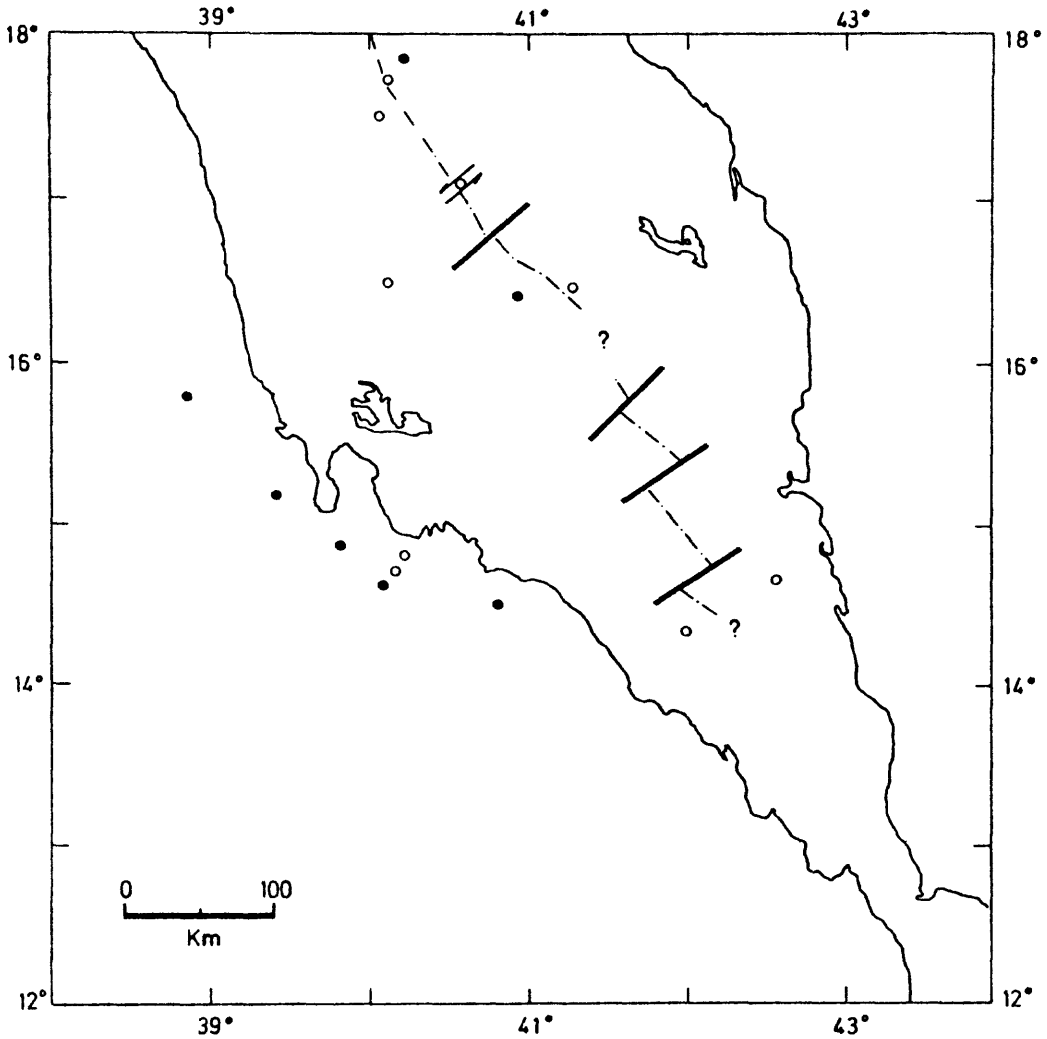

Figure 6.15 Location of transform faults inferred from offsets and/or sudden changes in direction of the magnetic pattern (fig. 6.7). —·—· axis of symmetry of magnetic pattern. Also shown are earthquake epicentres for events prior to 1963, O, and after 1963, ●. Arrows indicate sense and direction of fault plane solution obtained by Fairhead and Girdler (1970).

CHAPTER SEVEN

RED SEA FLOOR SPREADING, TRANSFORMS AND PLATE GEOMETRY

7.1 Extent of oceanic crust

The magnetic data indicate almost the entire width of the Red Sea is underlain by oceanic crust. In some areas, this crust also extends beneath part of the coastal plain, e.g. near 19.5°N 41.0°E, fig. 5.9. The age of the crust beneath the main trough and shelves, deduced from seafloor spreading models, is either from 41 to 34 My (Girdler and Styles, 1974) or from 29 to 23 My (Hall et al, 1977) and that beneath the axial trough from about 5 My to the present. Distributions of new and older oceanic crust (zones 1 and 2) and continental crust (zone 3), inferred from the magnetic anomalies, are shown in figs. 7.1 to 7.3 for the northern, central and southern Red Sea respectively. Zone boundaries are poorly defined in several places, e.g. in the northern Red Sea (fig. 7.1) where the data are sparse. Those on the African side are largely based upon the assumption of symmetrical spreading about the present deep water axis although Plate 1 has been used, where possible, to delineate the boundaries. There are several places where the deep water axis is noticeably closer to one coast than the other (see Laughton, 1970). For example, near 25.5°N the axis is about 70 km from Arabia and 130 km from Africa measured along N50°. This may be due to asymmetrical spreading but could also indicate that part of offshore Egypt is continental. Amounts of new and older oceanic crust determined at various latitudes assuming symmetrical spreading are given in Table 7.1.

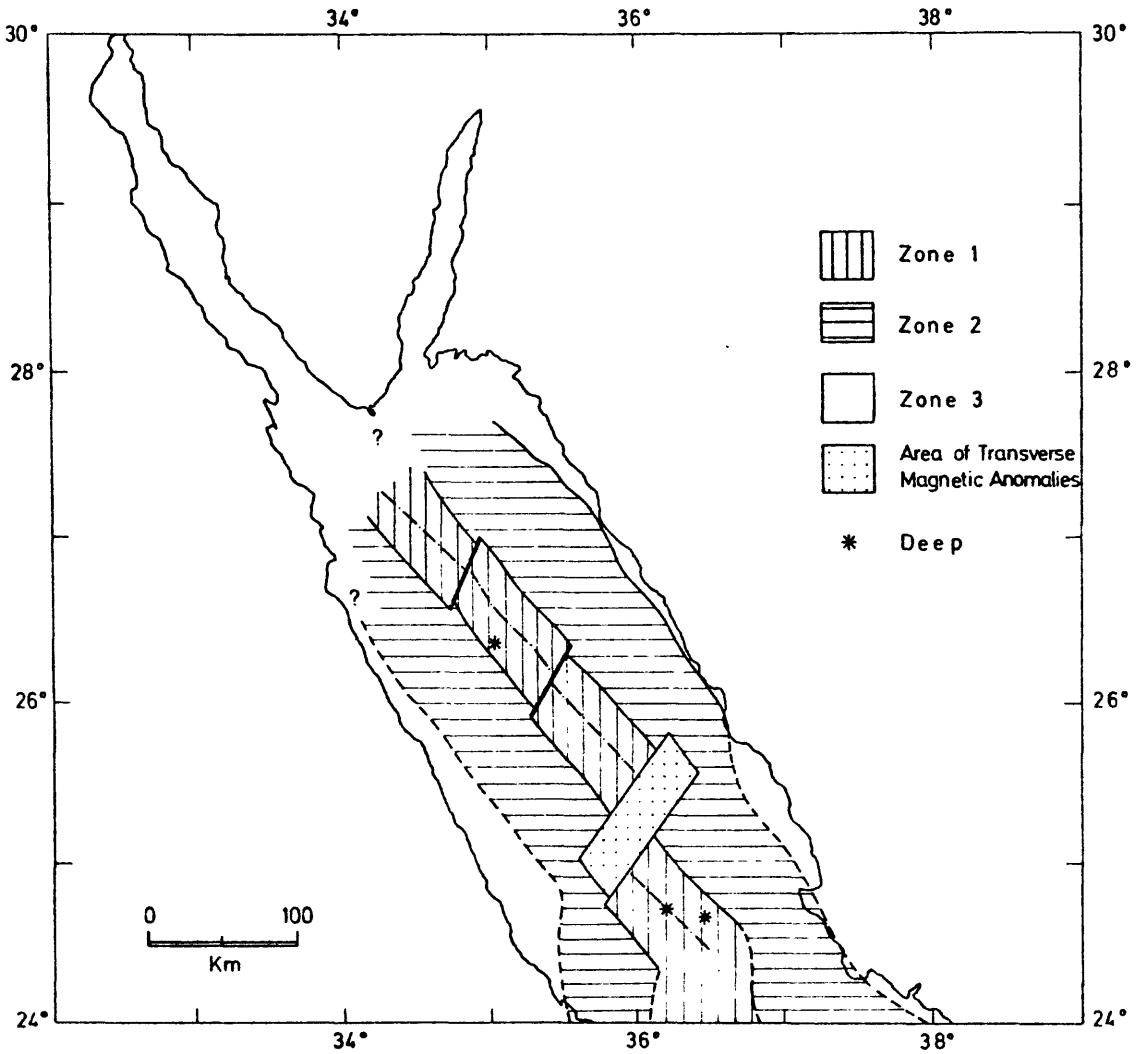

Figure 7.1 Crustal structure of the northern Red Sea deduced from the magnetic data. Zones 1 and 2 are underlain by oceanic crust and represent the two phases of seafloor spreading. Zone 3 is underlain by continental crust. —— · —— axis of spreading; — — — — tentative zone boundaries.

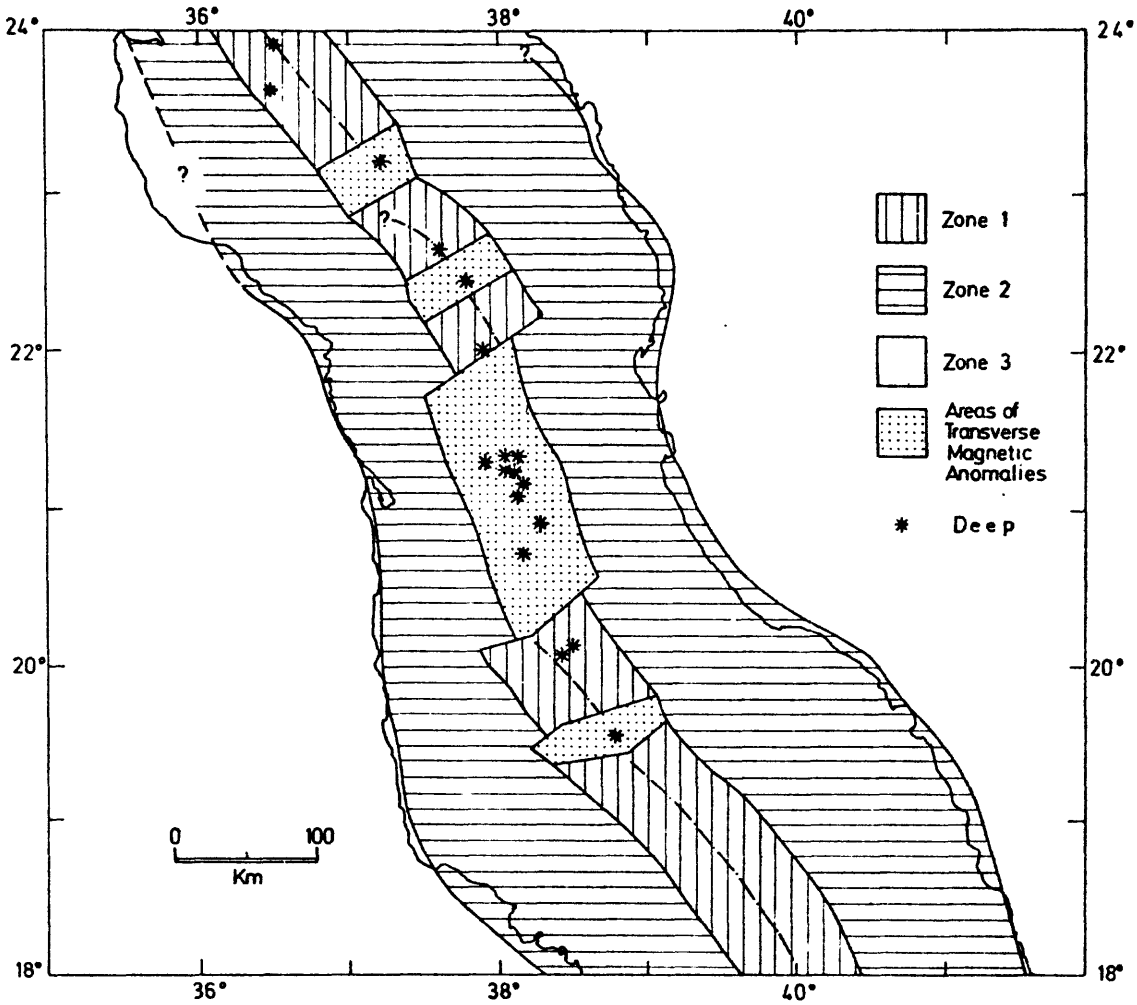

Figure 7.2 Crustal structure of the central Red Sea deduced from the magnetic data. Zones 1 and 2 are underlain by oceanic crust and represent the two phases of seafloor spreading. Zone 3 is underlain by continental crust. ——·——axis of spreading; — — — — tentative zone boundaries.

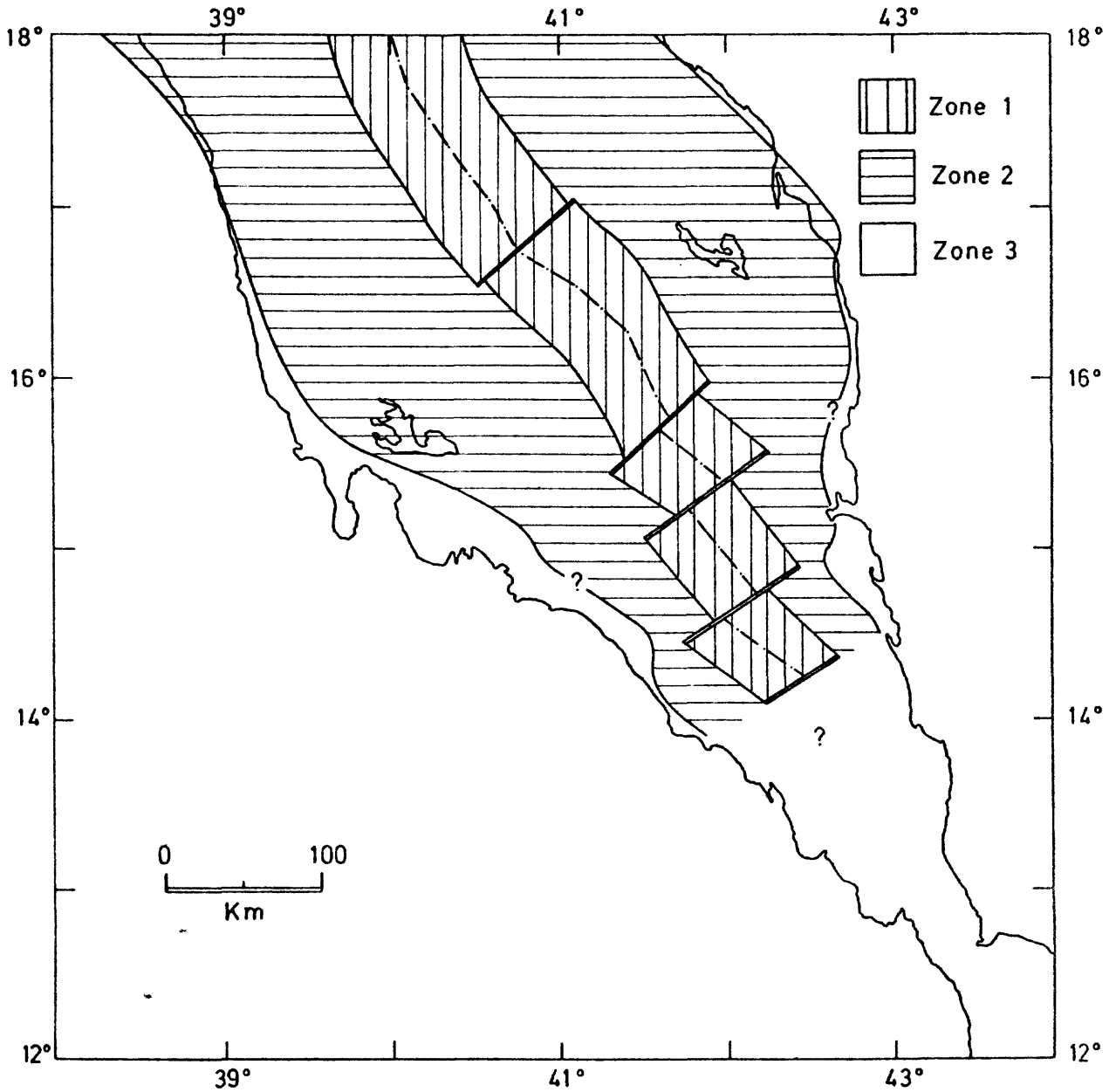

Figure 7.3 Crustal structure of the southern Red Sea deduced from the magnetic data. Zones 1 and 2 are underlain by oceanic crust and represent the two phases of seafloor spreading. Zone 3 is underlain by continental crust. ——·——axis of spreading; — — — —tentative zone boundaries.

TABLE 7.1

Amounts of recent and early spreading at various latitudes in Red Sea

Latitude (°N)	Longitude (°E)	Amount of recent spreading (km)	Azimuth of measurement	Amount of early spreading (km)	Azimuth of measurement	early spreading / recent spreading
27	34.75	60	040°	110	045°	1.8
26	35.70	60	045°	120	045°	2.0
23.5	37.00	70	050°	190	035°	2.7
22.5	37.75	70	050°	210	055°	3.0
19.0	39.40	80	050°	250	050°	3.1
18.5	39.75	80	050°	250	060°	3.1
17.0	40.70	80	055°	240*	050°	3.0

*not used in calculation of poles

Most geophysical data support the proposed amount of oceanic crust :

Gravity. The positive Bouguer anomaly was formerly attributed to a mass of basic material beneath the axial trough (Girdler, 1958) but the tremendous thicknesses of sediments (up to 5 km) since discovered in boreholes suggests this was a conservative estimate. When a correction is applied for the light sediments the zone of basic material becomes much wider. Recent gravity data over the Farasan Islands (Gettings, 1976) suggest the zone extends beneath the coastal plain at 17^{o}N.

Heat Flow. Most heat flow measurements are higher than the world mean, 59mW m^{-2}, including those over the main trough and shelves. Polyak and Smirnov (1968) have shown that the mean heat flow over continents decreases with increasing age of the orogenic province. The heat flow measured along the shelves (Girdler, 1970a; Evans and Tammemagi, 1974) is typically twice the world mean. To produce such a high heat flow over continental crust requires an orogenic event since the beginning of the Cenozoic. There is no evidence for such an event and the most recent orogeny appears to have taken place between 520 and 570 My ago (Brown, 1972). This event, the Najd orogeny, is expected to give rise to a heat flow of about the world mean. It appears more likely the shelves are underlain by oceanic crust emplaced 30 to 40 My ago. This is in broad agreement with the theoretical heat flow predicted by Sclater and Francheteau (1970) for a 100 km thick oceanic lithosphere of this age.

Seismic refraction. The seismic refraction results (Drake and Girdler, 1964; Girdler, 1969; Tramontini and Davies, 1969) are more difficult to reconcile with seafloor beneath the entire width of the Red Sea. Lines shot within the

axial trough give velocities typical of oceanic rift zones but some of those in the main trough give anomalous velocities for oceanic crust. Lines 170, 171-172, 175-176 and 184 (Drake and Girdler, 1964) and a DISCOVERY line (Girdler, 1969) detect a crustal layer with a velocity between 5.5 and 5.9 km s^{-1} lying at depths of 2 to 6 km. Velocities commonly associated with oceanic layer 2 are 4.5 to 5.5 km s^{-1} although the range of observed values is larger, viz 3.4 to 6.3 km s^{-1} (Ludwig et al, 1970). The 5.5 to 5.9 km s^{-1} layer therefore may represent layer 2 although the velocity is more typical of continental rocks. Similar values have been obtained in the Phillipine Sea (Murauchi et al, 1968) which is considered to be underlain by normal oceanic material. In the Phillipine Sea the observed range of seismic velocities of layer 2, viz. 3.5 to 5.8, is thought to be due to a complex system of basins and ridges (Murauchi et al, 1968). A similar explanation could be adopted for the velocities in the Red Sea but there is currently no other evidence to indicate the presence of such structures.

Analyses of samples obtained during DSDP Leg 23 show that anhydrite can have high seismic velocities (Whitmarsh et al, 1974). Velocities of about 5.6 km s^{-1} were determined for site 228 with a maximum value of 5.91 km s^{-1}. However, these samples were obtained from depths less than 325 metres whereas the 5.5 to 5.9 km s^{-1} layer occurs much deeper.

It is apparent from the above that an adequate explanation of the seismic refraction results remains to be given and the results should be reappraised in the light of the magnetic evidence.

Seismicity. The seismicity of the Red Sea (Fairhead and Girdler, 1970) indicates the axial trough is an area of active spreading.

Seismic Reflection. The reflection data indicate the axial trough is underlain by a intensely deformed, acoustially opaque material which probably represents seafloor. The absence of the S-reflector in the axial trough suggests seafloor spreading has taken place since the deposition of the sediments.

7.2 Seafloor spreading

The synthetic seafloor spreading anomalies correlate well with the observed data in many areas. In particular, the correlations obtained over the axial trough in the central and southern Red Sea are remarkably good (cf figs. 5.14 and 6.11). Those obtained over the main trough and shelves in these areas are not as good but still impressive (cf figs. 5.15 and 6.13). However, there are three areas where the correlations are poorer: (1) north of 22.6°N, (2) south of 15.5°N, and (3) areas over which there are transverse anomalies in the northern and central Red Sea. In these, the anomaly amplitudes are often smaller than those predicted (assuming an effective susceptibility of 0.01 emu cm^{-3}), and several of the seafloor anomalies are not observed. For example, to simulate the observed amplitudes in fig. 4.9 it is necessary to use an effective susceptibility of only 0.003 emu cm^{-3} and in fig. 5.20 the observed profiles are much smoother over the sides than the synthetic profiles.

In Chapter 3, the amplitude of the seafloor anomalies was shown to decrease with decreasing latitude, increasing depth and decreasing spreading rate. The shapes of the anomalies were also shown to change with the strike of the seafloor. Deeper seafloor does not provide an adequate explanation

as the observed amplitudes (~ 300 nT) require seafloor at depths of 7 to 8 km (see fig. 3.5) and this does not agree with seismic refraction data at 23^{o}N (line 180-181, Drake and Girdler, 1964) which show a 4.68 km s^{-1} layer, presumably layer 2, at a depth of only 2.5 km. Differences in spreading from north to south, viz. from 0.6 cm y^{-1} (27^{o}N) to 0.8 cm y^{-1} (19^{o}N), are also too small to account for a two to threefold decrease in amplitude. The strike of the seafloor, which is either N145^{o} or N50^{o} (transverse features), does not produce anomalies of the observed amplitude. Consequently other explanations of the smaller amplitudes and "missing" anomalies must be examined. One possibility is that in certain areas oceanic layer 2 may be missing altogether. Seismic refraction line 183 at 24.5^{o}N (Drake and Girdler, 1964) shows a velocity of 3.92 km s^{-1} overlying 7.34 km s^{-1}. Typical velocities for layer 2 are 4.5 to 5.5 km s^{-1} (Ludwig et al, 1970). It is possible, therefore, that near this refraction line a sedimentary formation (3.92 km s^{-1}) directly overlies layer 3 (7.34 km s^{-1}) and that the observed anomalies are due to layer 3 only. However, further south near 23^{o}N line 180-181 shows an approximately 3 km thick layer with a velocity of 4.68 km s^{-1} overlying a velocity 6.97 km s^{-1}. This layer is probably layer 2 but the magnetic anomalies observed nearby are also small (200 to 300 nT). It appears more likely, therefore, that at 24.5^{o}N layer 2 may have been intruded into the overlying sediments resulting in interlayering of the basalts with the sediments.

Two other factors discussed in detail below, are: (1) the relation of the spreading rate to the dyke injection mechanism, and (2) the possible significance of the presence of evaporites overlying the seafloor. The first is especially important in the case of the leaky transforms where the spreading

rates are small. The second is more significant for areas north of 22.6°N where there is no axial trough.

7.2.1 Dyke injection mechanism

In the simple seafloor model described in Chapter 3 and used throughout Chapter 4, 5 and 6, the boundaries between adjacent normally and reversely magnetised blocks are sharp such that the intensity of the magnetisation (I) changes sign abruptly at their interfaces. This situation, shown in fig. 7.4(a), assumes seafloor is generated along one, central, vertical line. However, recent, detailed studies of spreading axes (e.g. Atwater and Mudie, 1973; Lattimore et al, 1974) suggest seafloor is emplaced by a number of dykes within a comparatively narrow "intrusion zone". The width of this zone for spreading centres in the Pacific Ocean appears to be typically 2 to 3 km (Klitgord et al, 1975). If seafloor is generated within such a zone, then material of one magnetic polarity will be contaminated by opposite polarity material when the field reverses and the overall magnetisation will change more gradually (fig. 7.4(b)). A statistical model of this type of dyke injection process was presented by Matthews and Bath (1967) and a good correlation obtained with the anomalies observed over the Mid-Atlantic Ridge.

The amplitude of the anomalies produced by such a model depend mainly on: (1) spreading rate, and (2) the intrusion zone width. The intrusion zone widths found for the Pacific Ocean (Klitgord et al, 1975) indicate that these two parameters are not inter-related as widths of 2 to 3 km are found for spreading rates varying from 1.2 cm y^{-1} (Gorda Rise 41.5°N) to 4.8 cm y^{-1} (Pacific Antarctic ridge 51°S). Curves of the intensity of magnetisation versus

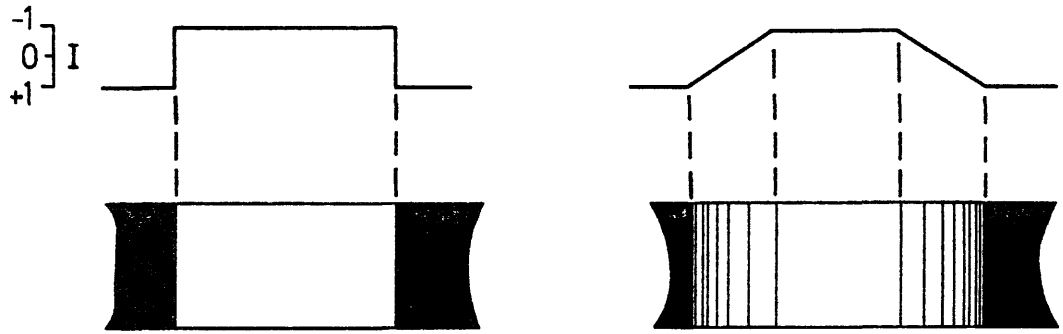

Figure 7.4 Variation of intensity of magnetisation (I), in arbitrary units, over two reversals of the geomagnetic field. In (a) I changes sign abruptly at each reversal (Vine-Matthews model); in (b) I changes more gradually as seafloor is generated within a finite intrusion zone.

age of seafloor for various spreading rates and intrusion zone widths are plotted in fig. 7.5. In each case, I is assumed to increase or decrease linearly across the boundaries only reaching ± 1 for reversals wider than the half-width of the intrusion zone. These curves were used to generate seafloor anomalies which were compared with observed profiles over areas (1), (2) and (3) of the Red Sea (see above). Synthetic seafloor anomalies which best simulate the observed data are shown in fig. 7.6; synthetic profiles obtained from the simple model are included for comparison. For those anomalies parallel to the deep water axis, profiles generated with the appropriate spreading rate for an intrusion zone width of 2 km give the optimum fit; for the transverse anomalies the best correlation is obtained using profiles generated for a width of 10 km. The models (fig. 7.6) have the advantage that the same value of the effective susceptibility of the seafloor, viz. 0.01 emu cm^{-3}, may be used for all profiles. Although a detailed seismic study of the Red Sea spreading centre is needed to check the results, comparison with the Atlantic Ocean at $37^{o}N$ (Whitmarsh, 1975) suggests a 2 to 3 km wide zone is approximately correct.

7.2.2 Possible effect of evaporites overlying seafloor

An alternative explanation of the reduced amplitudes and 'missing' anomalies is that the effective susceptibility of the seafloor is less in these areas and this has been assumed in the seafloor models shown in figs. 4.9 and 4.13. The magnetisation of oceanic basalts is predominantly due to thermoremnant magnetisation (TRM) with the induced magnetisation contributing less than 10% of the total (Pitman et al, 1968). The two to threefold difference in magnetisation

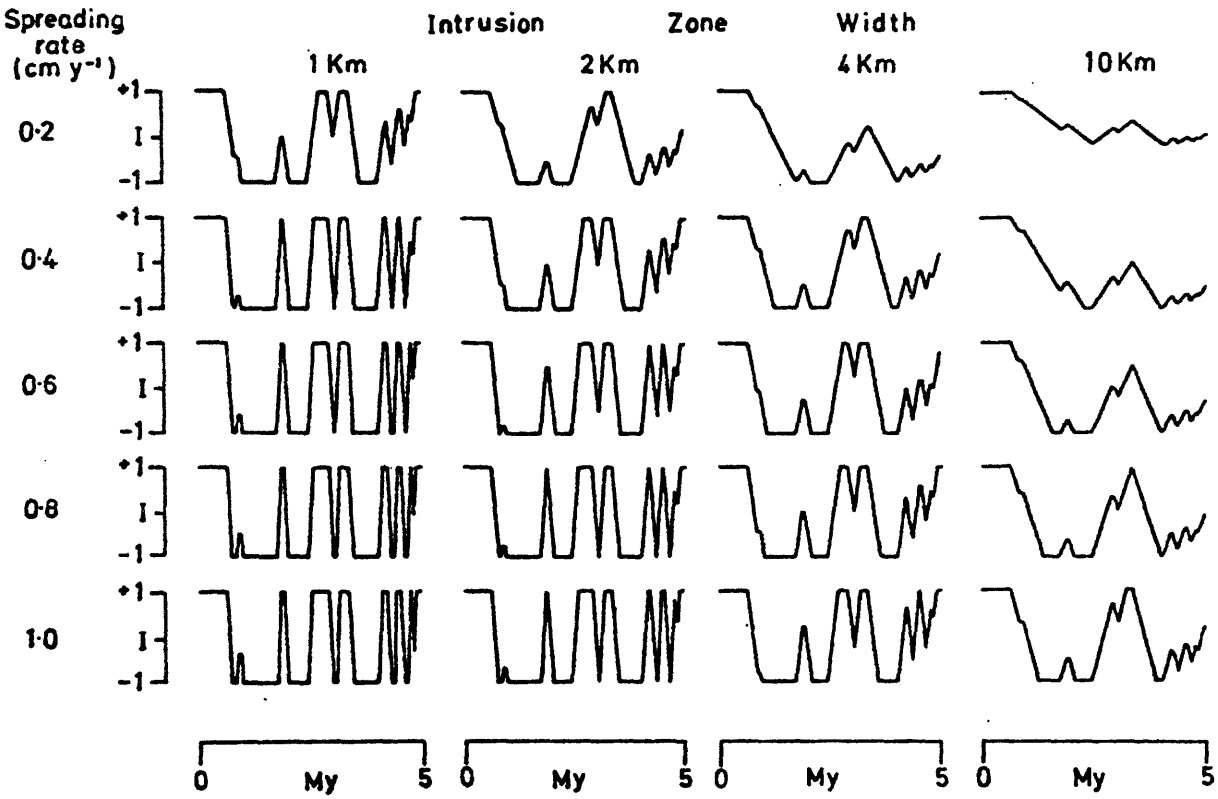

Figure 7.5 Plots of intensity of magnetisation (I) in arbitrary units versus age of the seafloor for various spreading rates and intrusion zone widths.

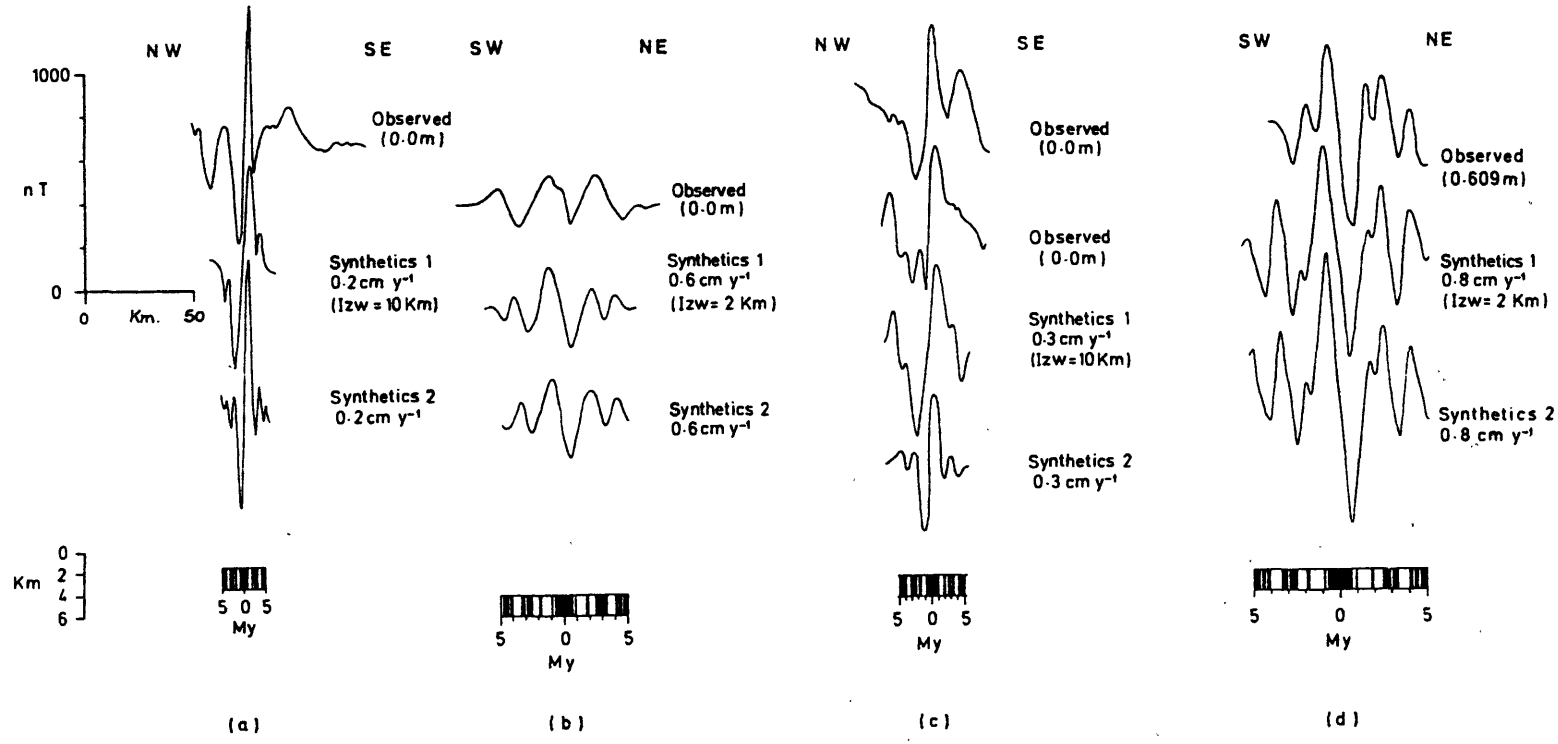

Figure 7.6 Seafloor spreading models for anomalies parallel (b and d) and transverse (a and c) to the axis in the northern and central Red Sea. Synthetics 1 are profiles calculated from the magnetisation curves in fig. 7.5. Synthetics 2 are the profiles used in figs 4.13, 4.9, 5.20 and 5.14 (a, b, c and d respectively). For Synthetics 1, $\chi_{eff} = 0.01$ emu cm^{-3}, for Synthetics 2, χ_{eff} is the value given in the appropiate figure. Izw is the intrusion zone width used in the calculation of the profile.

is, therefore, probably due to differences in TRM. These could be caused by differences in the magnetic mineral composition but since the bulk chemical composition of the seafloor is probably the same in each area it seems more likely the differences are due to other factors.

Seismic reflection studies (Knott et al, 1966; Phillips and Ross, 1970; Ross and Schlee, 1973) reveal the presence of a strong reflector (S-reflector) due to Late Miocene anhydrite (Whitmarsh et al, 1974) at depths of up to 500 metres beneath most areas of the Red Sea north of 24^{o}N (see fig. 21, Phillips and Ross, 1970) but, in general, absent from the axial trough in the central and southern Red Sea. Thus all the recent seafloor is covered by sediments in the northern Red Sea but not in central Red Sea. An estimate of the thickness of the overlying sediments may be obtained from seismic refraction line 183 (see fig. 4.1 and Drake and Girdler, 1964) which shows approximately 5 km of 3.92 km s^{-1} material overlying 7.34 km s^{-1} material. Since 3.92 km s^{-1} is close to that measured for the Red Sea evaporites, viz 4.2 ± 0.4 km s^{-1} (Wheildon et al, 1974), it seems reasonable to assume the presence of several kilometres of evaporites.

If the younger seafloor has been intruded into the base of the evaporites, it will have cooled more slowly than in areas where it is quenched by sea water. Thus differences in magnetisation of the seafloor between the northern and central Red Sea may simply reflect different rates of cooling of the magnetised layer. The mechanism envisaged is somewhat similar to the formation of sills beneath sedimentary formations. Studies of the intensity of magnetisation of several dolerite sills have been made (Irving, 1956b, Creer et al, 1959) and

although the chemical composition of these are different to oceanic basalts the magnetic carriers are probably similar. Results from the Great Whin Sill in northern England (Creer et al, 1959), which was intruded into Carboniferous sediments, indicate an average effective susceptibility of approximately 0.005 emu cm^{-3}. Similar values were obtained by Irving (1956b) for Tasmanian dolerite sills. The value is approximately that required to simulate the anomalies over the northern Red Sea.

Slower cooling produces larger grain, ferromagnetic minerals. Since the intensity of TRM decreases with increasing grain size, larger grain minerals will acquire a reduced magnetisation. Although studies of oceanic basalts from the Atlantic and Pacific Oceans (Lowrie et al, 1973(a); Lowrie et al, 1973(b))show they contain titanomagnetite grains of 1 to 5 microns, the TRM is thought to be predominantly due to finer grains that range in size from a few hundred Angstroms to 0.25 microns and which represent the single domain phase (Evans and Wayman, 1972). The TRM is large for single domain grains and small for multidomain grains. Grains of intermediate size, i.e. those in the pseudo-single domain range, have an intermediate value of TRM which decreases rapidly by a factor dependant on 1/d (Dunlop, 1973) where d is the mean grain diameter (fig. 7.7).

It seems likely, therefore, that the basalts beneath the evaporites have a different grain size distribution from those quenched in sea water with the result that fewer single domain grains are present.

If the evaporites have flowed as suggested by Girdler and Whitmarsh (1974), then, if the flowage exceeded the spreading rate, the early stages of

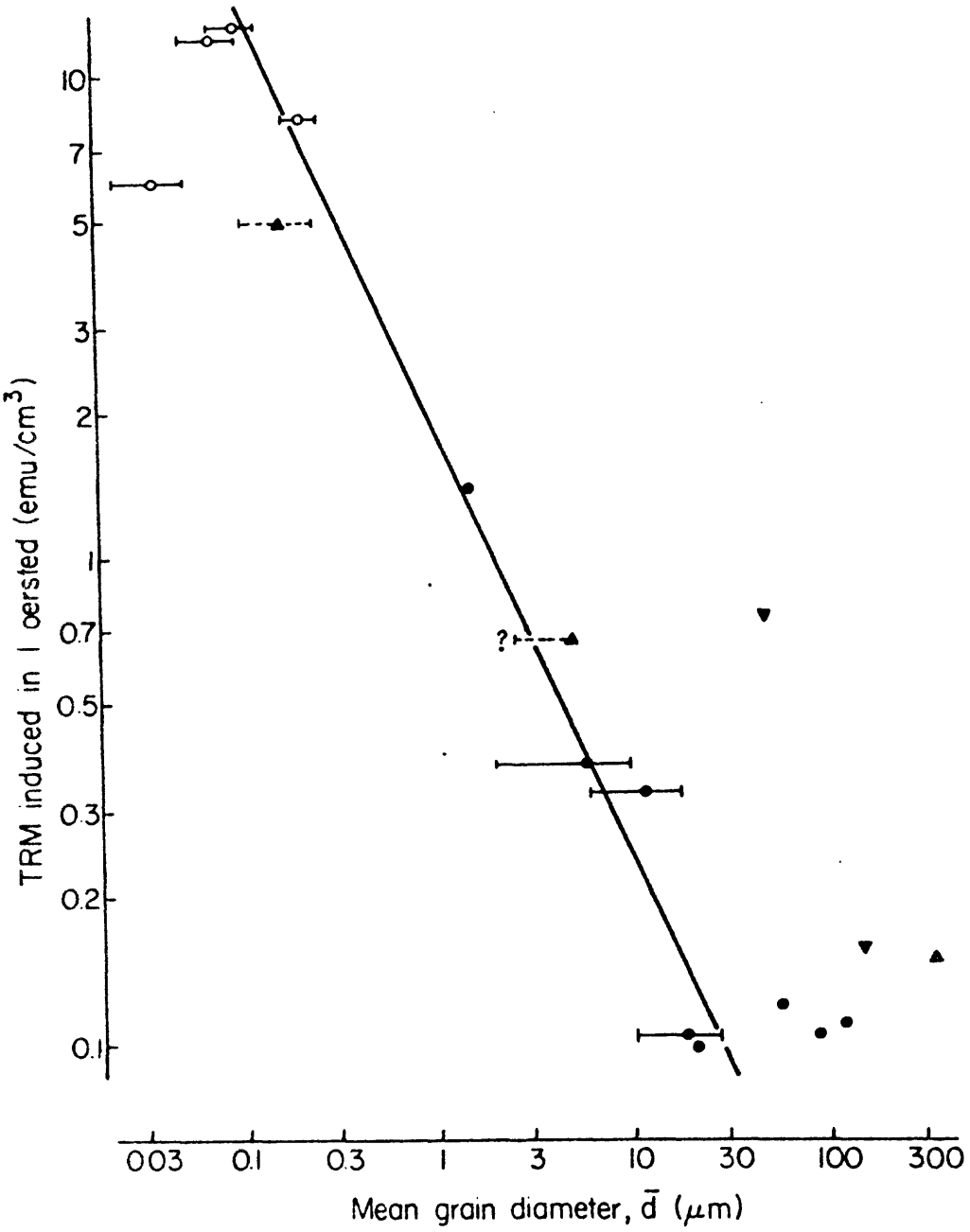

Figure 7.7 Variation in TRM intensity with grain size for magnetite (after Dunlop, 1973).

the recent spreading may have been affected in other areas of the Red Sea. The flowage is thought to have ceased by the late Pliocene (Girdler and Whitmarsh, 1974) and seismic reflection data (Ross and Schlee, 1973) indicate an approximately 40 km wide strip of the axial trough near 18^{o}N where the S-reflector is absent. This implies approximately 15 to 20 km of young seafloor on each side is covered by the evaporites. Thus seafloor created during the initial stages will be more weakly magnetised and this may explain the absence of the 4 to 5 My anomalies on many profiles. A model in which seafloor more than 25 km from the spreading axis has an effective susceptibility of one third that of seafloor less than 25 km is shown in fig. 7.8. The profile obtained using a constant effective susceptibility of 0.01 emu cm^{-3} throughout is superimposed for comparison. The solid profile correlates better but still has anomalies slightly larger than the observed suggesting the seafloor is still more weakly magnetised.

The effect of flowage in the leaky transform zone may also be large as gravity data (Searle and Ross, 1975) and bathymetric features (Backer et al, 1975) indicate evaporites may be present in several areas of the axial trough. Small magnetic anomalies away from the leaking axis are, therefore, to be expected.

7.3 Transforms

Seventeen possible transform faults have been located using the magnetic data. Two criteria were used: (1) offsets and/or abrupt changes in the direction of the magnetic lineations, and (2) the presence of anomalies transverse to the Red Sea trend. Four of the proposed faults satisfy both criteria, ten satisfy

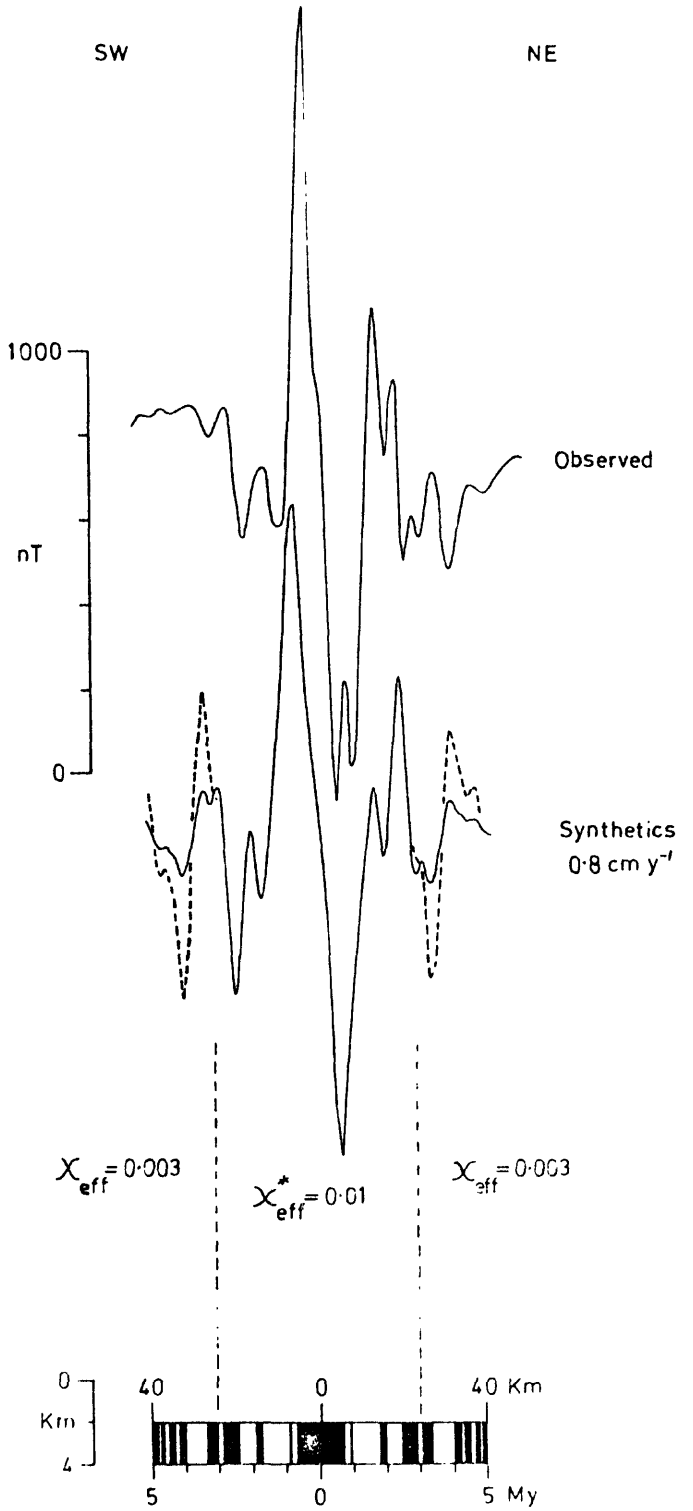

Figure 7.8 Seafloor model of recent spreading phase. Observed profile is from central Red Sea. Seafloor older than 3 My has an effective susceptibility of 0.003 emu cm^{-3}. Dashed line shows profile between 3 My and 5 My for model with χ_{eff} = 0.01 emu cm^{-3}. * central body χ_{eff} is 0.02 emu cm^{-3}.

(1) and three satisfy (2). Details of the faults are given in Table 7.2 and their locations shown in fig. 7.9. Ten faults are considered to be identified with reasonable certainty. Transverse anomalies are observed over two of the other seven but there are no corresponding data along the coast (see fig. 5.9). Fifteen faults appear to have dextral offsets and two, sinistral offsets although the sinistral offset of one of these is based upon the left lateral displacement of bathymetric features rather than magnetic lineations and as such is questionable.

Azimuths of the faults (Table 7.2) are measured from only short sections and consequently are poorly determined. Errors somewhat larger than $\pm 10^{o}$ may be present. The azimuths determined from transverse anomalies over the centre are approximately 20^{o} to 30^{o} larger than those obtained from offsets near the coasts. Although the errors are large, these differences suggest the directions of motion of Nubia and Arabia were different during the two spreading phases.

The poles of rotation (see section 7.4) predict that dextrally offset transforms formed during the earlier spreading will have leaked during the recent spreading. However, over five dextral faults, viz. numbers 2, 3, 5, 8 and 13 (Table 7.2), no transverse anomalies are observed. It is apparent from this that either the transverse anomalies are not due to leaky transforms or the faults have been identified incorrectly. Four of the faults are not reliably located being based upon the offsets of two or less magnetic features but one, viz.number 2 (Table 7.2), is based upon five offsets: three on the sea and two on the air data. Data coverage of the deep water near this fault is poor and a small transverse feature could be present. Further data are required to check this.

Table 7.2

Location and relevant details of the proposed transform faults

No.	Approx Location Lat(°N)	Long(°E)	Dextral (D) Sinistral (S)?	Offset No.of features	Offset Amount(Km)	Azimuth	Transverse feature present?	Offset on air or sea data?	Any bathymetric expression?	In known seismically active area?	Is deep present?
1*	26.9	34.8	S	7	10-12	021°	No	both	Widening of deep water	No	No
2	26.3	35.4	D	5	7-10	026°	No	both	No	No	No
3	26.3	36.1	D	1	10	033°	No	air	Widening of deep water	No	No
4*	25.4	36.0	D	3	40-50	036° [3]	Yes	both	NE-SW trending ridge	No	No
5	25.3	37.0	D	1	20	036°	No	air	No	No	Yes
6*	23.2	37.2	D	3	8	030°-040°(060°[3])	Yes	both	No	No	Yes
7*	22.4	37.7	D	2	9	025°-040°(060°[3])	Yes	both	No	No	Yes
8	22.8	38.7	D	2	10	030°-040°	No	air	No	No	No
9*	21.8	38.0	D	2	15-20	040°-050°(060°[3])	Yes	both	Widening of axial trough	No	No
10	21.3	38.0	D	-	?	055°-065°[3]	Yes	sea	Widening of axial trough	No	Yes
11*	20.8	38.2	D	-	?	070° [3]	Yes	sea	Offset of deep water axis	Yes	Yes
12*	19.5	38.8	D	-	?	055°-060°[3]	Yes	sea	No	Yes	Yes
13	20.0	40.4	D	2	10-12	055°	No	air	No	No	No
14*	16.8	40.8	S?[2]	0	10-15?[2]	049° [1]	No	both	Shallow water area	Yes	No
15*	15.8	41.7	D	7	9	045°	No	air	Shallow water area	No	No
16	15.3	41.9	D	2	30	055°	No	sea	Jebel Tair	No	No
17*	14.8	42.1	D	2	25	055°	No	both	No	Yes	No

[1] from nearby fault plane solution

[2] from offset of bathymetric features

[3] azimuth measured along transverse feature in centre of Red Sea

* transform faults identified with reasonable certainty

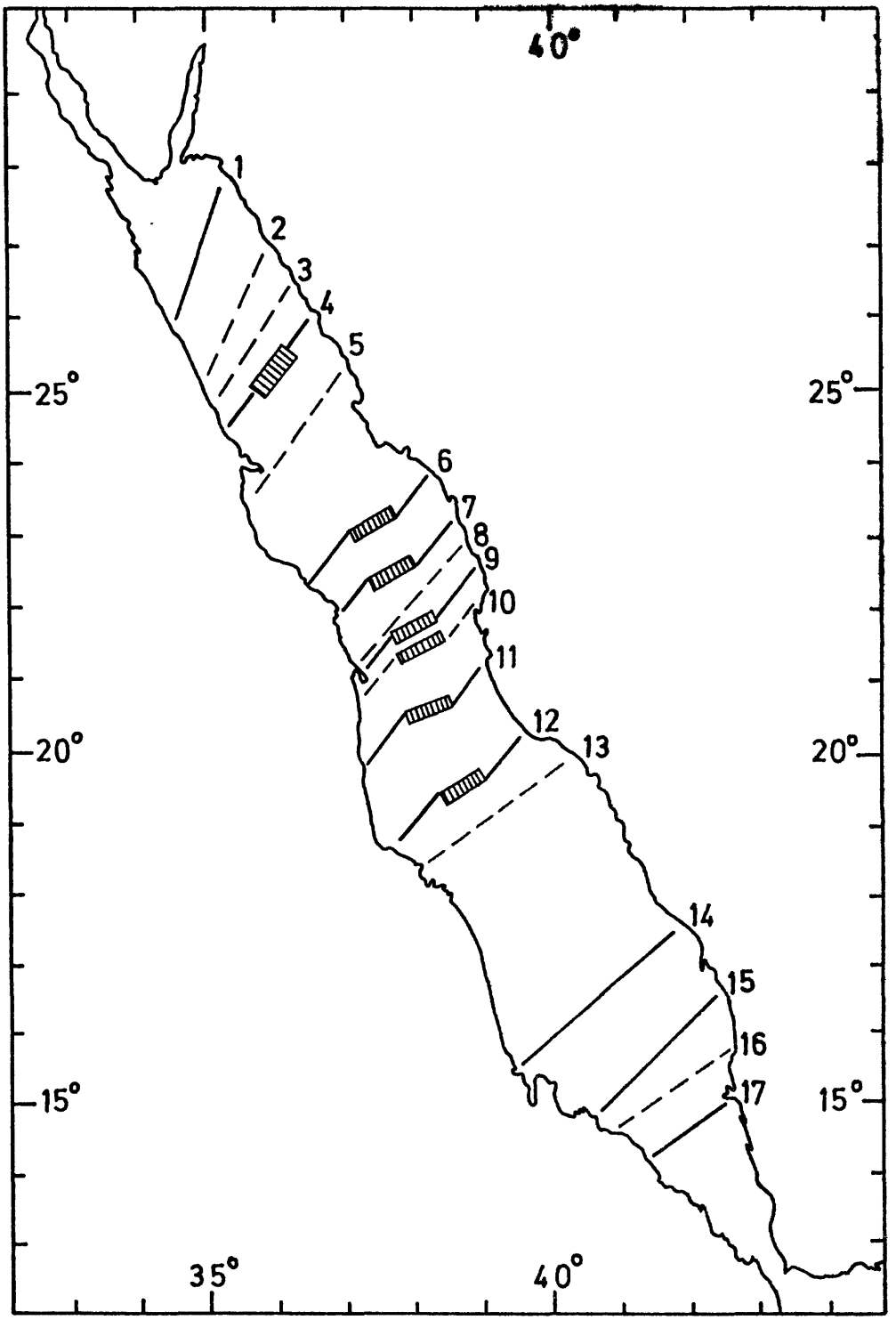

Figure 7.9 Locations of proposed transform faults. ——— transforms identified with reasonable certainty; — — — — tentative transforms; ▥▥▥▥▥▥ proposed leaky transforms. (Numbers are those used in Table 7.2)

Transverse anomalies are not observed south of 16°N where the faults are controlled by movements of Danakil and Arabia. This seems to indicate the motion of Danakil with respect to Arabia has not differed greatly during the two spreading phases.

Five of the six reliably located, dextral faults controlled by the movements of Nubia and Arabia are in areas where there are deep holes. In a recent article, Garson and Krs (1976) have suggested that each deep is associated with a transform fault and that consequently their formation is linked with transform motion. The magnetic evidence does not support this: in particular, several deeps, e.g. Port Sudan and Volcano Deeps, are located in areas where well developed, magnetic lineations, parallel to the Red Sea trend, are supported by extensive data. It appears more likely that the deeps are associated with spreading and therefore are not confined to transform faults, leaky or otherwise.

7.4 Poles of rotation for Nubia and Arabia

A pole of rotation for Nubia and Arabia was determined for each spreading phase using the amounts of new and old seafloor given in Table 7.1. These amounts were measured normal to the magnetic lineations and consequently represent the component of the true separation along the azimuths given in Table 7.1. In fig. 7.10, AB represents the true amount of separation of the plates and AC the component of AB normal to the magnetic lineations. Provided AB and AC are small enough to be considered as straight lines rather than arcs, the quantities are related by:

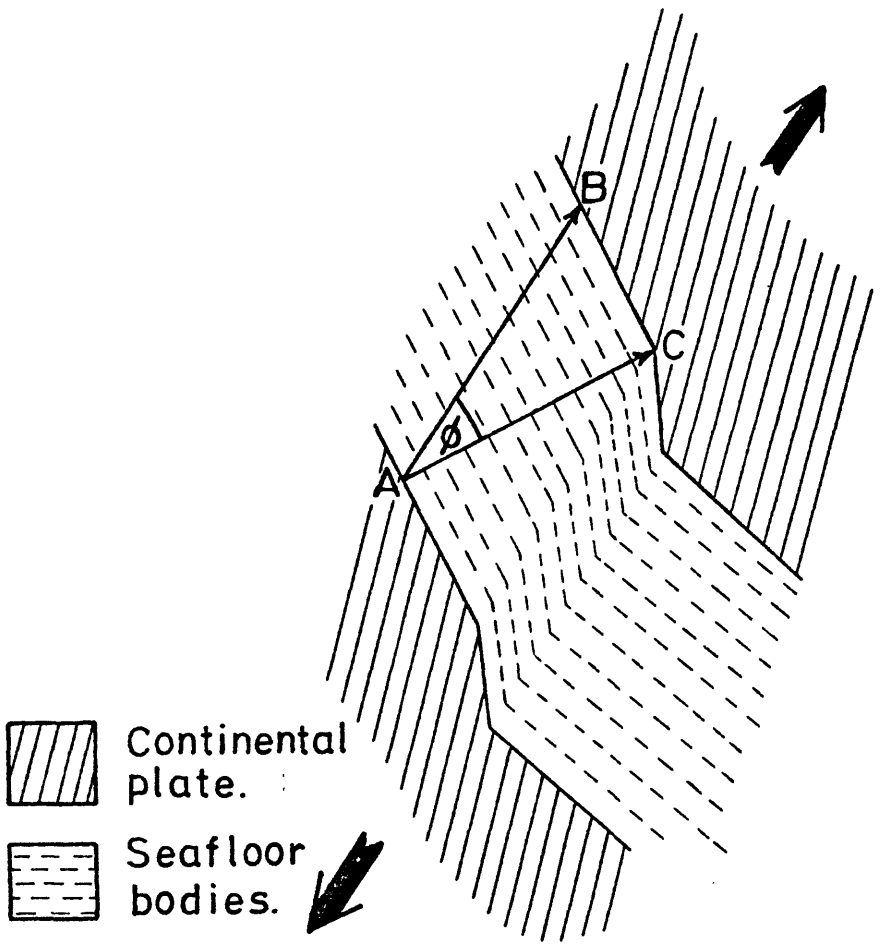

Figure 7.10 Separation of continental plate and generation of oceanic crust. Seafloor bodies formed parallel to continental edges. Large arrows indicate direction of separation, AB. AC is normal to seafloor bodies.

$$AB = AC/\cos \phi \qquad 7.1$$

where ϕ is the angle between AB and AC (fig. 7.10).

The pole of rotation for each phase was calculated as follows: an arbitrary pole position was chosen and the directions of motion calculated at the latitudes given in Table 7.1. Values of ϕ were obtained by subtracting the directions of motion from the azimuths in Table 7.1. Values of AB were calculated using equation 7.1 and these used to obtain estimates of the angle of opening at the pole. Values of the maximum amount of opening produced at the appropriate 'equator' were calculated from these estimates. A mean value of the maximum opening was calculated and the standard deviation of this determined. New pole positions were chosen and the procedure repeated until a minimum standard deviation was obtained; the corresponding pole position was the required pole of rotation. The mean pole position and angle of opening for each phase are:

Phase	Pole position	Angle of opening
Early	29.3^{o}N, 27.1^{o}E	$8.8^{o} \pm 0.5^{o}$
Recent	44.5^{o}N, 9.7^{o}E	$1.2^{o} \pm 0.03^{o}$

The locus of poles having standard deviations of 1.25 times the minimum was also determined as this gives an estimate of how quickly the minimisation of the standard deviation converges(Le Pichon, 1968). The pole positions and their corresponding loci are shown in fig. 7.11.

The poles, though not well determined, are sufficiently reliable to indicate a difference in the direction of motion for each spreading phase. The directions of motion at various latitudes, determined for each phase, are given in Table 7.3. The angular differences, i.e. differences in

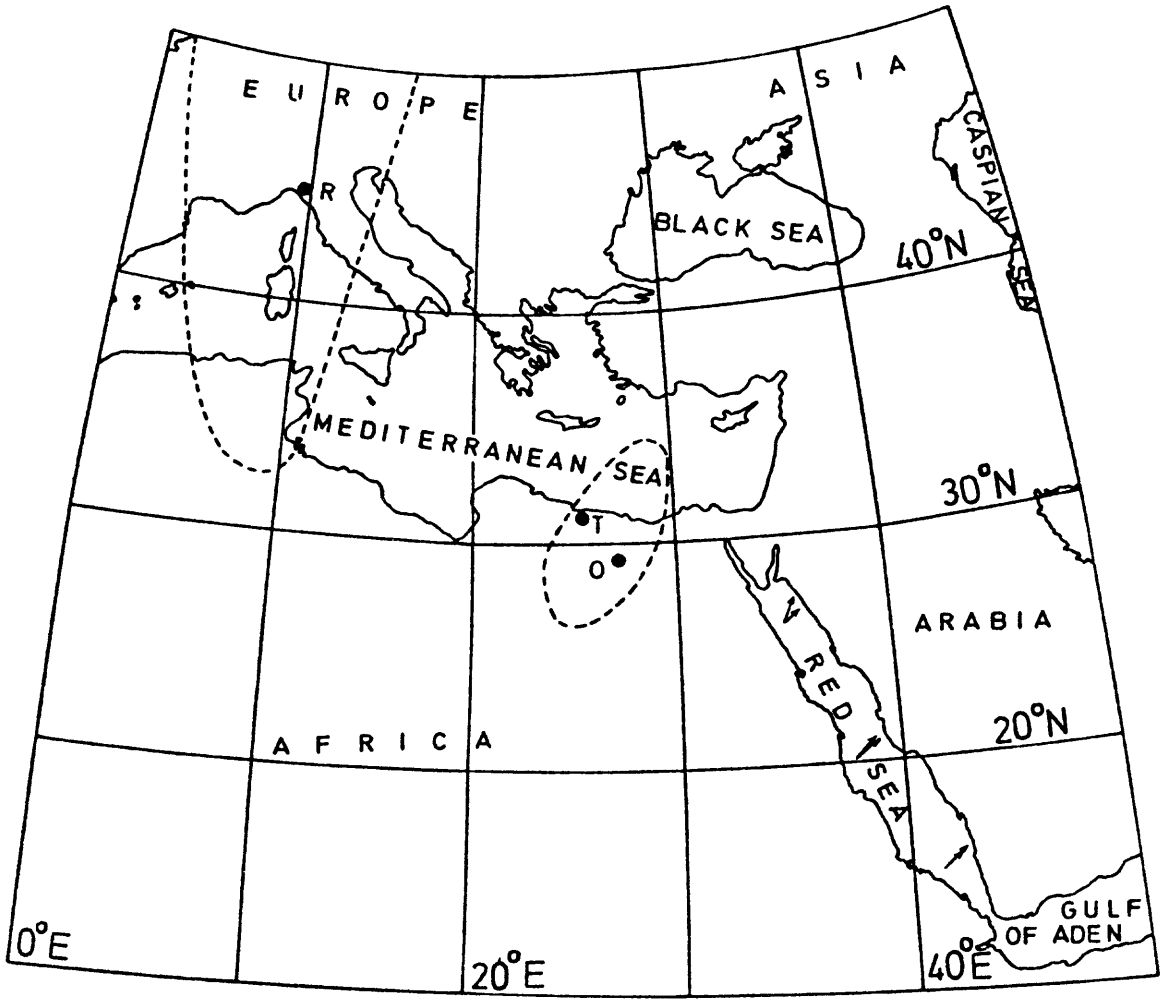

Figure 7.11 Regional map showing locations of rotation poles for the Red Sea determined from the magnetic data. O and R are the poles of rotation for the early and recent spreading phases respectively. Dashed lines are loci of points at which the standard deviation equals 1.25 times the minimum standard deviation. The extent of these loci indicate how fast the least squares determination converges. T is the pole of rotation obtained for the total movement of Arabia with respect to Nubia.

TABLE 7.3

Directions of motion of Arabia with respect to Nubia at various latitudes calculated from the poles of rotation in Fig. 7.11

Latitude (°N)	Longitude (°E)	Direction of motion			Difference in direction (recent - early)
		Old phase, O	Recent phase, R	Total, T	
31.5	35.5	345°	040°	359°	55°
30.0	35.0	004°	043°	010°	39°
27.0	34.75	021°	048°	029°	27°
25.4	36.0	028°	049°	034°	21°
23.5	37.0	035°	050°	039°	15°
22.5	37.75	038°	051°	041°	13°
20.0	40.4	040°	051°	043°	11°
18.5	39.75	046°	053°	047°	7°
17.0	40.7	047°	053°	048°	6°
14.0	42.5	050°	054°	051°	4°

directions of motion for early and recent phases, are approximately 10° to 20° and are in broad agreement with those found for transforms whose azimuths were measured at the coast and over the deep water (viz. numbers 6, 7 and 9,Table 7.2). Comparison of Tables 7.2 and 7.3 indicates the directions obtained from the poles agree reasonably well with the azimuths of the transform faults measured in the centre and at the coast. The poles, therefore, provide additional support for the view that the offsets of the magnetic lineations delineate transform faults and the transverse anomalies are due to dextrally offset, leaky transforms.

A mean pole for the total movement of Arabia with respect to Nubia was determined from the two poles. This is located at 31.2°N, 25.4°E with an angle of opening of 9.9°.

7.5 Plate movements and geometry

The poles of rotation were used in conjunction with geological and geophysical data to study the plate movements and their relative positions during each spreading phase. Three plate combinations are considered: (1) Arabia-Nubia, (2) Arabia-Sinai-Nubia, and (3) Arabia-Danakil-Nubia.

(1) Arabia - Nubia

The poles were used to obtain a two-stage reconstruction of Arabia and Nubia (fig. 7.12). The relative positions prior to spreading (fig. 7.12(c) are not unlike those obtained by McKenzie et al (1970) by fitting the coastlines. In fig. 7.12(c), however, the coastlines overlap in several places especially in the south where, at 17°N, there is about 40 km of overlap. Between the

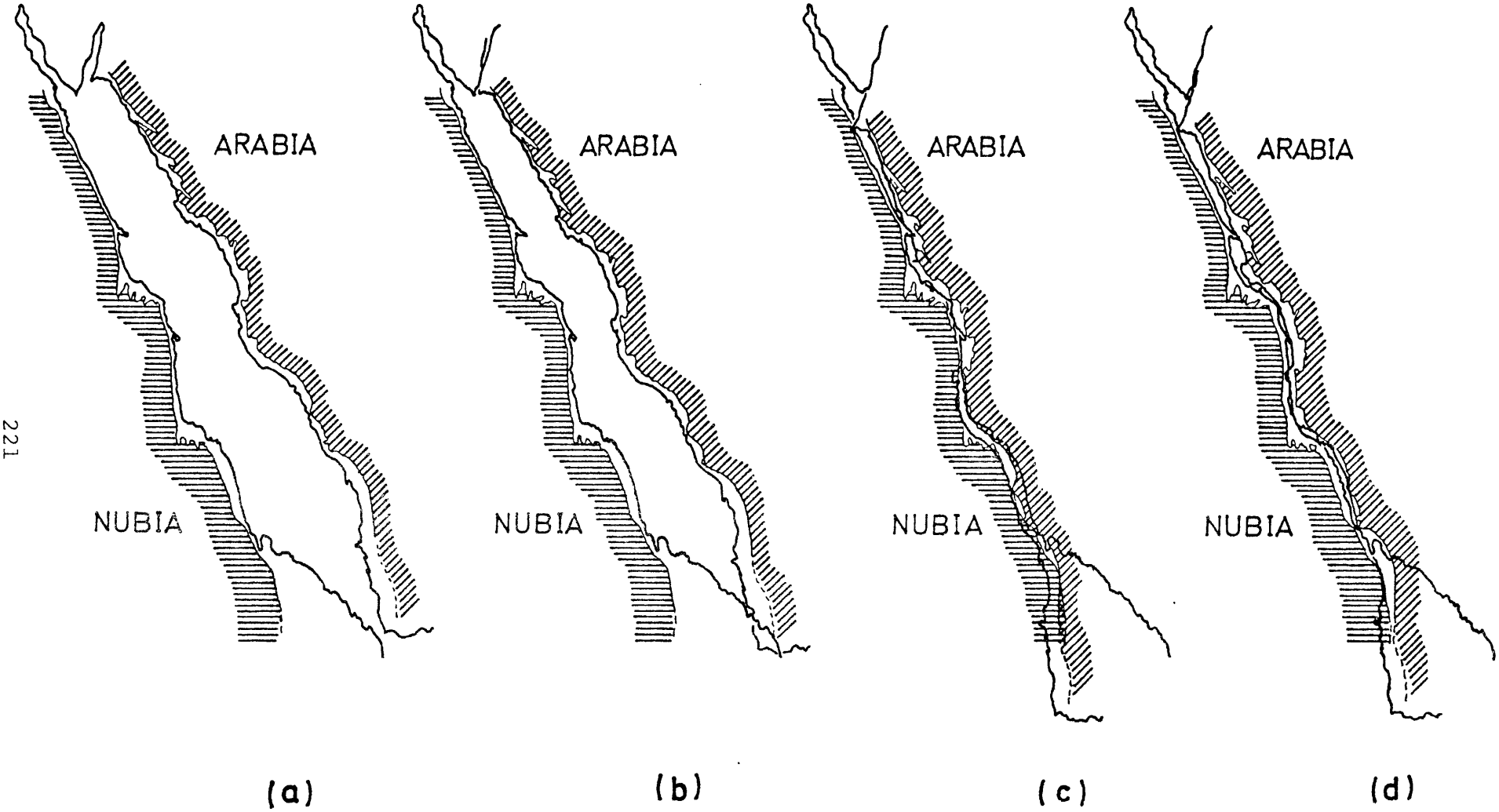

Figure 7.12 Schematic 2-stage reconstruction of Arabia and Nubia by rotation of Arabia about poles O and R in fig. 7.11. In (d) Arabia has been rotated away from Nubia about pole T to remove overlap of PreCambrian. Shading indicates mapped PreCambrian.

Gulf of Suez and the Buri peninsula, the mapped Pre-Cambrian overlap in only one place, viz. near 16°N where a tongue of Arabia Hali Schist (U.S. Geol. Survey 1963) crosses the African Pre-Cambrian by about 10 km. In fig. 7.12(d) the reconstruction has been adjusted to remove any overlap of the Precambrian. An interesting feature of the reconstruction is that Wadi Alhamd and Wadi Hafafit shear zones are continuous as suggested by Abdel-Gawad (1970).

The magnetic data and poles of rotation were used to construct a model of the evolution of the Red Sea (fig. 7.13). This involves four stages: (1) the initial continental fracture (fig. 7.13(a)), (2) fragmentation of the spreading axis and the introduction of several transform faults (cf. fig. 10(b) of Searle and Ross, 1975), (3) rotation of the spreading axes until they are approximately normal to the direction of motion (fig. 7.13(c)), and (4) the recent spreading along a new direction producing leaky transforms (black areas in fig. 7.13(d)). There is some support for asymmetry from the coast-to-coast profiles at 21°N (fig. 5.6) where the peaks and troughs show a small rotation between the coast and the centre (fig. 5.9). Process (2) seems to have been more important in the central Red Sea as most reliably located, dextral, transforms are found between 19.5°N and 23.2°N (see Table 7.2). This is in good agreement with the recent model of Searle and Ross (1975) in which transforms are predominantly formed in areas where the fracture is more oblique to the direction of motion, i.e. central Red Sea.

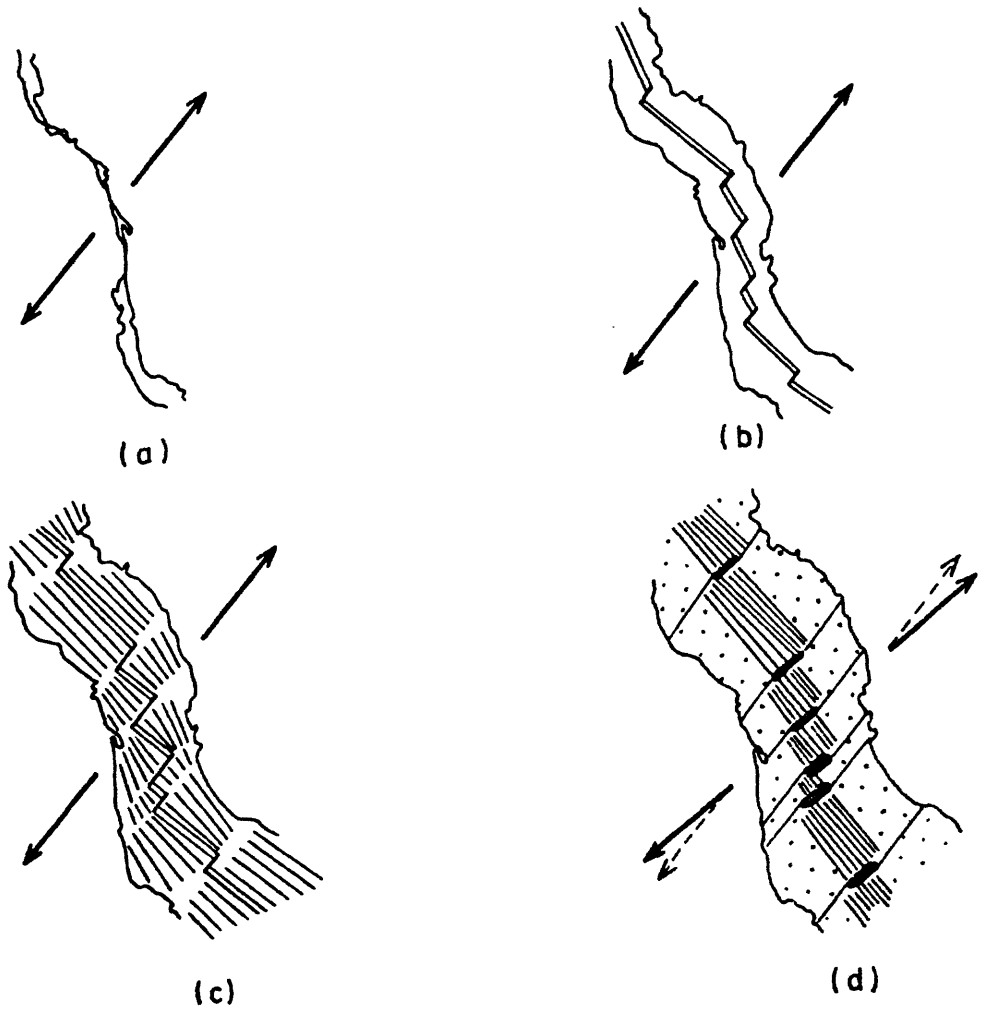

Figure 7.13 Schematic evolution of the Red Sea. (a) Initial continental fracture near present coastlines, (b) early spreading oblique to direction of motion with resulting formation of transform faults, (c) adjustment of spreading axes by asymmetric spreading, and (d) recent spreading along new direction with formation of leaky transforms. Dotted areas represent seafloor formed in early phase .

(2) Arabia - Sinai - Nubia

Calculations, based upon the poles of rotation, indicate a total extension between Arabia and Nubia at 30^{o}N, 35^{o}E of approximately 160 km along N10^{o}. As detailed studies of surface and subsurface geological features along the Dead Sea rift (Freund et al, 1970) indicate approximately 105 km left lateral movement between Arabia and Sinai (and its northern extension), it seems likely that Sinai forms a separate plate. If so the boundary between Nubia and a Sinai plate must be the Gulf of Suez as Triassic and older rocks are found throughout Sinai (Said, 1962). Although little is published about the underlying structure of the Gulf it is generally considered to be underlain by Pre-Cambrian. However, analyses of seismograms for an earthquake near Shadwan Island in the mouth of the Gulf indicate the presence of low Q material (R. Pearce, pers. comm.) suggesting the southern Gulf may be partly underlain by oceanic crust.

The magnetic data show the separation of Arabia and Nubia has occurred in two stages. Geological evidence (Freund et al, 1970) indicates the sinistral movement along the Dead Sea rift between Arabia and Sinai has also taken place in two stages. It follows from this that any motion, viz. extension, separation or shear, between Nubia and Sinai must have occurred in two stages. A schematic two stage reconstruction of the three plates is shown in fig. 7.14. The plate configurations were obtained by reversing the sequence of movements. Thus to obtain the situation prior to the recent spreading(fig. 7.14(b))the following adjustments to the present configuration (fig. 7.14(a)) were made: Arabia was moved along N223^{o} by 55 km at 30^{o}N and along N228^{o} by 60 km

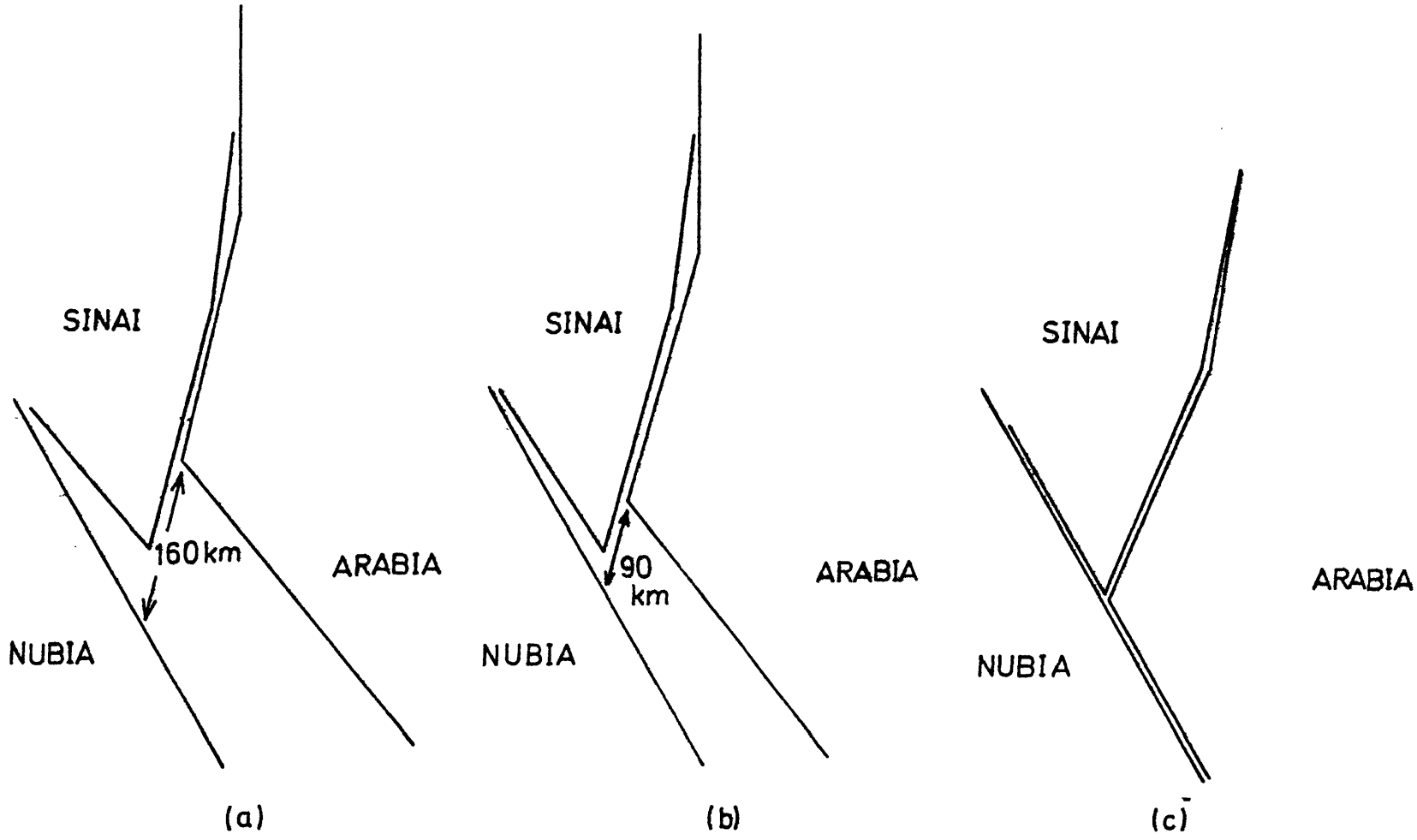

Figure 7.14 Proposed reconstruction of Arabia-Sinai-Nubia deduced from the 2-stage rotation of Arabia with respect to Nubia. (a)present position of Arabia-Sinai-Nubia, (b) position of plates at end of early spreading phase, and (c) plate geometry prior to the onset of spreading.

at 27°N. Sinai was then moved south westward so as to reduce the sinistral offset with Arabia from 105 km to 60 km, i.e. the amount of pre-Miocene offset reported (Freund et al, 1970). Nubia was kept stationary. To obtain the situation prior to the early spreading, Arabia was moved 110 km along N184° at 30°N and 120 km along N201° at 27°N. Sinai was then moved in such a manner as to close up the gaps as much as possible. There are no firm constraints on its motion at this time although the three plates probably formed one continuous plate prior to the onset of spreading.

During the early phase, parts of Arabia north of 31°N moved west of north (see Table 7.3). Although there is no control on the movements of the corresponding parts of the Sinai plate it seems probable that little westerly motion occurred since there was compression and folding in northern Israel and Lebanon (Picard, 1943; Bentor and Vroman, 1954; deSitter, 1962). Sinai moved approximately NNE to NE with respect to Nubia by 35 to 40 km.

During the recent phase Arabia moved along N40° to N45°. At 30°N the movement was 55 km with respect to Nubia giving a N-S component of about 40 km and an E-W component of 35 to 40 km. The N-S component agrees approximately with the amount of sinistral movement noted along the Dead Sea rift (Freund, 1965) since the Miocene implying there has been little N-S movement between Nubia and Sinai during the recent phase. The easterly movement of Arabia is responsible for the extensive faulting and the observed depression although small easterly movements of the Sinai plate may have reduced the amount of extension.

The total movement of Sinai with respect to Nubia appears to have been about 45 km along N45^{o} which implies approximately 40 km normal to the strike of the Gulf. This is substantially larger than previous estimates (Robson, 1971) but less than that suggested by others (McKenzie et al, 1970). The movement may have been achieved by faulting, crustal attenuation or separation or a combination of these processes. Unfortunately within the Gulf proper the existence of faults remains largely speculative. Upper Cretaceous sediments have been observed in boreholes within the Gulf (El Shinnawi and Sultan, 1973) indicating the amount of oceanic crust younger than this is not substantial.

Finally it is perhaps worth noting that moving Sinai approximately 40 km SW brings two basement highs, viz. Jebel Zeit and Jebel Araba, into continuity. These features are thought to have existed as islands or submerged highs in the middle of the Gulf during the Cretaceous (Said, 1962).

(3) Arabia - Danakil - Nubia

There is extensive evidence for the existence of a Danakil plate between Arabia and Nubia at the southern end of the Red Sea (see section 1.2). Any reconstruction of the major plates must leave sufficient space to accommodate the continental part of this plate. Unfortunately the exact size of Danakil is unknown although it is generally shown to extend from the Buri peninsula at 15.5^{o}N to 12^{o}N with a width varying from 15 km near 15^{o}N to 100 km at 12^{o}N. The area of exposed pre-Tertiary rocks is much smaller covering approximately 130 x 70 km^{2}. A great deal of its southern part is covered

by Tertiary and Quaternary volcanics (Mohr, 1967) and there is some reservation concerning the nature of the crust south of 13^{o}N (Marinelli et al, 1973).

The reconstruction shown in fig. 7.13(c) does not provide sufficient space to accommodate the Danakil plate indicating the pole positions and/or the angles of opening are incorrect. The pole for the early phase is located close to the N. Red Sea, consequently small errors in the angle of opening will not seriously affect northern areas but will produce large distance errors in the south. Such errors are probably responsible for the extent of the overlap observed in fig. 7.12(c). There are, however, several other factors which may also contribute to the overlap. First, the E-W size of the block may have been increased by stretching. There are numerous faults crossing Danakil (Mohr, 1972) and several kilometres extension may have been produced. Secondly, the coastal plain of Yemen, opposite Danakil, could be underlain by oceanic crust. There is an approximately 40 km wide strip on which no Pre-Cambrian rocks have yet been mapped. Unfortunately the spreading centre, inferred from the magnetic anomalies, lies nearly midway between the coasts (fig. 6.7), consequently considerably asymmetric spreading is required to emplace seafloor beneath the Yemeni coastal plain. Thirdly, the Danakil plate may be much smaller than previously supposed, consisting of several, small continental fragments separated by oceanic crust.

The poles of rotation were used to construct a model of the evolution of the Danakil plate from movements of Arabia and Nubia. This model is

shown in fig. 7.15 and assumes the major plates have loosely controlled Danakil's movements. In particular, Arabia and Danakil are assumed to have been connected at the southern end of the Red Sea until the beginning of the recent spreading phase so as to agree with the geological evidence. The rotation of Danakil was obtained from palaeomagnetic data which indicate a counter clockwise rotation of 25^{o} to 30^{o} since the early Miocene (Burek, 1970) and about 10^{o} over the past 6 to 7 My (Schult, 1974). In the model a total rotation of 30^{o} has been assumed: 20^{o} during the early phase and 10^{o} during the recent phase. The direction of motion of Arabia and Nubia is similar for both phases at this latitude viz $N50^{o}$ to $N55^{o}$ (Table 7.3). If Danakil was fixed to Arabia during the early spreading it must have moved northwards with respect to Nubia. Because of the errors in the poles and/or angles of opening it is not possible to specify accurately how much Arabia moved with respect to Nubia at this time. In fig. 7.15(b) Arabia has been moved approximately 250 km along $N50^{o}$. This moves Danakil NE with respect to Nubia opening up the Gulf of Zula to a width of approximately 30 km. During the recent phase Danakil became detached from Arabia and the Straits of Bab-el-Mandeb opened permitting the waters of the Indian Ocean to enter the Red Sea. Interpretation of satellite photography of the Straits (Abdel-Gawad, 1970) suggests that Arabia has moved approximately 40 km NNE with respect to southern Danakil. In fig. 7.15(c) Arabia has been moved 90 km along $N55^{o}$ as indicated by the poles of rotation. Danakil's position is fixed by three constraints: (1) a further 10^{o} rotation with respect to Nubia, (2) 40 km SSW movement with respect to southern Arabia, and (3) the width

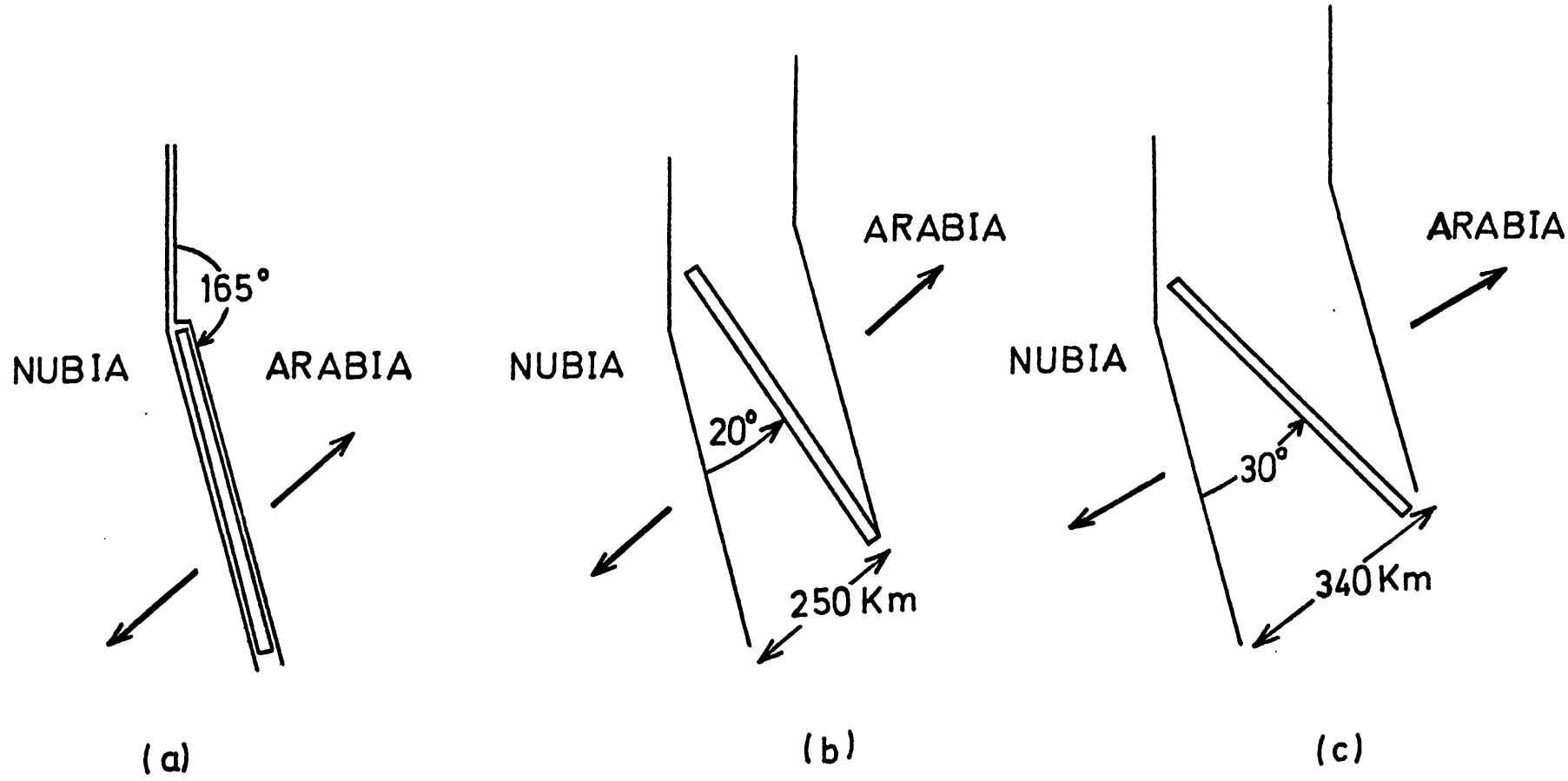

Figure 7.15 Proposed evolution of Danakil plate deduced from the 2-stage rotation of Arabia with respect to Nubia. (a) plate geometry prior to the onset of spreading, (b) position of Danakil at the end of the early spreading phase, and (c) present position of Danakil.

of the Gulf of Zula which must not exceed the distance between the Pre-Cambrian on either side, viz ~ 20 km.

An attempt to delineate the present boundaries of the Danakil plate is shown in fig. 7.16. The eastern boundary is based upon the magnetic data and follows the proposed axis of spreading (fig. 6.7). The western boundary is based upon geological evidence (Marinelli et al, 1973) and follows the Dallol - Borale - Erta Ale volcanic range between 15 ^{o}N and 13.5^{o}N, south of which it is drawn along the Tat'ali volcanic chain. The northern boundary with Nubia crosses the bend in the magnetic lineations at the coast (Girdler and Styles, 1974) and in the centre (see fig. 6.7) slightly north of the point at which the spreading rate begins to decrease (Girdler and Styles, 1974). The eastern boundary south of 14.2^{o}N is difficult to define as only high frequency magnetic anomalies are present. South of 13.5^{o}N the volcanic province in Afar widens abruptly from 35 km to approximately 110 km splitting into two volcanic chains, viz. Tat'ali and Alayta. As this coincides approximately with the disappearance of the linear anomalies in the southern Red Sea it is tempting to speculate that some spreading may be transferred from the Red Sea into Afar at this point.

One interesting feature of the plate geometry in fig. 7.16 is that sea-floor emplaced along the Arabian coast south of 17^{o}N will have been controlled by movements of Arabia and Danakil. The widening of the anomalies in this area (see section 6.4.3) does not support this and it appears more likely that the widening is due to spreading of Arabia and Nubia. An alternative

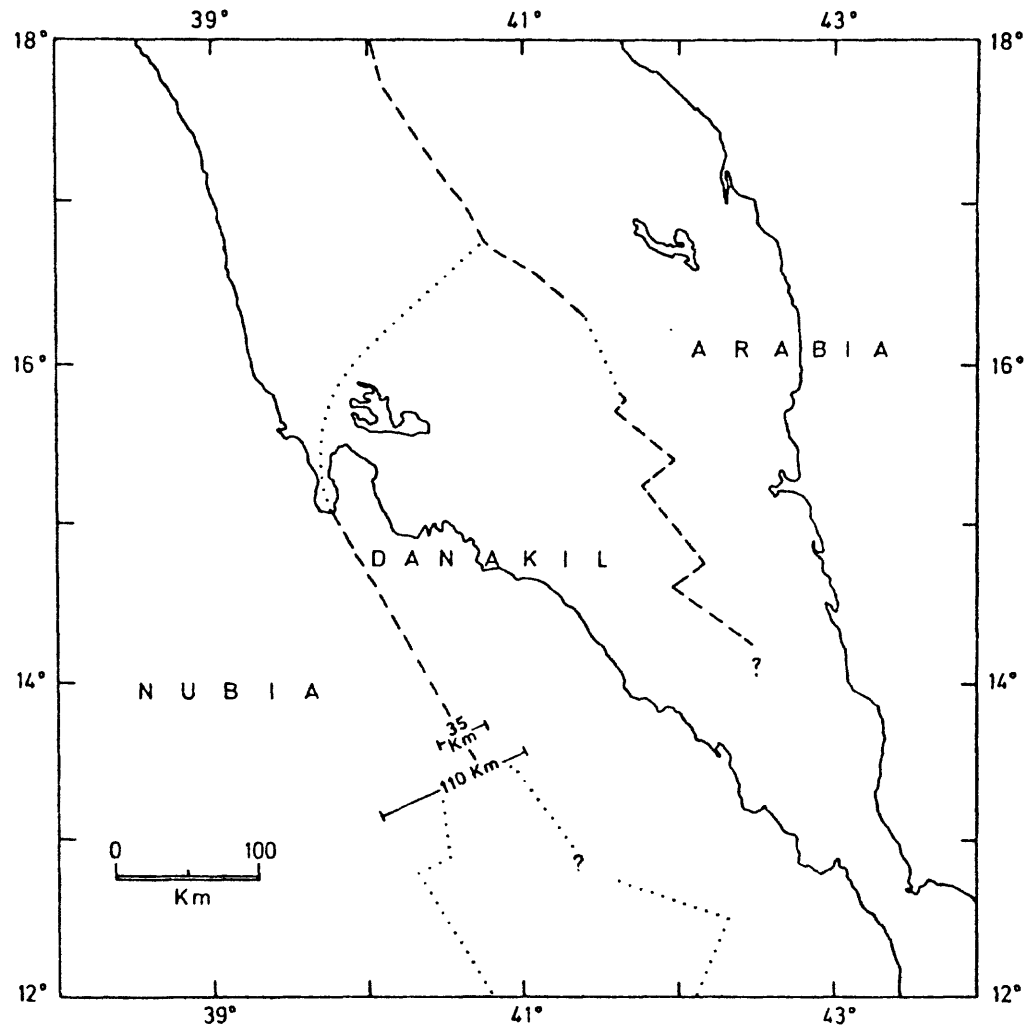

Figure 7.16 Present plate geometry at southern end of Red Sea. Dashed lines indicate reasonably well defined boundaries; dotted lines indicate poorly defined boundaries. Location of southern boundary between Danakil and Arabia unknown. ⊢—— 35 Km ——⊣ width of volcanic province in Afar.

explanation is the initial spreading between Danakil and Arabia may have been asymmetric with the spreading axis rotating to produce a narrowing of the anomalies on the west and a widening to the east. This situation is shown schematically in fig. 7.17.

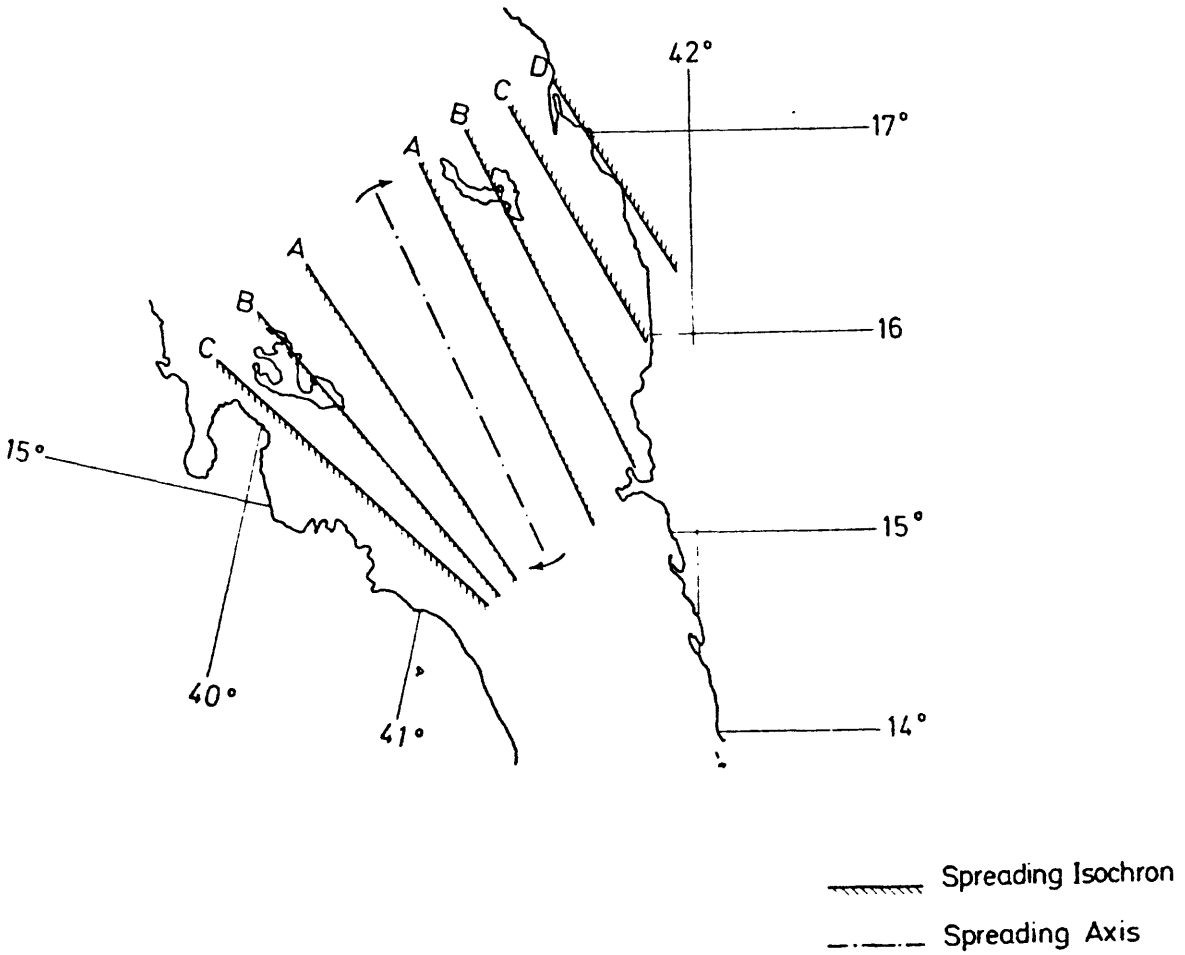

Figure 7.17 Formation of the southern Red Sea by the counterclockwise rotation of Danakil with respect to Arabia. Adjustment of spreading axis by asymmetric spreading leads to a widening of the anomalies to the east and a narrowing to the west.

CHAPTER EIGHT

IMPLICATIONS FOR THE FORMATION OF THE RED SEA DEEPS

8.1 Magnetic anomalies over the deeps

In general, large amplitude ($\sim$ 1000 nT), short wavelength (5 to 10 km), anomalies are observed over the deeps. Exceptions are Oceanographer, Gypsum and Vema Deeps and an unnamed deep at 23.67^{o}N, 36.43^{o}E over which there are smaller (100 to 200 nT), longer wavelength (15 to 20 km) anomalies. All deeps lie in zone 1 (figs. 7.1, 7.2 and 7.3) and therefore are associated with the young seafloor. Over Kebrit Deep there is a strong localised anomaly (fig. 4.14); such anomalies may be present over other deeps but at present there is insufficient detailed coverage to verify this. The large anomalies over the deeps in the central Red Sea are not localised but form part of the large, regional magnetic pattern. These deeps are therefore probably related to the seafloor spreading.

The deeps are located in areas over which there are linear anomalies that trend parallel to or transverse to the axis. There are only two areas of transverse anomalies in which no deeps have yet been discovered, viz. numbers 4 and 9, Table 7.2 and fig. 7.9. Detailed bathymetric surveys have been made over one of these, viz. 21.8^{o}N, 38.0^{o}E, (Backer et al, 1975) but no deeps detected.

8.2 Possible models for the formation of the deeps

Since the magnetic expressions of the deeps differ, it is difficult to find a model which will simulate each type of anomaly. Furthermore, as the deeps are located in leaky transform areas and 'normal' parts of the spreading axis their formation may involve more than one mechanism. Consequently there are several possible models, each of which agrees with some but not all of the data. Three such models are discussed below:

(1) Buried seamounts

The large anomaly over Kebrit Deep was simulated in Chapter 4 using a strongly magnetised body located beneath the deep. The body may be considered as a volcanic seamount covered by the evaporites. The magnetic anomalies on nearby tracks are small ($\sim$ 100 nT) indicating the seafloor is either deep or weakly magnetised (see section 7.2) in the vicinity of the deep. On the other hand, the amplitude and gradient of the large anomaly indicates the volcanic body is comparatively shallow implying it rises above the seafloor. Formation of the deep is due to seafloor spreading accompanied by localised injections of basalt into the base of the evaporites (fig. 8.1). Spreading causes slumping of the evaporites, some of which are pushed aside by the seamount.

The model has the following advantages: (1) it provides a localised source, compatible with the deeps, (2) the volcanic body provides heat which can elevate the water temperatures, (3) heat from the body can cause some evaporites to dissolve forming a dense brine pool, and (4) migration of the seamounts by seafloor spreading possibly accounts for those deeps located some way from the deep water axis, e.g. Gypsum Deep and the unnamed deep at

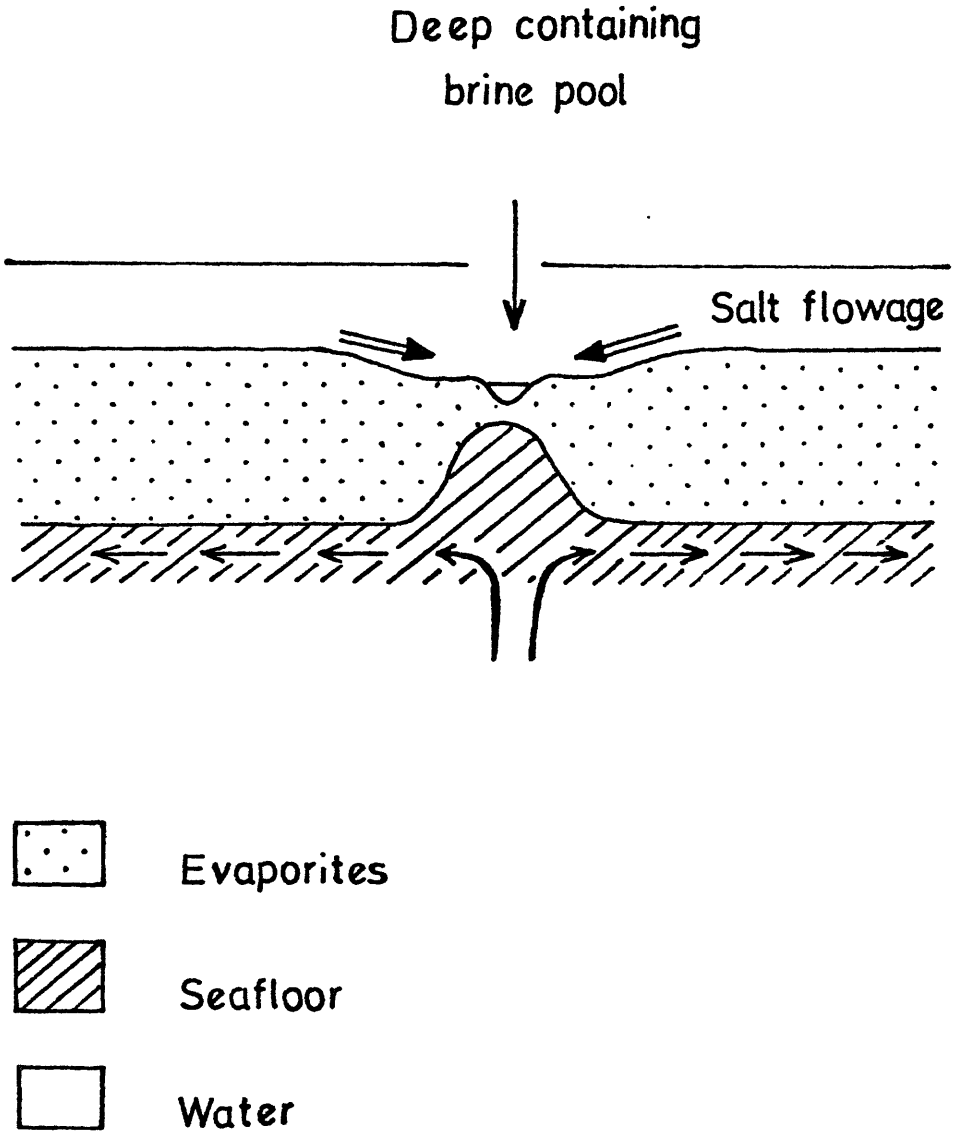

Figure 8.1 Formation of deep holes by seafloor spreading with localised injection of seafloor into evaporites.

23.67°N, 36.43°E. The absence of brine pools in such deeps may be partly explained by deposition in response to the water cooling as the seamounts spread away from the magma chamber. The disadvantages of the model are: (1) it is unlikely that so many seamounts, viz. 21, would be formed in such a small area of seafloor, (2) the morphology of the deeps differ so much that it is difficult to explain each by a seamount. Round structures such as Kebrit, Discovery and Valdivia Deeps have predictable shapes whereas Nereus, Suakin and Port Sudan/Volcano Deeps are elongated twin basin features, (3) the distribution of deeps is not random as might be expected but concentrated in the central Red Sea. The seamount model, therefore, provides a reasonable explanation of the smaller deeps but not the larger ones.

(2) Localised basins

A model for the initial generation of transform faults in the Red Sea has been presented recently by Searle and Ross (1975). The authors use the ideas of Menard and Atwater (1968) to demonstrate how the initial continental fracture has influenced the subsequent geometry of the seafloor. Where the direction of this fracture is oblique to the direction of motion the spreading axis adjusts by either asymmetrical spreading or fragmenting into several shorter spreading axes (cf. fig. 5, Menard and Atwater, 1968). The poles of rotation (section 7.4) indicate the central Red Sea was oblique to the direction of motion during the early spreading phase. Thus several transforms were probably formed producing a number of short spreading axes (fig. 7.13(b)).

If the motion of the plates changed at the beginning of the recent spreading phase, both transform faults and spreading axes will have generated seafloor (fig. 7.13(d)). A series of small basins may have been formed by the flowage of evaporites from all directions (fig. 8.2). Deeps formed by this process satisfy the following criteria: (1) the presence of a heat source giving high heat flow and elevated water temperatures, (2) a supply of salt to form brine pools, (3) the large, linear anomalies produced by seafloor spreading, (4) the presence of deeps in both leaky transforms and spreading axes, (5) the presence of inter-trough zones (Searle and Ross, 1975) in which the evaporites are continuous across the axial trough. Such zones are the NW and SE sides of leaky transforms (fig. 8.2(c)), (6) the absence of deeps in the southern Red Sea where the directions of motion for each spreading phase are approximately the same and little adjustment of the spreading axis is necessary.

The model is unable to account for: (1) the localised anomaly over Kebrit Deep, (2) the existence of off-axis deeps such as Gypsum Deep and the unnamed deep at 23.67^{o}N, 36.43^{o}E, and (3) the variations in morphology of the deeps, especially the NW-SE basins in Atlantis II Deep (Backer and Schoell, 1972; Backer et al, 1975), although these could be a consequence of salt flowage. The model does, however, predict that where there are longer sections of the spreading axis, any deep present will be located approximately midway between the appropriate transform faults; the salt on either side having flowed about the same distance. Also where the NW-SE length of the spreading axis exceeds the width of new seafloor, viz. approximately 70 to 80 km in the central Red Sea, the deep will be elongated NW-SE. Thus Port

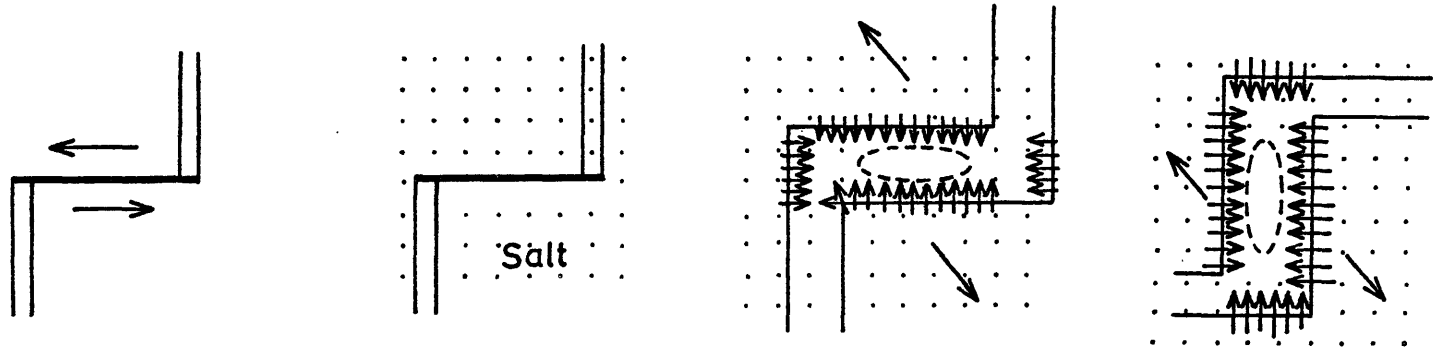

(a) Initial spreading phase.

(b) Hiatus in spreading. Deposition of evaporites.

(c) Recent spreading phase. Salt flows forming basin in leaky transform.

(d) Recent spreading phase. Salt flows forming basin in short spreading axis.

Figure 8.2 Development of localised basins due to salt flowage and seafloor spreading.

Sudan/Volcano Deeps lie on a 120 to 130 km long spreading axis, about midway between transforms 11 and 12 (fig. 7.9) and form an elongated feature.

(3) Caldera collapse

In a recent paper, Francis (1974) explains the seismicity of the Mid-Atlantic Ridge in terms of caldera collapse. In the model, the ridge axis is considered an area of general uplift produced by upwelling magmas. At equilibrium, the overburden pressure due to the ridge exactly matches the magmatic pressure. Further uplift reduces the magmatic pressure resulting in collapse of the ridge. The collapse produces roughly elliptical calderas elongated along the spreading axis which overlap forming an extended depression, i.e. the median valley.

Applying this model to the Red Sea which has comparable spreading rates and seismicity to the Mid-Atlantic Ridge it can be seen that the calderas provide suitable locations for the deeps. The advantages of such a model are similar to those in (2) with the additional advantage that off-axis deeps may be explained in terms of uplift of the calderas and spreading. The calderas will be raised as they spread away from the centre to the flanks of the spreading axis. Consequently such deeps would be shallower than those on the spreading axis because of this uplift and the increased deposition due to cooling. In fig. 8.3 the depth of each deep is plotted against it latitude; the off-axis deeps are shallower than on-axis deeps at the same latitude although an insufficient number have been discovered to make this more than tentative.

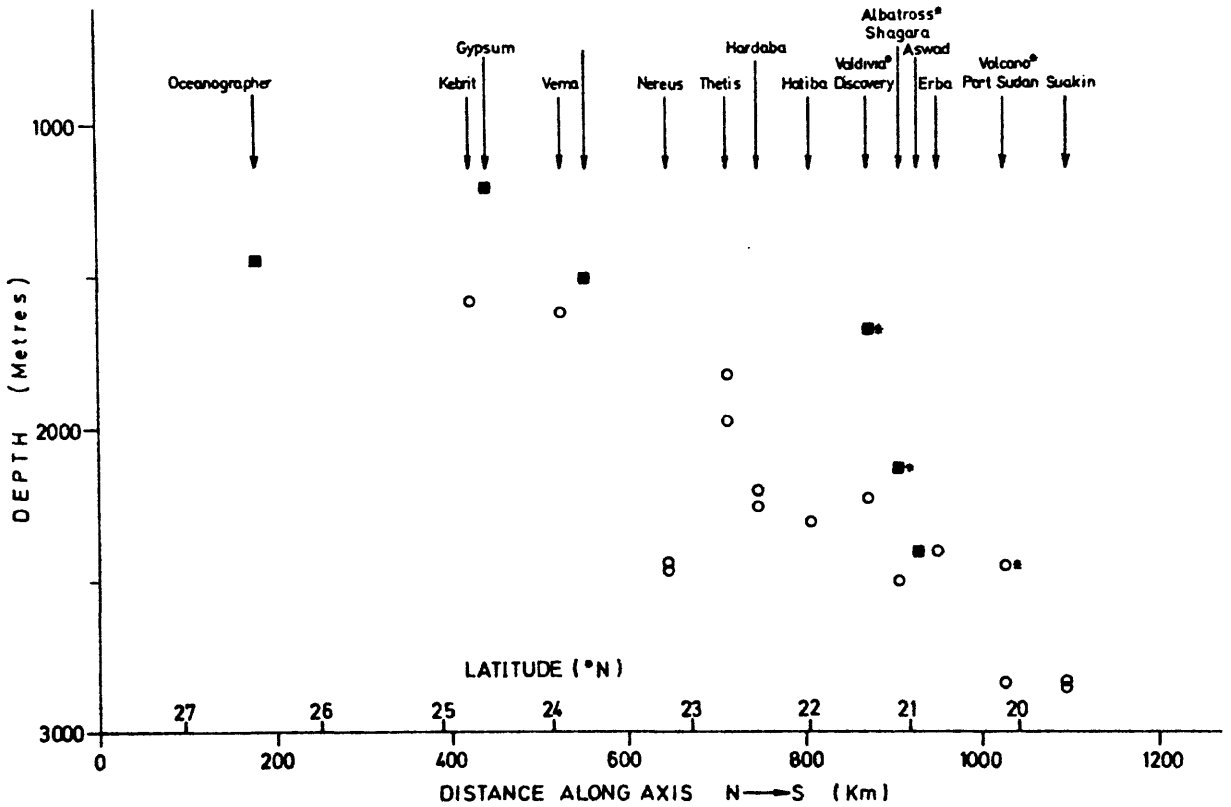

Figure 8.3 Plot of depth versus latitude of deep holes in the Red Sea. O on-axis deeps; ■ off-axis deeps.

There are two main disadvantages: (1) deeps in leaky transform are elongated NW-SE whereas the model predicts NE-SW, and (2) it is not clear why the calderas do not connect to produce an elongated valley rather than localised deeps. The first problem is common to each model. The second problem can be explained in terms of salt flowage which has modified the geometry of the original basins. Thus adjacent deeps may be separated by walls of salt. The physical and chemical composition of some brine pools suggest subsurface connections between several deeps, e.g. Atlantis II and Discovery Deeps, two basins within Suakin Deep (Backer and Schoell, 1972). An alternative explanation is that the calderas experience differential uplift and collapse in response to different thermal regimes; the deeps being separated by caldera walls which have vents that permit the brine pools to mix. Seismic reflection data (Ross et al, 1969) show that beneath the flanks of the deeps the S-reflector is often present. The deeps, therefore, probably represent minor depressions in the seafloor separated by salt flows rather than volcanic material.

Insufficient evidence is available to decide between the models. However as most deeps are found in leaky transform zones, the conditions in such areas must be especially favourable for their formation. Further data from such areas should be collected, therefore, and the models reappraised.

CHAPTER 9

CONCLUSIONS AND SUGGESTIONS FOR FURTHER WORK

9.1 Concluding remarks

The Red Sea is a young ocean formed by the separation of Arabia from Africa during the past 40 My. However, the continental edges and usual bathymetric expressions of seafloor spreading are concealed beneath huge thicknesses of sediments which have accumulated during an hiatus in spreading. As a result the plate geometry and relative motions cannot be studied directly. The magnetic data have provided an alternative estimate of the continental edge and enabled the directions of motion to be determined. The effects of the plate movements on the surrounding continents have not been studied and detailed correlation of tectonic events with the spreading is awaited with interest. The relationship of the mineralisation found in the deep holes to the plate geometry is not fully understood and additional research on this problem is required.

Although magnetic data have been used throughout this work there is a growing need for an integrated study involving other geophysical data. Such studies require detailed planning if they are to be effective. It is hoped that this work will prove helpful in this planning.

9.2 Major conclusions

1. Almost the entire width of the Red Sea is underlain by oceanic crust.
2. This oceanic crust has been emplaced during at least two phases of seafloor spreading: one between either 41 My and 34 My or 29 My and 23 My, the other from about 5 My to the present.

3. The direction of motion of Arabia with respect to Nubia was different for each spreading phase; Arabia moving more northerly during the early spreading phase.

4. Several dextral transform faults, created during the early spreading, have spread during the recent phase and are responsible for the transverse magnetic anomalies observed.

5. Several transform faults have been identified from offsets of the linear, magnetic pattern along the Arabian coast.

6. Sinai forms a separate plate which has moved approximately 45 km NE with respect to Nubia thereby opening the Gulf of Suez.

7. The lack of magnetic expression of the seafloor in the northern Red Sea is attributed to the presence of evaporites which permit the seafloor to cool more slowly and thereby acquire a reduced magnetisation.

8. Although all deeps are located in the area of seafloor created during the past 5 My, with the exception of Kebrit Deep, there is no evidence of localised anomalies associated with the holes. The large anomalies observed over the deeps are due to recent seafloor spreading.

9. A majority of deeps are found in leaky transform faults. Models of their formation, however, suggest they are produced by the combined effects of seafloor spreading and salt flowage.

10. The secular variation in the Red Sea over the period 1959 to 1972 was found to be $+18 \pm 3$ nT per year.

9.3 Suggestions for further work

It can be seen from fig. 2.1 that large areas exist where little or no data are available. The coverage of the northern Red Sea is particularly poor. Future work should be planned to augment existing data with particular attention being paid to the main trough and shallow shelves. In addition, some detailed studies might be carried out to substantiate and possibly modify the conclusions of this work, especially those concerning the leaky transform faults, the nature of the crust beneath the margins and the present plate geometry. These could include:

(1) A detailed study of one of the areas of transverse magnetic anomalies. Two of these occur some distance from the others (nos. 4 and 12, Table 7.2) and either would provide a suitable site. As detailed bathymetric and geochemical studies have been carried out in Suakin Deep (Baumann et al, 1973) this is possibly the best choice. A study including magnetics, gravity, seismic refraction and ocean bottom seismometry would enable the structure and seismic activity to be more accurately defined. Coverage might be extended as near to the coasts as possible to detect any changes in the direction of the features.

(2) A deep drilling site along the coastal plain of Arabia where the magnetic data indicate oceanic crust. The seafloor spreading models suggest the upper surface of the magnetised layer is probably at 4 to 5 km below sea level. Previous holes along the coast and offshore areas have been drilled to 3.5 to 3.9 km (Gillman, 1968; Coleman, 1974). Suitable locations showing impressive linear seafloor anomalies are near Jizan

(17^{o}N, 42.5^{o}E) and near Qunfudah (19^{o}N, 41.2^{o}E). Such a hole would provide evidence of the oceanic crust and enable its age to be determined. Analyses of the physical properties of the core material would be especially helpful in the interpretation of data from other boreholes.

(3) Local studies of the seismicity and microseismicity using either portable land stations or ocean bottom recording seismometers. These would help to accurately locate the plate boundaries and determine the direction of motion between the plates.

REFERENCES

Abdel-Gawad, M., 1969. Geological structures of the Red Sea area inferred from satellite pictures: in Degens, E.T., and Ross, D.A., eds., Hot brines and recent heavy metal deposits in the Red Sea : New York, Springer - Verlag, pp. 25-37.

Abdel-Gawad, M., 1970. Interpretation of satellite photographs of the Red Sea and Gulf of Aden : Phil Trans. Roy. Soc. Lond., v. A267, pp. 23-40.

Ahmed, S.S., 1972. Geology and petroleum prospects in eastern Red Sea : Am. Assoc. Petroleum Geologist Bull., v. 56, no. 4, pp. 707-719.

Allan, T.D., 1970. Magnetic and gravity fields over the Red Sea : Phil. Trans. Roy. Soc. London., v. A267, pp. 153-180.

Atwater, T., and Mudie, J.D., 1973. Detailed near-bottom geophysical study of the Gorda Rise : Jour. Geophys. Research, v. 78, pp. 8665 - 8686.

Backer, H., 1973. Rezente hydrothermal-sedimentare Lager stattenbildung : Erzmetall, v. 26, pp. 544-555.

Backer, H., Lange, K., and Richter, H., 1975. Morphology of the Red Sea central graben between Subair Islands and Abulkizaan.

Backer, H., and Richter, H., 1973. Die rezente hydrothermal-sedimentare Lagerstatte Atlantis II - Tief in Roten Meer : Geol. Rundschau, v. 62, pp. 697-740.

Backer, H., and Schoell, M., 1972. New Deeps with brines and metalliferous sediments in the Red Sea : Nature, Physical Sciences, v. 240, pp. 153-158.

Ball, J., 1916. The geology and geography of west central Sinai: Egypt Survey Dept. Cairo. pp. 1-219.

Barberi, F., Borsi, S., Ferrara, G., Marinelli, G., and Varet, J., 1970. Relations between tectonics and magmatology in the northern Danakil Depression (Ethiopia) : Phil. Trans. Roy. Soc. Lond., v. A267, pp. 293-311.

Barron, T., 1917. The topography and geology of the peninsula of Sinai (western portion) : Egypt. Survey Dept., Cairo, pp. 1-241.

Baumann, A., Richter, H., and Schoell, M., 1973. Suakin Deep : Brines and hydrothermal sediments in the deepest part of the Red Sea : Geol. Rundschau, v. 62, pp. 684-697.

Allan, T. D., Charnock, H., and Morelli, C., 1964, Magnetic, gravity and depth surveys in the Mediterranean and Red Sea: Nature, v. 204, no. 4965, pp. 1245-1248.

Beets, ., 1948. Unpublished report of Anglo-Egyptian Oilfields Ltd. (cited by Heybroek, F., 1965. p.21).

Ben-Menahem, A., and Aboodi, E., 1971. Tectonic patterns in the northern Red Sea region : Jour. Geophys. Research, v. 76, no.11, pp. 2674-2689.

Bentor, Y.K., and Vroman, A.J., 1954. A structural map of Israel (1 : 250,000) with remarks on its dynamical interpretation : Res. Counc. Israel Bull., v. 4, pp. 125-135.

Bergh, H.W., 1971. Seafloor spreading in the southwest Indian Ocean : Jour. Geophys. Research, v.76, pp. 6276-6282.

Bhattacharyya, B.K., 1965. Two dimensional harmonic analysis as a tool for magnetic interpretation : Geophysics, v. 30, no. 5, pp. 829-857.

Bignell, R.D., Tooms, J.S., Cronan, D.S., and Horowitz, A., 1974. An additional location of metalliferous sediments in the Red Sea : Nature, v. 248, pp.127-128.

Birch, F.S., and Halunen, A.J., 1966. Heat flow measurements in the Atlantic Ocean, Indian Ocean, Mediterranean Sea and Red Sea : Jour. Geophys. Research, v. 71, pp. 583-586.

Brown, G.F., 1970. Eastern margin of the Red Sea and coastal structures in Saudi Arabia : Phil. Trans. Roy. Soc. Lond., v. A267, pp. 75-87.

Brown, G.F., 1972. Tectonic map of the Arabian Peninsula : Saudi Arabian Dir. Gen. Mineral Resources, Arabian Peninsula Map AP-2, scale 1:4,000,000.

Brown, G.F., Jackson, R.O., Bogue, R.G., et al 1962. Geologic map of the southern Hijaz quadrangle, Kingdom of Saudi Arabia : U.S. Geol. Survey Misc. Geol. Inv. Map I-210A, scale 1:500,000.

Brown, G.F., Jackson, R.O., Bogue, R.G., et al, 1963a. Geologic map of the northwestern Hijaz quadrangle, Kingdom of Saudi Arabia : U.S. Geol. Survey Misc. Geol. Inv. Map I-204A, scale 1:500,000.

Brown, G.F., Layne, N.M., Goudarzi, G.H., et al. 1963b. Geologic map of the northeastern Hijaz quadrangle, Kingdom of Saudi Arabia : U.S. Geol. Survey. Misc. Geol. Inv. Map I-205A, scale 1:500,000.

Burek, P.J., 1970. Palaeomagnetic evidence for an anticlockwise rotation of the Danakil Alps, Ethiopia : Trans. Am. Geophys. Union, v.51, no.4. p.271.

Carella, R., and Scarpa, N., 1962. Geological results of exploration in Sudan by A.G.I.P. Mineraria Ltd : 4th Arab Petroleum Congress (Beirut).

Coleman, R.G., 1974. Geologic background of the Red Sea :from Whitmarsh, R.B., Weser, O.E., Ross, D.A., et al. Initial Reports of the Deep Sea Drilling Project, v.23, Washington (U.S. Govt. Printing Office), pp.813-819.

Cooley, J.W., and Tukey, J.W., 1965. An algorithm for the machine calculation of complex Fourier series, Maths. Comput. v.19, p.297.

Creer, K.M., Irving, E., and Nairn, A.E.M., 1959. Palaeomagnetism of the Great Whin Sill : Roy. Astron. Soc. Geophys. J. v.2, pp.306-323.

Darracott, B.W., Fairhead, J.D., Girdler, R.W., and Hall, S.A., 1972. The East African Rift system: in Tarling, D.H., and Runcorn, S.K. (eds) Implications of continental Drift to Earth Sciences, (Academic Press), London and New York, pp. 757-766.

Degens, E.T., and Ross, D.A., (eds). 1969. Hot brines and recent heavy metal deposits in the Red Sea : New York, Springer-Verlag, 600 pp.

de Sitter, L.U., 1962. Structural development of the Arabian Shield in Palestine : Geologie Mijnb., v.41, pp.116-124.

Drake, C.L., and Girdler, R.W., 1964. A geophysical study of the Red Sea : Roy. Astron. Soc. Geophy. J., v.8, pp.473-495.

Dubertret, L., 1932. Les formes structurales de la Syrie et de la Palestine; leur origine : C.r. hebd. Seanc. Acad. Sci., Paris, v. 195, pp.65-67.

Dubertret, L. 1970. Review of structural geology of the Red Sea and surrounding areas : Phil. Trans. Roy. Soc. Lond. v.A267, pp.9-20.

Ducruix, J., Le Mouel, J.L., and Courtillot, V., 1974. Continuation of three-dimensional potential fields measured on an uneven surface : Roy. Astron. Soc Geophy. J. v. 38, pp.299-314.

Dunlop, D.J., 1973. Thermoremanent magnetization in submicroscopic magnetite : Jour. Geophys. Research, v.78, pp.7602-7613.

El-Shinnawi, M.A., and Sultan, I.Z., 1973. Lithostratigraphy of some subsurface Upper Cretaceous sections in the Gulf of Suez area, Egypt : Acta Geol. Hungarica, v. 17, pp.469-494.

Erickson, A.J., and Simmons, G., 1969. Thermal measurements in the Red Sea : in Degens, E.T., and Ross, D.A., eds., Hot brines and recent heavy metal deposits in the Red Sea : New York, Springer-Verlag, pp. 114-121.

Evans, M.E., and Wayman, M.L., 1972. The Mid Atlantic Ridge at 45°N. XIX. An electron microscope investigation of the magnetic minerals in basalt samples : Can. Jour. Earth. Sci., v.9, pp.671-678.

E vans, T.R., and Tammemagi, H.Y., 1974. Heat flow and heat production in northeast Africa : Earth Planet. Sci. Lett. v. 23, pp. 349-356.

Fairhead, J.D., and Girdler, R.W., 1970. The seismicity of the Red Sea, Gulf of Aden and Afar triangle : Phil. Trans. Roy. Soc. Lond., v. A267, pp.49-74.

Fox, P.J., and Opdyke, N.D., 1973. Geology of the oceanic crust : Magnetic properties of oceanic rocks : Jour. Geophys. Research, v.78, pp. 5139-5154.

Francis, T.J.G., 1974. A new interpretation of the 1968 Fernandina Caldera collapse and its implications for the Mid-Oceanic Ridges : Roy. Astron. Soc. Geophys. J., v.39, pp.301-318.

Freund, R., 1965. A model of the structural development of Israel and adjacent areas since Upper Cretaceous times : Geol. Mag. (Great Britain) v. 102, pp.189-205.

Freund, R., 1970. Plate tectonics of the Red Sea and East Africa : Nature, v.228, p.453.

Freund, R., Garfunkel, Z., Zak.. I., et al., 1970. The shear along the Dead Sea Rift : Phil. Trans. Roy. Soc. Lond., v. A267, pp.107-130.

Garson, M.S., and Krs. M., 1976. Geophysical and geological evidence of the relationship of Red Sea transverse tectonics to ancient fractures : Geol. Soc. Amer. Bull, v.87, pp.169-181.

Gass, I.G., Mallick, I.J., and Cox, K.G., 1965. Royal Society volcanological expedition to the South Arabian Federation and the Red Sea : Nature, v.205, pp. 952-955.

Gass, I.G., Mallick, I.J., and Cox, K.G., 1973. Volcanic Islands of the Red Sea: Jour. Geol. Soc. Lond. v.129, pp.275-310.

Gettings, M.E., 1976. Delineation of the continental margin in southern Red Sea region from new gravity evidence : in Hilpert, L.S., (ed), Red Sea research : Saudi Arabian Dir. Gen. Mineral Resources Bulletin (in prep.)

Geukens, F., 1966. Geology of the Arabian Peninsula - Yemen : U.S. Geol. Survey Prof. Paper 560-B, 23pp.

Gillman, M., 1968. Preliminary results of a geological and geophysical reconnaissance of the Gizan coastal plain in Saudi Arabia: AIME Symp. Dhahran, Saudi Arabia, pp. 198-208.

Girdler, R.W., 1958. The relati onship of the Red Sea to the East African Rift System: Quart. Jour. Geol. Soc. Lond. v.114, pp.79-105.

Girdler, R.W., 1969. The Red Sea - a geophysical background : in Degens, E.T., and Ross, D.A., eds. Hot brines and recent heavy metal deposits in the Red Sea : New York, Springer-Verlag, pp. 38-58.

Girdler, R.W., 1970a. A review of the Red Sea heat flow : Phil. Trans. Roy. Soc. Lond., v. A267, pp. 191-203.

Girdler, R.W., 1970b. An aeromagnetic survey of the junction of the Red Sea, Gulf of Aden and Ethiopian rifts - a preliminary report: Phil. Trans. Roy. Soc. Lond. v. A267, pp. 359-368.

Girdler, R.W., and Darracott, B.W., 1972. African poles of rotation : Comments on Earth Sciences, Geophysics, v.2, pp. 131-138.

Girdler, R.W., Erickson, A J., and von Herzen, R., 1974. Downhole temperature and shipboard thermal conductivity measurements aboard D/V "Glomar Challenger" in the Red Sea : in Initial reports of the Deep Sea Drilling Project, v.23, Washington (U.S. Govt. Printing Office), pp. 879-886.

Girdler, R.W., and Hall, S.A., 1972. An aeromagnetic survey of the Afar Triangle of Ethiopia : in R.W. Girdler (ed), East African Rifts. Tectonophysics, 15, (1/2), p.53.

Girdler, R.W., and Harrison, J.C., 1957. Submarine gravity measurements in the Atlantic Ocean, Indian Ocean, Red Sea and Mediterranean Sea : Proc. Roy. Soc. Lond., v. A239, pp. 202-213.

Girdler, R.W., and Styles, P., 1974. Two stage Red Sea floor spreading : Nature, v. 247, pp. 7-11.

Girdler, R.W., and Styles, P., 1976. The relevance of magnetic anomalies over the southern Red Sea and Gulf of Aden to Afar : in press.

Girdler, R.W., and Whitmarsh, R.B., 1974. Miocene evaporites in Red Sea cores, their relevance to the problem of the width and age of oceanic crust beneath the Red Sea : from Whitmarsh, R.B., Weser, O.E., Ross, D.A., et al. Initial reports of the Deep Sea Drilling Project. v. 23, Washington (U.S. Govt. Printing Office), pp. 913-921.

Godson, R. H., 1974, GEOPAC: U.S. Geological Survey open-file rept. (IR)SA-162, 146 p., 17 figs.

Haenel, R., 1972. Heat flow measurements in the Red Sea and Gulf of Aden : Z. Geophysik, v. 38, pp. 1035-1047.

Hall, S.A., 1970. Total intensity magnetic anomaly chart of the junction of the Red Sea, Gulf of Aden and Ethiopian Rift.

Hall, S. A., Andreasen, G. E., and Girdler, R. W., 1977, Total-intensity magnetic anomaly map of the Red Sea and adjacent coastal areas, a description and preliminary interpretation: Saudi Arabian Directorate General of Mineral Resources Bull. 22, p. F1-F15.

Hecker, O., 1910. Bestimmung der Schwerkraft auf der Schwarzen Meere und an dessen Kuste sowie neue Ausgleichung der Schwerkraftmessungen auf dem Atlantischen, Indischen und Grossen Ozean. Veroffentl. des Zentralbureaus der Internat. Erd messung, Neue Folge, v. 17, no.20.

Heirtzler, J.R., Dickson, G.O., Herron, E.M., et al, 1968. Marine magnetic anomalies; geomagnetic field reversals and motions of the ocean floor and continents : Jour. Geophys. Research, v. 73, pp. 2119-2136.

Hess, H.H., 1962. History of ocean basins : in Engel, A.E.J., James, H.L., and Leonard, B.F., (eds.), Petrologic studies : a volume in honour of A.F. Buddington : Geol. Soc. Amer., pp. 599-620.

Heybroek, F., 1965. The Red Sea Miocene evaporite basin : in Salt basins around Africa, Inst. Petroleum, London., pp. 17-40.

Holmes, A., 1944. Principles of Physical Geology, Ronald Press, New York.

Hutchinson, R.W., and Engels, G.G., 1970. Tectonic significance of regional geology and evaporite lithofacies in northeastern Ethiopia : Phil. Trans. Roy. Soc. Lond., v. A267, pp. 313-329.

Irving, E., 1956a. Palaeomagnetic and palaeoclimatological aspects of polar wandering : Pure Appl. Geophys. v. 33, pp. 23-41.

Irving, E., 1956b. The Magnetization of the Mesozoic Dolerites of Tasmania : Proc. Roy. Soc. Tasmania, v. 90, pp. 157-168.

Isacks, B., Oliver, J., and Sykes, L.R., 1968. Seismology and the New Global Tectonics : Jour. Geophys. Research, v. 73, pp. 5855-5899.

Kabbani, F.K., 1970. Geophysical and structural aspects of the central Red Sea rift valley: Phil. Trans. Roy. Soc. Lond. v. A267, pp. 89-97.

Karpoff, R., 1957. Sur l'existence du maestrichtien au nord de Djeddah (Arabie seoudite): Comptes Rendus, Seances, Acad. des Sciences, v. 245, no.2, pp. 1322-1324.

Kazmin, V., 1971. Precambrian of Ethiopia: Nature Phys. Sci., v. 230, pp.176-177.

Klitgord, K.D., Huestis, S.P., Mudie, J.D., et al, 1975. An analysis of near-bottom magnetic anomalies : sea-floor spreading and the magnetised layer : Roy. Astron. Soc. Geophys. J., v. 43, pp. 387-424.

Klitgord, K.D., and Mudie, J.D., 1974. The Galapagos spreading centre : a near bottom geophysical survey : Roy. Astron Soc. Geophys. J. v.38, no. 3, pp. 563-586.

Knott, S.T., Bunce, E.T., and Chase, R.L., 1966. Red Sea seismic reflection studies : in The world rift system, Canada Geol. Survey paper 66-14, pp. 31-61.

Lamare, P., 1930. Les manifestations volcaniques post-cretacees de la Mer Rouge et des pays limitrophes : Soc. geol. France Mem., new. ser. 6, pp. 221-223.

Langseth, M.G., and Taylor, P.T., 1967. Recent heat flow measurements in the Indian Ocean : Jour. Geophys. Research, v. 72, pp. 6249-6260.

Lattimore, R.K., Rona, P.A., and DeWald, O.E., 1974. Magnetic anomaly sequence in the central North Atlantic : Jour. Geophys. Research, v. 79, pp. 1207-1209.

Laughton, A.S., 1966. The Gulf of Aden, in relation to the Red Sea and the Afar depression of Ethiopia : in The World Rift System, Canada Geol. survey paper 66-14, pp. 78-97.

Laughton, A.S. 1970. A new bathymetric chart of the Red Sea: Phil. Trans. Roy. Soc Lond. v. A267, pp. 21-22

Le Pichon, X., 1968. Sea-floor spreading and continental drift : Jour. Geophys. Research, v. 73, pp. 3661-3697.

Le Pichon, X., Francheteau, J., and Bonnin, J., 1973. Plate Tectonics : Developments in Geotectonics, no. 6, Elsevier, Amsterdam, 300 pp.

Lowrie, W., Løvlie, R., and Opdyke, N.D., 1973a. The magnetic properties of Deep Sea Drilling Project basalts from the Atlantic Ocean : Earth. Planet. Sci. Lett., v. 17, pp. 338-349.

Lowrie, W., Løvlie, R., and Opdyke, N.D., 1973b. Magnetic properties of Deep-Sea Drilling Project basalts from the North Pacific Ocean : Jour. Geophys. Research, v. 78, pp. 7647-7660.

Ludwig, W.J., Nafe, J.E., and Drake, C.L., 1970. Seismic Refraction : in A.E. Maxwell (ed.), The Sea, Vol. 4, Interscience, New York, pp. 53-84.

MacFadyen, W.A., 1932. On the volcanic Zebayir Islands, Red Sea : Geol. Mag. (Great Britain), v. 69, pp. 63-66.

McKenzie, B.P., Davies, D., and Molnar, P., 1970. Plate tectonics of the Red Sea and East Africa : Nature, v. 226, pp. 243-248.

McKenzie, D.P., and Parker, R.L., 1967. The North Pacific : an example of tectonics on a sphere : Nature, v. 216, pp. 1276 - 1280.

Marinelli, G., Barberi, F., Santacroce, R., et al, 1973. Geology of northern Afar (Ethiopia) : Rev. Geog. Phys. Geol. Dyn., v. 15, pp. 443-489.

Marshall, M., and Cox, A., 1971. Magnetism of pillow basalts and their petrology : Geol. Soc. Amer. Bull., v. 82, pp. 537-552.

Matthews, D.H., and Bath, J., 1967. Formation of magnetic anomaly pattern of mid-Atlantic ridge : Roy. Astron. Soc. Geophys. J., v. 13, pp. 349-357.

Matthews, D.H., Vine, F.J., and Cann, J.R., 1965. Geology of an area of the Carlsberg Ridge, Indian Ocean : Geol. Soc. Amer. Bull., v. 76, pp. 675-682.

Menard, H.W., and Atwater, T., 1968. Changes in direction of sea floor spreading, Nature, v. 219, pp. 463-467.

Mohr, P.A., 1962. The Geology of Ethiopia : Univ. Coll. Addis Ababa Press, 268 pp.

Mohr, P.A., 1967. The Ethiopia Rift System : Bull. Geophys. Obs., Addis Ababa, Ethiopia, v.11, pp 1-65.

Mohr, P.A., 1972. Surface structure and plate tectonics of Afar : in Girdler, R.W. (ed.), East African Rifts. Tectonophysics, v. 15, pp. 3-18.

Morgan, W.J., 1968. Rises, Trenches, Great Faults and Crustal Blocks : Jour. Geophys. Research, v.73, pp. 1959-1982.

Murauchi, S., Den, N., Asano, S., et al, 1968. Crustal structure of the Phillipine Sea : Jour. Geophys. Research, v. 73, pp. 3143-3171.

Ostapoff, F., 1969. A fourth brine hole in the Red Sea : in Degens, E.T., and Ross, D.A., eds. Hot brines and recent heavy metal deposits in the Red Sea : New York, Springer-Verlag, pp. 18-21.

Pearce, R. PhD Thesis, University of Newcastle upon Tyne (in prep.)

Phillips, J.D., 1970. Magnetic anomalies in the Red Sea : Phil. Trans. Roy. Soc. Lond., v. A267, pp. 205-218.

Phillips, J.D., and Ross, D.A., 1970. Continuous seismic reflection profiles in the Red Sea : Phil. Trans. Roy. Soc. Lond. v. A267, pp. 153-180.

Phillips, J.D., Woodside, J., and Bowin, C.O., 1969. Magnetic and gravity anomalies in the central Red Sea : in Degens, E.T., and Ross, D.A., eds., Hot brines and recent heavy metal deposits in the Red Sea: New York, Springer-Verlag, pp. 98-113.

Picard, L., 1943. Structure and evolution of Palestine : Bull. Hebrew Univ., Jerusalem, v.4, pp 1-134.

Picard, L., 1966. Thoughts on the graben system in the Levant : in The world rift system, Canada Geol. Survey paper 66-14, pp.22-32.

Pitman, W.C., Herron, E.M., and Heirtzler, J.R., 1968. Magnetic anomalies in the Pacific and sea-floor spreading : Jour. Geophys. Research, v. 73, pp. 2069-2085.

Plaumann, S., 1963. Kontinuierliche Schweremessungen in Roten Meer mit einen Askamia-Seagravimeter von Typ Gas 2 nach GRAF : Zeit fur Geophysik v. 29, pp 233-256.

Polyak, B.G., and Smirnov, Ya, B., 1968. Relationship between terrestial heat flow and the tectonics of continents : Geotectonics, pp. 205-213.

Quennell, A.M., 1958. The structural and geomorphic evolution of the Dead Sea Rift : Quart. J. Geol. Soc. Lond., v. 114, pp. 1-24.

Quennell, A.M. 1959. Tectonics of the Dead Sea Rift : 20th Int. Geol. Congr. Mexico, pp. 385-405.

Richter-Bernburg, G., and Schott, W., 1954. Geological researches in western Saudi Arabia : Saudi Arabian Dir. Gen. Mineral Resources open-file rept. 38, 69 pp.

Roberts, D.G., and Whitmarsh, R.B., 1969. A bathymetric and magnetic survey in the Gulf of Tadjura, western Gulf of Aden : Earth Planet. Sci. Lett., v. 5, pp. 253-258.

Robson, D.A. 1971. The structure of the Gulf of Suez (Clysmic) rift, with special reference to the eastern side : Jour. Geol. Soc. Lond. v. 127, pp. 247-276.

Ross, D.A., Hays, E.E., and Allstrom, F.C., 1969. Bathymetry and continuous seismic profiles of the hot brine region of the Red Sea : in Degens, E.T., and Ross, D.A., eds. Hot brines and recent heavy metal deposits in the Red Sea : New York, Springer-Verlag, pp. 82-97.

Ross, D.A., and Schlee, J., 1973. Shallow structure and geologic development of the southern Red Sea : Geol. Soc. Amer. Bull. v. 84, pp. 3827-3848.

Runcorn, S.K., 1956. Palaeomagnetic comparisons between Europe and North America : Geol. Ass. Canada, Proc., v.8, pp. 77-85.

Said, R., 1962. The Geology of Egypt : Elsevier Publishing Co., Amsterdam, New York, 377 pp.

Talwani, M., 1965. Computation with the help of a digital computer of magnetic anomalies caused by bodies of arbitrary shape : Geophysics, v. 30, pp. 797-817.

Talwani, M., and Heirtzler, J.R., 1964. Computation of magnetic anomalies caused by two dimensional structures of arbitrary shape : in Computers in the mineral industries, G.A. Parks (ed.), Stanford University.

Tazieff, H., Marinelli, G., Barberi, F., and Varet, J., 1969. Geologie de l'Afar Septentrionel. Premere expedition du CNRS-France et du CNR-Italia (decembre 67 - fevrier 68) : Bull. Volcan. v.33, no.4, pp. 1039-1072.

Tazieff, H., and Varet, J., 1969. Signification tectonique et magmatique de l'Afar septentrional (Ethiopia) : Rev. Geog. Phys. Geol. Dyn., v.11, pp.429-450.

Topping, J., 1955. Errors of observation and their treatment : Institute of Physics, London, Monograph for students.

Tramontini, G.B., and Davies, D., 1969. A seismic refraction survey in the Red Sea : Roy. Astron. Soc. Geophys. J. v.17, pp.225-241.

Tromp, S.W., 1951. Misir ve Bilhassa Kizildenizin Jeolojik Tarihcesi : Bull. Turk. Jeol. Kurumu, v. 3, pp. 51-95.

Truilzi, A.E..von, 1898. Expedition S.M. Schiff POLA in das Rote Mear, nordliche Halfte. Wissenschaftliche Ergebnisse 11. Relative Schwerebestimmungen. Denkschr. K. Akad. Wiss. Math-Nat. Classe, v.65, p.131.

Truilzi, A.E. von, 1901. Expedition S.M. Schiff POLA in das Rote Meer, suddliche Halfte. Wissenschaftliche Ergebnisse 12. Relative Schwerebestimmungen. Denkschr. K. Akad. Wiss. Math-Nat. Classe, v.69, p.143.

U.S. Geological Survey, 1963. Geologic map of the Arabian Peninsula : Misc. Geol. Inv. Map I-270A, scale 1:2,000,000.

U.S. Geological Survey, 1972. Topographic map of the Arabian Peninsula, A.P.-1.

Vening Meinesz, F.A., 1934. Gravity Expeditions at Sea, II, 1923-1932 : Delft, Netherlands Geod. Comm. Publ. 208 pp.

Vine, F.J., 1966. Spreading of the ocean floor : new evidence : Science, v.154, pp. 1405-1415.

Vine, F.J., and Matthews, D.H., 1963. Magnetic anomalies over ocean ridges : Nature, v. 199, pp. 947-949.

Vine, F.J., and Wilson, J.T., 1965. Magnetic anomalies over a young oceanic ridge off Vancouver Island : Science, v.150, pp. 485-489.

Said, R., 1969. General stratigraphy of the adjacent land areas of the Red Sea : in Degens, E.T., and Ross, D.A., eds. Hot brines and recent heavy metal deposits in the Red Sea : New York, Springer-Verlag, pp.71-81.

Scheuch, J., 1973. Warmestromdichtemessungen im Roten Meer zwichen 19° und 26° nordlicher Breite (Gebiet der Laugentiefs) : Z. Geophys., v. 39, pp. 859-862.

Schouten, H., 1974. Magnetic anomalies over fracture zones in the lower magnetic latitudes of the central north Atlantic : Trans. Amer. Geophys. Union, v. 55, p.232. (Abstract).

Schult, A., 1974. Palaeomagnetism of Tertiary volcanic rocks from the Ethiopian Southern Plateau and the Danakil Block : Zeit. Geophys. v. 40, pp. 203-212.

Schurmann, H.M.E., 1966. The Pre-Cambrian along the Gulf of Suez and the northern part of the Red Sea : Leiden : Brill.

Sclater, J.G., 1966. Heat flow in the north west Indian Ocean and Red Sea : Phil. Trans. Roy. Lond., v. A259, pp. 271-278.

Sclater, J.G., and Francheteau, J., 1970. The implications of terrestial heat flow observations on current tectonic and geochemical models of the crust and upper mantle of the earth : Roy. Astron. Soc. Geophys. J., v. 20, pp.509-537.

Searle, R.C., and Ross, D.A., 1975. A geophysical study of the Red Sea axial trough between 20.5°N and 22°N : Roy. Astron. Soc. Geophys. J., v. 43, pp. 555-572.

Sestini, J., 1965. Cenozoic stratigraphy and depositional history, Red Sea coast, Sudan : Am. Assoc. Petroleum, Geologists, Bull., v.49, pp.1453-1472.

Shanti, M.S., 1966. Oolitic iron ore deposits in Wadi Fatima between Jiddah and Mecca : Saudi Arabian Directorate General of Mineral Resources, Bulletin, no.2.

Styles, P. The tectonic evolution of the southern Red Sea and Gulf of Aden : PhD Thesis, University of Newcastle upon Tyne (in prep.)

Swarz, D.H., and Arden, D.D., Jr., 1960. Geologic history of the Red Sea area : Am. Assoc. Petroleum Geologists, Bull., v. 44, pp.1621-1637.

Sykes, L.R., 1968. Seismological evidence for transform faults, seafloor spreading and continental drift : in R.A. Phinney (ed), The History of the Earth's Crust, Princeton University Press, pp.120-150.

Watkins, N.D., Paster, T., and Ade-Hall, J. 1970. Variation of magnetic properties in a single deep-sea pillow basalt : Earth. Planet. Sci. Lett. v.8, pp. 322-328.

Wheildon, J., Evans, T.R., and Girdler, R.W., 1974. Thermal conductivity, density, and sonic velocity measurements of samples of anhydrite and halite from sites 225 and 227 : from Whitmarsh, R.B., Weser, O.E., Ross, D.A., et al. Initial Reports of the Deep Sea Drilling Project, v. 23, Washington (U.S. Govt. Printing Office), pp. 909-911.

Whiteman, A.J., 1968. Formation of the Red Sea depression : Geol. Mag. (Great Britain). v. 105, pp. 231-246.

Whiteman, A.J., 1971. The geology of the Sudan Republic : Oxford, Clarendon Press, 290 pp.

Whitmarsh, R.B., 1975. Axial intrusion zone beneath the median valley of the Mid-Atlantic Ridge at 37^{o}N detected by explosion seismology : Roy. Astron. Soc. Geophys. J., v.42, pp. 189-215.

Whitmarsh, R.B., Weser, O.E., Ross, D.A., et al., 1974. Initial reports of the Deep Sea Drilling Project, v. 23, Washington (U.S. Govt. Printing Office).